# LIM kinase and metanephric mesenchymal cell migration in the developing mouse kidney.

Alexander James Sparrow, BSc. (Hons), MSc.

Thesis submitted to the University of Nottingham for the degree of Doctor of Philosophy

July 2016

# Abstract

The adult mammalian kidney forms from the reciprocal interaction between two tissues; the ureteric bud which will form the collecting duct system and the metanephric mesenchyme which will form all the cells in the nephrons. This thesis used *ex-vivo* embryonic kidney culture to show that during mouse kidney development metanephric mesenchymal cells migrated towards the periphery of the kidney. When this migration is pharmacologically inhibited the Six2 expressing metanephric mesenchyme cells no longer expanded their population and kidney development ceases. LIM kinase, which had been shown to regulate cell migration, when inhibited not only prevented cell migration in both embryonic mouse kidneys and in HK2 cells but also prevented embryonic kidney cells from completing mitosis and caused them to undergo apoptosis. This thesis showed that inhibition of LIM kinase in HK2 cells resulted in the formation of multiple alpha-tubulin foci, multiple centrosomes, the premature dispersal of the cohesin complex protein SMC3 in the absence of a fully formed spindle, and cell death. Thus concluding that active LIM kinase is required for the generation of the mitotic spindle and the appropriate dispersal of SMC3. This thesis furthered the understanding of how the metanephric mesenchyme develops and showed that these cells migrated away from the ureteric bud and this migration is required for further growth of the kidney. This thesis also showed that active LIM kinase is required for the completion of mitosis in both embryonic kidneys and HK2 cells.

# Publications

## Paper

Gray C., Al-Dujaili E.A., **Sparrow A.J.**, Gardiner S.M., Craigon J., Welham S.J., and Gardner D.S. (2013). Excess maternal salt intake produces sex-specific hypertension in offspring: putative roles for kidney and gastrointestinal sodium handling. PLoS One. 8(8), e72682.

## Conference abstract

**Sparrow A**, Sweetman D, Welham S. 2014. Active LIM kinase is required for metanephric mesenchyme migration, SIX2 expression and Mitosis in mesenchymal cells. Abstract at UK Kidney week 2014; 2014 April 29-May 2; Glasgow, UK.

# Acknowledgments

I would like to thank my supervisors Simon and Dylan for their invaluable help, and my parents and sister who have been supportive throughout these past 4 years.

I wish to thank everyone in nutritional sciences and at the BSU. In particular Cathy, Zoe, and Kirsty for all their help in the lab. And all the postgrads in office 50 and 51 for making these 4 years fun.

Finally I would like to thank Bethan for being the most amazing friend these past 4 years and always being there for me.

# Table of Contents

Abstract……..i

Publications……..ii

Acknowledgments……..iii

Table of Contents……...iv

Table of Figures…….……...x

Table of Tables…….……xviii

Abbreviations……..……xix

Chapter 1: Introduction ..... 1

1.1 – Kidney Development ..... 1

1.1.1 – Introduction ..... 1

1.1.2 – Induction ..... 1

1.1.3 – Branching and growth ..... 5

1.1.4 – Mesenchyme..... 7

1.1.5 – Nephron Formation ..... 10

1.1.6 – LIM kinase in the kidney ..... 12

1.2 – Cell Cycle ..... 13

1.2.1 – Introduction ..... 13

1.2.2 – Interphase ..... 13

1.2.3 – M Phase..... 13

1.2.4 – LIM kinase during mitosis ..... 17

1.3 – Cell Migration ..... 18

1.3.1 – Introduction ..... 18

1.3.2 – Mechanism ..... 18

1.3.3 – LIM kinase and cell migration ..... 22

1.4 – Summary, hypothesis and aims ..... 24

Chapter 2: Materials and Methods ..... 26

2.1 – Tissue culture ..... 26

2.1.1 – Matings ..... 26

2.1.2 – Kidney dissection ..... 26

2.1.3 – Kidney culture ..... 26

2.1.4 – Micro-Injections ..... 27

2.1.5 – Fixing ..... 28

2.1.6 – Whole mount immunofluorescence ..... 28

2.1.7 – TUNEL whole mount ..... 29

2.1.8 – Cell number assay ..... 30

2.1.9 – Mitotic number and anaphase quantification ..... 31

2.1.10 – Western blot ..... 31

2.1.11 – Kidney area measurements ..... 33

2.2 – Cell culture ..... 34

2.2.1 – Human proximal tubule cells (HK2 cells) ..... 34

2.2.2 – Mouse myoblast cells (C2C12 cells) ..... 35
2.2.3 – Human hepatocellular carcinoma cells (HEPG2 cells) ..... 35
2.2.4 – Mouse embryonic fibroblast cells (3T3 cells) ..... 36
2.2.5 – Wound healing assay ..... 36
2.2.6 – Cell number assay ..... 36
2.2.7 – Trypan blue assay ..... 37
2.2.8 – MTT assay ..... 38
2.2.9 – Fixing ..... 38
2.2.10 – Immunofluorescence ..... 39
2.2.11 – Mitotic number and anaphase quantification ..... 40
2.3 – Imaging ..... 41
2.3.1 – Kidney culture light and DiI images ..... 41
2.3.2 – Live kidney confocal time-lapse imaging ..... 41
2.3.3 – Whole mount IF and TUNEL images ..... 41
2.3.4 – Cell culture images ..... 42
2.3.5 – Cell culture immunofluorescence images ..... 42
2.4 – Statistics ..... 43
Chapter 3: The effect of LIMK inhibition during kidney development. ..... 44
3.1 – Introduction ..... 44
3.2 – Results ..... 47
3.2.1 – BMS5 inhibits LIMK activity ..... 47

3.2.2 – BMS5 effects on kidney growth ..... 57

3.2.3 – BMS5 causes mitotic arrest in kidney development ..... 62

3.2.4 – BMS5 effects on Six2 expression is not due to a Phosphorylated Cofilin pathway ..... 65

3.2.5 – BMS5 effects on Six2 expression cannot be explained by the loss of Cofilin phosphorylation ..... 72

3.2.6 – Mitosis inhibitors do not replicate the loss of Six2 or cell death 77

3.3 – Conclusions ..... 88

Chapter 4: The effect of LIMK inhibition during the cell cycle in HK2 cells. 92

4.1 – Introduction ..... 92

4.2 – Results ..... 94

4.2.1 – BMS5 inhibits Cofilin phosphorylation ..... 94

4.2.2 – BMS5 inhibits completion of mitosis ..... 98

4.2.3 – BMS5 prevents spindle formation ..... 114

4.2.4 – BMS5 has no effect on the degradation of the nuclear lamina or Securin 117

4.2.5 – BMS5 causes the mis-localisation of Pericentrin and centrosomes ..... 120

4.2.6 – BMS5 causes the inappropriate dispersal of SMC3 ..... 124

4.2.7 – LIMK inhibition with BMS5 has no effect on Stathmin phosphorylation, or Vimentin ..... 126

4.2.8 – Mitotic inhibition by BMS5 is independent of cell type..... 130

4.2.9 – Is Cofilin phosphorylation responsible for the generation of α-tubulin foci? ..... 133

4.2.10 – Actin filament disruption is not the mechanism by which BMS5 generates α-tubulin foci ..... 138

4.2.11 – Mitosis inhibition cannot replicate the BMS5 phenotype in HK2 cells ..... 148

4.3 – Conclusions ..... 153

Chapter 5: Metanephric mesenchymal cell migration. ..... 156

5.1 – Introduction ..... 156

5.2 – Results ..... 158

5.2.1 – DiI labelled populations of cells in the metanephric mesenchyme separate ..... 158

5.2.2 – DiI labelled cells migrate towards the periphery of the kidney 162

5.2.3 – BMS5 stops cell movement in kidneys ..... 168

5.2.4 – Migration inhibitors in HK2 cells ..... 170

5.2.5 – Migration inhibitors stop mesenchyme cell migration ..... 177

5.2.6 – Consequences of the inhibition of cell migration with Cytochalasin B ..... 180

5.2.7 – Does CK666 affect mitosis? ..... 189

5.2.8 – Consequences of cell migration inhibition with CK666..... 195

5.2.9 – Can the effect of inhibiting migration with CK666 be reversed by transfer back to control media? ..... 204

5.2.10 – Can the inhibition of growth with migration inhibitors be replicated with an anti-MMP9 antibody? ..... 212

5.3 – Conclusions ..... 219

Chapter 6: Discussion ..... 222

6.1 – LIM kinase role in mitosis ..... 222

6.2 – Metanephric mesenchymal cell migration ..... 226

6.3 – Limitations and future directions ..... 230

6.4 – Significance and conclusions ..... 232

Chapter 7: References ..... 234

# Tables of Figures

Figure 1.1 – Development of the nephric duct. ..... 4

Figure 1.2 – Nephric duct growing into the metanephric mesenchyme. ..... 5

Figure 1.3 – Nephron formation from the metanephric mesenchyme. ..... 10

Figure 1.4 – Mitosis. ..... 16

Figure 1.5 – Lamellipodia formation. ..... 22

Figure 3.1 – LIMK1, LIMK2 and pLIMK1/2 in E12.5 cultured kidneys. ..... 49

Figure 3.2 – Phosphorylated Cofilin in E11.5 kidneys cultured in 10µM BMS5. ..... 51

Figure 3.3 – Phosphorylated Cofilin in E12.5 kidneys cultured in 50µM BMS5 (24 hours). ..... 54

Figure 3.4 – Phosphorylated Cofilin in E12.5 kidneys cultured in 50µM BMS5 (48 hours). ..... 55

Figure 3.5 – Western blot of E12.5 kidneys cultured in 50µM BMS5. ..... 56

Figure 3.6 – Kidney size after 24 and 48 hours cultured in 50µM BMS5. ..... 58

Figure 3.7 – Light micrographs of E12.5 kidneys cultured in 50µM BMS5. ... 59

Figure 3.8 – Six2 in E12.5 kidneys cultured in 50µM BMS5. ..... 60

Figure 3.9 – Cell counts on E12.5 kidneys cultured in 50µM BMS5. ..... 61

Figure 3.10 – Mitosis analysis of E12.5 kidneys cultured in 50µM BMS5. ..... 63

Figure 3.11 – Apoptosis in E12.5 kidneys cultured in 50µM BMS5. ..... 64

Figure 3.12 – Kidney size after 48 hours cultured in 100µM FIPI and 1.5% Butanol. ..... 67

Figure 3.13 – Light micrographs of E12.5 kidneys cultured in 100µM FIPI. .... 69

Figure 3.14 – Light micrographs of E12.5 kidneys cultured in 1.5% Butanol. 70

Figure 3.15 – Six2 in E12.5 kidneys cultured in 100µM FIPI and 1.5% Butanol. ..... 71
Figure 3.16 – Phosphorylated Cofilin in E12.5 kidneys cultured in 25µM A23187. ..... 73
Figure 3.17 – Phosphorylated Cofilin in E12.5 kidneys cultured in 10mM Histamine..... 74
Figure 3.18 – Six2 in E12.5 kidneys cultured in 25µM A23187. ..... 75
Figure 3.19 – Six2 in E12.5 kidneys cultured in 10mM Histamine. ..... 76
Figure 3.20 – Mitosis analysis of E12.5 kidneys cultured in 10µM Paclitaxel. 79
Figure 3.21 – Mitosis analysis of E12.5 kidneys cultured in 1µg/ml Colchicine. ..... 81
Figure 3.22 – Kidney size after 24 hours cultured in 10µM Paclitaxel. ..... 82
Figure 3.23 – Light micrographs of E12.5 kidneys cultured in 10µM Paclitaxel. ..... 83
Figure 3.24 – Kidney size after 24 hours cultured in 1µg/ml Colchicine. ..... 84
Figure 3.25 – Light micrographs of E12.5 kidneys cultured in 1µg/ml Colchicine. ..... 85
Figure 3.26 – Six2 in E12.5 kidneys cultured in 10µM Paclitaxel. ..... 86
Figure 3.27 – Six2 in E12.5 kidneys cultured in 1µg/ml Colchicine. ..... 87
Figure 4.1 – Phosphorylated Cofilin in HK2 cells cultured in 10µM and 50µM BMS5. ..... 95
Figure 4.2 – LIMK1, LIMK2, and pLIMK1/2 in cultured HK2 cells. ..... 96
Figure 4.3 – TESK1 and TESK2 in cultured HK2 cells. ..... 97
Figure 4.4 – Cell counts on HK2 cells cultured in 10µM and 50µM BMS5. . 102

Figure 4.5 – Cell counts on HK2 cells cultured in 10µM and 50µM BMS5 at 0 hours, 24 hours, and 48 hours. ..... 103
Figure 4.6 – Cell counts on confluent HK2 cells cultured in 10µM and 50µM BMS5. ..... 104
Figure 4.7 – Cell counts on HEPG2 cells cultured in 10µM and 50µM BMS5. ..... 105
Figure 4.8 – Cell counts on sub confluent and confluent C2C12 cells cultured in 10µM and 50µM BMS5. ..... 106
Figure 4.9 – Trypan blue assay on HK2 cells cultured in 10µM and 50µM BMS5. ..... 107
Figure 4.10 – MTT assay on HK2 cells cultured in BMS5. ..... 108
Figure 4.11 – MTT assay on confluent HK2 cells cultured in BMS5. ..... 109
Figure 4.12 – Mitosis analysis on HK2 cells cultured in 10µM and 50µM BMS5. ..... 111
Figure 4.13 – Phalloidin and pH3 in HK2 cells cultured in 10µM and 50µM BMS5. ..... 113
Figure 4.14 – α-tubulin in HK2 cells cultured in 10µM and 50µM BMS5. ..... 115
Figure 4.15 – α-tubulin in HK2 cells cultured in 10µM and 50µM BMS5 (interphase). ..... 116
Figure 4.16 – Lamin A and α-tubulin in HK2 cells cultured in 10µM and 50µM BMS5. ..... 118
Figure 4.17 – Securin and pH3 in HK2 cells cultured in 10µM and 50µM BMS5. ..... 119
Figure 4.18 – Pericentrin and α-tubulin in HK2 cells cultured in 10µM and 50µM BMS5. ..... 121

Figure 4.19 – Pericentrin and α-tubulin in HK2 cells cultured in 10μM and 50μM BMS5 (interphase)..... 122
Figure 4.20 – γ-tubulin and Pericentrin in HK2 cells cultured in 10μM and 50μM BMS5..... 123
Figure 4.21 – SMC3 and α-tubulin in HK2 cells cultured in 10μM and 50μM BMS5..... 125
Figure 4.22 – Stathmin p37 and α-tubulin in HK2 cells cultured in 10μM and 50μM BMS5..... 127
Figure 4.23 – Stathmin p63 and α-tubulin in HK2 cells cultured in 10μM and 50μM BMS5..... 128
Figure 4.24 – Vimentin and α-tubulin in HK2 cells cultured in 10μM and 50μM BMS5..... 129
Figure 4.25 – α-tubulin and pH3 in 3T3 cells cultured in 10μM and 50μM BMS5..... 131
Figure 4.26 – Mitosis analysis on 3T3 cells cultured in 10μM and 50μM BMS5. ..... 132
Figure 4.27 – Phosphorylated Cofilin in HK2 cells cultured in 5μM, 25μM and 50μM A23187. ..... 134
Figure 4.28 – Phosphorylated Cofilin in HK2 cells cultured in 1mM and 10mM Histamine..... 135
Figure 4.29 – α-tubulin and pH3 in HK2 cells cultured in 5μM and 50μM A23187. ..... 136
Figure 4.30 – α-tubulin and pH3 in HK2 cells cultured in 1mM and 10mM Histamine..... 137

Figure 4.31 – Phalloidin and pH3 in HK2 cells cultured in 1µM, 10µM, and 30µM Cytochalasin B..... 140
Figure 4.32 – Cell counts on HK2 cells cultured in 1µM, 10µM, and 30µM Cytochalasin B..... 141
Figure 4.33 – Mitosis analysis on HK2 cells cultured in 1µM, 10µM, and 30µM Cytochalasin B..... 142
Figure 4.34 – α-tubulin in HK2 cells cultured in 1µM, 10µM, and 30µM Cytochalasin B..... 144
Figure 4.35 – Pericentrin and α-tubulin in HK2 cells cultured in 1µM, 10µM, and 30µM Cytochalasin B..... 145
Figure 4.36 – SMC3 and α-tubulin in HK2 cells cultured in 1µM, 10µM, and 30µM Cytochalasin B..... 147
Figure 4.37 – Mitosis analysis on HK2 cells cultured in 10µM and 50µM Paclitaxel. ..... 150
Figure 4.38 – SMC3 and α-tubulin in HK2 cells cultured in 10µM and 50µM Paclitaxel ..... 152
Figure 5.1 – DiI injected mesenchyme showing cells moving to the periphery of the kidney. ..... 160
Figure 5.2 – DiI labelled cells overlay with Six2 in E12.5 kidneys..... 161
Figure 5.3 – Confocal images of DiI injected mesenchyme showing a cell moving towards the periphery of the kidney. ..... 164
Figure 5.4 – Time lapse confocal images of a DiI labelled cell migrating in the kidney. ..... 165
Figure 5.5 – Time lapse confocal images of DiI labelled cells migrating in the kidney. ..... 166

Figure 5.6 – Time lapse confocal images of a DiI labelled cell migrating towards the periphery of the kidney. ..... 167
Figure 5.7 – Failure of DiI labelled cells to move in E12.5 kidneys cultured in 50µM BMS5. ..... 169
Figure 5.8 – Cell wound assay on HK2 cells cultured in 10µM and 50µM BMS5. ..... 172
Figure 5.9 – Cell wound assays on HK2 cells cultured in 100µM, 500µM, and 1000µM CK666. ..... 173
Figure 5.10 – Cell wound assay on HK2 cells cultured in 10µM and 30µM Cytochalasin B. ..... 174
Figure 5.11 – Cell wound assay on HK2 cells cultured in 1.5% Butanol. ..... 175
Figure 5.12 – Cell wound assay on HK2 cells cultured in 100µM FIPI. ..... 176
Figure 5.13 – DiI labelled cells not migrating in E12.5 kidneys cultured in CK666. ..... 178
Figure 5.14 – DiI labelled cells not migrating in E12.5 kidneys cultured in Cytochalasin B. ..... 179
Figure 5.15 – Kidney size after 48 hours cultured in 10µM and 30µM Cytochalasin B. ..... 182
Figure 5.16 – Light micrographs of E12.5 kidneys cultured in 10µM Cytochalasin B. ..... 183
Figure 5.17– Light micrographs of E12.5 kidneys cultured in 30µM Cytochalasin B. ..... 184
Figure 5.18 – Six2 in E12.5 kidneys cultured in 10µM and 30µM Cytochalasin B. ..... 185

Figure 5.19 – Mitosis analysis of E12.5 kidneys cultured in 10µM Cytochalasin B. ..... 186
Figure 5.20 – Mitosis analysis of E12.5 kidneys cultured in 30µM Cytochalasin B. ..... 188
Figure 5.21 – Mitosis analysis of E12.5 kidneys cultured in 100µM CK666. 191
Figure 5.22 – Mitosis analysis of E12.5 kidneys cultured in 500µM CK666. 192
Figure 5.23 – Mitosis analysis of E12.5 kidneys cultured in 1000µM CK666. ..... 194
Figure 5.24 – Kidney size over 5 days cultured in 100µM, 500µM, and 1000µM CK666. ..... 197
Figure 5.25 – Kidney size over 5days cultured in 50µM BMS5. ..... 198
Figure 5.26 – Light micrographs of E12.5 kidneys cultured in 100µM CK666. ..... 199
Figure 5.27 – Light micrographs of E12.5 kidneys cultured in 500µM CK666. ..... 200
Figure 5.28 – Light micrographs of E12.5 kidneys cultured in 1000µM CK666. ..... 201
Figure 5.29 – Light micrographs of E12.5 kidneys cultured in 50µM BMS5. 202
Figure 5.30 – Six2 in E12.5 kidneys cultured in 100µM, 500µM, and 1000µM CK666. ..... 203
Figure 5.31 – Kidney size after 24 hours cultured in 100µM, 500µM, and 1000µM CK666, followed by 48 hour ‘rescue’. ..... 206
Figure 5.32 – Light micrographs of E12.5 kidneys cultured in 100µM CK666 for 24 hours followed by 48 hour ‘rescue’. ..... 207

Figure 5.33 – Light micrographs of E12.5 kidneys cultured in 500µM CK666 for 24 hours followed by 48 hour ‘rescue’. ..... 208
Figure 5.34 – Light micrographs of E12.5 kidneys cultured in 1000µM CK666 for 24 hours followed by 48 hour ‘rescue’. ..... 209
Figure 5.35 – Kidney size after 24 hours cultured in 50µM BMS5 followed by 48 hour ‘rescue’. ..... 210
Figure 5.36 – Light micrographs of E12.5 kidneys cultured in 50µM BMS5 for 24 hours followed by 48 hour ‘rescue’. ..... 211
Figure 5.37 – Light micrographs of E12.5 kidneys cultured in 1µg/ml MMP9 antibody. ..... 214
Figure 5.38 – Light micrographs of E12.5 kidneys cultured in 5µg/ml MMP9 antibody. ..... 215
Figure 5.39 – Kidney size after 48 hours cultured in 1µg/ml and 5µg/ml MMP9 antibody. ..... 216
Figure 5.40 – Light micrographs of E12.5 kidneys cultured in 1µg/ml MMP9 (Novus) antibody. ..... 217
Figure 5.41 – Light micrographs of E12.5 kidneys cultured in 5µg/ml MMP9 (Novus) antibody. ..... 218

# Table of Tables

Table 4.1 – MTT assay on HK2 sub confluent cells..... 108

Table 4.2 – MTT assay on HK2 confluent cells. ..... 110

# Abbreviations

| | |
|---|---|
| 3T3 | Mouse embryonic fibroblast cells |
| Anova | Analysis of variance |
| APC | Anaphase promoting complex |
| C2C12 cells | Mouse myoblast cells |
| DAPI | 4',6-diamidino-2-phenylindole |
| E | Embryonic day |
| EGF | Epidermal growth factor |
| FBS | Fetal bovine serum |
| FGF | Fibroblast growth factor |
| GDNF | Glial cell derived neurotrophic factor |
| GREM1 | Gremlin 1 |
| HEPG2 cells | Human hepatocellular carcinoma cells |
| HK2 cells | Human proximal tubule cells |
| LIM | Lin-11, Isl-1, and Mec-3 domain |
| LIMK | LIM kinase |
| MM | Metanephric mesenchyme |
| MMP9 | Matrix Metalloproteinase 9 |
| MTT | 3-(4,5-dimethylthiazol-2-yl)-2,5-diphenyltetrazolium bromide |

| | |
|---|---|
| PBS | Phosphate buffered saline |
| PFA | Paraformaldehyde |
| PIP2 | Phosphatidylinositol 4,5-bisphosphate |
| pLIMK1/2 | Phosphorylated LIMK 1 and 2 |
| ROCK | Rho-associated protein kinase |
| SDS | Sodium dodecyl sulfate |
| siRNA | Small interfering RNA |
| SSH | Slingshot protein phosphatase |
| TBS | Tris buffered saline |
| TBS-T | TBS with Tween-20 |
| TUNEL | Terminal deoxynucleotidyl transferase dUTP nick end labeling |
| UB | Ureteric bud |
| WASP | Wiskott–Aldrich syndrome protein |

# Chapter 1: Introduction

## 1.1 – Kidney Development

### 1.1.1 – Introduction

The adult kidney is a highly complex organ with at least 26 different cell types (Al-Awqati and Oliver, 2002) all working together to filter the blood and re-absorb key nutrients. In the mouse the kidney begins to form at embryonic day (E) 10.5 from 2 pieces of tissue in the intermediate mesoderm that interact to create a branched structure terminating with nephrons to filter the blood. Normal development of the kidney is crucial to lifelong health and a lower number of nephrons formed during development has been shown to be a cause of hypertension and renal disease (Hoy et al., 2008).

### 1.1.2 – Induction

The adult mammalian kidney forms from the reciprocal interaction between two tissues; the ureteric bud (UB) and the metanephric mesenchyme (MM). The UB arises from the nephric duct (also termed the Wolffian duct or mesonephric duct) whereas the MM arises from the nephrogenic cord within the intermediate mesoderm. The first stage in kidney development in the mouse is at E8.5 when the nephric duct starts to form, this grows parallel to the nephrogenic cord (Morris et al., 2003). The nephric duct grows down the embryo towards the distal end over the course of 3 days, along this growth there are three embryonic kidneys that will form; the pronephros, mesonephros, and the metanephros (Figure 1.1; Kuure et al., 2000). The

metanephros is the kidney that goes on to form the adult mammalian kidney while the pronephros and mesonephros die off by apoptosis by E14 (Pole et al., 2002). By E10.5 the nephric duct has reached a physical point alongside the nephrogenic cord where the genes are located in for the induction of the UB (Figure 1.1). Glial derived neurotrophic factor (GDNF) is normally inhibited throughout the nephrogenic cord except in the location where the MM is formed (Sainio et al., 1997; Vega et al., 1996; Shakya et al., 2005). GDNF signals to the nephric duct through the RET receptor causing the high RET expressing cells in the nephric duct to migrate and proliferate towards the region with the highest concentration of GDNF (Chi et al., 2009).

In the area of the nephrogenic cord which give rise to the mammalian kidney, the MM, Gremlin 1 (GREM1) inhibits bone morphogenetic protein 4, BMP4, which would normally inhibit GDNF in the rest of the nephrogenic cord (Brophy et al., 2001), thus the expression of GREM1 allows the expression of GDNF (Michos et al., 2004). Pax2 will also act to positively regulate GDNF in the nephrogenic cord (Brophy et al., 2001) and FoxC1 acts to restrict GDNF expression to this location (Kume et al., 2000). Other genes are also involved in the correct localisation of GDNF, SLIT2 and its receptor ROBO2 repress GDNF expression, and it has been shown that mice lacking SLIT2 produce excess ureteric buds (Grieshammer et al., 2004). This shows that GDNF is the key protein that determines UB growth in the correct location. UB outgrowth is also regulated by Wnt signalling. Wnt11 expression is localised to the tip of the UB through RET where it increases GDNF levels. Sprouty1, a Wnt inhibitor, is expressed in the nephric duct where it prevents GDNF from acting on RET by inhibiting the downstream effect of Wnt11 by RET (Basson

et al., 2006). Mice lacking Sprouty1 have multiple ureteric buds (Basson et al., 2005) as they cannot inhibit UB outgrowth to one location.

The precise expression of GDNF causes the RET expressing cells on the nephric duct to form an outgrowth which ‘invades’ the nephrogenic cord, now the termed the MM, it is this outgrowth that forms the UB (Figure 1.2).

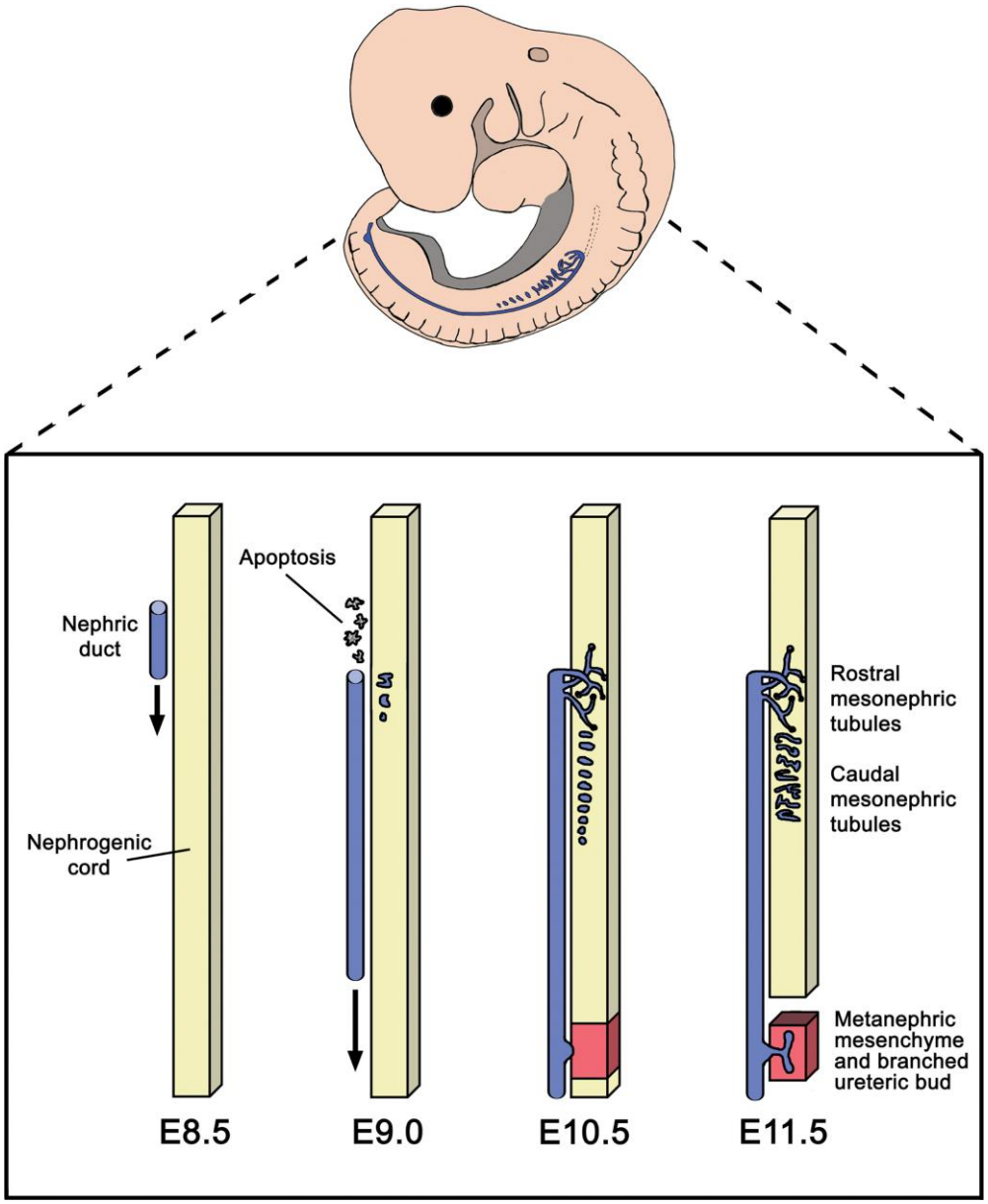



Figure 1.1 – Development of the nephric duct.

The growth of the nephric duct parallel to the nephrogenic cord from E8.5 to E11.5 when the adult kidney begins to form from the reciprocal interacting between the nephric duct and nephrogenic cord. Ret and GDNF are inhibited in other parts of the nephric duct and nephrogenic cord by BMP4 and FoxC1/C2 respectively. Adapted from Davidson (2009).

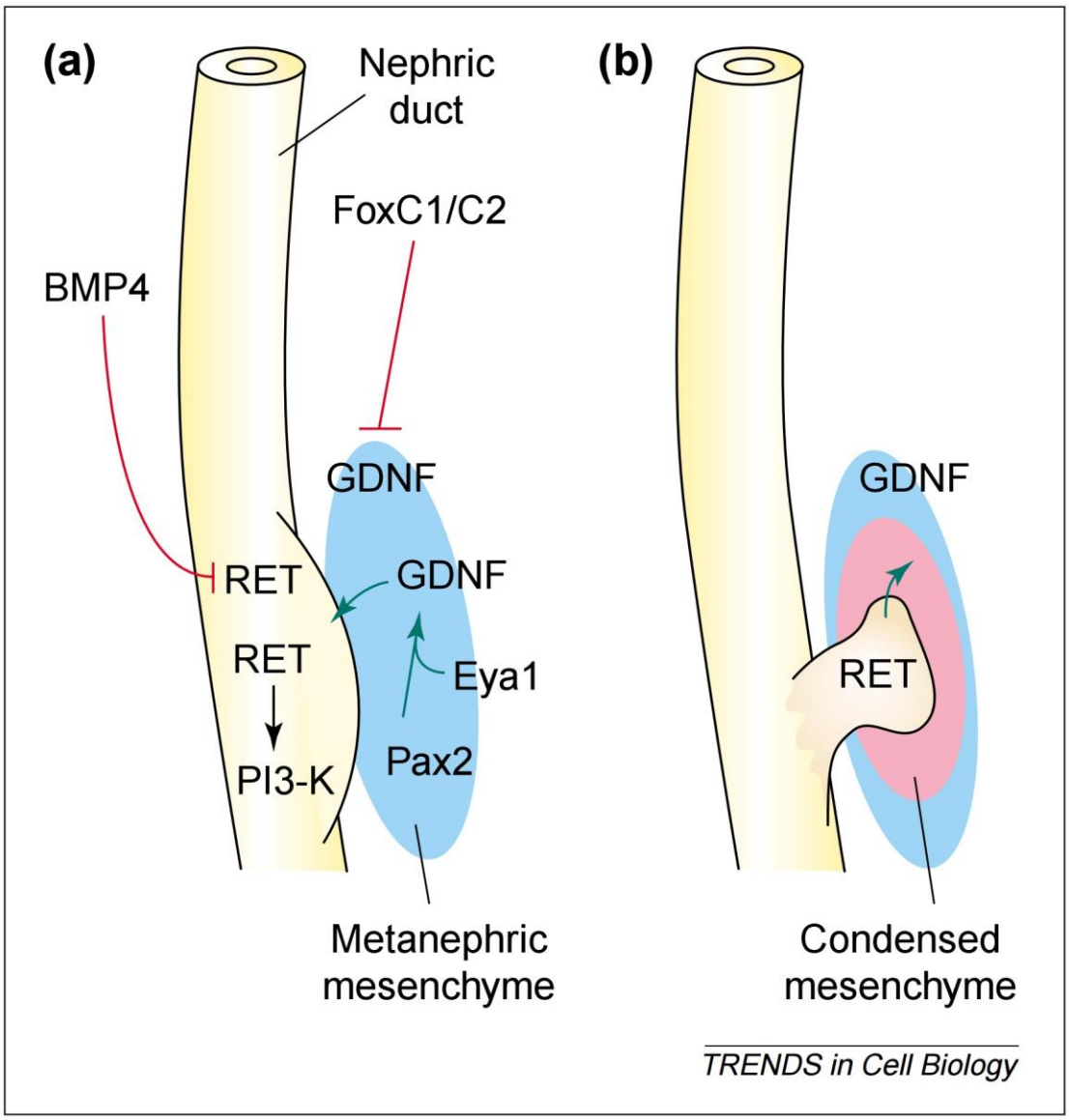



Figure 1.2 – Nephric duct growing into the metanephric mesenchyme.

GDNF acts on Ret expressing cells to induce the outgrowth of the nephric duct (ureteric bud) into the metanephric mesenchyme (nephrogenic cord). From Dressler (2002).

## 1.1.3 – Branching and growth

In the mouse the UB then continues to grow into the MM and branches repeatedly (Srinivas et al., 1999). UB branching is caused by the attraction of

UB tips to local sources of GDNF in the MM, which act on RET expressing cells in the UB (Vega et al., 1996) to increase cell proliferation causing the UB tips to grow towards GDNF (Pepicelli et al., 1997). GDNF is essential for UB branching, as addition of GDNF in organ culture increases UB branching, while adding an antibody against GDNF inhibits this branching (Vega et al., 1996). As the UB grows “mitosis-associated cell dispersal” occurs in the UB tips whereby an epithelial cell delaminates and enters the lumen of the UB where it divides and one daughter cell goes back in the same location, while the other daughter cell inserts 1 to 3 positions away from the original parent cell location (Packard et al., 2013). It is not yet fully known why this occurs but this is a possible method by which rapid cell division can take place the UB tips.

Fibroblast growth factor (FGF) signalling has also been implicated in regulation of UB branching. Mice lacking FGF7 have reduced numbers of nephrons and is also required of UB survival (Qiao et al., 1999). FGF receptor (FGFR) 2, though not FGFR1, is crucial for normal UB branching as mice lacking FGFR2 in the UB have “thin ureteric bud stalks, and fewer ureteric bud tips”, while those lacking FGFR1 in the UB had no renal abnormalities (Zhao et al., 2004). Whereas in mice where both FGFR1 and FGFR2 have been deleted from the MM no GDNF is produced which leads to the failure of the UB to invade the MM (Poladia et al., 2006).

## 1.1.4 – Mesenchyme

The mesenchyme will give rise to all nephron cells (Kobayashi et al., 2008), and is characterised by expression of Six2 by which its premature deletion results in early differentiation into renal vesicles (Self et al., 2006). At the onset of UB branching there are approximately 10,000 Six2+ cells in the mesenchyme that will form the approximately 13,000 nephrons present in the adult mouse kidney. To produce this many nephrons the Six2+ cells need to self-renew, but this self-renewal capacity is lost once the cell begins to form a renal vesicle (Kobayashi et al., 2008). The mesenchyme is surrounded by stromal cells, characterised by expression of Foxd1, these stromal cells go on to form renal interstitial pericytes, vascular smooth muscle cells and mesangial cells in the adult kidney (Humphreys et al., 2010; Sequeira Lopez and Gomez, 2011). Genetic deletion of Foxd1 results in smaller kidneys that have structural deformities (Levinson et al., 2005), thus implying the presence of stromal cells to be required for normal kidney development although the renal stroma has not been studied in as much detail compared to the UB and the MM (Hum et al., 2014).

As the UB branches, pre-tubular aggregates form from the mesenchyme, which give rise to renal vesicles and ultimately nephrons (Figure 1.3). The MM contains two separate populations of cells; the capping mesenchyme and the induced mesenchyme. The capping mesenchyme cells have the gene profile of Six2 positive, Cited1 positive, and Wnt4 negative, which proliferates to expand the nephron progenitor pool. While the induced mesenchyme cells, which form from the capping mesenchyme and are induced to create a pre-tubular aggregate, have the gene profile of Six2 positive, Cited1 negative and

Wnt4 positive (Mugford et al., 2009). It is these cells, $Six2^+$, $Cited1^-$, and $Wnt4^+$ which are now destined to become nephrons.

The nephrons form from the induction of $Six2^+$ cells by Wnt9b which is secreted from the UB tips (Carroll et al., 2005). Wnt9b causes the activation Wnt4 expression via FGF8 (Grieshammer et al., 2005), which in turn is required for the generation of pre-tubular aggregates (Stark et al., 1994). It has been suggested that cells with high levels of Six2 respond to Wnt9b by proliferating and maintaining a pool of nephron progenitors, while cells with lower levels of Six2 expression (those forming a pre-tubular aggregate) respond to the Wnt9b signal by differentiating along the pathway to form a nephron (Karner et al., 2011). Therefore once Wnt4 has been activated by Wnt9b, Wnt9b will now induce the differentiation within these cells. Wnt9b also causes the stabilization of β-catenin (i.e. not phosphorylated and targeted for degradation) which is required for mesenchymal to epithelial transition (Park et al., 2007). Since β-catenin is now not targeted for ubiquitination, it becomes translocated to the nucleus where it binds to the Tcf and Six2 complex and promotes FGF8 and Wnt4 transcription (Park et al., 2012). Six2 will also cause the expression of Osr1 which acts to maintain the mesenchyme in an undifferentiated state by interacting with Tcf proteins. It is this interaction with between Osr1 and Tcf proteins that enables the binding of Groucho proteins which represses transcription (Xu et al., 2014). Groucho and β-catenin compete for binding to Tcf (Roose et al., 1998; Range et al., 2005). It is this increased β-catenin level by Wnt9b which causes the activation of the transcription of the genes required for mesenchymal to epithelial transition, the first stage in nephron development. The mesenchyme

cells need to become epithelia to form tubules that make up the nephron which will later become specified into the bowman's capsule, the proximal tubule, the loop of Henle, and the distal tubule (Herzlinger et al., 1992).

In addition to Wnt9b causing the proliferation of Six2 expressing cells, Six2 itself has also been shown to activate its own promotor in addition to activating GDNF expression (Brodbeck et al., 2004) which enables the continued growth of the UB. The nephron progenitor pool of capping mesenchyme cells continues expanding at an increasingly slower rate (Short et al., 2014) until postnatal day 3 in the mouse by which all the Cited1$^{+}$ cells have been used up (Hartman et al., 2007).

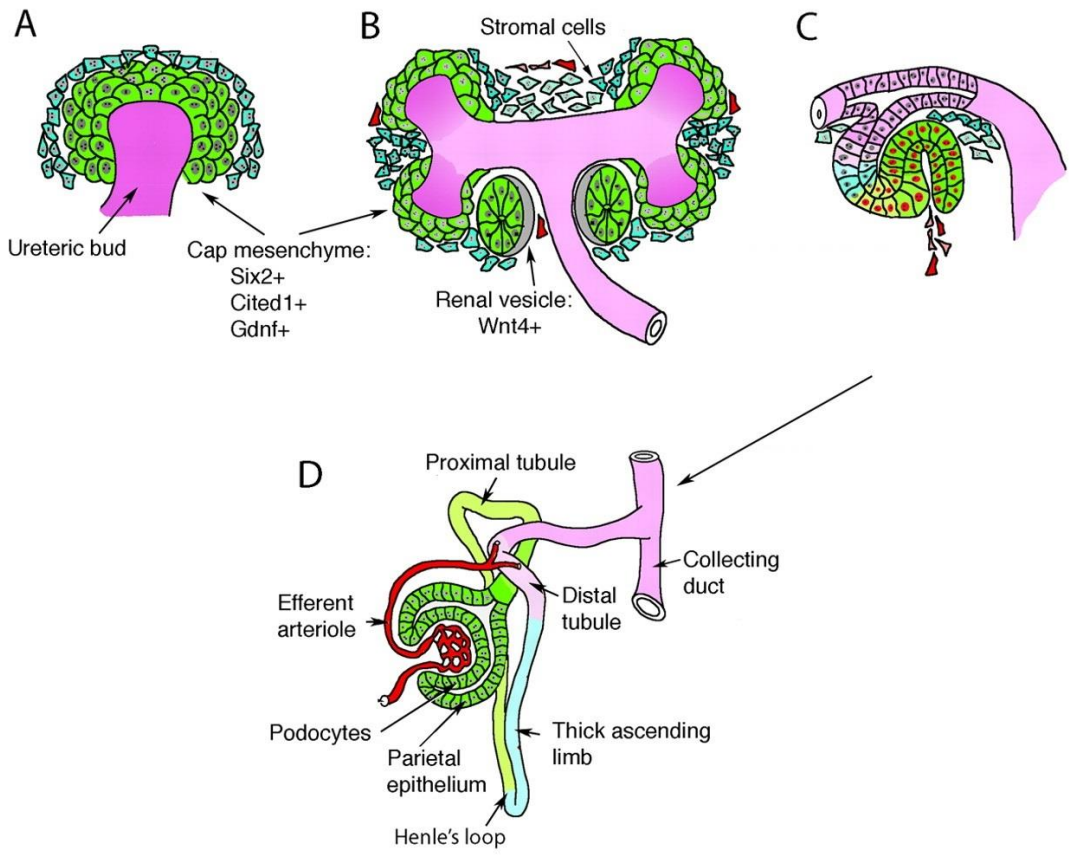



Figure 1.3 – Nephron formation from the metanephric mesenchyme.

The ureteric bud is surrounded by mesenchyme cells (A), which then branches and induces a renal vesicle to form at a branch point (B). The comma and s-shaped bodies will then form from this renal vesicle (C) and elongate to form a nephron (D). From Dressler (2009).

## 1.1.5 – Nephron Formation

The expression of a wide variety of genes are required to enable the patterning of the proximal to distal axis of the nephron from the renal vesicle stage through a comma shaped body and s-shaped body to formation of a full nephron (Figure 1.3). The proximal and medial nephron segments are

characterised by expressing Notch (Cheng et al., 2007) and having low levels of both β-catenin and PI3K (Lindström et al., 2015). Since the distal end has a higher level of β-catenin this creates an increasing gradient of β-catenin from proximal to distal. It is this Wnt mediated Notch signalling that causes the mesenchymal to epithelial transition to form the proximal tubule (Boyle et al., 2011). Wnt4 is itself upstream of Lhx1 (Lim1; Kobayashi et al., 2005) which distinguishes the distal end of the renal vesicle from the proximal end. There is limited knowledge on Lhx1 as Lhx1 knockouts die at E10, before the kidneys start to form (Shawlot and Behringer, 1995). Although it is known that Lhx1 is upstream of both Brn1 and Dll1 (Kobayashi et al., 2005), and Brn1 is known to be crucial for the formation of the loop of Henle and distal convoluted tubule (Nakai et al., 2003). The cells in the proximal end of the nephron will form the bowman's capsule and the proximal tubule, with the medial and distal end forming the loop of henle and distal tubule which connects to the UB, now termed the collecting duct. As mentioned earlier (1.1.4), development does not cease at birth in the mouse, with the nephron progenitor cells only being lost by postnatal day 3 (Hartman et al., 2007). This results in more than 50% of the nephrons being formed after branching has completed (Short et al., 2014). At birth there is no inner medulla (Kim et al., 1996) and significant development occurs after birth with most of the loop of Henle's being formed and elongated (Cha et al., 2001) and large scale cell division still occurring in the early post natal period (Coles et al., 1993). Using the mouse as a model organism it has been show that, postnatally, the size of the kidney increases from 3-4 mm at E19.5 to approximately 9-10 mm by postnatal day 28 (Wu et al., 2013).

## 1.1.6 – LIM kinase in the kidney

Lin-11, Isl1, and Mec-3 (LIM) kinase (LIMK) is an enzyme that phosphorylates Cofilin which in turn depolymerises actin filaments. However there is limited knowledge of what, if any, specific role LIMK might have during kidney development or kidney specific diseases. LIMK1 is present in the MM although no specific role for it has been suggested during kidney development beyond its known roles in actin remodelling (Lindström et al., 2011). Lack of Cofilin (LIMK phosphorylation target) in the UB had no effect on kidney development, however when Cofilin was deleted along with Destrin (another actin depolymerising enzyme, which its deletion had no effect on kidney development) UB branching was inhibited (Kuure et al., 2010). This implies there might be some role for Cofilin in combination with Destrin in UB branching, but no roles have been suggested for LIMK or Cofilin the MM.

It is known to be one of the genes deleted in Williams-Beuron syndrome. Williams-Beuron syndrome is a genetic disorder that is characterised by a 1.5-1.6 megabase deletion in the q11.23 region of chromosome 7 containing between 25 to 30 genes (Francke U, 1999; Bayés et al., 2003). This region includes LIMK1 (Tassabehji et al., 1996). Approximately 18% of patients with Williams-Beuron syndrome have renal abnormalities (Pober et al., 1993; Pankau et al., 1996). Due to the large number (25-30) genes deleted in patients with Williams-Beuron syndrome it is unlikely that only the gene this thesis looks at (LIMK1) would be solely responsible for the renal abnormalities observed, although it might play a role.

# 1.2 – Cell Cycle

## 1.2.1 – Introduction

Cells undergo cell division (mitosis) to create 2 new ‘daughter’ cells, to accomplish this the cell needs to replicate everything in the cell to enable 2 new daughter cells to function. The cell cycle is split into 4 phases; G1, S, G2, and M, the first 3 (G1, S, and G2) are termed interphase while M phase is mitosis where the cell divides.

## 1.2.2 – Interphase

Interphase is where the cell prepares itself for cell division or decides not to undergo cell division and enter a state called G0 (non-dividing). In the G1 phase the cell rapid protein synthesis occurs (Pardee, 1989). Next the DNA gets replicated in S phase ready to be separated during mitosis. A further gap phase (G2) then occurs where the cell becomes ready to pass through the G2/M checkpoint and begin mitosis. The G2/M checkpoint is where the cell can check the DNA that has been replicated is not damaged and therefore ok to continue to undergo cell division (Cuddihy and O'Connell, 2003).

## 1.2.3 – M Phase

Mitosis is the phase of the cell cycle where the chromosomes separate and nuclear division occurs, immediately following mitosis cytoplasmic division occurs (Cytokinesis). The first stage of mitosis is prophase where the chromatin condenses into chromosomes, being held together in pairs joined

at the centromere (Figure 1.4; Beaudouin et al., 2002). Centrosomes were duplicated in S phase and separate early on in prophase (Meraldi and Nigg, 2002). Centrosomes are part of the pericentriolar matrix which, with γ-tubulin act as a nucleator for the mitotic spindle to begin to form (Moritz and Agard, 2001). In Prometaphase the nuclear membrane consisting of lamins breakdown (Gerace and Blobel, 1980) which allow the microtubules of the mitotic spindle to be able to attach to the kinetochores at the centromeres of the chromosomes (Figure 1.4; Salina et al., 2003). The chromosomes will also begin to move towards alignment on the metaphase plate. Once all the chromosomes are attached to the microtubules via the kinetochores and aligned on the metaphase plate this signals to allow the anaphase promoting complex (APC) to be active (once all the kinetochores are attached, the spindle assembly checkpoint) and this triggers the cell to undergo anaphase (Figure 1.4; Minshull et al., 1994; Musacchio and Salmon, 2007). The APC activates Securin which releases Separase which breaks down the cohesin complex (Nasmyth, 2001) which is a ring of 4 proteins (Scc1, Scc3, SMC1 and SMC3) holding the sister chromatids together (Gruber et al., 2003). APC also targets cyclin A and cyclin B for degradation which allows the cell to complete mitosis (Acquaviva and Pines, 2006). Now the cell can undergo anaphase and pull apart the chromosomes, as the chromosomes are pulled apart the kinetochore microtubules attached to them get shorter as the chromosome get closer to the spindle poles (Figure 1.4; Forer and Wilson, 2000). Now the chromosomes have been separated the cell undergoes telophase where the nuclear membrane re-forms and the chromosomes de-condense (Figure 1.4; Schooley et al., 2012). Mitosis is now complete,

nuclear division has finished, and now the cytoplasm will separate during cytokinesis (Figure 1.4). A contractile ring of actin and myosin filaments forms around the plasma membrane which constricts to create a cleavage furrow that will split the cell into 2 new cells (Glotzer, 2005). Once the contractile ring has fully constricted, the plasma membrane needs to be split, this is carried out by a SNARE mediated mechanism of membrane fusion (Low et al., 2003). Now the cell has fully divided into 2 genetically identical ‘daughter’ cells which will now either go on to another cell cycle and divide again or enter the G0 ‘quiescent’ phase (Pardee, 1989).

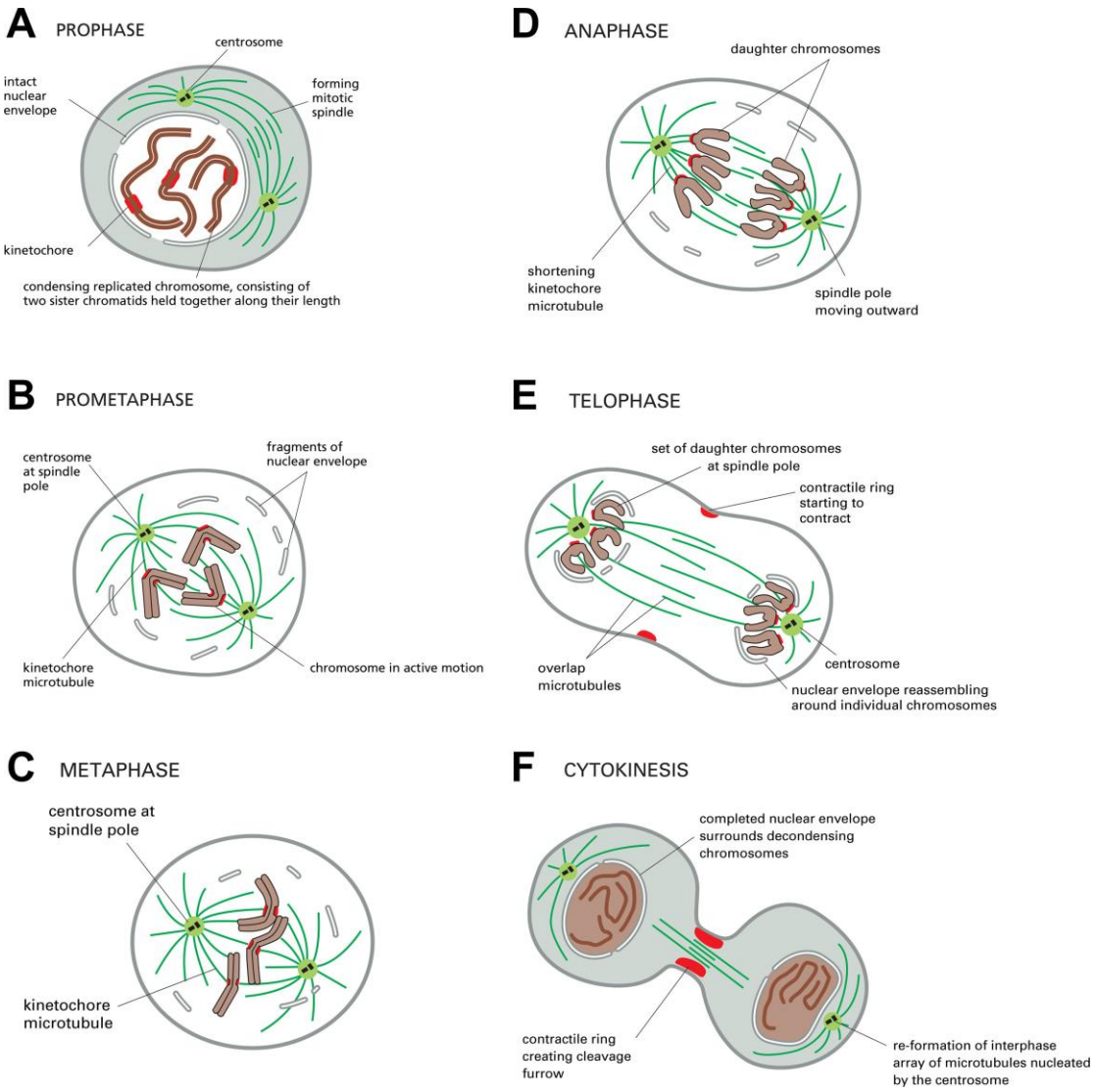



Figure 1.4 – Mitosis.

M phase begins with prophase (A) where the chromosomes condense and the centrosomes move to the poles are the cell. At prometaphase (B) the nuclear membrane (envelope) breaks down and the chromosomes begin to align on the metaphase plate. The mitotic spindles attach to the kinetochores at the centromeres of the chromosomes in metaphase (C). At anaphase (D) the chromosomes are pulled apart and the cytoplasm begins to separate in telophase (E). The cell separates into 2 daughter cells in cytokinesis (F). Adapted from Alberts et al. (2008).

## 1.2.4 – LIM kinase during mitosis

LIMK has been shown to have a role during mitosis, not only by regulating Cofilin and therefore the actin cytoskeleton but also directly. Cofilin needs to be phosphorylated by LIMK during mitosis to enable a stable actin cytoskeleton around the edge of the cell to form and act as a scaffold for the mitotic spindle to orientate correctly (Kaji et al. 2008). LIMK activity was highest during mitosis and low during interphase, which suggest that active LIMK has a crucial role during cell division (Sumi et al., 2002). The phosphorylation state of Cofilin increases from prophase to metaphase then slowly reduces in telophase (Amano et al., 2002), which shows that the activity of LIMK correlates to the phosphorylation state of Cofilin during mitosis.

LIM kinases have been shown to have a role in astral microtubule organization with LIMK2 only, not LIMK1, having a role in regulating astral microtubules and orientation of the mitotic spindle through TPPP (Heng et al., 2012). Although Kaji et al. (2008) stated that it is the phosphorylation state of Cofilin that had a role in the mitotic spindle orientation Heng et al. (2012) argues this role of regulating mitotic spindle orientation via phosphorylation of Cofilin would be through LIMK1 and not LIMK2.

# 1.3 – Cell Migration

## 1.3.1 – Introduction

Cell migration is the process by which cells move and is crucial for development (Weijer, 2009), the immune system (Luster et al., 2005), cancer invasion and metastasis (Friedl et al., 1995; Christiansen and Rajasekaran, 2006), and healing after injury (Krawczyk, 1971). Cells migrate by pushing forward the membrane and the cell moving in this direction.

Cells can migrate by pushing the cell membrane and creating membrane protrusions called lamellipodia, filopodia, invadopodia, and membrane blebs. These four protrusions can all act to enable the cell to move within the tissue, Lamellipodia are protrusions of the cell membrane consisting of actin filaments that push and pull the cell (Ridley et al., 2003), filopodia consist of actin filaments that explore the cell surroundings (Svitkina et al., 2003), invadopodia participate in degrading the extra cellular matrix (Kelly et al., 1994), and membrane blebs push the cell membrane forward with the cytoplasm filling the space enabling the cell to move (Fackler and Grosse, 2008). In most eukaryotic cells cell migration is carried out by the formation of lamellipodia (Bravo-Cordero et al., 2013).

## 1.3.2– Mechanism

Lamellipodia push forward the cell membrane to enable cell migration, they consist of actin filaments which contain pointed (Minus -) and barbed (Plus +) ends; polymerisation occurs at the barbed end where free actin monomers

(G-actin) are added which allows the actin filament to grow (DesMarais et al., 2005). To generate new free actin monomers, actin filaments need to be depolymerised primarily by Cofilin. Cofilin binds to ADP-actin, located at the pointed (-) end of the actin filament, more readily than ATP-actin which is found at the barbed (+) end (growing tip). Cofilin induces a small change in the angular rotation of the ADP-actin which accelerates the dissociation rate, causing depolymerisation (dos Remedios et al., 2003). The actin monomer then binds to profilin which catalyses the ADP to ATP reaction, the actin monomer is then ready to be added to the growing top of the actin filament (Goldschmidt-Clermont et al., 1992). A mechanism to control the length of an actin filament is to 'cap' the growing (barbed) end of the actin filament. This can be done by a capping and severing protein such as gelsolin (Kwiatkowski, 1999), or purely capping the growing end with capping protein (Edwards et al., 2014).

By severing actin filaments, thereby creating new actin monomers which can be utilised for polymerisation, Cofilin also depolymerises old actin filaments which are no longer required by the cell. Cofilin is regulated by phosphorylation on the Serine-3 residue (Agnew et al., 1995) which inhibits the ability of Cofilin to bind to actin filaments (Moriyama et al., 1996).

Cofilin activity is controlled by phosphatases and kinases. Cofilin in its active non-phosphorylated form can be inactivated by phosphorylation by either LIMKs (Arber et al., 1998; Yang et al., 1998; Sumi et al., 1999) or testicular kinases (TESK; Toshima et al., 2001a; Toshima et al., 2001b). Phosphorylated Cofilin can be de-phosphorylated by the phosphatases Slingshot (SSH) and Chronophin (Niwa et al., 2002; Gohla et al., 2005).

LIM Kinases are activated by PAK1, PAK4, and Rho-associated protein kinase 1 (ROCK1) (Edwards et al., 1999; Dan et al., 2001; Ohashi et al., 2000). Cofilin can also be phosphorylated at tyrosine residue Y68 by v-SRC which targets Cofilin for ubiquitination and therefore reduces the amount of Cofilin available for actin depolymerisation and therefore reduces cell migration (Yoo et al., 2010).

To create the branched structure required for lamellipodia formation, new actin filaments need to be nucleated from existing actin filaments. The Arp2/3 complex binds to the actin filament and nucleates the formation of a new actin filament at a 70° angle, thereby creating a branched network of actin filaments (Mullins et al., 1998). The Rho protein, Cdc42, regulates the Arp2/3 complex through the Wiskott-Aldrich syndrome proteins (WASPs) which in turn activates the Arp2/3 complex (Pollard and Borisy, 2003; Machesky and Insall, 1998). Another group of proteins related to WASPs, WAVEs also activate the Arp2/3 complex, however instead of being activated by Cdc42 they are primarily activated by Rac (Miki et al., 1998; Bompard and Caron, 2004).

Another mechanism by which actin dynamics are regulated is by the binding of Cofilin to PtdIns(4,5)P2 (PIP2) located at the plasma membrane thereby inactivating it, when PIP2 is cleaved Cofilin is released and becomes active. Cofilin at the leading edge of a migratory cell is found within the plasma membrane compartment (van Rheenen et al., 2007). This inactivation occurs due to the un-phosphorylated Cofilin binding to PIP2 which is located in the plasma membrane (Yonezawa et al., 1990; Yin and Janmey, 2003). Epidermal growth factor (EGF) binds to the EGF receptor on the plasma membrane and causes Phospholipase C γ to be activated (Mouneimne et al.,

2004), resulting in the cleavage of PIP2 into diacylglycerol and inositol 1,4,5-trisphosphate. The reduction of PIP2 at the plasma membrane causes the activation of Cofilin by releasing its inhibitory complex with PIP2 at the plasma membrane (Song et al., 2006).

For cells to migrate, the extracellular matrix needs to be digested, one of the proteolytic enzymes that carries this out is matrix metalloprotease 9 (MMP9). MMP9 has been shown to be required for migration in breast cancer cells, when these cells are treated with small interfering RNA (siRNA) for LIMK then the ability to migrate is lost and loss of focalized MMP9 immunostaining is observed along with a lack of active MMP9 in the media of treated cells (Scott et al., 2010). MMP9 has also be shown to be required for normal kidney development, as MMP9 deficient mice have a 30% decrease in nephron number, 20% decrease in adult kidney weight, and a 2.5 fold increase in apoptosis (Arnould et al., 2009).

There are multiple pathways that achieve the same goal of moving the cell forwards. Most cell migration requires the formation of lamellipodia and this requires actin turnover, therefore Cofilin and LIMK.

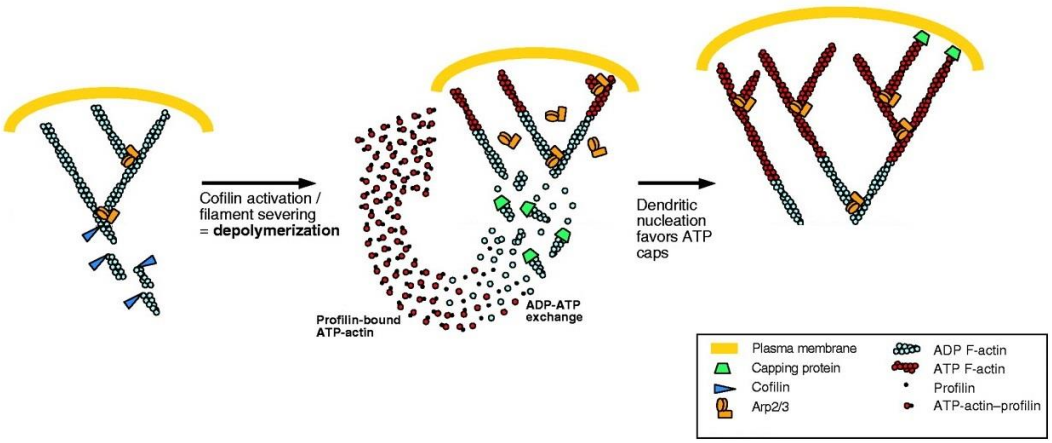



Figure 1.5 – Lamellipodia formation.

Lamellipodia are formed by Cofilin depolymerising actin freeing actin monomers to be added at the growing end of the actin filament. Branch points are created by the Arp2/3 protein nucleating a new actin filament at an angle to an existing actin filament. From DesMarais et al. (2005).

## 1.3.3 – LIM kinase and cell migration

LIMK is a key protein in cell migration as it phosphorylates one of the key actin depolymerising enzymes, Cofilin. It is known that the inhibition of Cofilin by a constitutively active LIMK domain results in the failure to produce lamellipodia and thereby inhibiting cell migration (Zebda et al., 2000). Additionally is has been shown that knockdown of LIMK1 by siRNA inhibits cell migration (Nishita et al., 2005). This shows that targeting LIMK is a useful method to analyse cell migration.

There are several pharmacological inhibitors of LIMK, Damnacanthal and Nischarin are inhibitors of LIMK that are known to have effects on other proteins (Ohashi et al., 2014; Ding et al., 2008). Pyr1 inhibits LIMK (Prudent et

al., 2012), but the only known specific inhibitor of LIMK at the start of this work was N-(5-(1-(2,6-dichlorophenyl)-3-(difluoromethyl)-1H-pyrazol-5-yl)thiazol-2-yl)cyclopropanecarboxamide (compound 3 in Ross-Macdonald et al. (2008)), which is commercially available as BMS5 from SYNkinase in China. BMS5 (also termed LIMKi and BMS3) has been shown to inhibit LIMK and stop cell migration (Scott et al., 2010; Li et al., 2013). Recently more specific inhibitors have been discovered including the specific LIMK2 inhibitor, T-56, which has no activity on LIMK1 (Mashiach-Farkash et al., 2012; Rak et al., 2014).

## 1.4 – Summary, hypothesis and aims

Development of the kidney is a complex process where a large number of cell types are produced, and the complex organization of these cell types need to be controlled. LIMK1 has been shown to be expressed in the developing kidney (Lindström et al., 2011), along with its downstream target, Cofilin (Welham et al., 2005), therefore the hypothesis is that LIMK has a role to play in the development of the kidney. It is known that LIMK is involved in both mitosis (Amano et al., 2002; Sumi et al., 2002; Kaji et al. 2008; Heng et al., 2012) and cell migration via its control over Cofilin phosphorylation (Nishita et al., 2005) and therefore both of these main downstream effects of LIMK are addressed in the context of kidney development.

Our hypothesis is that LIMK plays a crucial role during the development of the kidney through its regulation of mitosis and cell migration.

*Ex-vivo* embryonic mouse kidney cultures were utilised in order to study the development of the kidney. This method (Chan et al., 2010; Barak and Boyle., 2011) has been extensively used previously to look at various aspects of kidney development (Grobstein C., 1953; Gupta et al., 2003; Giuliani et al., 2003) as it is much easier to manipulate the kidney in a tissue culture system (*ex-vivo*) than *in-vivo*. In addition you can use one kidney as a control while using the other contralateral kidney as the treatment kidney thereby having a genetically identical control to compare and therefore the only difference between the kidneys are the treatments or manipulations performed.

The aim of this PhD is to look at what role LIMK has during kidney development using the mouse as a model organism. LIMK will be

pharmacologically inhibited in *ex-vivo* kidney culture and the morphological effects analysed using light micrographs and immunofluorescent. There are two cell processes that LIMK is known to be involved in the regulation of; mitosis and cell migration, both of these will be investigated. This thesis will aim to elucidate what effects the inhibition of LIMK has on mitosis in HK2 cells using immunofluorescent analysis of proteins involved in cell division. This thesis will also look at if cell migration occurs during kidney development and what role cell migration has by immunofluorescently labelling and tracking cells and pharmacologically inhibiting cell migration in *ex-vivo* kidney culture.

# Chapter 2: Materials and Methods

## 2.1 – Tissue culture

### 2.1.1 – Matings

Mice were mated overnight (12.30pm to 9am the following morning) and midday after the vaginal plug was found was considered to be E0.5.

### 2.1.2 – Kidney dissection

On day E12.5, mice were euthanized in accordance with Schedule 1 from the Animals (Scientific Procedures) Act 1986. The embryos were dissected out and kept in Dulbecco's Modified Eagle Medium: Nutrient Mixture F-12 (DMEM/F12) (D8437, Sigma) on ice. The kidneys were dissected from the embryos using 25 gauge needles (NN-2516R 25G x 5/8", Thin Wall Needle, Terumo Medical Corporation, USA) under a dissecting microscope (Olympus Microscope BSZ60, Olympus Microscopy) and light (Schott KL 150B, SCHOTT UK Ltd.) in a laminar flow hood (Barak and Boyle., 2011).

### 2.1.3 – Kidney culture

Kidneys cultured as per Chan et al. (2010). Dissected kidneys were transferred using a 1ml pipette, with the tip cut off, onto 12mm Millicell cell culture inserts (PIHA01250, Merck Millipore, USA) with 0.4µm filters in a 24 well culture plate and 0.5ml media per well was added: DMEM/F12, supplemented with penicillin (100 units/ml) and streptomycin (100µg/ml) (Pen

Strep, Gibco, Life Technologies Ltd), ITS (10mg/l Insulin, 5.5mg/l Transferrin, and 6.7µg/l Sodium Selenite; Gibco, Life Technologies Ltd). Excess liquid from around the kidney on the filter was removed before culturing. Kidneys were grown at 37°C in 5% $CO_2$ in an incubator (RS Biotech Galaxy S+, New Brunswick Scientific, USA). All treatments were sterile filtered before adding to the cells. The following compounds were added to the media as treatments; BMS5 ((N-(5-(1-(2,6-dichlorophenyl)-3-(difluoromethyl)-1H-pyrazol-5-yl)thiazol-2-yl)isobutyramide) SYN-1024, Synkinase, China), CK666 (SML0006, Sigma), Colchicine (C9754, Sigma), Paclitaxel (P3456, Invitrogen, Life Technologies Ltd), Butanol (Butan-1-ol, B/4850/15, Fisher Scientific), FIPI hydrochloride hydrate (F5807, Sigma), Cytochalasin B (228090010, Acros Organics, Fischer Scientific), A23187 (328080050, Acros Organics, Fischer Scientific), and Histamine (411710010, Acros Organics, Fischer Scientific).

All experiments were at least n=3 unless specified.

## 2.1.4 – Micro-Injections

The day after dissection the kidneys were injected in the metanephric mesenchyme using a micro injector (FemtoJet, Eppendorf UK Limited) and a borosilicate glass capillary (GC100TF-15, Harvard Apparatus) pulled out on a P-97 micropipette puller (Sutter Instrument Company, USA) using the following settings; heat = 480, pull = 120, velocity = 200, time = 50. DiI (CellTracker™ CM-DiI, C-7001, Molecular Probes, Life Technologies Ltd) at 1mg/ml in ethanol is diluted 1:1 in 0.3M sucrose in phosphate buffered saline (PBS; Phosphate buffered saline tablets, BPE9739-1, Fisher Scientific). 3 to

5µl of diluted DiI (0.5mg/ml) was loaded into the pulled glass capillary and injected into the metanephric mesenchyme.

## 2.1.5 – Fixing

The kidneys were fixed in 4% Paraformaldehyde (PFA; P/0840/53, Fisher Scientific) in PBS for 20 minutes, on the filters, then washed in PBS twice and stored in PBS at 4°C with the plate wrapped tightly with Parafilm.

## 2.1.6 – Whole mount immunofluorescence

After culture and fixing, kidneys were washed in PBS and transferred to a 0.2ml tube, then washed in PBS and left in 0.2% Triton X-100 (93420, Fluka, Sigma) in PBS overnight at 4°C on a roller (SRT6 Roller mixer, Stuart, Bibby Scientific Limited). The following day the kidneys were washed in PBS three times then the appropriate primary antibody was added, diluted in PBS, and left overnight on a roller at 4°C. The next day the kidneys were washed in PBS three times and the appropriate fluorescent secondary antibody was added at the appropriate concentration, 1 in 100 for anti-mouse Texas red and 1 in 40 for anti-rabbit FITC, in PBS and placed overnight at 4°C on a roller. The next day the kidneys were washed once in PBS then 2µg/ml Hoechst (Bisbenzimide (Hoechst 33258), Sigma) in PBS was added, if not staining with 4',6-diamidino-2-phenylindole (DAPI), for 10 to 15 minutes followed by four washes in PBS (5 PBS washes in total for DAPI staining). The kidneys were then mounted on slides in Citifluor (AF1, Citifluor Ltd),

within two stacked reinforcement washers (330356, 5 Star Office) (to preserve the 3d structure), with a cover slip and sealed with DPX (44581, Sigma) and/or nail varnish, and allowed to dry. Or if staining with DAPI, DPX was added in a ring shape on the slides and allowed to dry (to preserve the 3d structure), then the kidney was transferred into the ring and Vectashield Hardset with DAPI (H1500, Vector Laboratories LTD.) was added a coverslip was added. Vectashield mounted slides were stored at 4°C in the dark for 24 hours then at room temperature in the dark thereafter and Citifluor mounted slides in the dark at room temperature.

Primary Antibodies, all 1 in 100 unless indicated: Calbindin (D-28K) (C9848, Sigma), Laminin (L9393, Sigma), Cytokeratin (CK8) (C2562, Sigma), Total Cofilin (ab42824, AbCam), Phospho-Cofilin (77G2, Cell Signalling Technology), Six2 (11562-1-AP, ProteinTech), pH3 (1 in 500, Histone H3 (phospho S10), ab5176, AbCam), LIMK1 (AP7813a, Abgent.com), LIMK2 (SAB4501760, Sigma).

Fluorescent secondary antibodies: Anti-Mouse IgG, Texas red (T-862, Invitrogen, Life Technologies Ltd), Anti-Rabbit IgG, FITC - F0205 (Dako UK Ltd.).

## 2.1.7 – TUNEL whole mount

After culture and fixing, kidneys were washed in PBS and transferred to a 0.2ml tube, then washed in PBS and left in 0.2% Triton X-100 in PBS overnight at 4°C on a roller. The next day the kidneys were washed in PBS three times and 23.4µg/ml Proteinase K (P4850, Sigma) in PBS was added

for 15 minutes at 37°C, then washed in PBS three times and the anti-Calbindin D-28K primary antibody was added, 1 in 100 in PBS, and left overnight on a roller at 4°C. The next day the kidneys were washed in PBS three times and the terminal deoxynucleotidyl transferase dUTP nick end labeling (TUNEL) reaction mixture was added for 1 hour at 37°C. (TUNEL - In Situ Cell Death Detection Kit, Fluorescein. Cat. No. 11 684 795 910, Roche Diagnostics Ltd.) The anti-mouse Texas red fluorescent secondary antibody was added at 1 in 100 in PBS and placed overnight at 4°C on a roller. The next day the kidneys were washed once in PBS then 2µg/ml Hoechst was added for 10 to 15 minutes followed by four washes in PBS. The kidneys were then mounted on slides in Citifluor, within two stacked reinforcement washers (to preserve the 3d structure), with a cover slip and sealed with DPX and/or nail varnish, and allowed to dry. The slides were stored in the dark.

## 2.1.8 – Cell number assay

Kidneys after treatment were individually dissociated in 0.25% trypsin/EDTA (25200-072, Gibco, Life Technologies Ltd) for 8 minutes at 37°C, then pipetted up and down repeatedly until no clumps of cells were visible then the same volume of 10% fetal bovine serum (FBS; 10500-064, Gibco, Life Technologies Ltd) in PBS (Sterile filtered) was added to stop the trypsin reaction. 10µl of this was taken and cells were counted on a haemocytometer (Paul Marienfeld GmbH & Co. KG, Germany) on an inverted microscope (Olympus CK2 inverted microscope, Olympus Microscopy), using a cell counter. The number of cells was calculated by taking the average of the

number of cells in the 4 large corner squares on the haemocytometer and multiplying by 10,000 to get cell number per ml, then dividing to get the number of cells present in the sample), the cell count was repeated with another 10µl sample. Blanks were run in parallel using the same amount of 0.25% trypsin/EDTA and 10% FBS in PBS for the same time, and these were counted on the haemocytometer as well to ensure no cells were present in the blanks.

## 2.1.9 – Mitotic number and anaphase quantification

After culture and fixing, kidneys were whole mount immunofluorescently labelled with a phosphorylated Histone H3 (pH3) antibody (2.1.6). Images were acquired of random non-overlapping regions per kidney at 20x magnification (5 for BMS5, 4 for Colchicine and Paclitaxel, and 3 regions for Cytochalasin B due to the treatments causing these organs to be smaller, all the controls used the same number of regions as the treatment in each case). Numbers of pH3 labelled cells were counted, anaphase nuclei were determined by a clear separation of pH3 labelled chromosomes.

## 2.1.10 – Western blot

Kidneys, cultured with and without BMS5, were snap frozen in liquid nitrogen and stored at -80°C. Kidneys were thawed, loading buffer added, and samples boiled for 5 minutes. A protein assay was performed (2d Quant kit, GE Healthcare) and 20µg protein loaded per lane along with a protein ladder

(P7710s, New England Biolabs) in a separate lane and run on a 10% acrylamide gel at 200mV until the first band (10kDa) of ladder reached the bottom of the gel. The proteins were then transferred from the gel onto a nitrocellulose membrane (Hybond-C Extra, RPN203E, GE Healthcare) at 200mA for 2 hours in western blotting transfer buffer. The membrane was washed in tris-buffered saline (TBS) with 0.1% Tween-20 (TBS-T) and blocked in 2% Marvel dried skimmed milk powder (Marvel) in TBS-T. Primary antibodies were diluted in 2% Marvell in TBS-T at 1 in 1000 and left incubating the membrane overnight at 4°C on a roller. The next day the membrane were washed in TBS-T and the HRP conjugated secondary antibodies were added at 1 in 5000 in 2% Marvell in TBS-T and left for 1 hour, rocking at room temperature. The membrane was washed in TBS-T and the ECL plus mix (RPN2132, GE Healthcare) was added for 2 minutes, liquid was tapped off and the membrane placed onto the cassette and developed on to Amersham Hyperfilm ECL (GE Healthcare).

Primary Antibodies: Cofilin (ab42824, AbCam), Phospho Cofilin1 Ser-3 (77G2, Cell Signalling Technology, New England Biolabs (UK) Ltd.).

Secondary Antibody: Rabbit IgG HRP-linked antibody (NA934V, GE Healthcare).

The following standard solutions were used:

Loading buffer – 2ml Glycerol, 1.25ml 1M Tris-HCL pH 6.8, 4ml 10% (w/v) sodium dodecyl sulfate (SDS), 1ml 1M Dithiothreitol (DTT; 0.154g/ml), 1 - 5mg Bromophenol blue, and made up to 10ml with distilled water.

10% acrylamide main gel – 3.33ml Acrylamide, 1.88ml 2M Tris-HCL pH 8.8, 0.1ml 10% SDS, 4.6ml water, 80µl 10% AMPS, 8µl Tetramethylethylenediamine (TEMED).

Gel stack – 0.85ml Acrylamide, 0.63ml 1M Tris-HCL pH 6.8, 50µl 10% SDS, 3.4ml water, 80µl 10% AMPS, 8µl Tetramethylethylenediamine (TEMED).

Western blotting transfer buffer – 60g Gylcine, 6g Tris, 100ml Isopropanol, made up to 2000ml with distilled water.

10 X TBS – 72g NaCl, 160ml 1M Tris pH 7.5, made up to 1000ml with distilled water.

TBS-T – 200ml 10 X TBS, 1800ml distilled water, 2ml Tween-20.

## 2.1.11 – Kidney area measurements

Microscope images were taken every 24 hours in culture and images opened in Image J (NIH), the polygon selection tool was used to draw around the kidney. This area was measured and expressed as a percentage of the time 0 value.

## 2.2 – Cell culture

All cell culture work was carried out using sterile techniques inside an ESCO Class II BSC.

### 2.2.1 – Human proximal tubule cells (HK2 cells)

Human proximal tubule cells (HK2 cells) were thawed from storage in liquid nitrogen up to 37°C, and transferred to a T25 cell culture flask and 10ml of media was added and grown in an incubator at 37°C in 5% $CO_2$. Once they had grown sufficiently to be split, they were subcultured into a T75 cell culture flask as below and cultured.

HK2 cells were maintained in T75 cell culture flasks at 37°C in 5% $CO_2$ in an incubator. The cells were maintained in Dulbecco's Modified Eagle's Medium – high glucose with 4500mg/L glucose, sodium pyruvate, and sodium bicarbonate, without L-glutamine (D6546, Sigma). Supplemented with penicillin (100 units/ml) and streptomycin (100µg/ml) (Pen Strep, Gibco, Life Technologies Ltd) 10% FBS, and 2mM L-glutamine (25030-024, Gibco, Life Technologies Ltd). All sterile filtered into the media, using 0.2µm syringe filters (Minisart® NML Syringe Filters 16534----------K, Sartorius Mechatronics UK Ltd.).

The media was changed every 48 hours and the cells were subcultured approximately every 4 days or as necessary (before 90% confluence is reached) by washing in sterile PBS then adding 0.25% trypsin/EDTA for 30 seconds at 37°C in 5% $CO_2$ in an incubator, followed by using media

containing 10% FBS to quench the trypsin activity (4:1 Media containing 10% FBS: trypsin/EDTA). Cells were then spun at 1000 RPM for 5 minutes in a centrifuge (5702 R - Eppendorf UK Limited) and the supernatant discarded, the resulting pellet was re-suspended in media, and then diluted approximately 1 in 10 into fresh media in a new T75 flask.

All treatments were sterile filtered before adding to the cells. The following compounds were added to the media as treatments; BMS5 ((N-(5-(1-(2,6-dichlorophenyl)-3-(difluoromethyl)-1H-pyrazol-5-yl)thiazol-2-yl)isobutyramide) SYN-1024, Synkinase, China), CK666 (SML0006, Sigma), Paclitaxel (P3456, Invitrogen, Life Technologies Ltd), Cytochalasin B (228090010, Acros Organics, Fischer Scientific), A23187 (328080050, Acros Organics, Fischer Scientific), and Histamine (411710010, Acros Organics, Fischer Scientific).

### 2.2.2 – Mouse myoblast cells (C2C12 cells)

Mouse myoblast cells (C2C12 cells) were cultured the same and with the same media as HK2 cells (2.2.1). BMS5 was also added to the media as a treatment.

### 2.2.3 – Human hepatocellular carcinoma cells (HEPG2 cells)

Human hepatocellular carcinoma cells (HEPG2 cells) were cultured the same and with the same media as HK2 cells (2.2.1). BMS5 was also added to the media as a treatment.

## 2.2.4 – Mouse embryonic fibroblast cells (3T3 cells)

Mouse embryonic fibroblast cells (3T3 cells) were cultured the same as HK2 cells (2.2.1). BMS5 was also added to the media as a treatment.

## 2.2.5 – Wound healing assay

Cells were seeded and grown on 16mm circular coverslips (12313138 - Cover slip No. 1 circle 16mm diameter, Fisherbrand, Fisher Scientific) at 37°C in 5% $CO_2$ in an incubator until confluence. The tip of a p1000 pipette tip was used to create a 'wound' cell free area across the middle of the coverslip, the cells were washed in media and incubated in either control media or treatment media at 37°C in 5% $CO_2$ in an incubator. The cell 'wound' was imaged on an inverted microscope at the start of treatment and 24 hours later and the gap measured, using a mark made by a marker pen on the underside of the 12 well plate to identify the region imaged. The gap was measured at 3 points equal distance from each other evenly spaced in the field of view, then averaged and converted into micrometres.

## 2.2.6 – Cell number assay

Cells were seeded on to 12 well plates and left to attach to the plates overnight then control or treatment media was added and grown at 37°C in 5% $CO_2$ in an incubator. At the appropriate time point the media was removed and 0.25% trypsin/EDTA was added to the wells, to detach the cells from the

surface of the 12 well plate, for 4 minutes at 37°C and media containing 10% FBS was added to quench the trypsin activity. 10µl of this was taken and cells were counted on a haemocytometer on an inverted microscope (Olympus CK2 inverted microscope, Olympus Microscopy), using a cell counter. The number of cells in each well was calculated by taking the average of the number of cells in the 4 large corner squares on the haemocytometer and multiplying by 10,000 to get cell number per ml, then divided to get the number of cells per well, the cell count was repeated with another 10µl sample. Blanks were run in parallel using the same amount of 0.25% Trypsin/EDTA and media for the same time, and these were counted on the haemocytometer as well to ensure no cells were present in the blanks.

## 2.2.7 – Trypan blue assay

Cells were seeded onto 12 well plates and left to attach to the plates overnight, then control or treatment media was added to the wells and grown for 24 hours at 37°C in 5% $CO_2$ in an incubator. The cells were washed in sterile PBS and 0.2% Trypan blue (Trypan Blue solution, T8154, Sigma) in media was then added for 5 minutes at 37°C. Images were taken on an inverted microscope and the percentage of cells that took up the dye was calculated. Cells that took up the dye are non-viable (dead) as their cell membrane is no longer intact.

## 2.2.8 – MTT assay

Cells were grown in 96 well cell culture plates until 60% confluence or 100% confluence, the treatment media was then added for 24 hours. The following protocol and reagents are from the Molecular Probes Vybrant MTT Cell Proliferation Assay Kit (V13154, Molecular Probes, Life Technologies Ltd): The media was removed and 100µl fresh media without phenol red (21063-029, Gibco, Life Technologies Ltd.) was added to each well, then 10µl of 12mM 3-(4,5-dimethylthiazol-2-yl)-2,5-diphenyltetrazolium bromide (MTT) was added to each well and left at 37°C in 5% $CO_2$ in an incubator for 4 hours. A negative control of media and MTT alone was also performed. After 4 hours 85µl was removed from each well and 50µl DMSO (Dimethyl sulfoxide, 154938, Sigma) was added per well, mixed with a pipette and left for 10 minutes at 37°C in 5% $CO_2$ in an incubator. Mixed again with a pipette and the plate was then read on a spectrophotometer at 550nm. Each treatment had 3 wells per plate which were averaged and repeated on 3 plates for an n=3.

## 2.2.9 – Fixing

All cells were fixed in 4% PFA in PBS for 15 minutes at room temperature. Washed with PBS twice and stored in PBS in the cell culture plates wrapped tightly with Parafilm at 4°C.

## 2.2.10 – Immunofluorescence

Cells grown and treated on 16mm circular coverslips were washed in PBS three times, and then fixed in 4% PFA (2.2.9). Washed in PBS three times, then permeabilised with 0.1% Triton X-100 in PBS for 15 minutes. Washed in PBS three times then the appropriate primary antibodies were added diluted in PBS) and left overnight at room temperature. The cells were washed three times in PBS and the appropriate secondary antibodies were added, along with a fluorescently tagged Phalloidin if needed, diluted in PBS and left for 1 hour at room temperature in a dark box. The cells were then washed four times in PBS and mounted on slides in Vectashield Hardset with DAPI. The slides were stored at 4°C in the dark for 24 hours then at room temperature in the dark thereafter.

Primary antibodies, 1 in 100 unless indicated: Alpha Tubulin (T9026, Sigma), Cofilin (ab42824, AbCam), Phospho Cofilin1 Ser-3 (77G2, Cell Signalling Technology, New England Biolabs (UK) Ltd.), pH3 (1 in 500, Histone H3 (phospho S10), ab5176, AbCam), Pericentrin (ab4448, Abcam), Lamin A (ab26300, Abcam), Securin (ab3305, Abcam), SMC3 (ab9263, Abcam), Vimentin (D21H3, 9854, Cell Signalling Tech), LIMK1 (AP7813a, Abgent.com), LIMK2 (SAB4501760, Sigma), TESK1 (D49D4, 4655, Cell Signalling Tech), TESK2 (GTX103902 (N2C3), GeneTex).

Secondary antibodies, 1 in 100: Anti-Rabbit IgG, FITC - F0205 (Dako UK Ltd), Anti-Mouse IgG, Texas red (T-862, Invitrogen, Life Technologies Ltd).

Phalloidins, 1 in 40: Phalloidin 555 (A34055, Invitrogen, Life Technologies Ltd).

## 2.2.11 – Mitotic number and anaphase quantification

Cells were grown on 16mm circular coverslips with and without treatment media, fixed (2.2.9) and immunofluorescently labelled with a phosphorylated Histone H3 (pH3) antibody (2.2.10). Images were acquired of 4 random non-overlapping regions per coverslip at 5x magnification on a fluorescent microscope. Numbers of pH3 labelled cells were counted, and anaphase nuclei were determined by a clear separation of pH3 labelled chromosomes.

## 2.3 – Imaging

### 2.3.1 – Kidney culture light and DiI images

Light and fluorescent images were taken on an inverted microscope (Leica DMIL, Leica DFC-420c camera and LAS v.3.2 software, Leica Microsystems (UK) Ltd). DiI images were overlaid onto the light image using GIMP software using layers and setting the opacity at 50% for the DiI layer.

### 2.3.2 – Live kidney confocal time-lapse imaging

One E12.5 kidney was cultured (2.1.3) and injected with DiI (2.1.4), then imaged on a LSM 710 laser scanning microscope/Axio Observer (Carl Zeiss Ltd., UK) with a C-Apochromat 10x/0.3 W M27 lens taking a 19 section Z-stack (total image size; x = 849.36µm, y = 849.36µm, z = 165.63µm, each Z plane is 9.2µm) every 30 minutes for 16 hours on an incubated stage (37°C) with humidified 5% $CO_2$ then fixed (2.1.5). The excitation laser was set at 561nm, 1.0%, and the filters set between 566nm to 685nm. LSM files were processed with Zen 2012 software (Carl Zeiss Ltd., UK) into TIFF and AVI files. Light/fluorescent overlaid images were also acquired at the start and end of the time lapse. The microscope/time lapse was set up with help from Tim Self (School of Life Sciences, University of Nottingham).

### 2.3.3 – Whole mount IF and TUNEL images

Images were taken on a fluorescent microscope (Leica DM5000 B microscope, Leica DFC420 camera and LAS v.3.8 software, Leica

Microsystems (UK) Ltd). Overlays were created with the Leica V3.8 software for triple red, green, and blue overlays. Overlays of 2 colours were created using Image J (NIH, USA).

### 2.3.4 – Cell culture images

Light images were taken on an inverted microscope (Leica DMIL, Leica DFC-420c camera and LAS v.3.2 software, Leica Microsystems (UK) Ltd).

### 2.3.5 – Cell culture immunofluorescence images

Images were taken on a fluorescent microscope (Leica DM5000 B microscope, Leica DFC420 camera and LAS v.3.8 software). Overlays were created with the Leica V3.8 software for triple red, green, and blue overlays. Overlays of 2 colours were created using Image J (NIH, USA). All cell culture immunofluorescence images are n=3 unless specified.

## 2.4 – Statistics

All experiments were repeated 3 times (n=3) unless otherwise stated and ± values are standard error of the means (standard deviation divided by the square root of the number of samples). For embryonic kidney culture experiments, one embryo per biological replicate was used, using 1 kidney as the control and the contralateral kidney as the treatment culture, each biological replicate was from a different litter. Cell line experiments were repeated on separate cell culture plates.

For experiments with control and only 1 treatment group, p values were obtained using two-tailed T-tests (two sample assuming equal variance) compared to the control for each experiment. One-way analysis of variance (ANOVA) with Tukey post-hoc analyses were performed for experiments with more than 1 treatment group and two-way ANOVAs with Tukey post-hoc analyses for more than 1 treatment group over multiple days. Statistical significance was considered to be $p<0.05$, T-tests were performed in Microsoft Excel, and One-way and two-way ANOVAs were performed in GraphPad Prism.

# Chapter 3: The effect of LIMK inhibition during kidney development.

## 3.1 – Introduction

LIMK1 and its target Cofilin are both expressed in the developing kidney (Lindström et al., 2011; Welham et al., 2005). The expression of LIMK1 localised to the MM is interesting and would suggest that LIMK might have a specific role in these cells. LIMK phosphorylates Cofilin which is also expressed, this suggests that LIMK's role in these cells would be mediated by phosphorylating Cofilin.

LIMK and Cofilin are involved in a variety of cell processes including mitosis (Kaji et al. 2008) and cell migration (Scott et al., 2010), both of which will be examined in chapters 4 and 5. The role of LIMK during kidney development is unknown and one or both (mitosis and cell migration) of these processes might be crucial for normal kidney development. The Six2 expressing MM is a highly proliferative cell population (Self et al., 2006; Kobayashi et al., 2008), and as such regulation and progression through mitosis is key. LIMK and Cofilin are involved in mitosis in a number of cell types so it would be logical that LIMK and Cofilin might be involved in the regulation and/or the progression through mitosis in Six2 cells. A LIMK1/2 double knockout mouse has been produced (Meng et al., 2004) although it has no renal abnormalities. The group never looked for any renal abnormalities as this was a neurological study and the effectiveness of the knockout has been questioned (Bernard, 2007). Bernard, 2007 suggested that, because only a small region of the

protein sequence was deleted, a protein with kinase activity might still be produced.

A method to overcome this issue would be to use a pharmacological inhibitor of either LIMK or an upstream activator of LIMK. The ROCK inhibitor, y27632, has been used in embryonic kidney culture and although this produced a significant increase in growth (Meyer et al., 2006), there are other pathways affected by ROCK. The ROCK inhibitor will cause the loss of phosphorylated (active) LIMK and phosphorylated Cofilin (Song et al., 2006), but ROCK also acts on a number of proteins in addition to LIMK including; myosin light chain (Amano et al., 1996) and the myosin-binding subunit (Kawano et al., 1999), thus showing the need to use a more specific inhibitor in order to study LIMK in kidney development.

To examine the role of LIMK in kidney development mice were mated and embryos collected at E12.5, the kidneys were dissected out and cultured on filters. This enabled the kidneys to be cultured in a specific small molecule pharmacological inhibitor of LIMK, N-(5-(1-(2,6-dichlorophenyl)-3-(difluoromethyl)-1H-pyrazol-5-yl)thiazol-2- yl)cyclopropanecarboxamide (compound 3 in Ross-Macdonald et al. (2008), which is commercially available as BMS5 from SYNkinase, China). There have been no off-target effects by BMS5 shown to occur in living cells (Ross-Macdonald et al., 2008). The appearance and size of kidneys was analysed after 24 and 48 hours in culture in BMS5, and BMS5 effects on the MM and mitosis was analysed using whole mount immunofluorescence techniques with antibodies against the metanephric mesenchyme marker Six2 and mitosis marker pH3.

LIMK phosphorylates Cofilin therefore any inhibition of LIMK will result in a decrease in the amount of phosphorylated Cofilin. To specifically attribute any effect seen with LIMK inhibition to its effects on Cofilin phosphorylation will require looking at other methods to decrease the amount of phosphorylated Cofilin such as using A23187 or Histamine (Wang et al., 2005).

Phosphorylated Cofilin is also involved in activating the PLD1 pathway, therefore this pathway downstream of LIMK was investigated to see if it is responsible for the effects seen with LIMK inhibition. PLD1 can be inhibited by FIPI (Su et al., 2009) and Butanol (Skippen et al., 2002).

## 3.2 – Results

### 3.2.1 – BMS5 inhibits LIMK activity

Using whole mount immunofluorescence LIMK1, LIMK2, and the active form of these, phosphorylated LIMK 1/2 (pLIMK1/2; the antibody detects both pLIMK1 and pLIMK2), were shown to be present in cultured kidneys (Figure 3.1, n=3). Initially kidneys were cultured in 10μM BMS5, as this had previously been shown to inhibit LIMK activity in cell culture (Scott et al., 2010), however at this concentration whole mount immunostaining still showed the presence of phosphorylated Cofilin in both the UB and MM (Figure 3.2 arrows, n=1). Consequently the efficacy of increasing the concentration of BMS5 to 50μM was assessed, this showed partial loss of phosphorylated Cofilin by 24 hours (Figure 3.3, n=3) and complete loss in the MM by 48 hours (Figure 3.4, n=3), while total-Cofilin was unaffected. Western blotting showed a band for phosphorylated and total Cofilin at approximately 19kDa. Phosphorylation of Cofilin was diminished in kidneys cultured in 50μM BMS5 for 48 hours, similarly total Cofilin was unaffected (Figure 3.5, 3 separately cultured contralateral pairs of kidneys pooled). A loading control was performed using β-actin, showing no difference between the control and treated kidneys.

Previous work has shown that kidney explants cultured in concentrations of both 5μM and 50μM Y27632 (ROCK inhibitor) were still able to grow (Meyer et al., 2006) although in cell culture 10μM is generally used (Coleman et al., 2001; Watanabe et al., 2007; Zhang et al., 2011), therefore a 5 times increase for *ex-vivo* kidney culture compared to the concentration used in cell culture has been shown to be appropriate. In cell culture the cells are covered by,

and therefore the cells are in contact with, a large volume of the media whereas in organ culture the cells are not in direct contact with the media (through a filter) and therefore a higher concentration is needed to penetrate the tissue.

Instead of using a pharmacological inhibitor siRNA molecules could be used to target LIMK though there is the problem of siRNA molecules penetrating the organ, as has been shown by Lee et al. (2008), where fluorescently labelled siRNA was shown to only penetrate the periphery of the kidney in culture, thus siRNA penetrates mesenchyme better than the epithelial tissue which is generally deeper in the organ (Lee et al., 2008).

In cell culture the LIMK inhibitor BMS5 has been used at 10µM (Scott et al., 2010) and 25µM (Prudent et al., 2012). It was shown that 10µM in organ culture for 24 hours had no effect on phosphorylated Cofilin (Figure 3.2), therefore it was decided to use a higher concentration of LIMK inhibitor, 50µM. Later in this thesis, BMS5 is shown to be non-toxic to non-dividing cells (4.2.2).

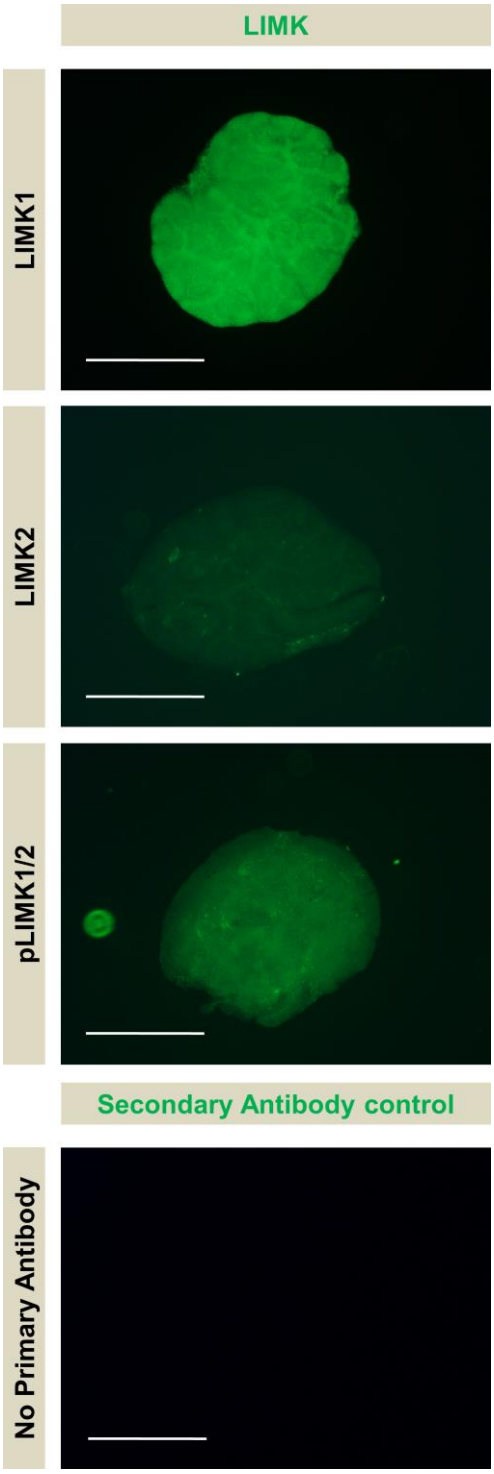



Figure 3.1 – LIMK1, LIMK2 and pLIMK1/2 in E12.5 cultured kidneys.

E12.5 kidneys cultured for 24 hours, fixed and whole mount immunofluorescently labelled with LIMK1, LIMK2 or pLIMK1/2 antibodies (green). Showing the presence of LIMK1, LIMK2 and pLIMK1/2 in cultured

kidneys. Control (bottom image) labelling with the secondary antibody only (no primary antibody) showing no unspecific staining. Scale bars = 400µm. N=3.

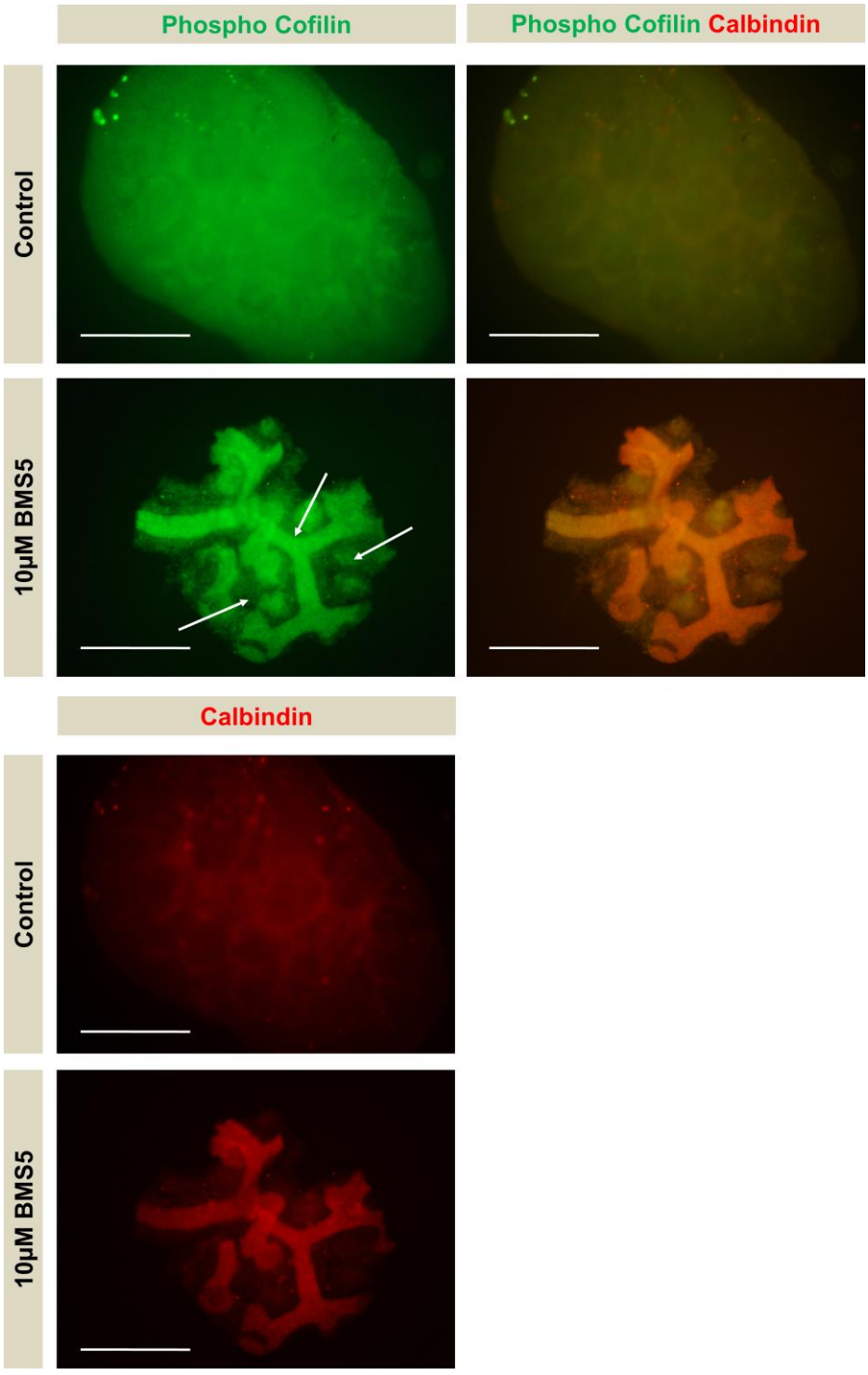



Figure 3.2 – Phosphorylated Cofilin in E11.5 kidneys cultured in 10µM BMS5.

E11.5 kidneys cultured in 10µM BMS5 for 24 hours, fixed and whole mount immunofluorescently labelled with phosphorylated Cofilin (green), and Calbindin (red, labelling the ureteric tree), arrows show phosphorylated Cofilin

is present in the metanephric mesenchyme in kidneys cultured in 10µM BMS5 for 24 hours. Scale bars = 200µm.

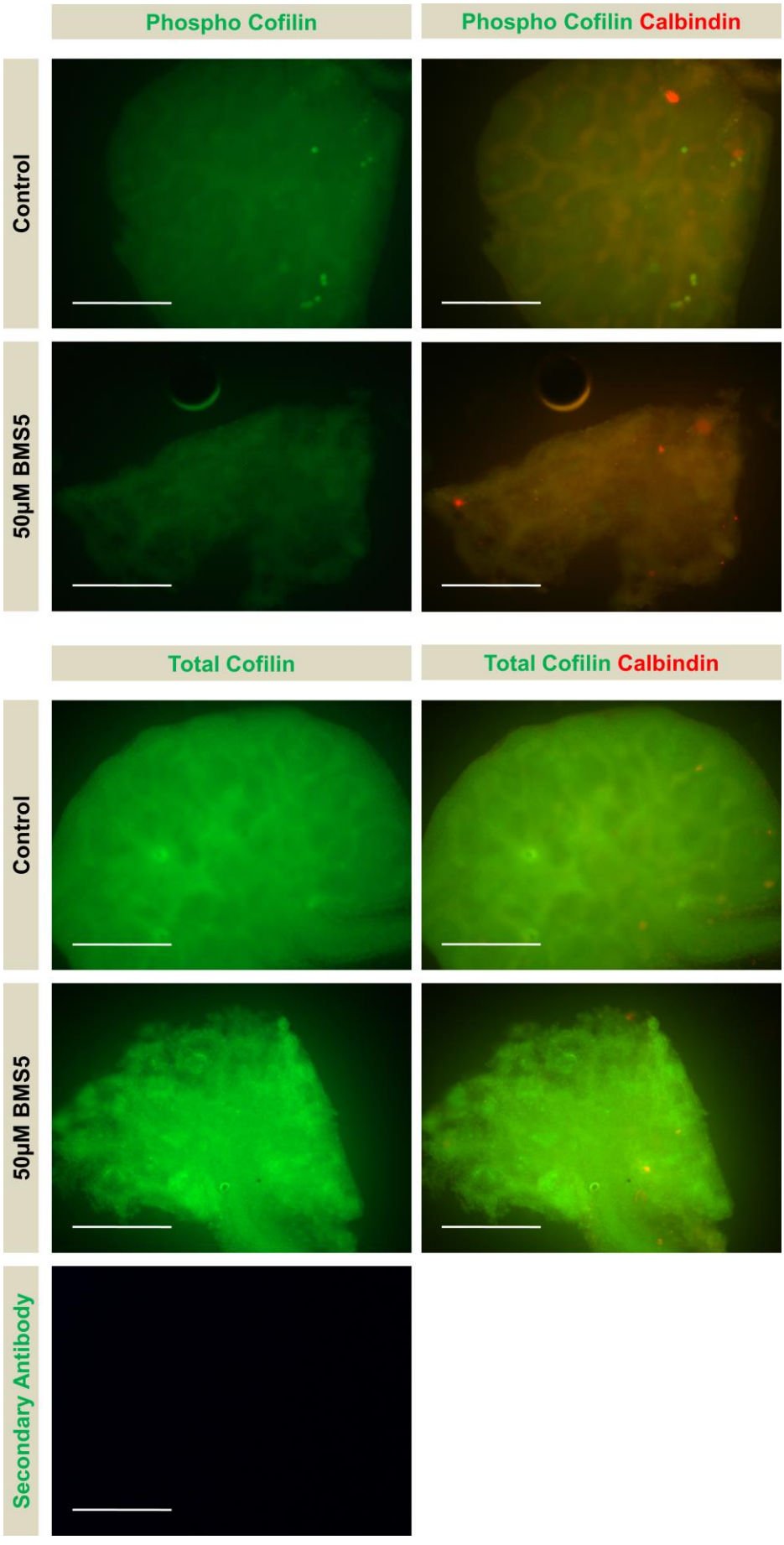

Phospho Cofilin
Phospho Cofilin Calbindin
Control
50µM BMS5
Total Cofilin
Total Cofilin Calbindin
Control
50µM BMS5
Secondary Antibody

Figure 3.3 – Phosphorylated Cofilin in E12.5 kidneys cultured in 50µM BMS5 (24 hours).

E12.5 kidneys cultured in 50µM BMS5 for 24 hours, fixed and whole mount immunofluorescently labelled with phosphorylated Cofilin (green), and Calbindin (red, labelling the ureteric tree). Showing phosphorylated Cofilin reduced to a small amount in BMS5 treated kidneys while total Cofilin remains the same in both control and treated. Scale bars = 200µm. N=3.

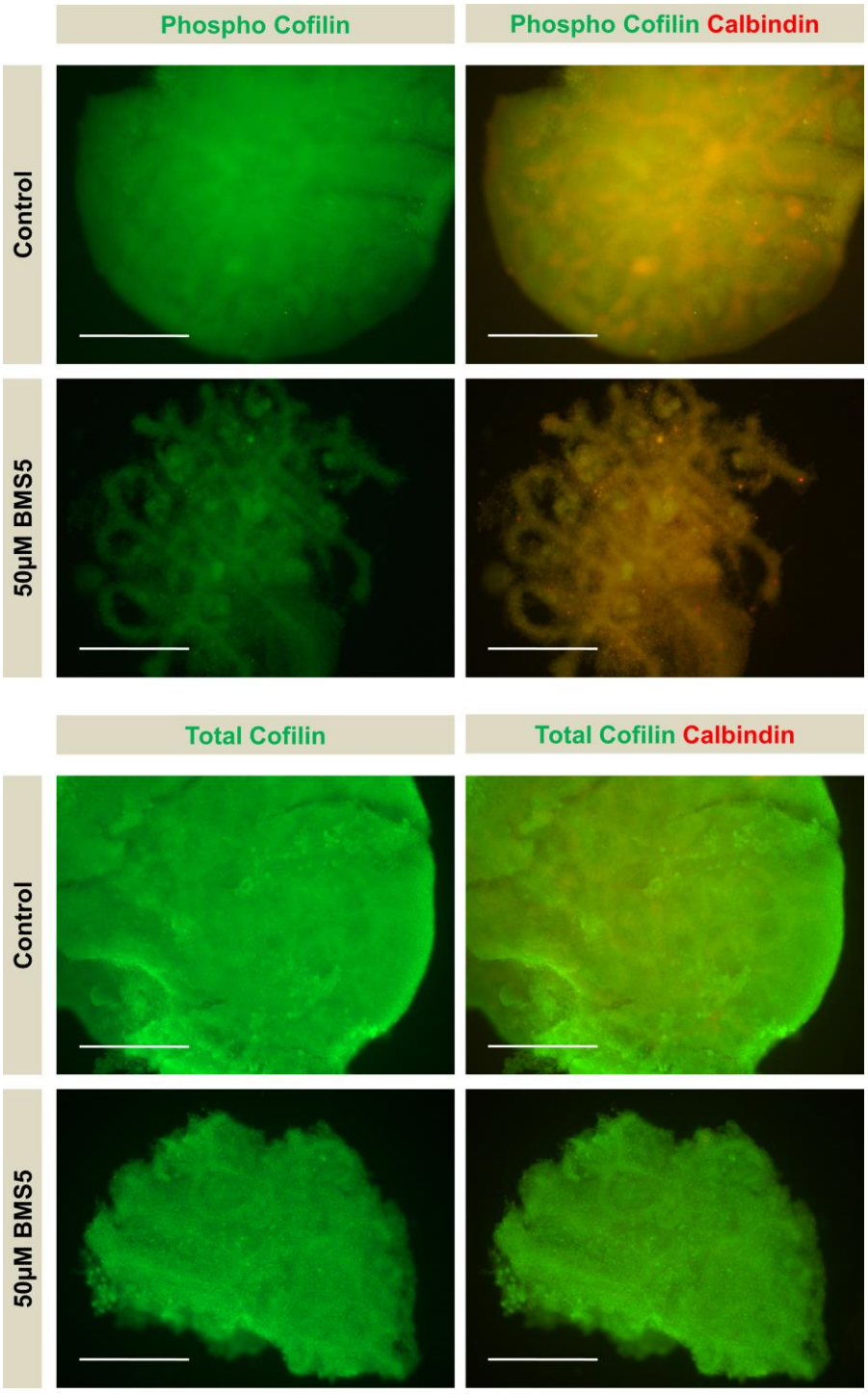



Figure 3.4 – Phosphorylated Cofilin in E12.5 kidneys cultured in 50µM BMS5 (48 hours).

E12.5 kidneys cultured in 50µM BMS5 for 48 hours, fixed and whole mount immunofluorescently labelled with phosphorylated Cofilin (green), and Calbindin (red). Showing a large reduction in the amount of phosphorylated

Cofilin (green) present in the mesenchyme of 50µM BMS5 treated kidneys, while the amount of total Cofilin remains the same in both control and treated kidneys. Scale bars = 200µm. N=3.

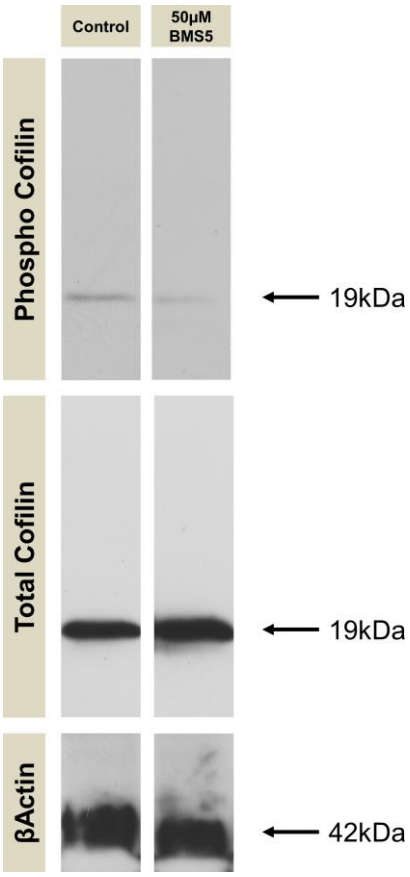



Figure 3.5 – Western blot of E12.5 kidneys cultured in 50µM BMS5.

Western blot of E12.5 kidneys cultured in 50µM BMS5 for 48 hours, labelled with phosphorylated Cofilin (top) and total Cofilin (bottom). Arrow indicates the molecular size, 19kDa, derived from the ladder. Bottom panel showing the loading control, β-actin (42kDa), showing largely no difference between the control and 50µM BMS5 treated kidneys.

### 3.2.2 – BMS5 effects on kidney growth

Kidneys cultured with 50µM BMS5 showed an inhibition of growth, with a significant decrease in the percentage area increase over 24 and 48 hours compared to controls (Figure 3.6). After 24 hours in culture control kidneys had grown 129.99% ± 2.44, while 50µM BMS5 cultured kidneys had only grown 120.66% ± 3.23 ($p=0.032$, $n=11$). During 48 hours in culture controls kidneys had grown 150.61% ± 3.53 while 50µM BMS5 cultured kidneys had grown 124.90% ± 3.68 ($p<0.001$, $n=6$). Figure 3.7 shows light microscope images over 24 hours ($n=11$) and 48 hours ($n=6$), in these kidneys the mesenchyme appeared to lose definition and became darker (Figure 3.7 arrow heads), and branching of the UB halted (Figure 3.7 arrows). Whole mount immunofluorescence with the MM marker, Six2 which is only expressed in the MM of the developing kidney, began to lose Six2 expression by 24 hours, and total loss of Six2 expression by 48 hours (Figure 3.8, $n=3$). The loss of further UB growth and branching (Figure 3.7 arrows) along with the loss of Six2 expression (Figure 3.8) shows that BMS5 inhibits growth of both the UB and the MM. Due to the inhibition of growth, a cell count was performed on kidneys after 48 hours in culture. Control kidneys had 144375 ± 31291.12 cells, while 50µM BMS5 had 35833 ± 12114.27 cells ($p=0.032$, $n=3$) (Figure 3.9) showing a significant reduction in the number of cells compared to their contralateral controls, thus providing further evidence that active LIMK is required for the continued growth and development of the kidney.

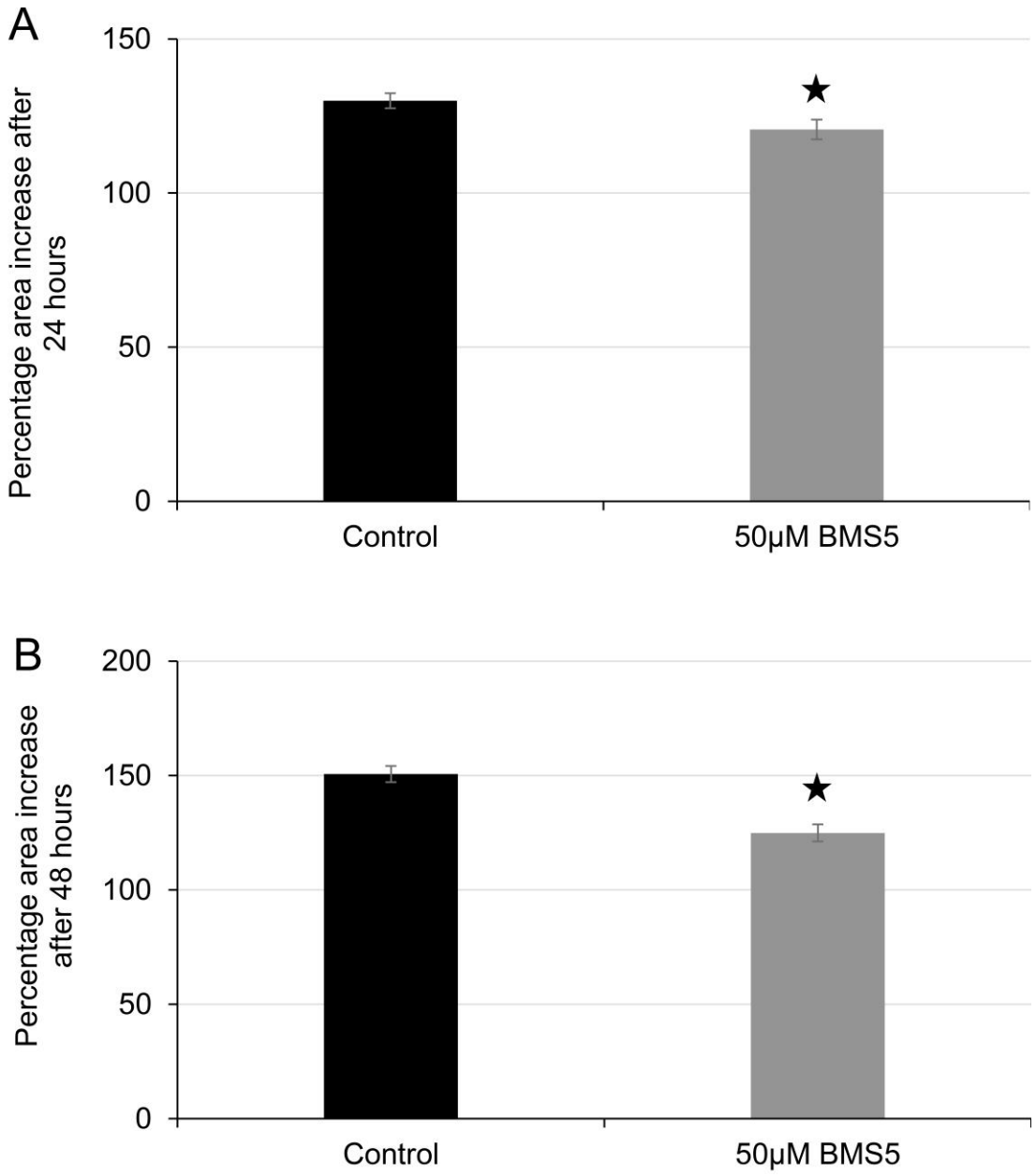



Figure 3.6 – Kidney size after 24 and 48 hours cultured in 50µM BMS5.

Graph showing the percentage area increase over 24 hours (A) and 48 hours (B) in culture in 50µM BMS5. (A) Control kidneys had grown 129.99% ± 2.44, 50µM BMS5 cultured kidneys had grown 120.66% ± 3.23 ($p=0.032$, $n=11$) after 24 hours in culture. (B) Control kidneys had grown 150.61% ± 3.53, 50µM BMS5 cultured kidneys had grown 124.90% ± 3.68 ($p<0.001$, $n=6$) after 48 hours in culture. * $p<0.01$ compared to control.

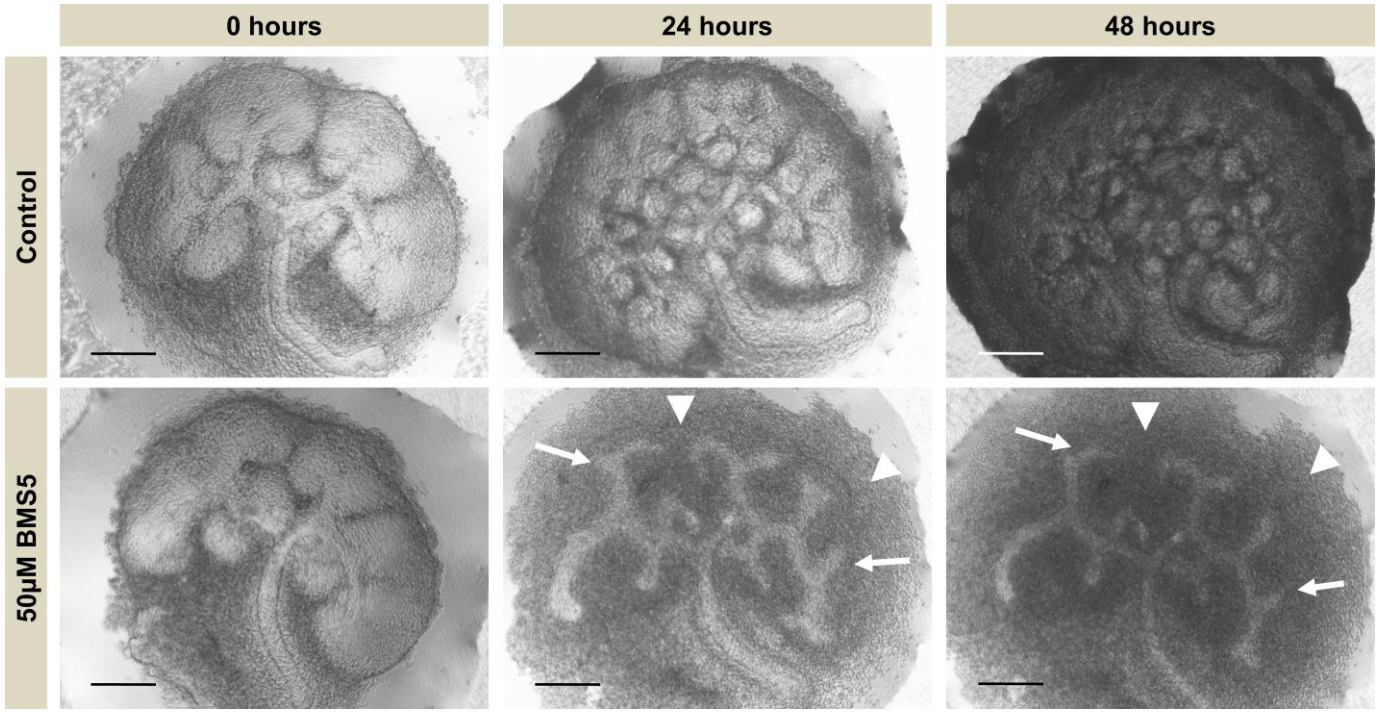



Figure 3.7 – Light micrographs of E12.5 kidneys cultured in 50µM BMS5.

E12.5 kidneys cultured in 50µM BMS5 for 48 hours showing lack of growth of the ureteric bud and loss of mesenchyme definition. Arrows indicate lack of UB growth, arrow heads show loss of mesenchyme definition. Scale bars = 200µm. N=6.

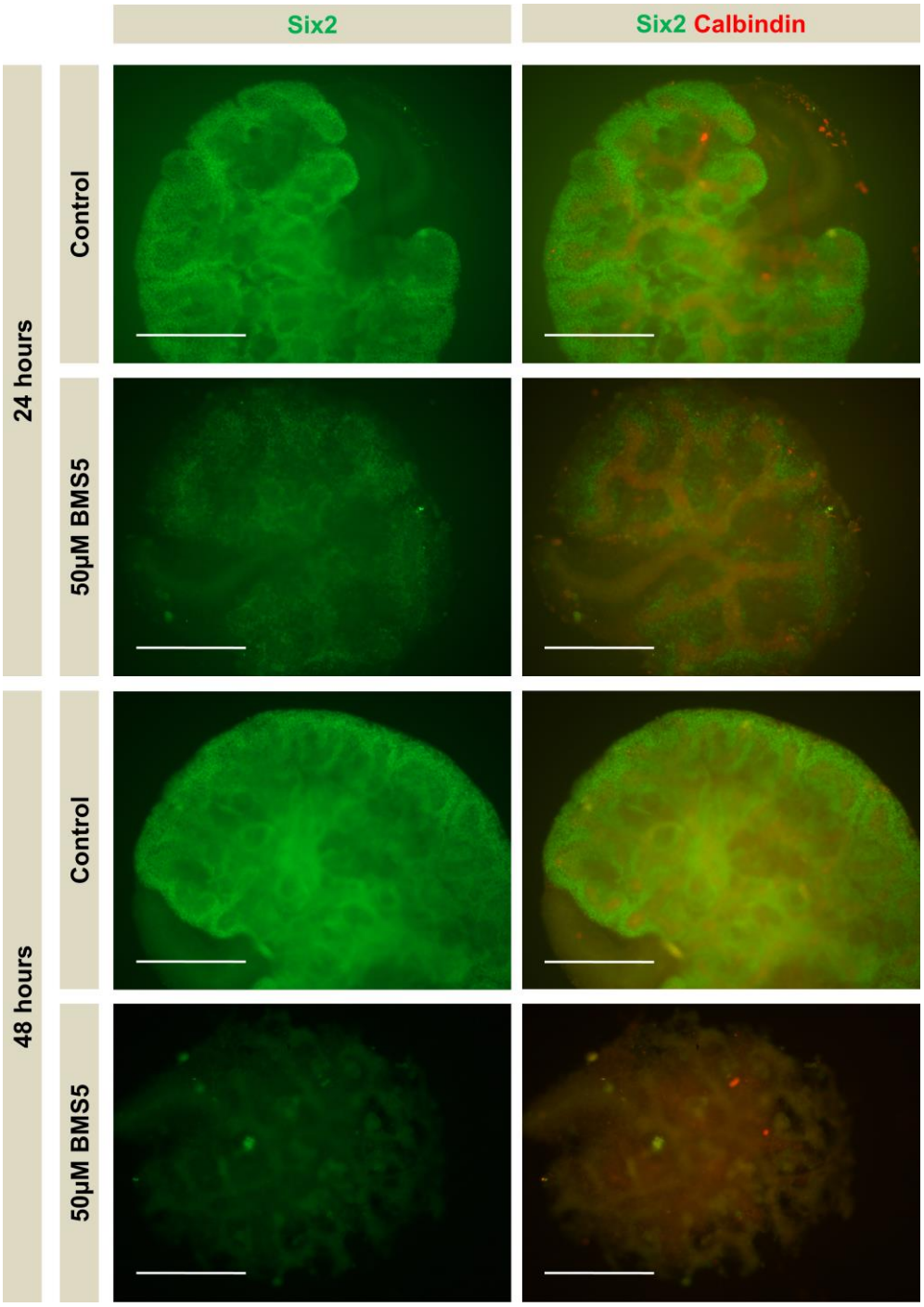



Figure 3.8 – Six2 in E12.5 kidneys cultured in 50µM BMS5.

E12.5 kidneys cultured in 50µM BMS5 for 24 and 48 hours, fixed and whole mount immunofluorescently labelled with Six2 (green, metanephric mesenchyme marker), and Calbindin (red, labelling the ureteric tree). 24 hour images show loss of Six2 staining in kidneys cultured in 50µM BMS5, while

after 48 hours, there was complete loss of Six2 in kidneys cultured in 50µM BMS5 compared to the control (no BMS5). Ureteric bud branching (red) is reduced in kidneys cultured in 50µM BMS5 at both 24 and 48 hours. Scale bars = 200µm. N=3.

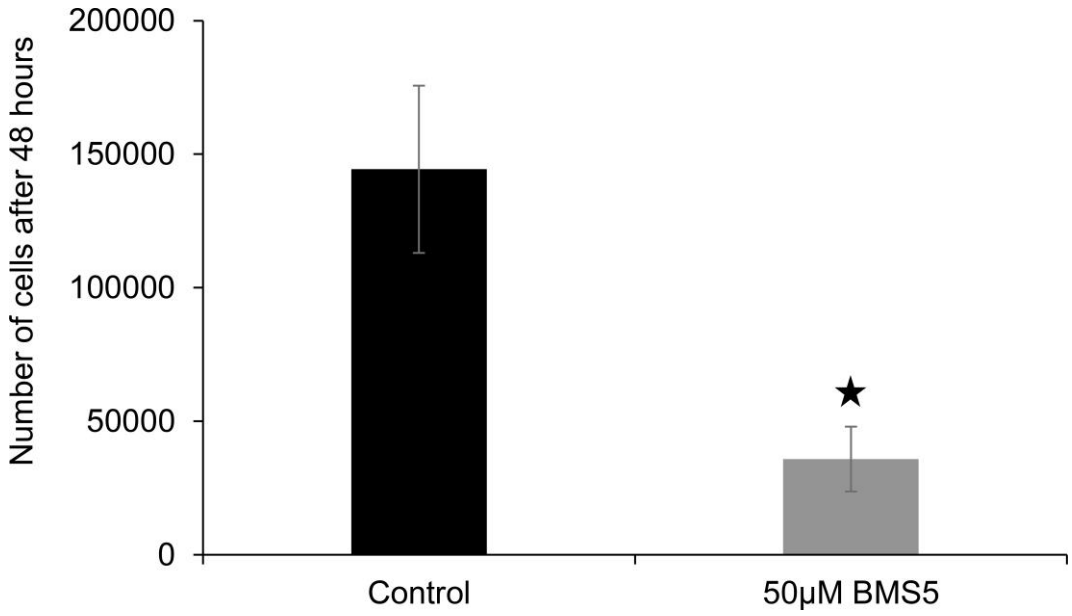



Figure 3.9 – Cell counts on E12.5 kidneys cultured in 50µM BMS5.

Graph showing the number of cells after 48 hours in culture with and without 50µM BMS5. Control kidneys had 144375 ± 31291.12 cells, 50µM BMS5 had 35833 ± 12114.27 cells ($p=0.032$, $n=3$). Showing fewer cells present in kidneys cultured in 50µM BMS5. * $p<0.05$ compared to control.

### 3.2.3 – BMS5 causes mitotic arrest in kidney development

It is known that the Six2 expressing MM is a highly proliferative cell population (Kobayashi et al., 2008) and therefore the observation of a loss of Six2 expression could be due to cell cycle arrest. Therefore kidneys were labelled with the mitotic marker pH3, to look to see what, if any, impact LIMK inhibition has on mitosis. In control kidneys there were 7.75% ± 0.82 of mitotic cells in anaphase while only 0.79% ± 0.57 of mitotic cells in anaphase in the 50µM BMS5 treated kidneys ($p=0.0022$, $n=3$) (Figure 3.10). The total number of cells in mitosis was unaffected with 100.33 cells ± 11.21 in mitosis per field of view in control kidneys, and 112.80 cells ± 18.81 in mitosis in 50µM BMS5 treated kidneys, ($p=0.60$, $n=3$, Figure 3.10). This suggests that the cells were stalled during mitosis and because there was not an accumulation of cells in mitosis the cells were either dying or were prevented from embarking on mitosis. To determine if the cells were dying a TUNEL assay was performed which showed a large increase in the number of apoptotic cells in the BMS5 treated kidney after 18 hours in culture (Figure 3.11, $n=3$). This indicated that the loss of Six2 expressing cells seen in Figure 3.8 and the decrease in cell number (Figure 3.9) could potentially be explained by these cells undergoing apoptosis after becoming stalled during mitosis due to the lack of active LIMK.

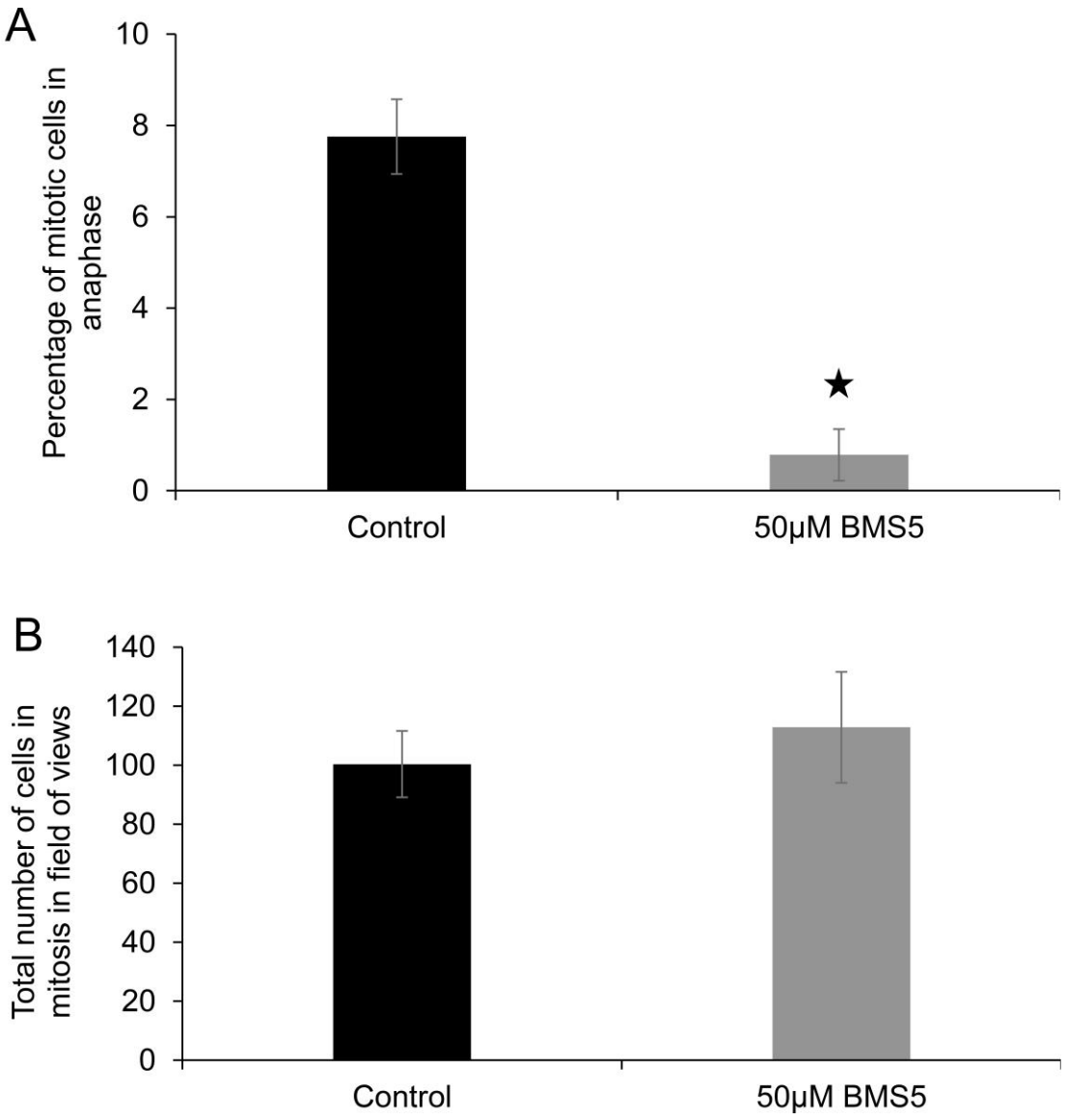



Figure 3.10 – Mitosis analysis of E12.5 kidneys cultured in 50μM BMS5.

Graphs showing kidneys cultured in 50μM BMS5 for 48 hours, fixed and whole mount immunofluorescently labelled with pH3. (A) Percentage of mitotic cells in anaphase. Control kidneys had 7.75% ± 0.82 of mitotic cells in anaphase while only 0.79% ± 0.57 of mitotic cells in anaphase in the 50μM BMS5 treated kidneys ($p=0.0022$, $n=3$). (B) Total number of cells in mitosis in field of views. Control kidneys had 100.33 cells ± 11.21 in mitosis per field of view, and 112.80 cells ± 18.81 in mitosis in 50μM BMS5 treated kidneys, ($p=0.60$, $n=3$). * $p<0.01$ compared to control.

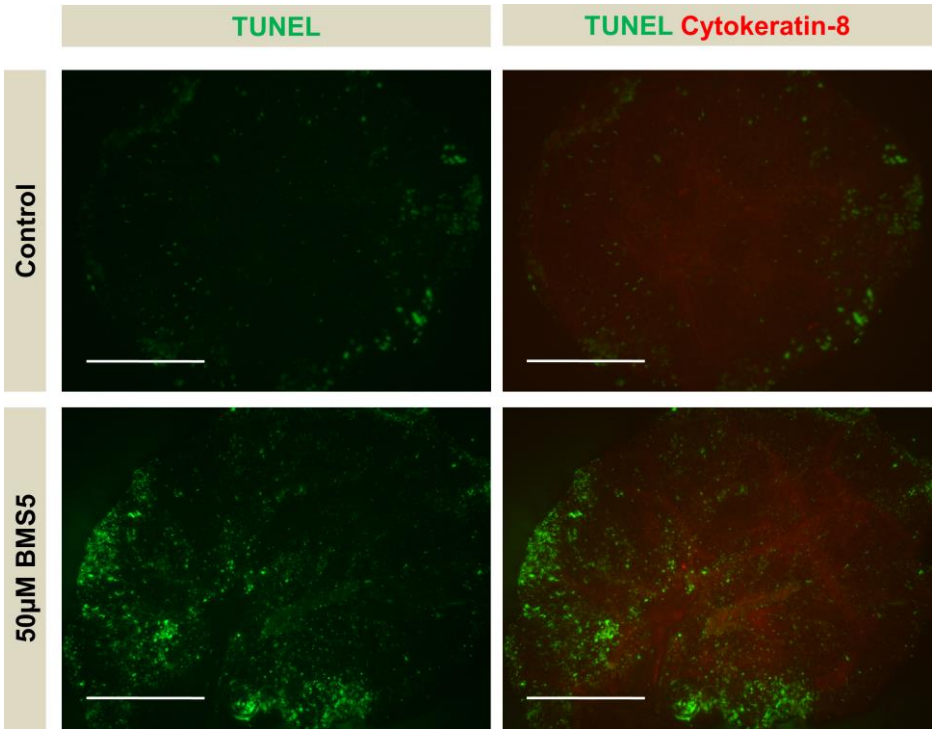



Figure 3.11 – Apoptosis in E12.5 kidneys cultured in 50µM BMS5.

E12.5 kidneys cultured in 50µM BMS5 for 18 hours, fixed and a whole mount TUNEL assay labelling TUNEL (green) and immunofluorescently labelling cytokeratin-8 (red, labelling the ureteric tree). Kidneys cultured in 50µM BMS5 for 18 hours showed more apoptosis (TUNEL, green). Scale bars = 200µm. N=3.

### 3.2.4 – BMS5 effects on Six2 expression is not due to a Phosphorylated Cofilin pathway

The most well documented role of LIM kinases is to inactivate Cofilin by phosphorylation. Phosphorylated Cofilin can activate phospholipase D1 (PLD1; Han et al., 2007) to catalyse the conversion of phosphatidylcholine to phosphatidic acid, which has been shown to affect gene transcription (Yao et al., 2013; Fang et al., 2001). Therefore two PLD1 inhibitors, FIPI (Su et al., 2009) and Butanol (Skippen et al., 2002) were used to see if the loss of Six2 expression can be explained by the BMS5 induced loss of phosphorylated Cofilin. There was a significant increase of growth for kidneys cultured in 1.5% Butanol (Figure 3.12), during 48 hours in culture controls kidneys had grown 125.13% ± 7.01 whereas 1.5% Butanol cultured kidneys had grown 157.18% ± 5.06 ($p=0.010$, $n=4$). Kidneys cultured in 100µM FIPI did not show this increase in growth, control kidneys grew 174.30% ± 8.95 over 48 hours in culture whereas 100µM FIPI cultured kidneys had grown 119.74% ± 10.65 ($p=0.066$, $n=3$). The light images showed a different phenotype to BMS5, with 100µM FIPI showing the kidneys becoming darker, and no further growth (Figure 3.13, $n=3$). Kidneys treated in 1.5% Butanol appeared dark (Figure 3.14, $n=4$), and while there was an increase in growth the appearance of kidneys cultured in 1.5% Butanol suggested that these kidneys were not growing appropriately.

Whole mount immunofluorescence with Six2 showed a decrease in Six2 expression in both 100µM FIPI and 1.5% Butanol (Figure 3.15, $n=3$ for 100µM FIPI and $n=3$ for 1.5% Butanol) treated kidneys but this was not as dramatic

as that seen following treatment with BMS5. The green staining showed in FIPI and Butanol treated kidneys was diffuse and hard to draw any definitive conclusions as this was not quantified. This would indicate that because of the difference in mesenchyme structure observed in brightfield images and the continued expression of some Six2, the phosphorylated Cofilin pathway in regulating PLD1 is unlikely to be responsible for the BMS5 phenotype.

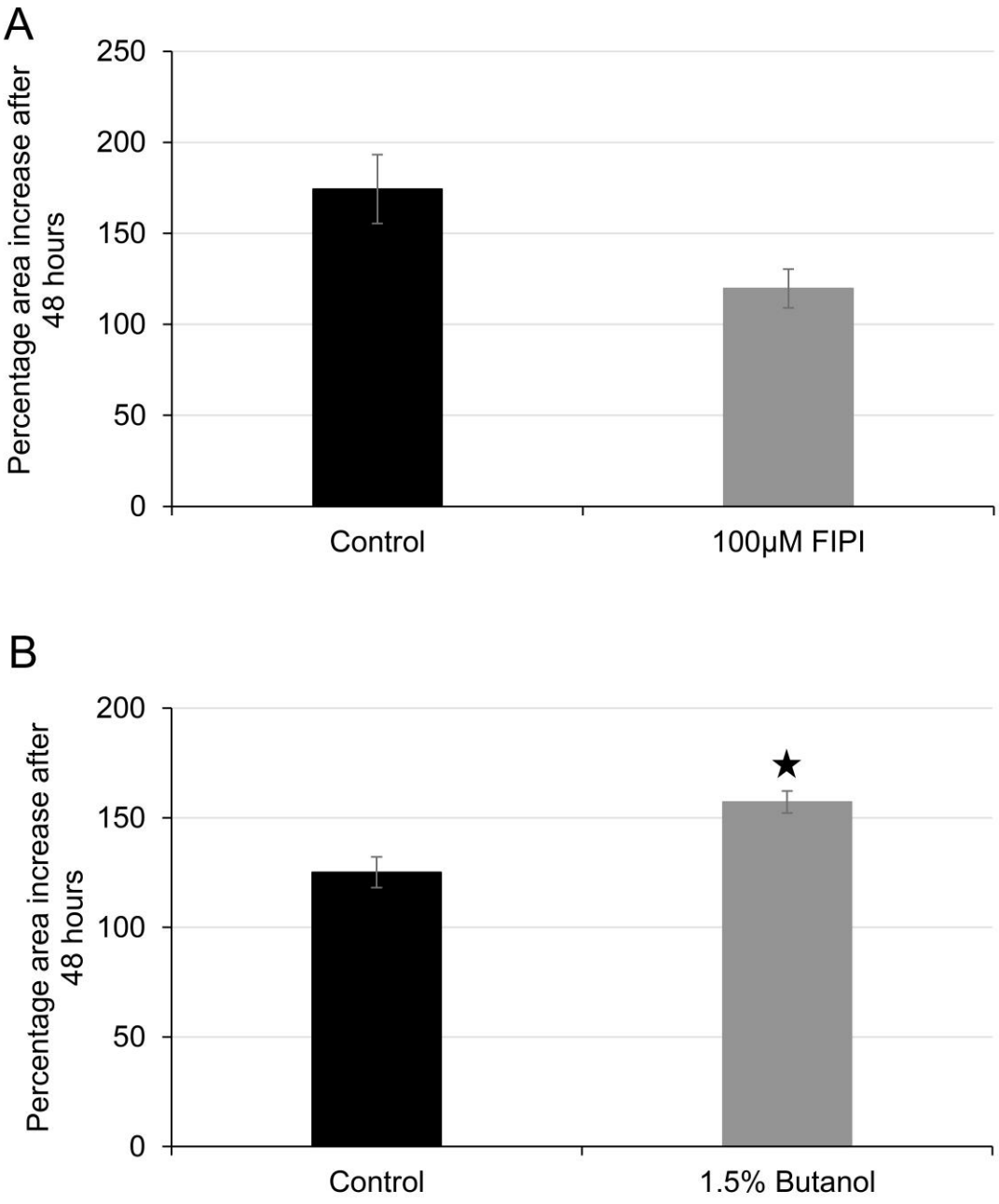



Figure 3.12 – Kidney size after 48 hours cultured in 100µM FIPI and 1.5% Butanol.

Graph showing the percentage area increase over 48 hours in culture in 100µM FIPI (A) and 1.5% Butanol (B). (A) Control kidneys had grown 125.13% ± 7.01 while 1.5% Butanol cultured kidneys had grown 157.18% ± 5.06 (p=0.010, n=4). (B) Control kidneys had grown 174.30% ± 8.95 over 48

hours in culture and kidneys cultured in 100μM FIPI had grown 119.74% ± 10.65 ($p=0.066$, $n=3$). * $p<0.05$ compared to control.

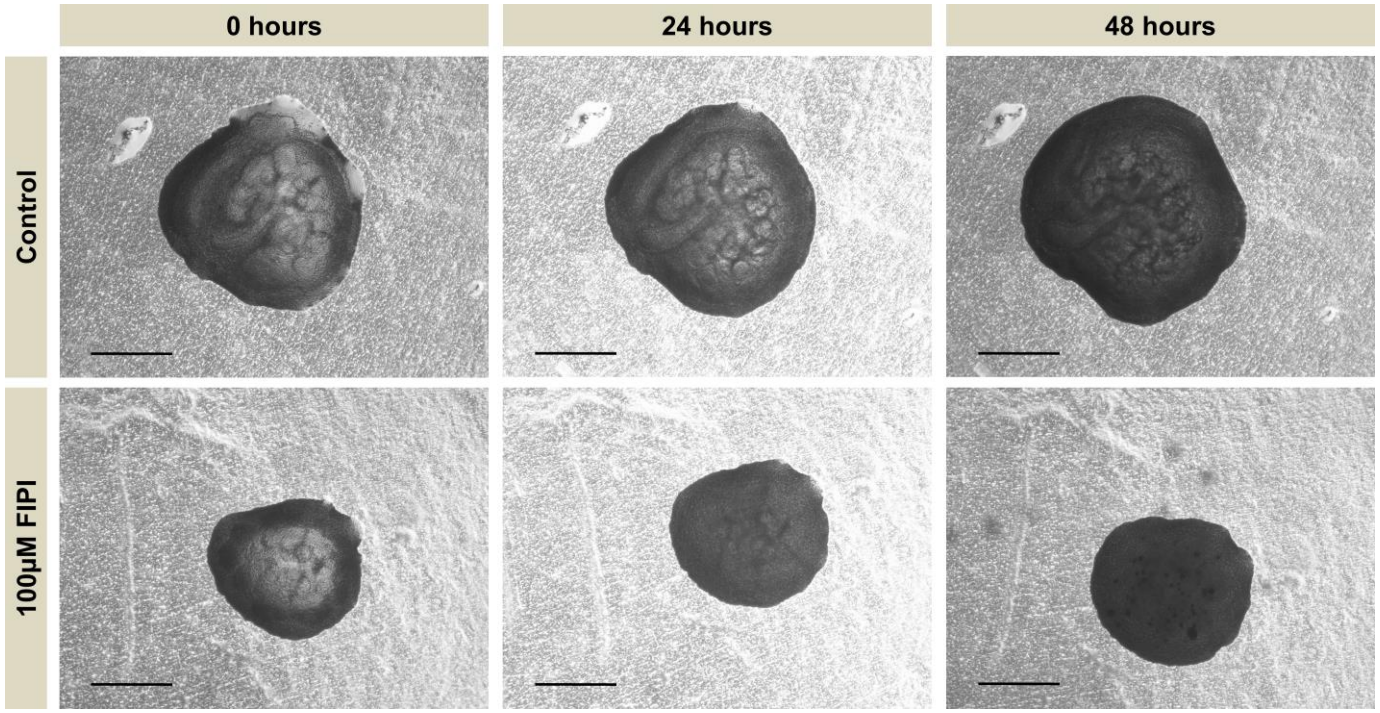



Figure 3.13 – Light micrographs of E12.5 kidneys cultured in 100µM FIPI.

E12.5 kidneys cultured in 100µM FIPI for 48 hours, showing kidneys cultured in 100µM FIPI are smaller than the controls. Scale bars = 500µm. N=3.

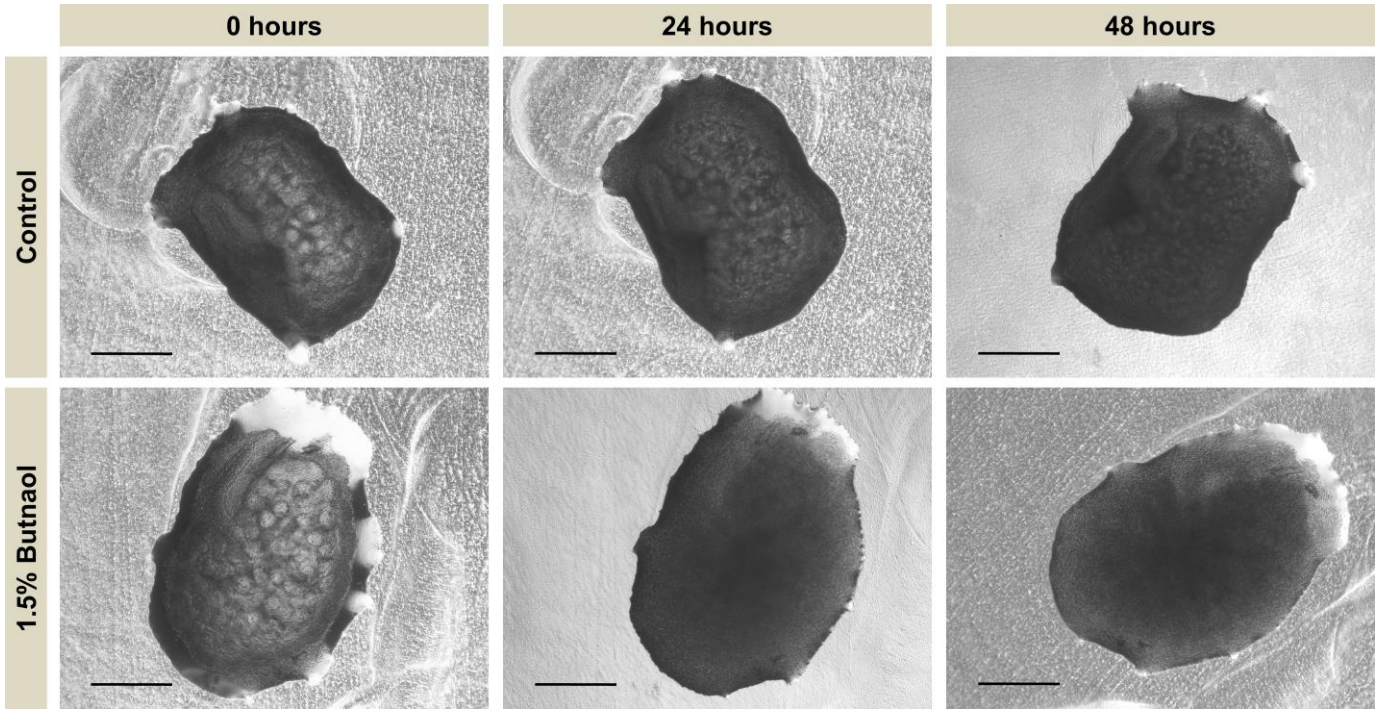



Figure 3.14 – Light micrographs of E12.5 kidneys cultured in 1.5% Butanol.

E12.5 kidneys cultured in 1.5% Butanol for 48 hours, showing kidneys cultured in 1.5% Butanol appear darker. Scale bars = 500µm. N=4.

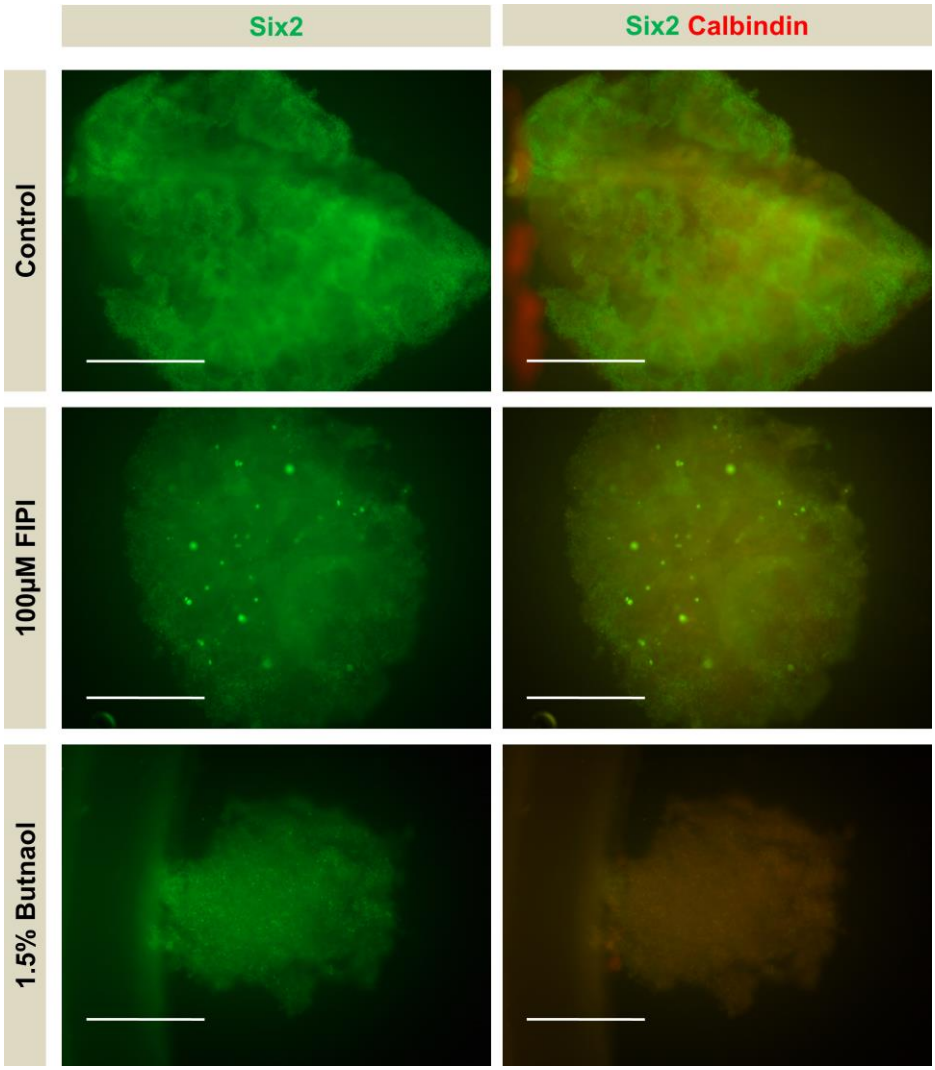



Figure 3.15 – Six2 in E12.5 kidneys cultured in 100µM FIPI and 1.5% Butanol.

E12.5 kidneys cultured in 100µM FIPI and 1.5% Butanol for 48 hours, fixed and whole mount immunofluorescently labelled with Six2 (green), and Calbindin (red, labelling the ureteric tree). Showing a decrease in Six2 staining in both 100µM FIPI and 1.5% Butanol treated kidneys. Scale bars = 200µm. N=3.

## 3.2.5 – BMS5 effects on Six2 expression cannot be explained by the loss of Cofilin phosphorylation

To further investigate whether the BMS5 phenotype is due to a Cofilin mediated effect or another LIMK driven effect this thesis looked to see if the loss of Six2 expression could be explained by the loss of the ability to phosphorylate Cofilin and not some other downstream effect of LIMK. Both the calcium ionophore, A23871 and the $Ca^{2+}$ mobilising agonist, Histamine, cause Cofilin dephosphorylation (Wang et al., 2005). While this group showed both A23187 and histamine does decrease the amount of Cofilin phosphorylation, this was not observed using 25µM A23187 (Figure 3.16, n=3) or 10mM Histamine (Figure 3.17, n=3). The concentration of A23187 employed (25µM) was 5 times that used in the original paper (Wang et al., 2005), and we failed to achieve a reduction in phosphorylated Cofilin. As such it was no surprise that whole mount immunofluorescence showed Six2 was only slightly reduced in kidneys cultured in 25µM A23187 (Figure 3.18, n=3) and still expressed when cultured in 10mM Histamine (Figure 3.19, n=3). The difference in Six2 expression seen in kidneys cultured in 25µM A23187 cannot be attributed to a lack of phosphorylated Cofilin as phosphorylated Cofilin was still expressed similarly to controls; this reduction might be as a consequence of other calcium mediated effects within the cell because it is known that A23187 increases intracellular $Ca^{2+}$ ions (Campbell and Siddle, 1976).

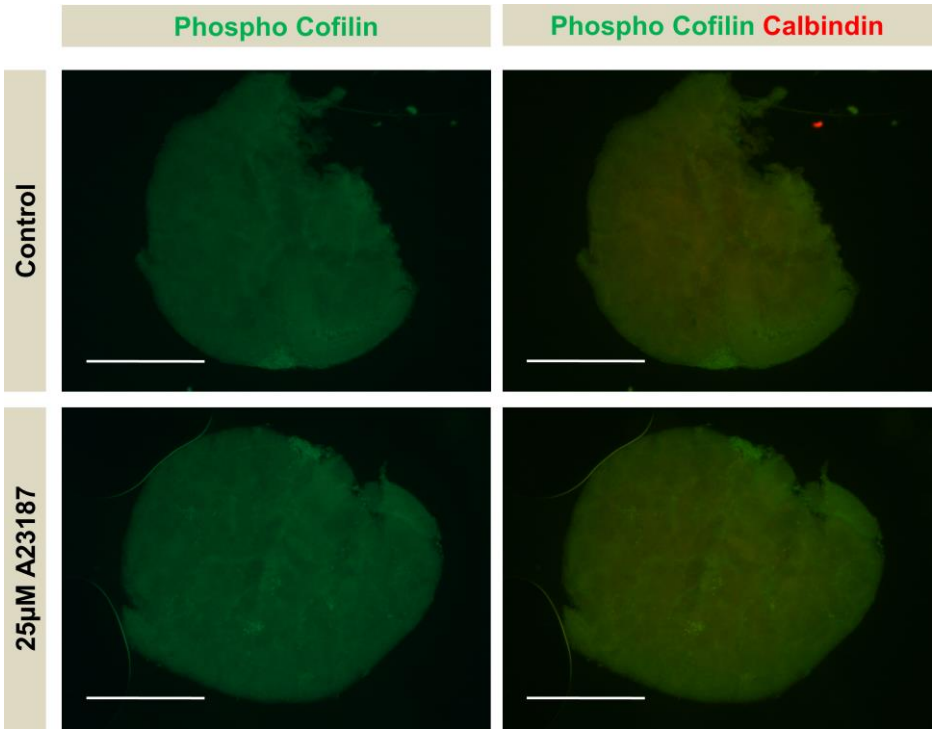



Figure 3.16 – Phosphorylated Cofilin in E12.5 kidneys cultured in 25µM A23187.

E12.5 kidneys cultured in 25µM A23187 for 48 hours, fixed and whole mount immunofluorescently labelled with phosphorylated Cofilin (green), and Calbindin (red, labelling the ureteric tree). Showing no difference in the amount of phosphorylated Cofilin (green) between the control (no A23187) and treated kidneys. Scale bars = 400µm. N=3.

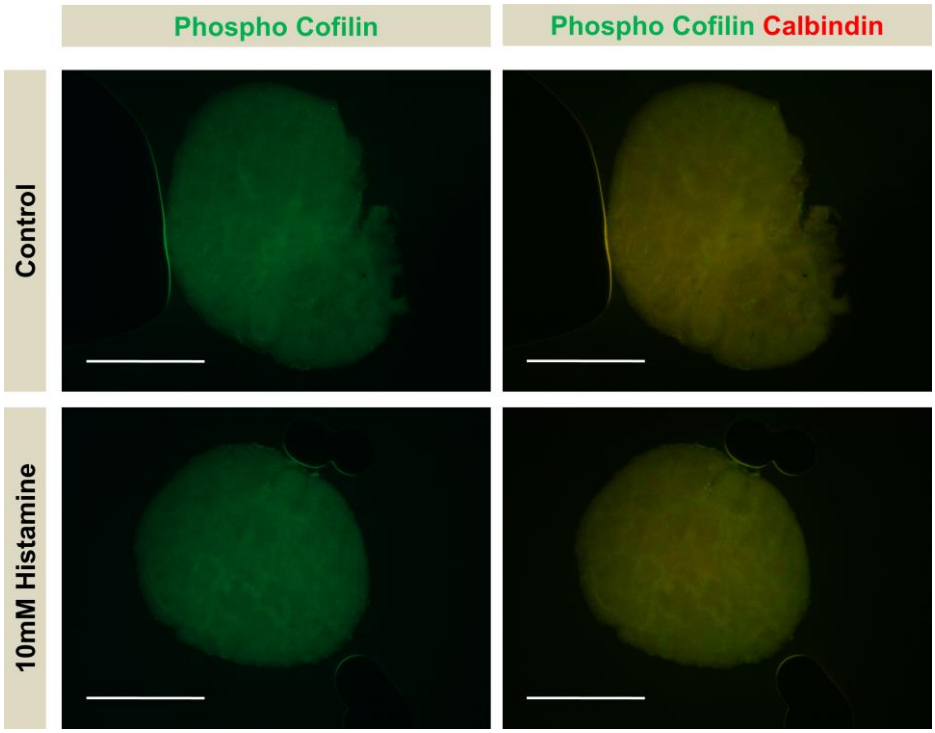



Figure 3.17 – Phosphorylated Cofilin in E12.5 kidneys cultured in 10mM Histamine.

E12.5 kidneys cultured in 10mM Histamine for 48 hours, fixed and whole mount immunofluorescently labelled with phosphorylated Cofilin (green), and Calbindin (red, labelling the ureteric tree). Showing no difference in the amount of phosphorylated Cofilin (green) between the control (no Histamine) and treated kidneys. Scale bars = 400µm. N=3.

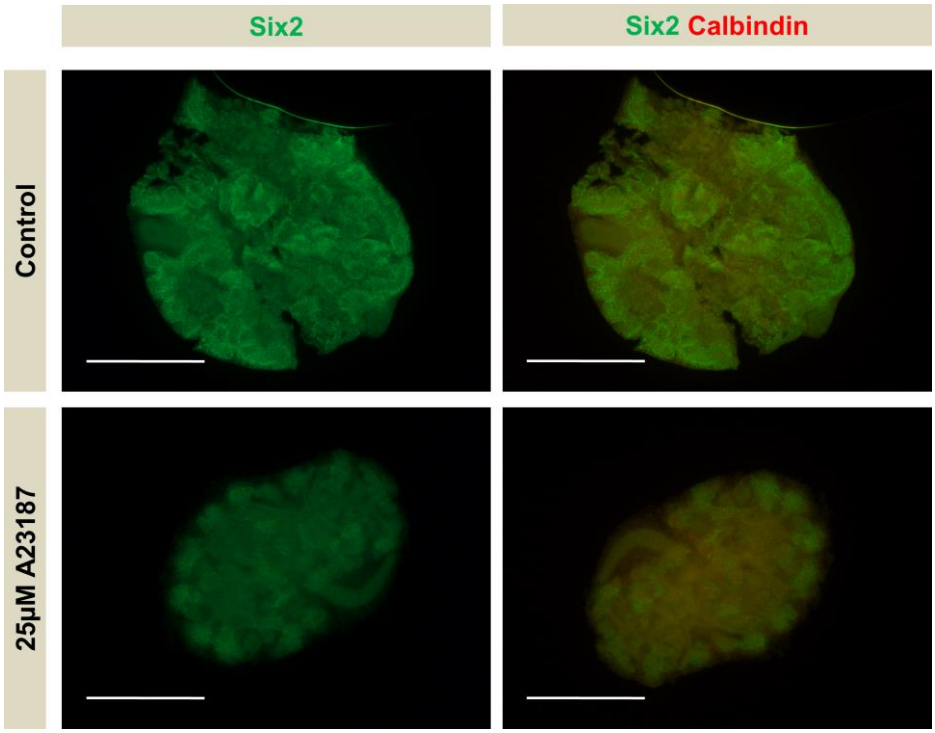



Figure 3.18 – Six2 in E12.5 kidneys cultured in 25µM A23187.

E12.5 kidneys cultured in 25µM A23187 for 48 hours, fixed and whole mount immunofluorescently labelled with Six2 (green), and Calbindin (red, labelling the ureteric tree). Showing a small reduction in the amount of Six2 (green) in the kidneys cultured in A23187. Scale bars = 400µm. N=3.

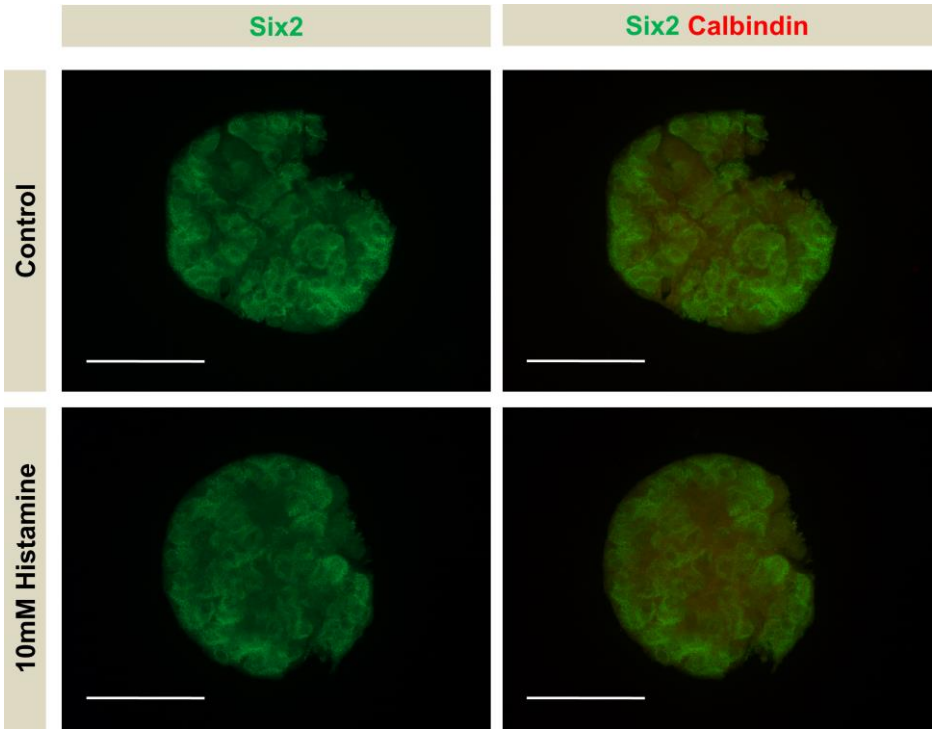



Figure 3.19 – Six2 in E12.5 kidneys cultured in 10mM Histamine.

E12.5 kidneys cultured in 10mM Histamine for 48 hours, fixed and whole mount immunofluorescently labelled with Six2 (green), and Calbindin (red, labelling the ureteric tree). Showing no difference in the amount of Six2 (green) between the control (no Histamine) and treated kidneys. Scale bars = 400µm. N=3.

### 3.2.6 – Mitosis inhibitors do not replicate the loss of Six2 or cell death

Since BMS5 arrests cells during mitosis (Figure 3.10), it was therefore decided to see if the phenotype observed with BMS5 could be explained solely by the inhibition of mitosis. Paclitaxel and Colchicine both disrupt tubulin during the cell cycle and thereby inhibit mitosis (Schiff and Horwitz, 1980; Taylor, 1965). If the effects observed following LIMK inhibition were solely due to mitotic arrest then other mitotic inhibitors should produce the same phenotype.

To confirm that these mitosis inhibitors were indeed stopping mitosis kidneys were cultured in 10μM Paclitaxel for 24 hours and whole mount immunofluorescently labelled with pH3, which showed 2.55% ± 0.46 of mitotic cells in anaphase in controls and 0% ± 0 of mitotic cells in anaphase ($p=0.0015$, $n=4$) for kidneys cultured in 10μM Paclitaxel. The total number of mitotic cells in an average field of view was 103.5 ± 14 in control kidneys but kidneys cultured in 10μM Paclitaxel had 237.4 ± 38 cells in mitosis ($p=0.016$, $n=4$) (Figure 3.20). This showed that Paclitaxel effectively stalls cells before anaphase (the majority were in prophase), and that the cells have not died in the time frame observed (due to the increase in cells in mitosis).

When kidneys were cultured in 1μg/ml Colchicine, control kidneys had 4.69% ± 1.15 mitotic cells in anaphase and Colchicine cultured kidneys had 0% ± 0 mitotic cells in anaphase ($p=0.015$, $n=3$). The total number of cells in mitosis in an average field of view was 98.5 ± 1.66 in control kidneys and 120.83 ± 15.77 ($p=0.23$, $n=3$) in kidneys cultured in 1μg/ml Colchicine (Figure 3.21).

Kidneys grown with Paclitaxel were not significantly smaller than contralateral controls (Figure 3.22). Control kidneys had grown to 126.62% ± 6.36 over 24 hours and 10µM Paclitaxel cultured kidneys had grown to 116.90% ± 4.67 (p=0.25, n=5) of their original size but their appearance was darkened and the mesenchyme and renal vesicles appeared to lose definition (Figure 3.23, n=5). Kidneys cultured in Colchicine were significantly smaller (Figure 3.24), over 24 hours controls kidneys had grew 135.42% ± 4.39, whereas kidneys cultured in 1µg/ml Colchicine had shrunk to 75.55% ± 4.95 of their original size (p=0.00000032, n=8), light microscope images showed that further development was halted (Figure 3.25, n=8).

Whole mount immunofluorescence with Six2 showed Paclitaxel treated kidneys had Six2 expression (Figure 3.26, n=3), although there appears slightly less Six2 expression compared to their contralateral controls. Colchicine treated kidneys showed green staining indicative of Six2 although fewer nuclei were visible (Figure 3.27, n=2). This data does not indicate complete absence of Six2 staining as seen with kidneys treated with BMS5.

From this data it can be concluded that BMS5 not only stalls the cells in mitosis but they also die which leads to the loss of Six2 expression.

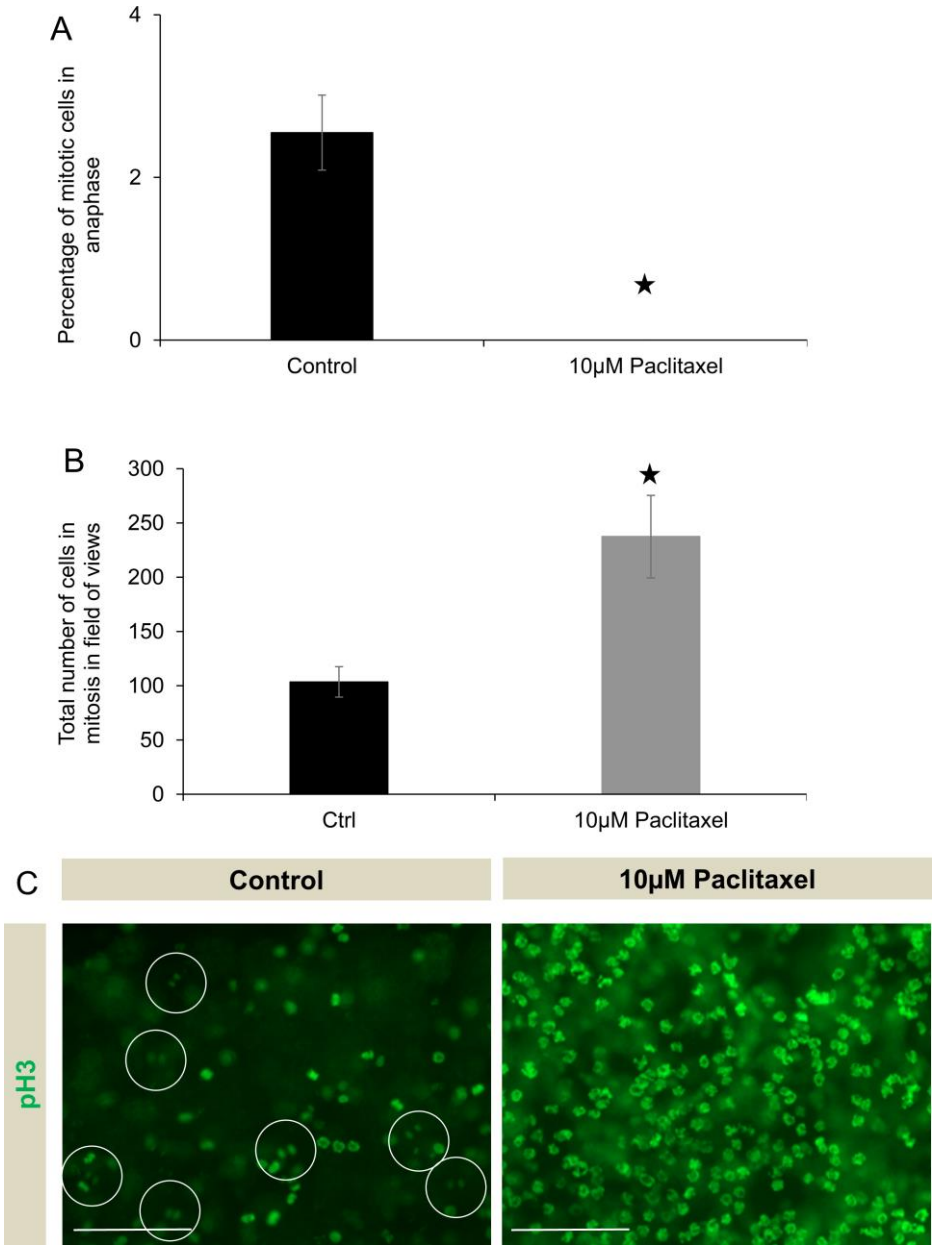



Figure 3.20 – Mitosis analysis of E12.5 kidneys cultured in 10μM Paclitaxel.

Graphs showing kidneys cultured in 10μM Paclitaxel for 24 hours, fixed and whole mount immunofluorescently labelled with pH3. (A) Percentage of mitotic cells in anaphase. 2.55% ± 0.46 of mitotic cells in anaphase in controls and 0% ± 0 of mitotic cells in anaphase ($p=0.0015$, $n=4$) in kidneys cultured in 10μM Paclitaxel. (B) Total number of cells in mitosis in field of views. 103.5 ± 14 cells in mitosis in control kidneys but kidneys cultured in 10μM Paclitaxel

had 237.4 ± 38 cells in mitosis ($p=0.016$, $n=4$). (C) Cropped images showing pH3 (green) in control and kidneys cultured in 10µM Paclitaxel. Nuclei in white circles show anaphase stage nuclei (chromosomes are separated) are present in control kidneys but not in 10µM Paclitaxel treated kidneys. * $p<0.05$ compared to control.

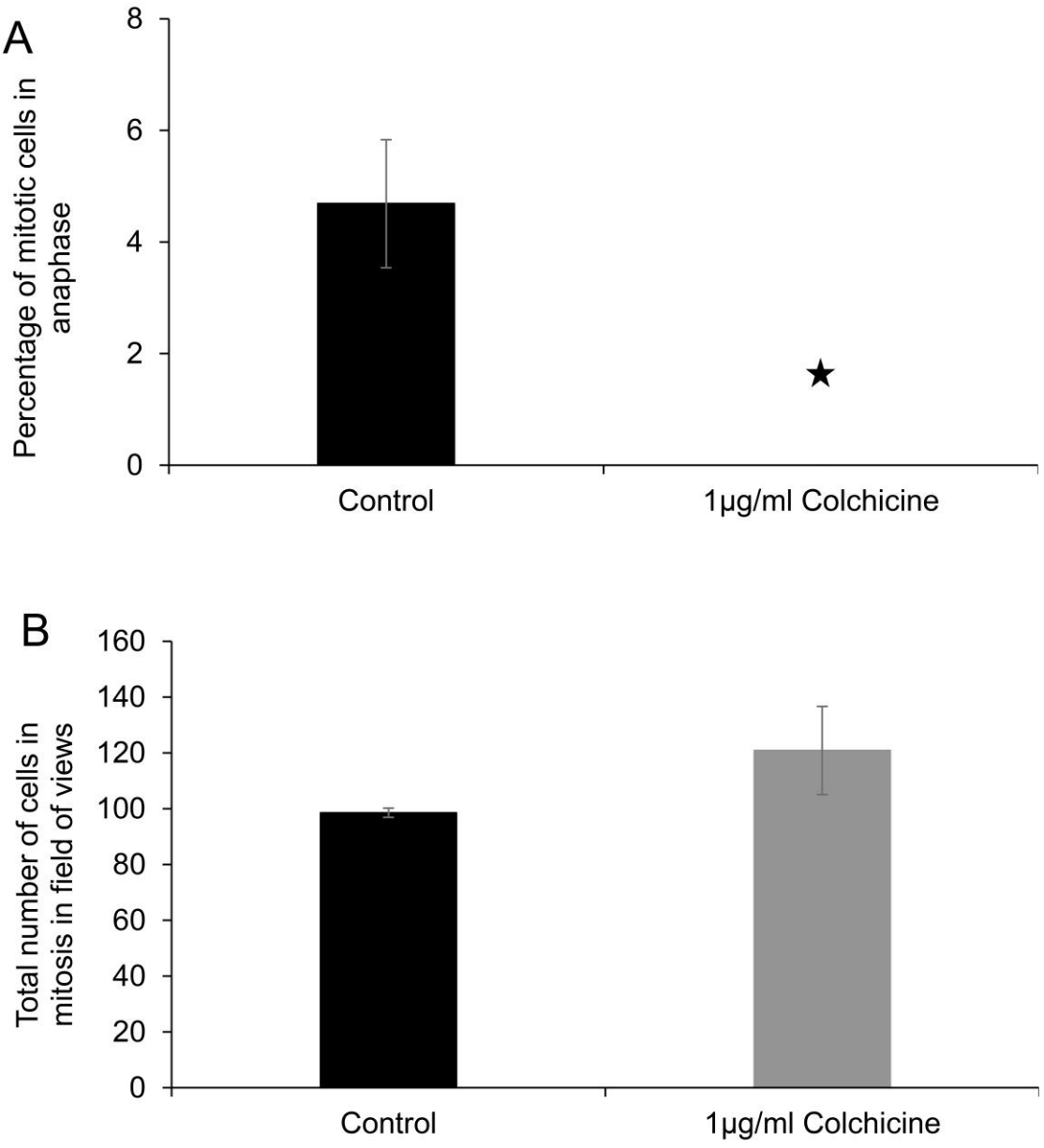



Figure 3.21 – Mitosis analysis of E12.5 kidneys cultured in 1µg/ml Colchicine.

Graphs showing kidneys cultured in 1µg/ml Colchicine for 24 hours, fixed and whole mount immunofluorescently labelled with pH3. (A) Percentage of mitotic cells in anaphase. Control kidneys had 4.69% ± 1.15 mitotic cells in anaphase and Colchicine cultured kidneys had 0% ± 0 mitotic cells in anaphase ($p=0.015$, $n=3$). (B) Total number of cells in mitosis in field of views. Control kidneys had 98.5 ± 1.66 cells in mitosis, while kidneys cultured in 1µg/ml Colchicine had 120.83 ± 15.77 ($p=0.23$, $n=3$). * $p<0.05$ compared to control.

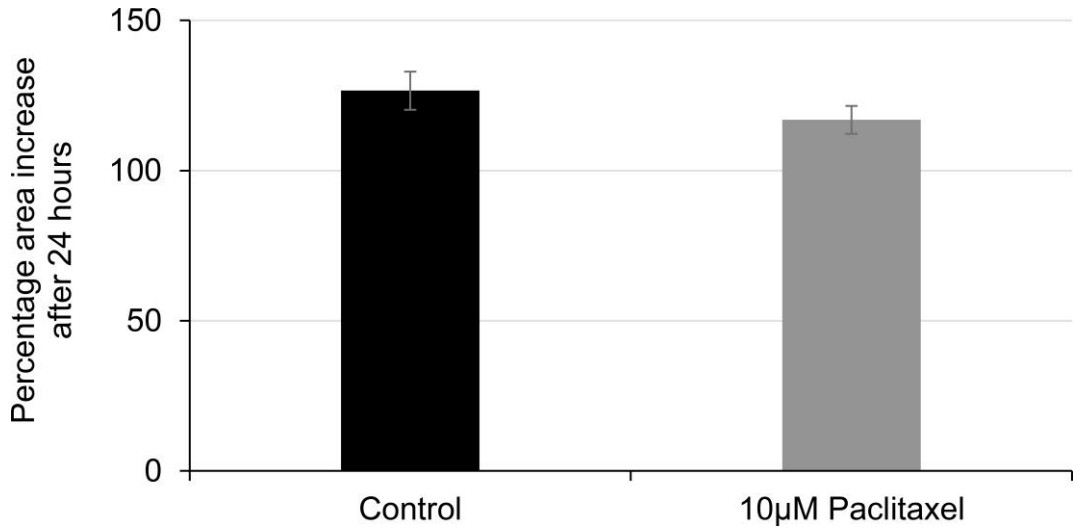



Figure 3.22 – Kidney size after 24 hours cultured in 10µM Paclitaxel.

Graph showing the percentage area increase over 24 hours in culture in 10µM Paclitaxel. Control kidneys had grown to 126.62% ± 6.36 over 24 hours and 10µM Paclitaxel cultured kidneys had grown to 116.90% ± 4.67 (p=0.25, n=5).

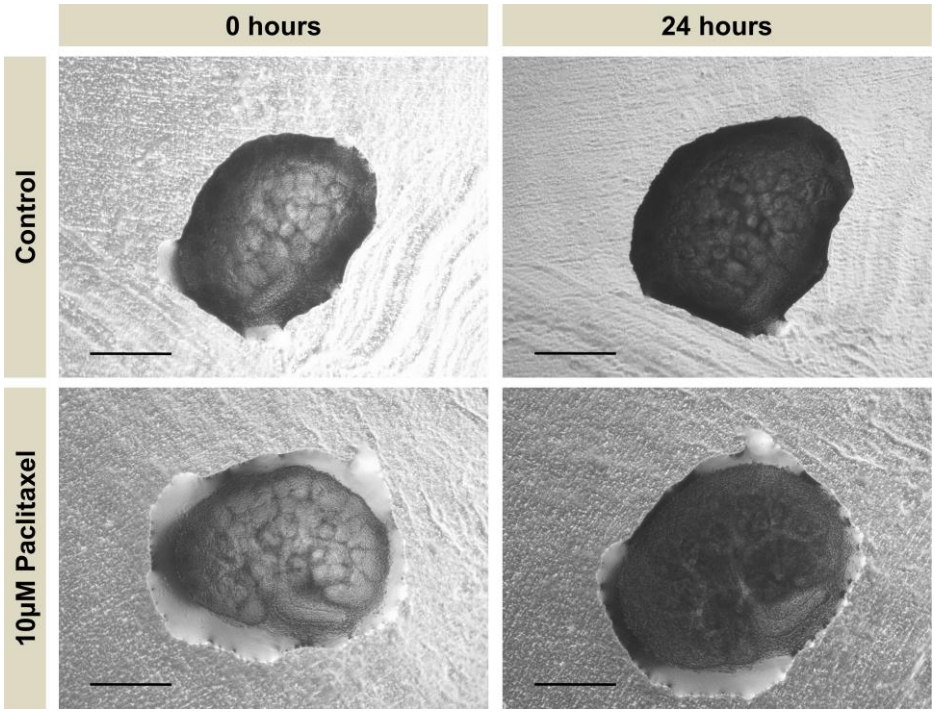



Figure 3.23 – Light micrographs of E12.5 kidneys cultured in 10μM Paclitaxel.

E12.5 kidneys cultured in 10μM Paclitaxel for 24 hours. Showing kidneys cultured in 10μM Paclitaxel are darker and the mesenchyme appeared to loose definition. Scale bars = 500μm. N=5.

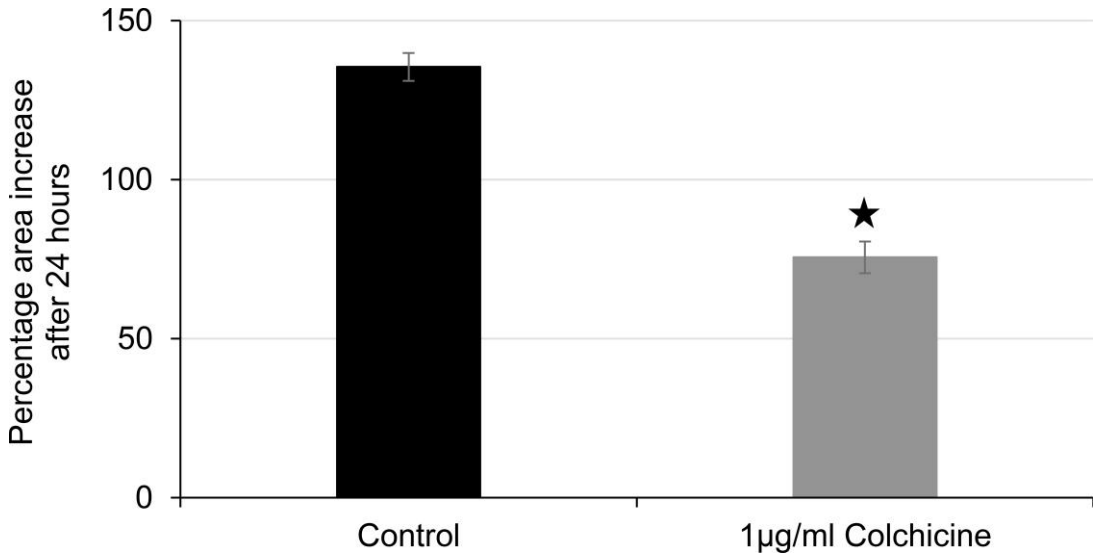



Figure 3.24 – Kidney size after 24 hours cultured in 1µg/ml Colchicine.

Graph showing the percentage area increase over 24 hours in culture in 1µg/ml Colchicine. Controls kidneys had grown 135.42% ± 4.39, whereas kidneys cultured in 1µg/ml Colchicine had shrunk to 75.55% ± 4.95 of their original size ($p=0.00000032$, $n=8$). * $p<0.001$ compared to control.

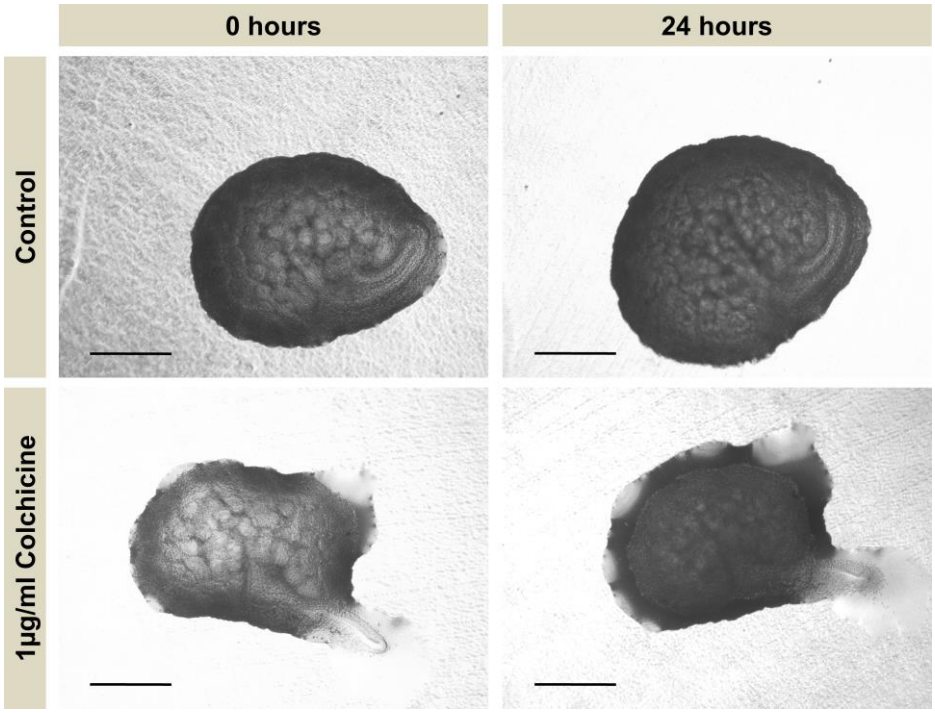



Figure 3.25 – Light micrographs of E12.5 kidneys cultured in 1µg/ml Colchicine.

E12.5 kidneys cultured in 1µg/ml Colchicine for 24 hours. Showing kidneys cultured in 1µg/ml Colchicine were smaller and no further growth is seen. Scale bars = 500µm. N=8.

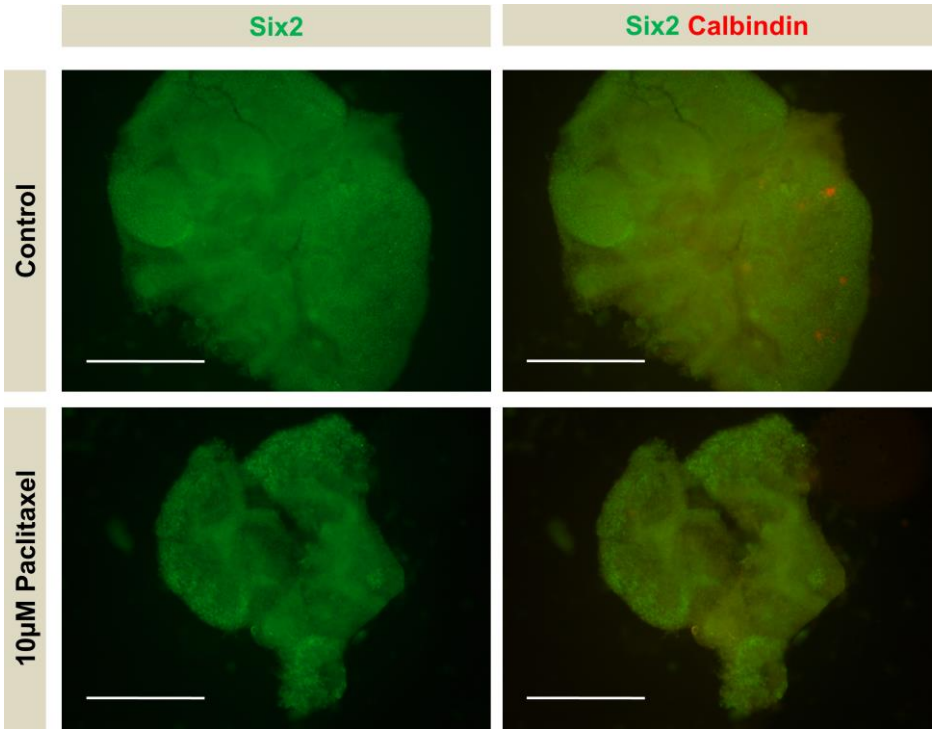



Figure 3.26 – Six2 in E12.5 kidneys cultured in 10µM Paclitaxel.

E12.5 kidneys cultured in 10µM Paclitaxel for 24 hours, fixed and whole mount immunofluorescently labelled with Six2 (green), and Calbindin (red, labelling the ureteric tree). Kidneys cultured in 10µM Paclitaxel still had Six2 (green) present although less compared to the control (no Paclitaxel). Scale bars = 200µm. N=3.

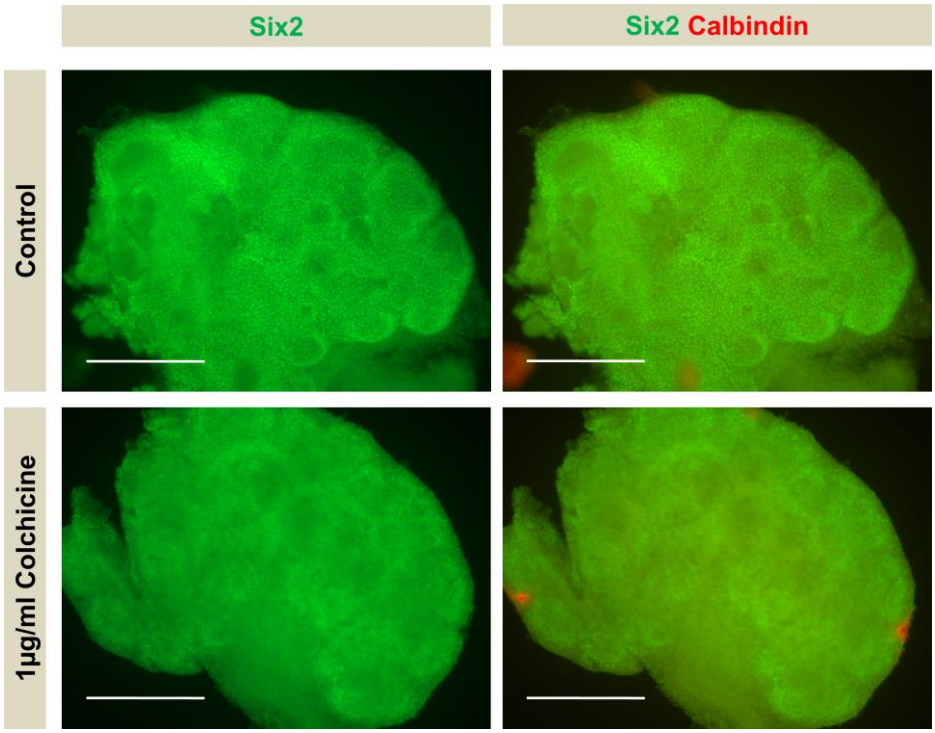



Figure 3.27 – Six2 in E12.5 kidneys cultured in 1µg/ml Colchicine.

E12.5 kidneys cultured in 1µg/ml Colchicine for 24 hours, fixed and whole mount immunofluorescently labelled with Six2 (green), and Calbindin (red, labelling the ureteric tree). Six2 was still present in kidneys cultured in 1µg/ml Colchicine. Scale bars = 200µm. N=2.

## 3.3 – Conclusions

This chapter shows that BMS5 reduces the amount of phosphorylated Cofilin present indicating inhibition of LIMK. This causes severe inhibition of growth, loss of Six2 expression, loss of cells, and prevents progression of mitosis beyond metaphase. The LIMK 1, 2 and phospho-LIMK antibodies were acquired at the end of the project and therefore time constraints meant kidneys cultured in BMS5 could not be immunolabelled with these antibodies.

The act of inhibiting mitosis alone did not replicate the complete loss of Six2 observed with BMS5 because Six2 expression was maintained in kidneys stalled in mitosis with Paclitaxel. The large increase of cells in mitosis in cells cultured in Paclitaxel shows that Paclitaxel, as expected, stalled the cells in mitosis causing them to accumulate at prophase. While cells cultured in BMS5 stalled cells in mitosis, no cells could progress beyond metaphase, there was no large increase in the number of cells in mitosis. The cells could enter mitosis and reach metaphase but instead of staying there, as what happens with Paclitaxel stalling cells at prophase, the cells died via apoptosis due to the observation of a large increase in the number of apoptotic cells after 18 hours (Figure 3.11).

Additionally it was shown that the phosphorylated Cofilin pathway in regulating PLD1 is unlikely to be responsible for the BMS5 phenotype. Phosphorylated Cofilin will activate the PLD1 pathway therefore PLD1 inhibitors were used to see if this pathway was responsible for the inhibition of kidney growth and loss of Six2 seen with BMS5. Both PLD1 inhibitors, FIPI

and Butanol, failed to replicate the reduction in kidney growth and while Six2 expression was diffuse, there was not a complete absence of Six2 staining.

In Figure 3.12 there is a difference in the amount of growth in control kidneys between the FIPI and Butanol experiments, this is due to the natural variation in the size of the kidneys at the time of dissection. The mice were mated overnight and as a result there is some variation in the exact age of the embryos at the time of dissection and culture. All experiments were carried out using contralateral kidneys from the embryos, e.g. one kidney for control, the other for treatment to minimize any variation although between experiments there will be variation in kidney size due to the overnight mating protocol used.

The brightfield images of kidneys cultured in FIPI and Butanol showed the mesenchyme darkening and not the complete loss of integrity seen with BMS5, this would indicate that the lack of phosphorylated Cofilin is unlikely to be the reason why inhibition of LIMK prevents kidney growth and loss of Six2.

This chapter attempted to use an alternative pathway using the SSH activators A23187 and Histamine to induce loss of phosphorylated Cofilin however these treatments did not effectively reduce levels of phosphorylated Cofilin. This is contrary to previously published work suggesting it might be cell type specific or because Wang et al., 2005 used shorter time points to analyse the reduction in Cofilin phosphorylation than we did. Therefore there might have been a reduction in Cofilin phosphorylation in our kidneys but we did not use the correct time points to see any effect. As such this work should be repeated using the same time points as Wang et al., 2005 in our kidneys.

Another method by which a similar end point could be achieved would be by utilising siRNA, but this is difficult as it has been shown before that siRNA does not penetrate far into cultured kidneys (Lee et al., 2008), and therefore it would be difficult to knockdown LIMK throughout the tissue. If an experiment were to have been performed to knockdown LIMK in kidneys then the effect might be different because there would be no LIMK protein present, while when LIMK is pharmacologically inhibited with BMS5 the protein is still present just can't act to phosphorylate Cofilin. Therefore having no protein present might have a different effect compared to the protein being present but having no activity.

Loss of LIMK activity prevents further growth of the kidney, the UB fails to grow and branch, while the MM appears to disintegrate and no renal vesicles are formed. The loss of MM definition cannot be completely attributed to the inhibition of mitosis seen with BMS5 administration as both paclitaxel and colchicine did not show the same disintegration of mesenchyme. Inhibition of LIMK results not only a decrease in growth and disintegration of the mesenchyme but also a large increase in apoptosis. Inhibition of LIMK activity causes cell death in addition to prevention of completion of mitosis. These two events may or may not be linked, i.e. the inhibition of mitosis by inhibition of LIMK causes the cells to die or the inhibition of LIMK causes the stalling of cells during mitosis and causes them to die but independently. In the second of these LIMK would have two separate effects, one during mitosis and another through a separate mechanism, possibly due to LIMK's role in cell migration.

Inhibition of LIMK results in the inhibition of mitosis in MM cells, although LIMK also has a role in cell migration. If cell migration take place in the MM then LIMK might be involved in both mitosis and cell migration during kidney development. Chapter 4 will investigate how LIMK prevents the completion of mitosis while chapter 5 will look at cell migration in the MM.

# Chapter 4: The effect of LIMK inhibition during the cell cycle in HK2 cells.

## 4.1 – Introduction

Progression through mitosis in embryonic kidneys is prevented by LIMK inhibition (see 3.2.3) therefore the role of LIMK during the cell cycle was examined in cultured human kidney cells (HK2 cells).

It is known that the LIMK mediated Cofilin phosphorylation is required for mitosis completion, Kaji et al. (2008) showed that knockdown of LIMK prevented normal spindle orientation due to an unstable actin cytoskeleton around the edge of the cell and hindered anaphase onset. However while relatively normal spindles formed they were misaligned. This would suggest that while Cofilin phosphorylation is needed for correct mitosis completion it is not producing the same effect that was shown in kidneys in chapter 3, specifically no progression beyond metaphase was shown (Figure 3.10).

Knockdown by siRNA of LIMK1 and LIMK2 has shown the generation of multiple pericentrin clumps and α-tubulin spindles which were outside the DNA compartment and crucially Heng et al. (2012) state that “cells treated with LIMK siRNAs do undergo cytokinesis” (Heng et al., 2012). In chapter 3 it was shown that inhibition of LIMK with BMS5 prevented the completion of mitosis contrary to the results with siRNA of LIMK1 and LIMK2 show. This would suggest that if you knockout LIMK1 and LIMK2 in a mouse then the mouse would not be viable as no cells could complete division and replicate. This was not the case when Meng et al. (2004) created a LIMK1 and LIMK2

double knockout mouse to look at synaptic function in the brain. They successfully created a viable mouse, though they did not mention any renal abnormalities. They created the knockout mice by removing a LIM domain and part of the PDZ domain however the kinase domain was untouched (Meng et al., 2002; Takahashi et al., 2002). Therefore if a resultant protein is produced then this would still have kinase activity, which calls into question whether these are full knockouts with zero LIMK activity (Bernard, 2007). The kinase domain would have to be deleted in knockout mice for any concrete conclusions to be drawn.

How the inhibition of LIMK prevents the completion of mitosis and induces cell death is unknown, various groups have shown loss of LIMK results in a slowing of progression through mitosis but none showed prevention of mitosis completion or cell death as a result. In this chapter human kidney (HK2) cells were used along with a number of other cell types (C2C12, HEPG2, 3T3) to look at the effects of inhibiting LIMK activity on mitosis progression. Proteins involved in the process of mitosis were labelled with antibodies to visualise what, if any, effects LIMK inhibition had on these proteins. By looking at how the mitotic machinery is affected by LIMK inhibition and other potential pathways or targets of LIMK this chapter will elucidate how the inhibition of LIMK results in the prevention of mitosis completion.

# 4.2 – Results

## 4.2.1 – BMS5 inhibits Cofilin phosphorylation

To confirm that BMS5 does inhibit LIMK and therefore Cofilin phosphorylation in HK2 cells, cells were grown in the presence or absence of BMS5 and immunofluorescently labelled for phosphorylated Cofilin, there was some loss of phosphorylated Cofilin at 10µM and near complete loss at 50µM (Figure 4.1).

LIMK1 and LIMK2 proteins were observed to be present and active (pLIMK1/2, arrows in Figure 4.2) in HK2 cells (n=2, Figure 4.2). TESK1 and TESK2 also phosphorylate Cofilin (Toshima et al., 2001a; Toshima et al., 2001b) and were observed in HK2 cells (Figure 4.3, n=1). This indicates that even after inhibiting both LIMK1 and LIMK2 by BMS5 there might still be some Cofilin phosphorylation by TESK's that could happen in HK2 cells. This work observing LIMK1, LIMK2, TESK1, and TESK2 in HK2 cells needs to be confirmed by repeating and increasing the n numbers.

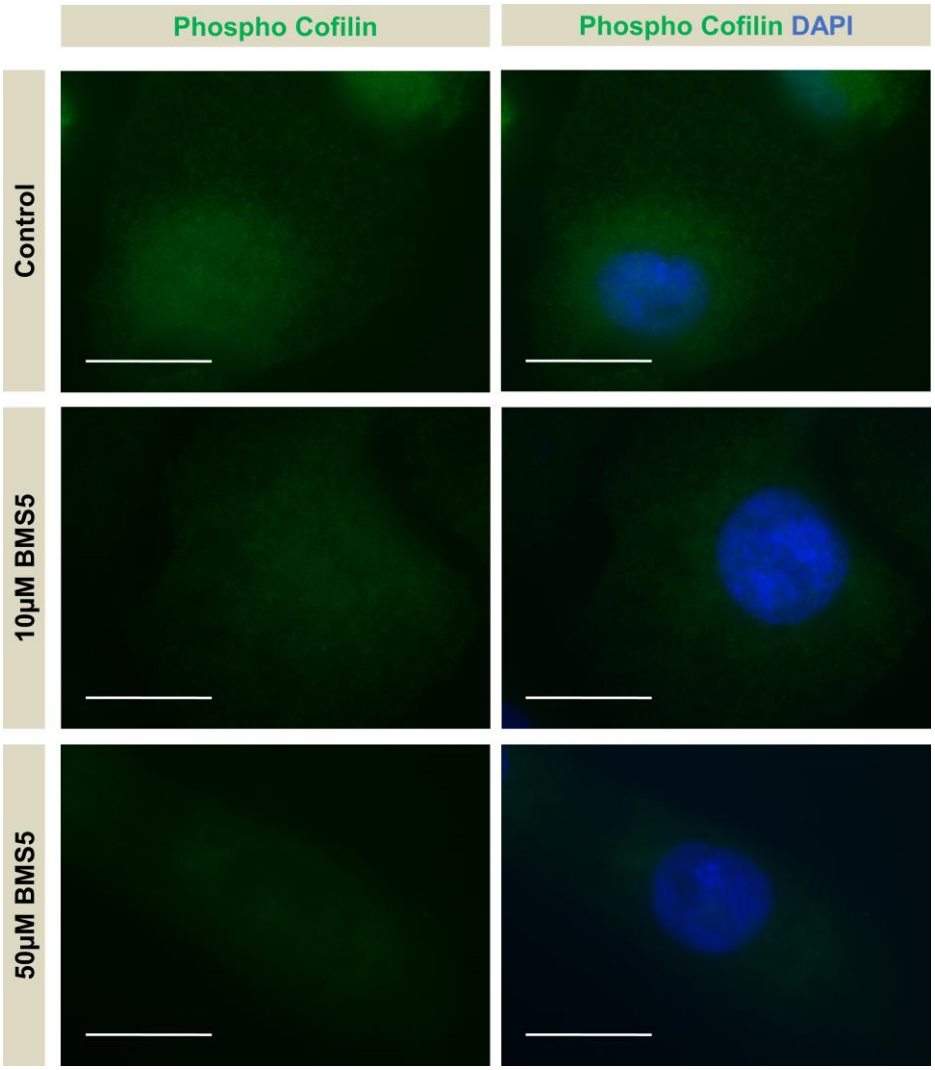



Figure 4.1 – Phosphorylated Cofilin in HK2 cells cultured in 10µM and 50µM BMS5.

HK2 cells cultured in BMS5 for 24 hours, fixed and immunofluorescently labelled with phosphorylated Cofilin (green) and DAPI (blue). Phosphorylated Cofilin (green) is present in the control, slightly less in 10µM BMS5 treated cells, and not present in 50µM BMS5 treated cells. Scale bars = 10µm.

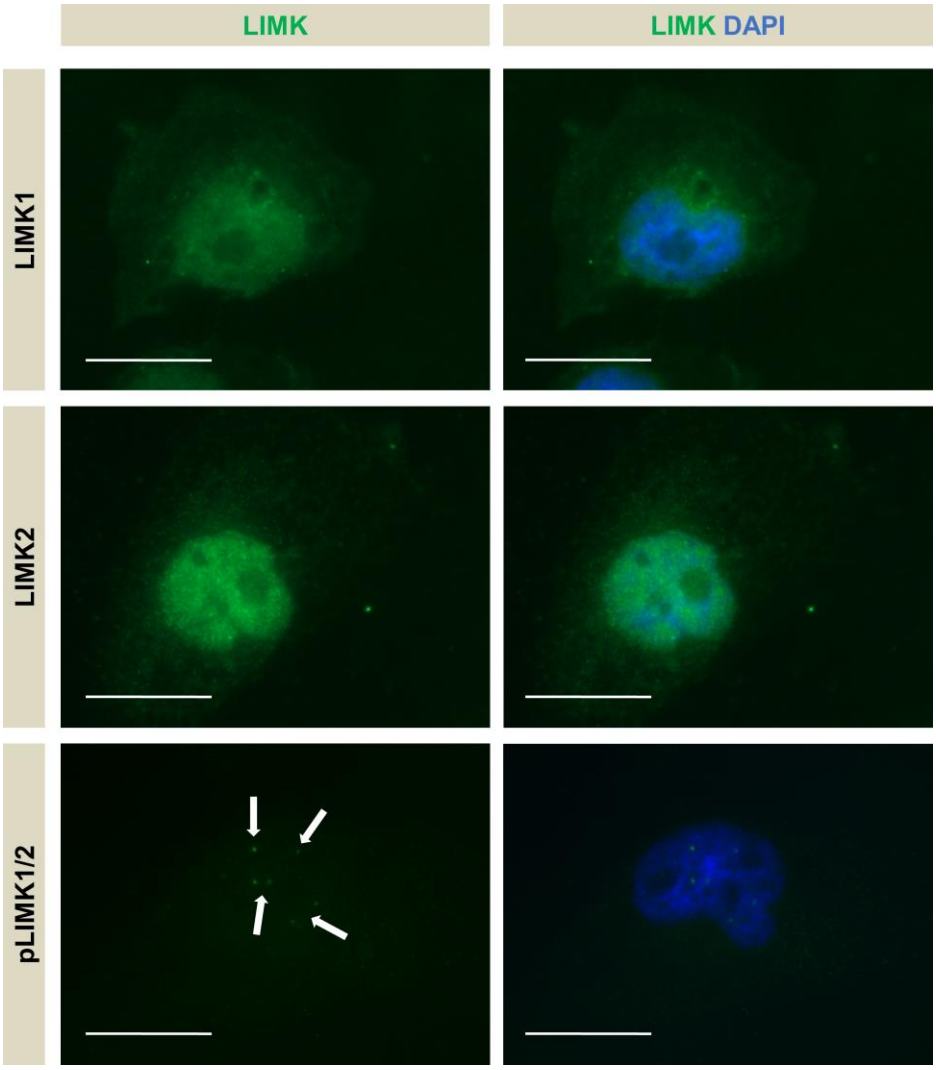



Figure 4.2 – LIMK1, LIMK2, and pLIMK1/2 in cultured HK2 cells.

HK2 cells cultured for 24 hours, fixed and immunofluorescently labelled with LIMK1, LIMK2 and pLIMK1/2 (green, arrows indicating small regions of green staining) and DAPI (blue). LIMK1, LIMK2 and the active form, pLIMK1/2 (arrows), are present in HK2 cells. Scale bars = 10µm.

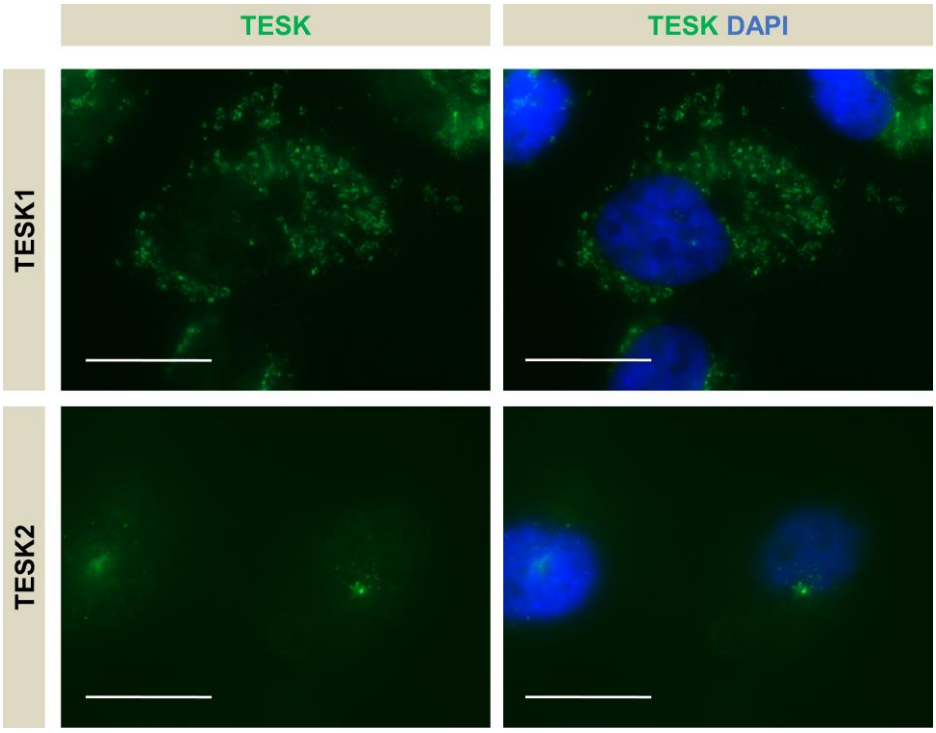



Figure 4.3 – TESK1 and TESK2 in cultured HK2 cells.

HK2 cells cultured for 24 hours, fixed and immunofluorescently labelled with TESK1 and TESK2 (green) and DAPI (blue). TESK1 and TESK2 are observed in HK2 cells. Scale bars = 10µm.

## 4.2.2 – BMS5 inhibits completion of mitosis

When cells were cultured in the presence of BMS5 it was observed that there were fewer cells after culturing in BMS5 compared to the controls. After 24 hours in culture in 10μM BMS5 there were 50.2% fewer cells than controls ($p=0.0001$) and 83.6% fewer cells with 50μM BMS5 ($p<0.001$) compared to controls (n=4, Figure 4.4). Cell counts from time 0, 24 hours and 48 hours of treatment with two way ANOVA with Tukey post-hoc analysis revealed a significant increase in the number of cells in the control ($p<0.0001$) over 48 hours, and no significant change in cells cultured in 10μM BMS5 ($p=0.17$) although there was a significant decrease in the number of cells in cells cultured in 50μM BMS5 indicating that the cells were dying (time 0 = 20781 cells ± 1260, time 48 hours = 5781 cells ± 1033, $p<0.0001$, n=4, Figure 4.5). There were also significant differences at both 24 hours and 48 hours between control group and cells treated with 10μM BMS5 and between control and cells treated with 50μM BMS5 ($p<0.0001$) with fewer cells being present in the BMS5 cultures.

To determine whether BMS5 affects only cells during mitosis, HK2 cells were grown to confluence and counted cells after treatment with BMS5. HK2 cells at confluence grew much more slowly and therefore had fewer cells in mitosis. After 24 hours treatment, control cultures had 540625 cells ± 9544, cultures treated with 10μM BMS5 had 511875 cells ± 6804 ($p=0.11$), and cultures treated with 50μM BMS5 had 528281 cells ± 9817 ($p=0.60$, n=4, Figure 4.6). The decrease in cell number only occurred in populations of cells that were undergoing mitosis. In addition this also shows that BMS5 at both concentrations is not toxic to all cells and seems to be having a specific effect

during mitosis. This phenotype was also tested in HEPG2 cells, sub confluent cells were treated for 24 hours. Cells cultured in control media had 877344 cells ± 43217, cells treated with 10μM BMS5 had 592969 cells ± 25629 ($p=0.0004$), and cells treated with 50μM BMS5 had 525000 cells ± 24154 ($p<0.0001$, $n=4$, Figure 4.7). The same cell number decrease with increasing BMS5 concentration occurs in other cells types.

To confirm that BMS5 only affects cells undergoing mitosis, C2C12 cells were grown to 60% confluence and 100% confluence and cell counts were performed after 24 hours treatment with 10μM and 50μM BMS5. Sub confluent (60%) control C2C12 cultures had 404375 cells ± 18767, cultures treated with 10μM BMS5 had 102813 cells ± 5306 ($p<0.0001$), and cultures treated with 50μM had only 93698 cells ± 10633 ($p<0.0001$, $n=4$). Confluent C2C12 cells do not show any significant difference with control cell cultures containing 419115 cells ± 51070, cultures treated with 10μM had 372135 cells ± 35853 ($p=0.78$), and cultures treated with 50μM had 366510 cells ± 57279 ($p=0.74$, $n=4$, Figure 4.8). This further validates the conclusion that BMS5 only caused cells to die when they were undergoing mitosis.

A Trypan blue assay was carried out on BMS5 treated HK2 cells. This assay measures membrane integrity, cells which have damaged membranes can uptake the Trypan blue dye into the cytoplasm, while those which have intact membranes exclude the dye. Therefore cells which uptake the dye have damaged membranes, which is indicative of cell death. After 24 hours there were 7.15% ± 0.25 non-viable cells in the control cultures, 14.87% ± 1.93 ($p=0.054$) in 10μM BMS5 treated cultures, and 43.32% ± 2.47 ($p<0.0001$,

n=3) non-viable cells in 50µM BMS5 treated cultures. This shows that the cells that were being lost were dying (Figure 4.9).

An MTT assay was performed to determine the toxicity of the BMS5 inhibitor by measuring mitochondrial activity. The MTT assay measures how much MTT is converted to insoluble formazan (purple) by the mitochondria which is solubilized by DMSO and measured on a spectrophotometer. Cells were cultured to sub-confluence and confluence levels with and without increasing concentrations of BMS5, then the MTT reaction was performed.

Compared to control cells, cells treated with 3µM, 10µM, 25µM, 50µM and 100µM BMS5 all showed significant reduction in mitochondrial activity in sub confluent cells (Figure 4.10, Table 4.1), whereas when the cells were grown to confluence only cells treated with 25µM, 50µM and 100µM BMS5 showed a significant reduction in mitochondrial activity (Figure 4.11, Table 4.2). Although this is a useful measure for cell activity it does not preclude the possibility that LIMK inhibition might affect mitochondrial activity, which would explain the reduction of activity in confluent and hence non-dividing cells. When looking at the amount of percentage reduction in activity, sub confluent cells cultured in 50µM BMS5 showed a 73% reduction in mitochondrial activity whereas confluent cells cultured in 50µM BMS5 only showed a 53% reduction, implying less of an effect in confluent cells.

As histones become phosphorylated during mitosis it is possible to visualise the condensation of the chromosomes and progression through alignment on the metaphase plate to the separation of sister chromatids. A phosphorylated Histone3 antibody (pH3) was used to look at this progression through mitosis.

HK2 cells cultured in BMS5 were immunofluorescently labelled with an anti-pH3 antibody, and the percentage of mitotic cells in anaphase were counted. 13.6% ± 2.1 of mitotic cells were in anaphase in the control cultures, 1.39% ± 1.39 of mitotic cells were in anaphase in cultures treated with 10μM BMS5 ($p=0.0025$), and 0% ± 0 in cultures treated with 50μM BMS5 ($p=0.0014$, $n=3$, Figure 4.12). The total number of cells in mitosis per an average field of view was unaffected, with 60.7 ± 19.7 cells in mitosis in control cultures, 38.3 ± 5.8 cells in cultures treated with 10μM BMS5 ($p=0.56$), and 63 ± 15.1 cells in cultures treated with 50μM BMS5 ($p=0.99$, $n=3$).

BMS5 treated cells also showed cytoskeletal abnormalities with the Actin cytoskeleton being severely affected in both interphase cells and mitotic cells. Cells treated with BMS5 showed a loss of stress fibres and circular actin structures forming in interphase cells (boxes; 10μM BMS5 with circle showing less stress fibres), while mitotic cells showed a less severe phenotype (arrows) as no stress fibres were normally seen in mitotic cells (Figure 4.13).

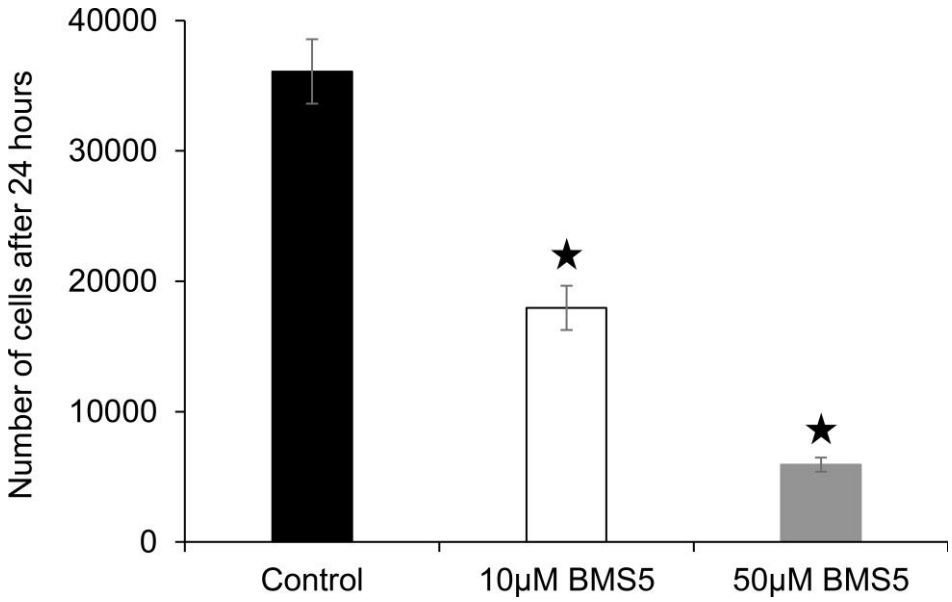



Figure 4.4 – Cell counts on HK2 cells cultured in 10μM and 50μM BMS5.

Graph showing a cell count from HK2 cells cultured in 10μm and 50μM BMS5 for 24 hours. After 24 hours in culture in 10μM BMS5 there are 50.2% fewer cells than controls ($p=0.0001$) and 83.6% fewer cells with 50μM BMS5 ($p<0.001$) compared to controls ($n=4$). * $p<0.001$ compared to control.

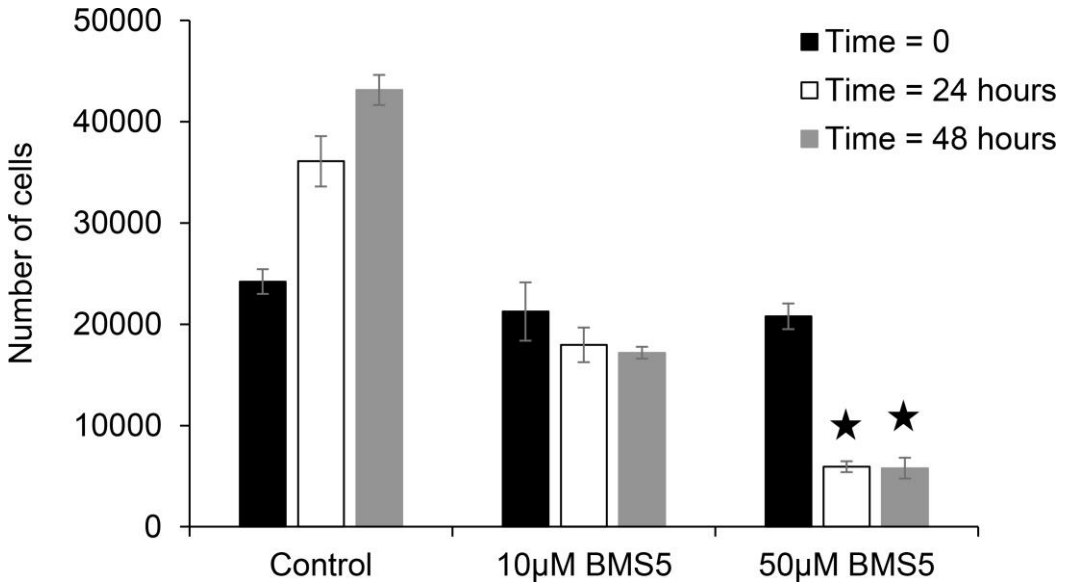



Figure 4.5 – Cell counts on HK2 cells cultured in 10μM and 50μM BMS5 at 0 hours, 24 hours, and 48 hours.

Graph showing cell counts from HK2 cells cultured in 10μm and 50μM BMS5 for 0 hours, 24 hours and 48 hours. No significant change in cells cultured in 10μM BMS5 ($p=0.17$). Cells cultured in 50μM BMS5 showed a significant decrease in the number of cells over time; time 0 = 20781 cells ± 1260, time 48 hours = 5781 cells ± 1033, $p<0.0001$, $n=4$).

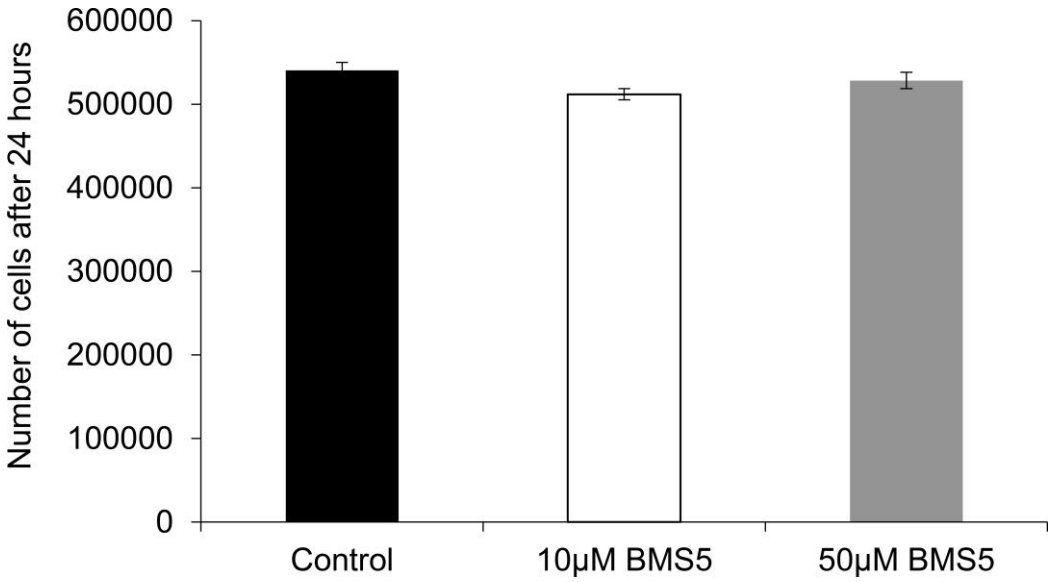



Figure 4.6 – Cell counts on confluent HK2 cells cultured in 10µM and 50µM BMS5.

Graph showing a cell count from confluent HK2 cells cultured in 10µm and 50µM BMS5 for 24 hours. Control cultures had 540625 cells ± 9544, cultures treated with 10µM BMS5 had 511875 cells ± 6804 (p=0.11), and cultures treated with 50µM BMS5 had 528281 cells ± 9817 (p=0.60, n=4).

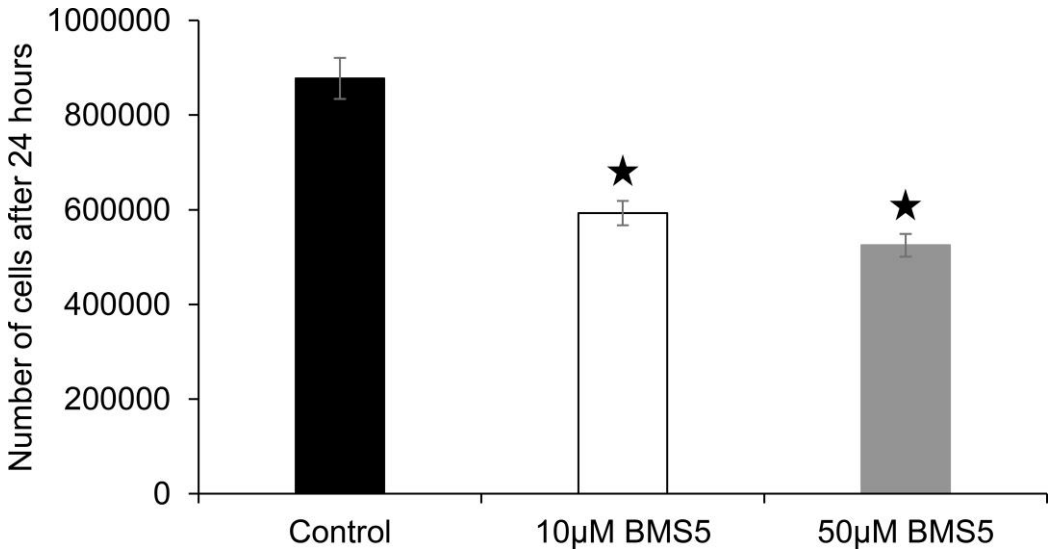



Figure 4.7 – Cell counts on HEPG2 cells cultured in 10μM and 50μM BMS5.

Graph showing a cell count from HEPG2 cells cultured in 10μm and 50μM BMS5 for 24 hours. Cells cultured in control media had 877344 cells ± 43217, cells treated with 10μM BMS5 had 592969 cells ± 25629 ($p=0.0004$), and cells treated with 50μM BMS5 had 525000 cells ± 24154 ($p<0.0001$, $n=4$). * $p<0.001$ compared to control.

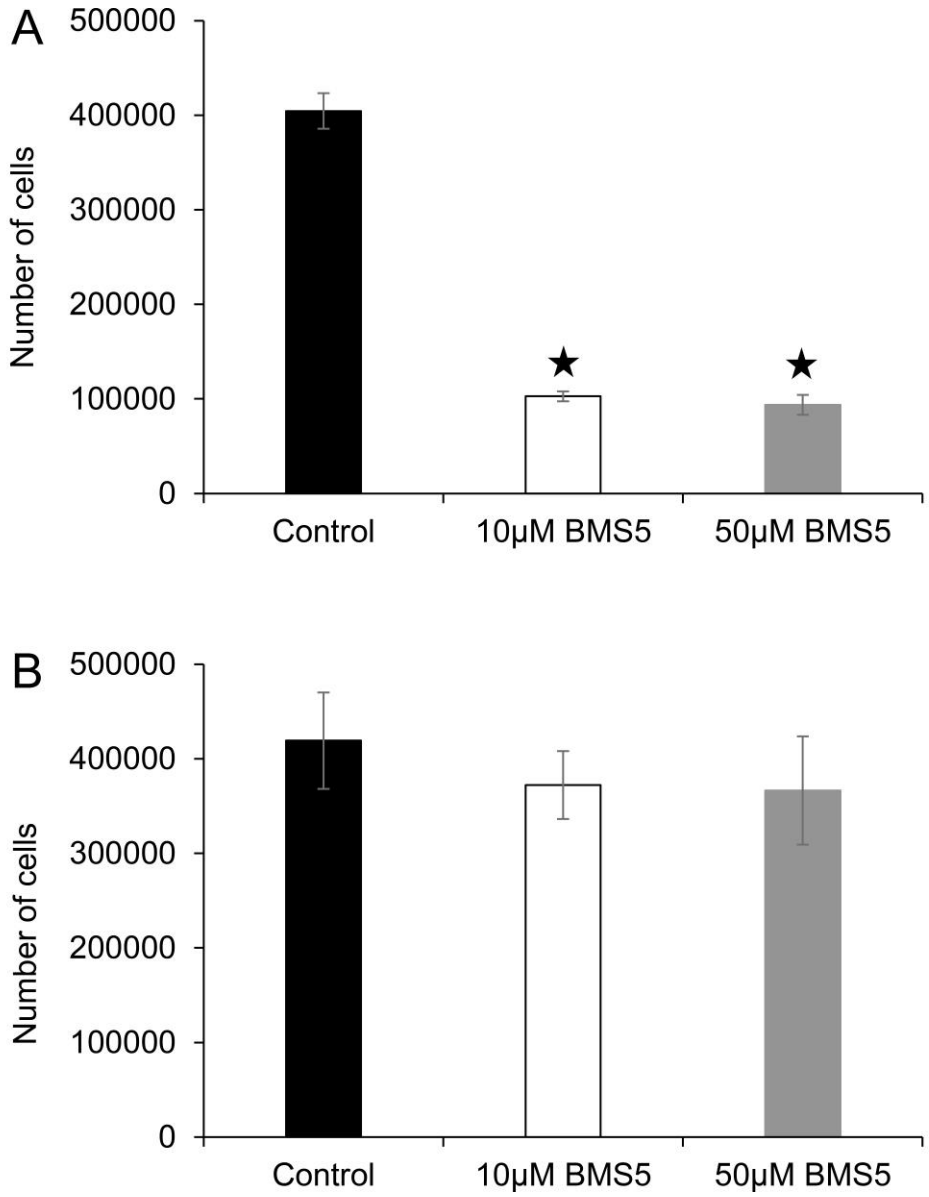



Figure 4.8 – Cell counts on sub confluent and confluent C2C12 cells cultured in 10μM and 50μM BMS5.

Graphs showing a cell count from sub-confluent (A) and confluent (B) C2C12 cells cultured in 10μm and 50μM BMS5 for 24 hours. (A) Sub confluent (60%) control C2C12 cultures had 404375 cells ± 18767, cultures treated with 10μM BMS5 had 102813 cells ± 5306 ($p<0.0001$), and cultures treated with 50μM had only 93698 cells ± 10633 ($p<0.0001$, $n=4$). (B) Confluent C2C12 cells do not show any significant difference with control cell cultures containing

419115 cells ± 51070, cultures treated with 10µM had 372135 cells ± 35853 (p=0.78), and cultures treated with 50µM had 366510 cells ± 57279 (p=0.74, n=4). * p<0.0001 compared to control.

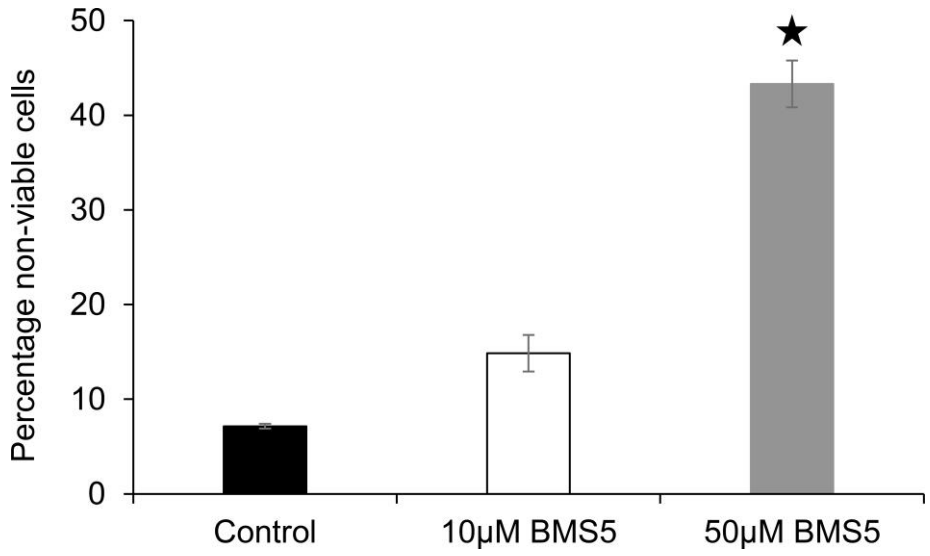



Figure 4.9 – Trypan blue assay on HK2 cells cultured in 10µM and 50µM BMS5.

Graph showing a Trypan blue assay on HK2 cells cultured in 10µm and 50µM BMS5 for 24 hours, showing the percentage of non-viable cells. After 24 hours there were 7.15% ± 0.25 non-viable cells in the control cultures, 14.87% ± 1.93 (p=0.054) in 10µM BMS5 treated cultures, and 43.32% ± 2.47 (p<0.0001, n=3) non-viable cells in 50µM BMS5 treated cultures. * p<0.0001 compared to control.

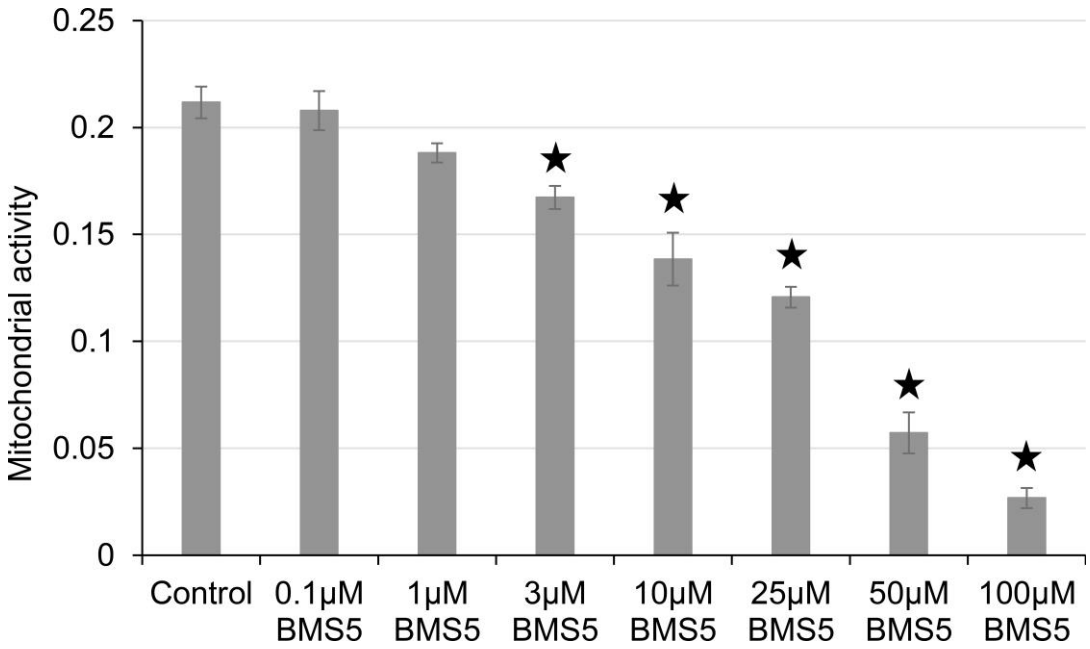



Figure 4.10 – MTT assay on HK2 cells cultured in BMS5.

HK2 sub confluent cells grown in BMS5 for 24 hours and an MTT assay performed. Showing a significant reduction in mitochondrial activity in cells cultured in 3μM, 10μM, 25μM, 50μM, and 100μM BMS5. * p<0.01 compared to control. N=3.

| BMS5 | Average | SEM | p |
|---|---|---|---|
| **Control** | 0.21 | 0.0075 | |
| **0.1μM BMS5** | 0.21 | 0.0091 | >0.9999 |
| **1μM BMS5** | 0.19 | 0.0044 | 0.42 |
| **3μM BMS5** | 0.17 | 0.0054 | 0.016 |
| **10μM BMS5** | 0.14 | 0.012 | 0.0001 |
| **25μM BMS5** | 0.12 | 0.0049 | <0.0001 |
| **50μM BMS5** | 0.057 | 0.0096 | <0.0001 |
| **100μM BMS5** | 0.027 | 0.0047 | <0.0001 |

Table 4.1 – MTT assay on HK2 sub confluent cells.

HK2 sub confluent cells grown in BMS5 for 24 hours and an MTT assay performed. Showing a significant reduction in mitochondrial activity in cells cultured in 3µM, 10µM, 25µM, 50µM, and 100µM BMS5. p=relative to control. SEM = standard error of the mean. 2 significant figures. N=3.

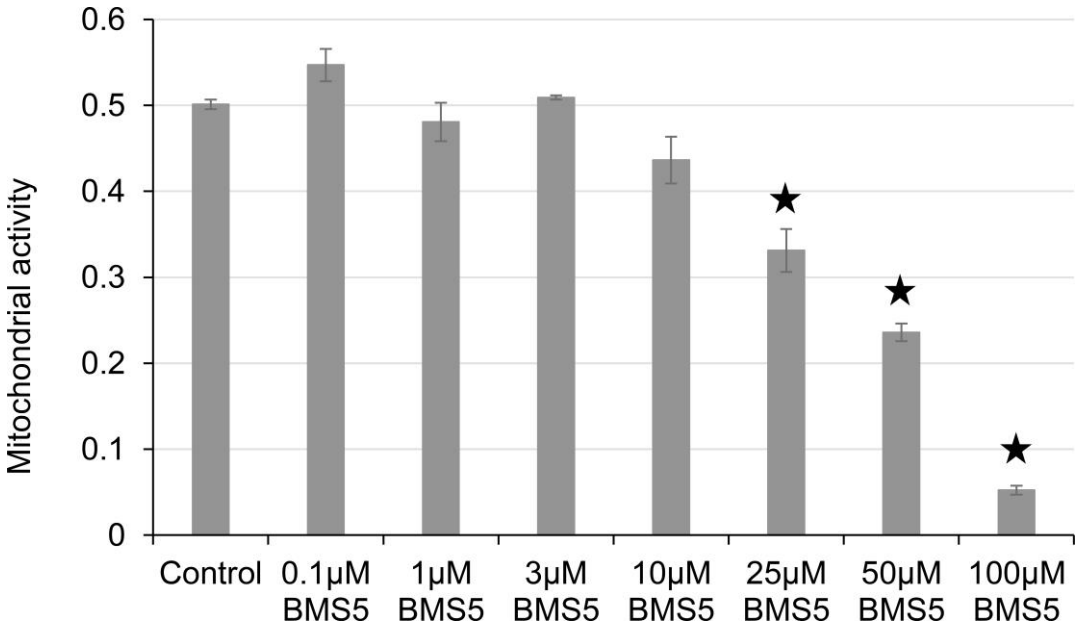



Figure 4.11 – MTT assay on confluent HK2 cells cultured in BMS5.

HK2 confluent cells grown in BMS5 for 24 hours and an MTT assay performed. Showing a significant reduction in mitochondrial activity in cells cultured in 25µM, 50µM, and 100µM BMS5. * $p<0.01$ compared to control. N=3.

| BMS5 | Average | SEM | p |
|---|---|---|---|
| **Control** | 0.50 | 0.0056 | |
| **0.1µM BMS5** | 0.55 | 0.019 | 0.59 |
| **1µM BMS5** | 0.48 | 0.022 | 0.99 |
| **3µM BMS5** | 0.51 | 0.0024 | >0.9999 |
| **10µM BMS5** | 0.44 | 0.027 | 0.21 |
| **25µM BMS5** | 0.33 | 0.025 | <0.0001 |
| **50µM BMS5** | 0.24 | 0.010 | <0.0001 |
| **100µM BMS5** | 0.052 | 0.0052 | <0.0001 |

Table 4.2 – MTT assay on HK2 confluent cells.

HK2 confluent cells grown in BMS5 for 24 hours and an MTT assay performed. Showing a significant reduction in mitochondrial activity in cells cultured in 25µM, 50µM, and 100µM BMS5. p=relative to control. SEM = standard error of the mean. 2 significant figures. N=3.

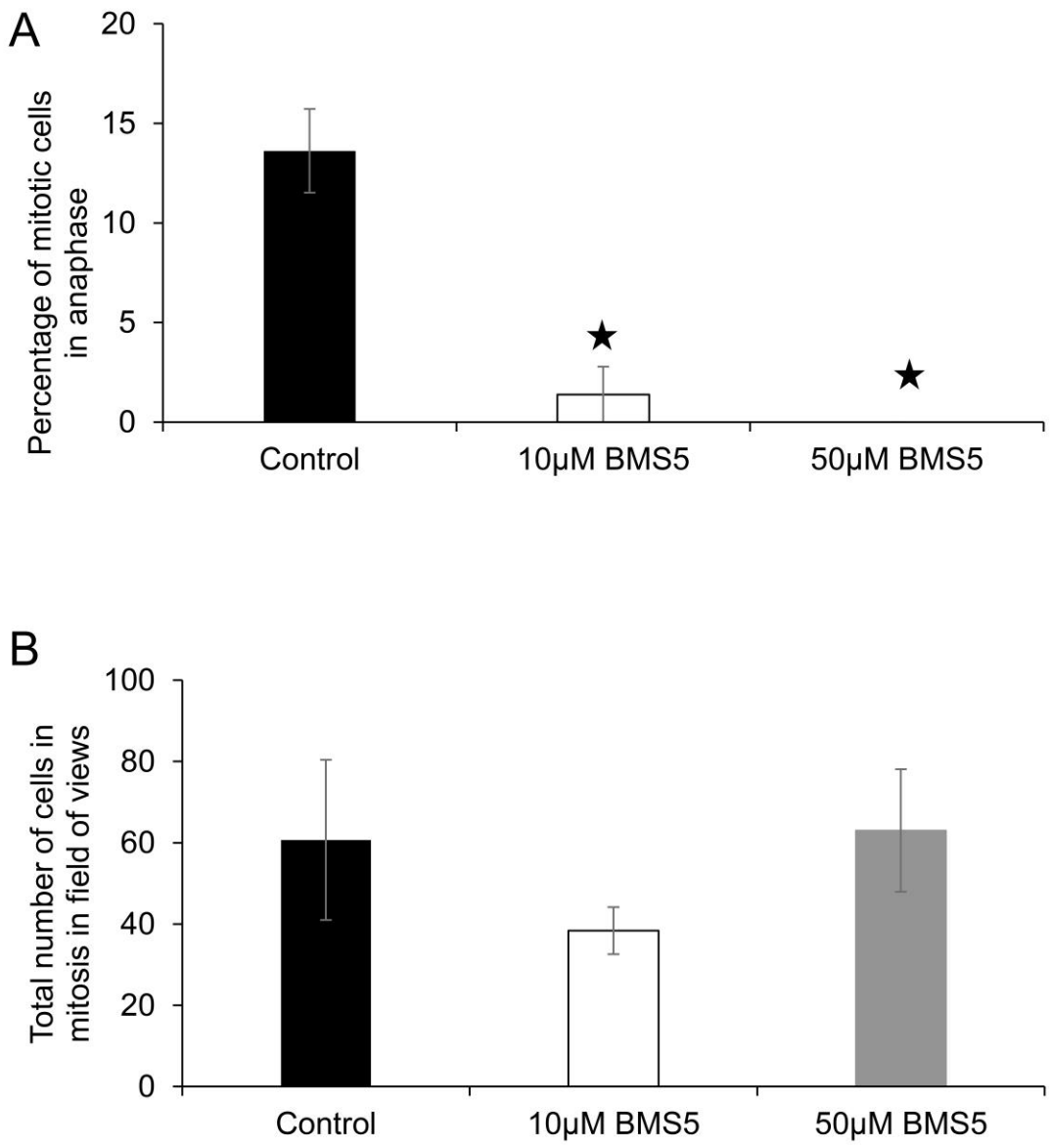



Figure 4.12 – Mitosis analysis on HK2 cells cultured in 10μM and 50μM BMS5.

Graphs showing HK2 cells cultured in 10μM and 50μM BMS5 for 24 hours, fixed and immunofluorescently labelled with pH3. (A) Percentage of mitotic cells in anaphase. 13.6% ± 2.1 of mitotic cells were in anaphase in the control cultures, 1.39% ± 1.39 of mitotic cells were in anaphase in cultures treated with 10μM BMS5 (p=0.0025), and 0% ± 0 in cultures treated with 50μM BMS5 (p=0.0014, n=3, Figure 4.12). (B) Total number of cells in mitosis in field of

views. The total number of cells in mitosis per an average field of view was unaffected, 60.7 ± 19.7 cells in mitosis in control cultures, 38.3 ± 5.8 cells in cultures treated with 10μM BMS5 ($p=0.56$), and 63 ± 15.1 cells in cultures treated with 50μM BMS5 ($p=0.99$, $n=3$). * $p<0.01$ compared to control.

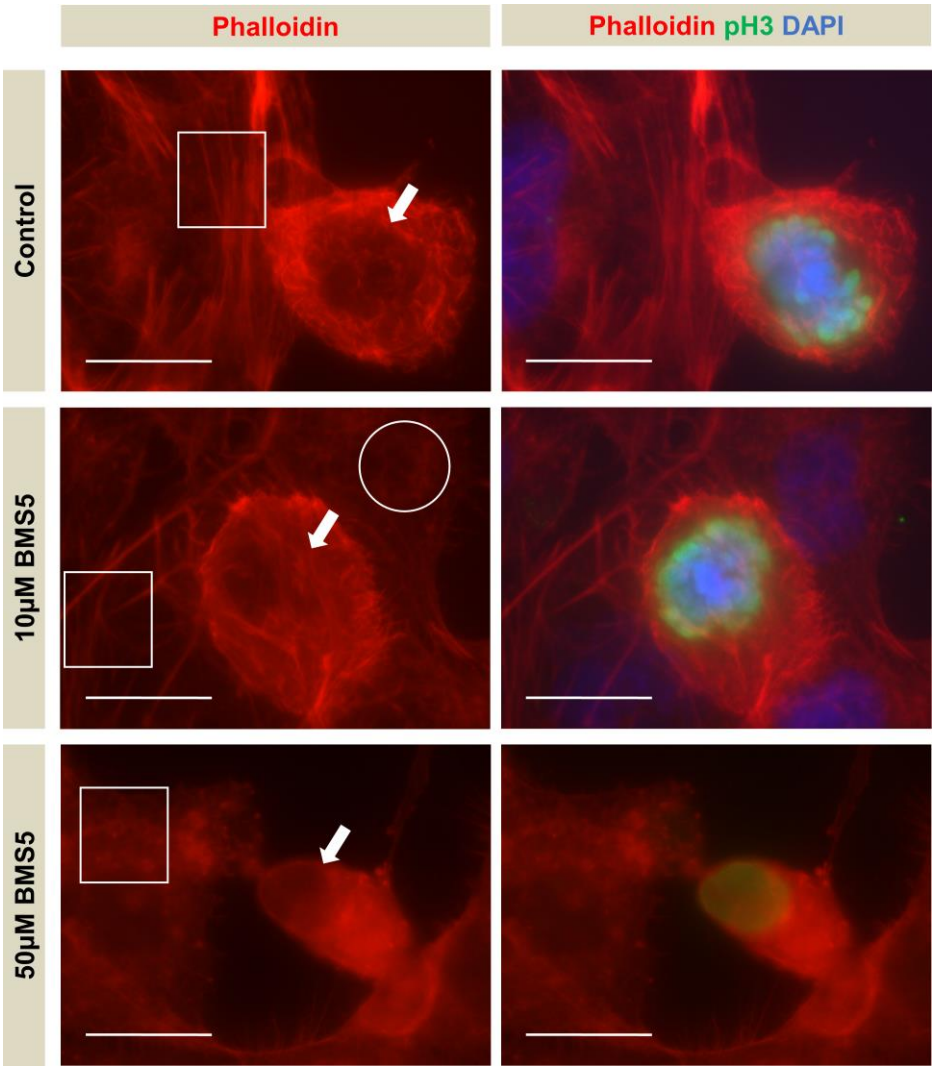



Figure 4.13 – Phalloidin and pH3 in HK2 cells cultured in 10µM and 50µM BMS5.

HK2 cells cultured in BMS5 for 24 hours, fixed and immunofluorescently labelled with Phalloidin (red), pH3 (green), and DAPI (blue). Boxes showing loss of stress fibres in interphase cells with increasing concentration of BMS5, circle showing some loss of stress fibres at 10µM BMS5 in an interphase cell, arrows showing mitotic cells. This was repeated 3 times (n=3) and the same results (loss of stress fibres with increasing concentration of BMS5) was observed in all 3 cultures. Scale bars = 10µm.

## 4.2.3 – BMS5 prevents spindle formation

BMS5 inhibited progression through mitosis by preventing the cells from reaching anaphase, therefore the formation of the mitotic spindle that will pull apart the chromosomes was investigated, cells were cultured in BMS5 and were immunofluorescently labelled with the spindle fibre component of the mitotic spindle, α-tubulin. When cells were cultured in 10μM and 50μM BMS5 the mitotic spindle failed to form and multiple α-tubulin foci were observed (arrows) located within the same space as the DNA (DAPI, blue, Figure 4.14). In BMS5 treated interphase cells, α-tubulin localisation appeared normal (Figure 4.15), indicating that BMS5 had no effect on α-tubulin in non-mitotic cells. This strongly implies that BMS5 caused the mitotic spindle to fail to form completely and was localised in the DNA compartment rather than the cytoplasm at the poles of the cell. In addition only 2 spindles per cell should form, not the multiple α-tubulin foci observed with culturing HK2 cells in BMS5. This inhibition of the mitotic spindle formation would be a possible reason as to why the cells could not complete mitosis; if the mitotic spindle fails to form then the chromosomes could not be pulled apart and therefore anaphase could not have occurred.

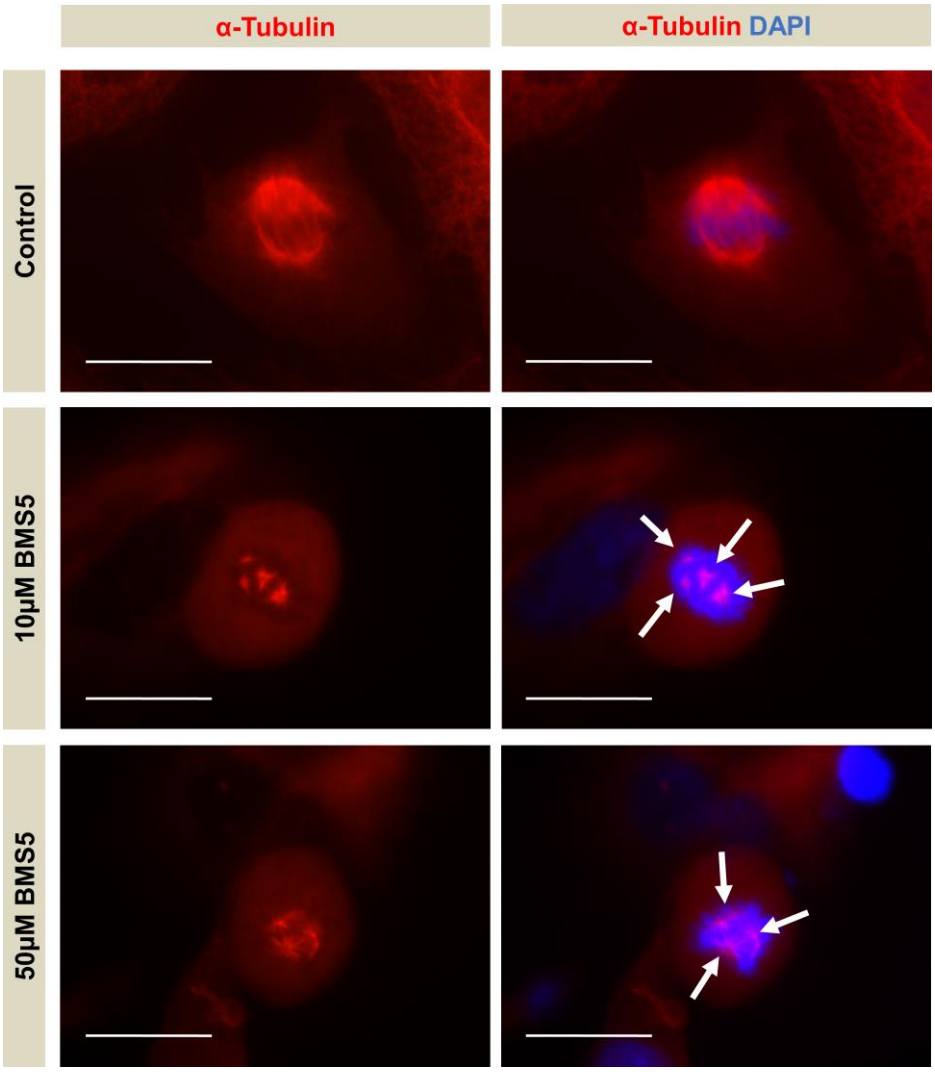



Figure 4.14 – α-tubulin in HK2 cells cultured in 10μM and 50μM BMS5.

HK2 cells in mitosis cultured in BMS5 for 24 hours, fixed and immunofluorescently labelled with α-tubulin (red) and DAPI (blue). Arrows in cells cultured in 10μM and 50μM BMS5 show α-tubulin foci present in these cells. Scale bars = 10μm. N=3.

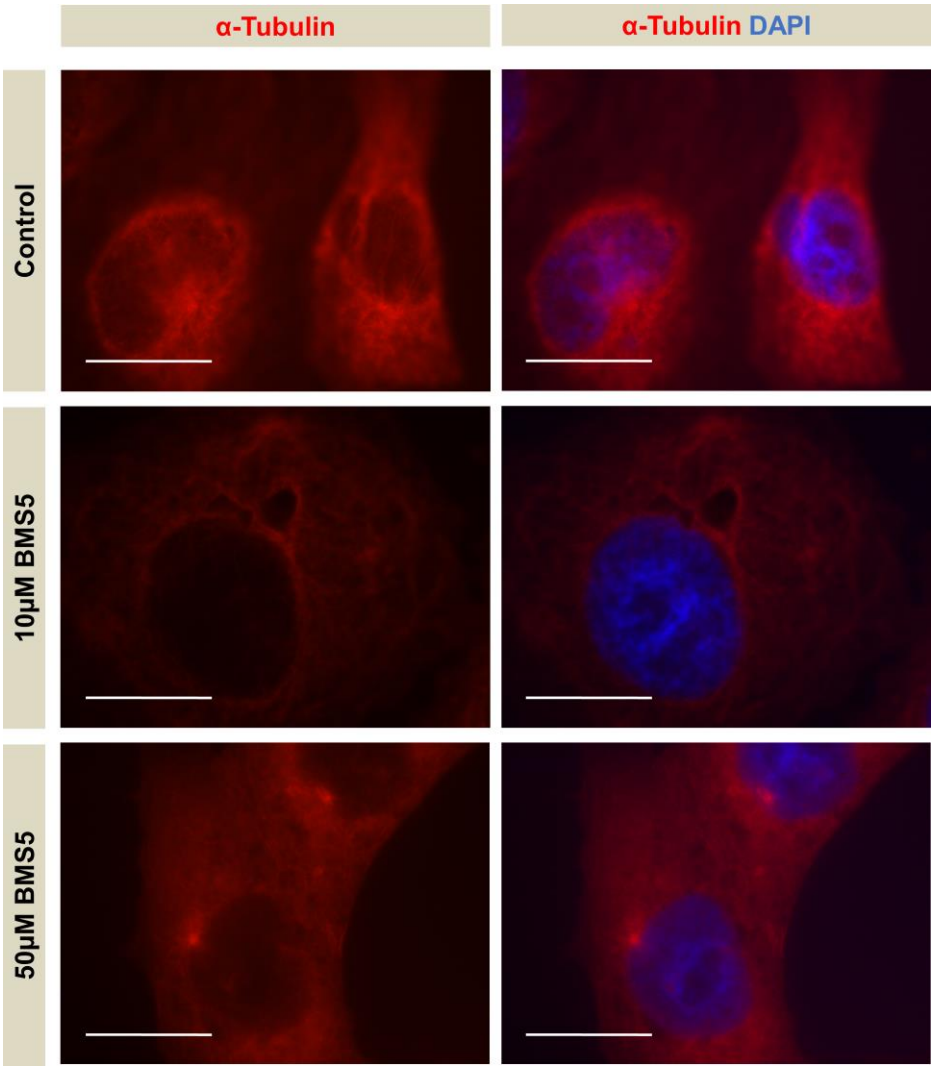



Figure 4.15 – α-tubulin in HK2 cells cultured in 10μM and 50μM BMS5 (interphase).

HK2 cells in interphase cultured in BMS5 for 24 hours, fixed and immunofluorescently labelled with α-tubulin (red) and DAPI (blue). No difference in α-tubulin (red) is observed between cells cultured in control media, or 10μM, or 50μM BMS5. Scale bars = 10μm. N=3.

### 4.2.4 – BMS5 has no effect on the degradation of the nuclear lamina or Securin

The mitotic spindle fails to form in cells cultured in BMS5, therefore it was investigated to see if a critical step (whether the nuclear lamina could be degraded) before metaphase and anaphase might be affected by BMS5. If the nuclear lamina could not be degraded then there would be a physical barrier (the nuclear lamina) to the spindle fibres attaching to the chromosomes. Cells were immunofluorescently labelled for Lamin A (a component of the nuclear lamina, which degrades at prophase and becomes dispersed throughout the cytoplasm). Lamin A was dispersed and broken down in BMS5 treated cells, showing no observable differences to control cells during mitosis (Figure 4.16).

Securin inhibits Separase, which cleaves the cohesin complex that holds together the chromatids before anaphase. Therefore Securin localisation was examined to see if it was affected by LIMK inhibition. There was no difference in mitotic cells treated with BMS5 at 10μM or 50μM or in interphase cells, with Securin localised in the DNA compartment in mitotic cells and not in the interphase cells (Figure 4.17). This indicates that BMS5 treated cells can still break down the nuclear lamina and they have Securin localised in the correct sub cellular location ready for anaphase.

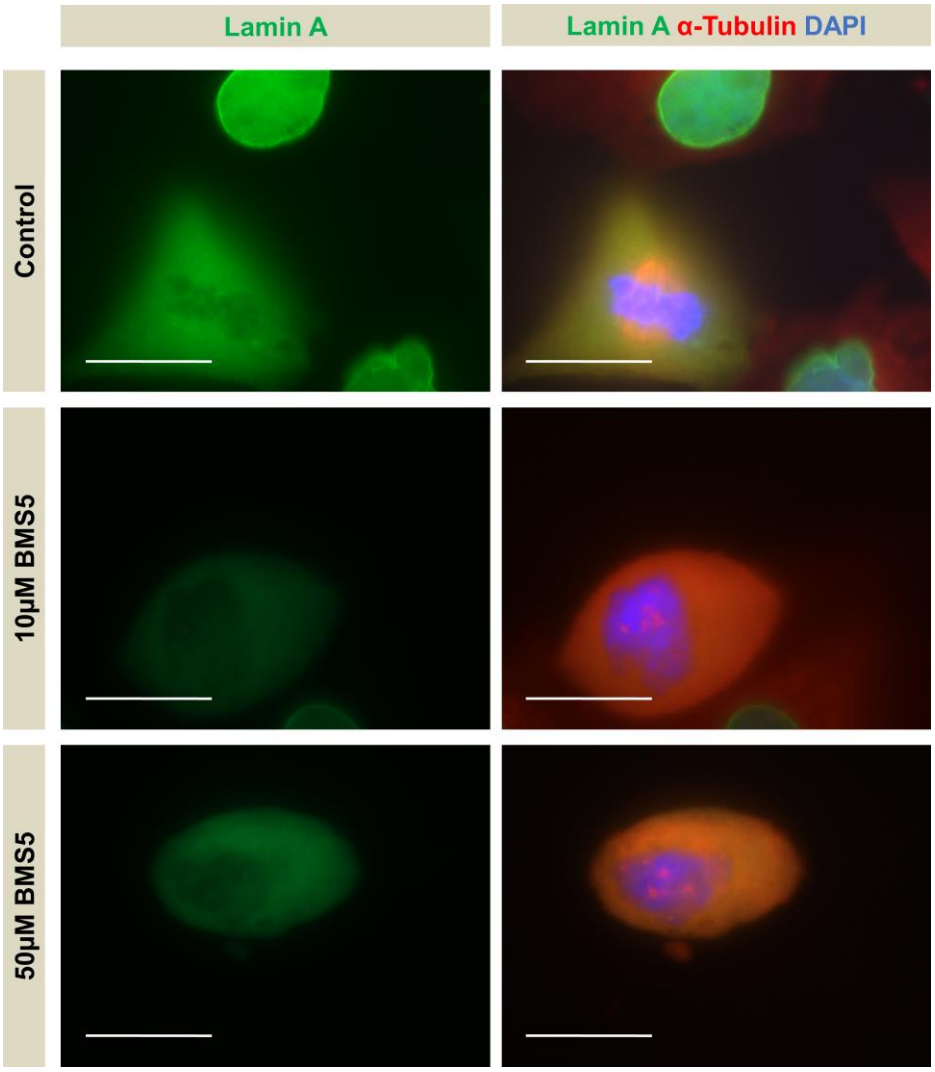



Figure 4.16 – Lamin A and α-tubulin in HK2 cells cultured in 10μM and 50μM BMS5.

HK2 cells cultured in BMS5 for 24 hours, fixed and immunofluorescently labelled with Lamin A (green), α-tubulin (red), and DAPI (blue). No difference is observed in the dispersal of Lamin A (green) between controls and cells cultured in 10μM and 50μM BMS5. Scale bars = 10μm. N=3.

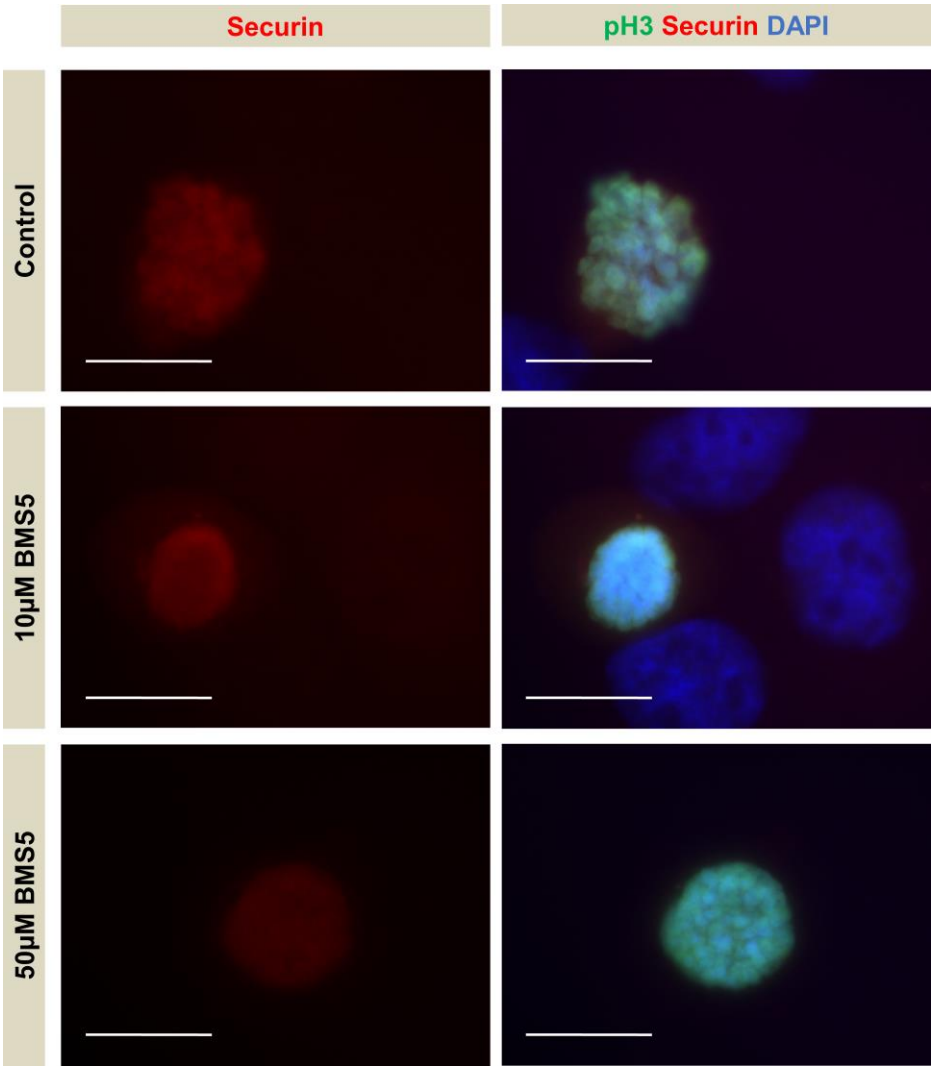



Figure 4.17 – Securin and pH3 in HK2 cells cultured in 10μM and 50μM BMS5.

HK2 cells cultured in BMS5 for 24 hours, fixed and immunofluorescently labelled with Securin (red), pH3 (green), and DAPI (blue). There is no difference in Securin localisation between controls and cells cultured in 10μM and 50μM BMS5. Scale bars = 10μm. N=3.

### 4.2.5 – BMS5 causes the mis-localisation of Pericentrin and centrosomes

Due to the observation of multiple α-tubulin foci in BMS5 treated cells, we looked to see if these foci were co-localised with centrosomes or just an accumulation of α-tubulin, and if BMS5 caused more than the normal 2 centrosomes to be produced and/or mis-localised them. Cells cultured in BMS5 were immunofluorescently dual labelled with Pericentrin and α-tubulin, there was no co-localisation between Pericentrin and α-tubulin in BMS5 treated cells, indicating that the α-tubulin foci were not localised to centrosomes (Figure 4.18). Pericentrin localisation and number appeared normal (1 per cell) in interphase cells cultured in BMS5 (Figure 4.19).

Another marker of centrosomes, γ-tubulin, was used to confirm the Pericentrin as centrosomes. Pericentrin and γ-tubulin were co-localised in control and BMS5 treated cells (Figure 4.20), indicating that BMS5 treated cells had produced multiple centrosomes (more than 2) and they were mis-localised, i.e. not at opposite poles of the cell.

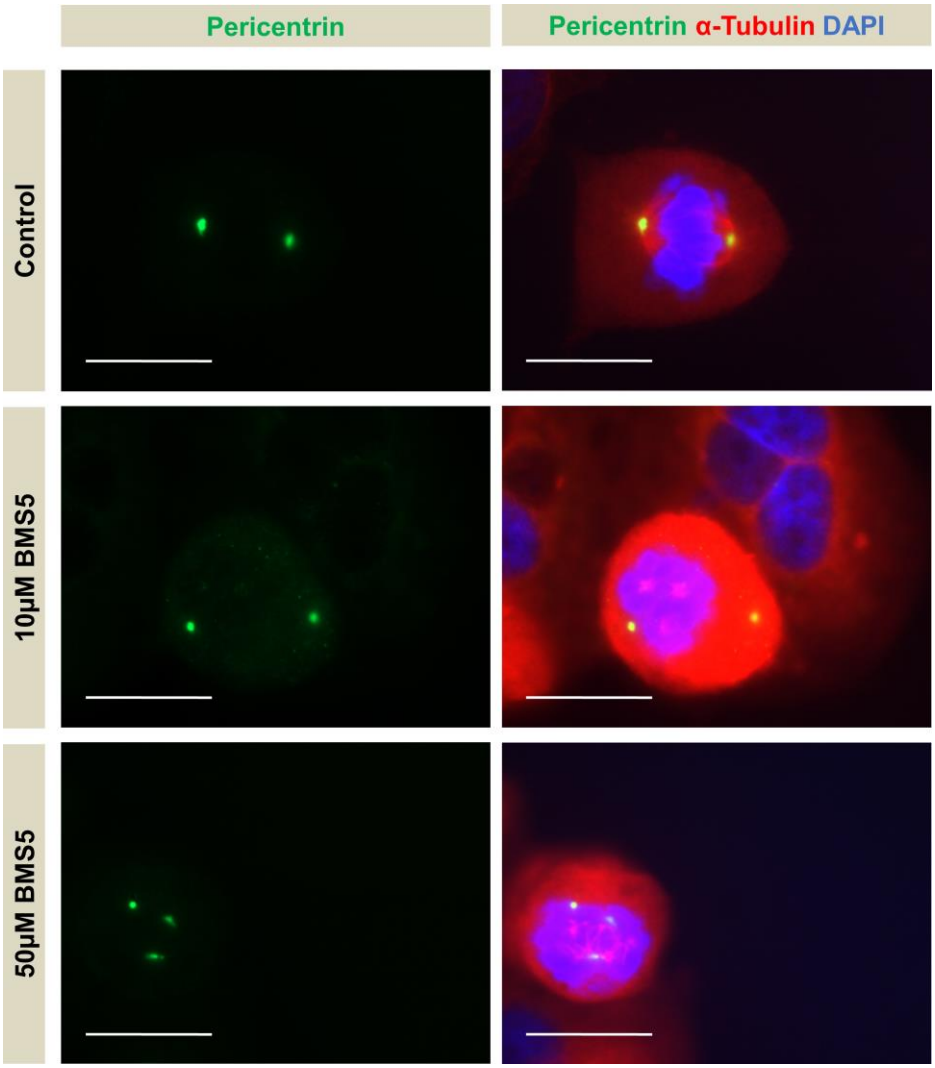



Figure 4.18 – Pericentrin and α-tubulin in HK2 cells cultured in 10μM and 50μM BMS5.

HK2 cells in mitosis cultured in BMS5 for 24 hours, fixed and immunofluorescently labelled with Pericentrin (green), α-tubulin (red), and DAPI (blue). Cells cultured in 10μM or 50μM BMS5 show incorrect Pericentrin (green) localisation that does not overly with α-tubulin (red). Scale bars = 10μm. N=3.

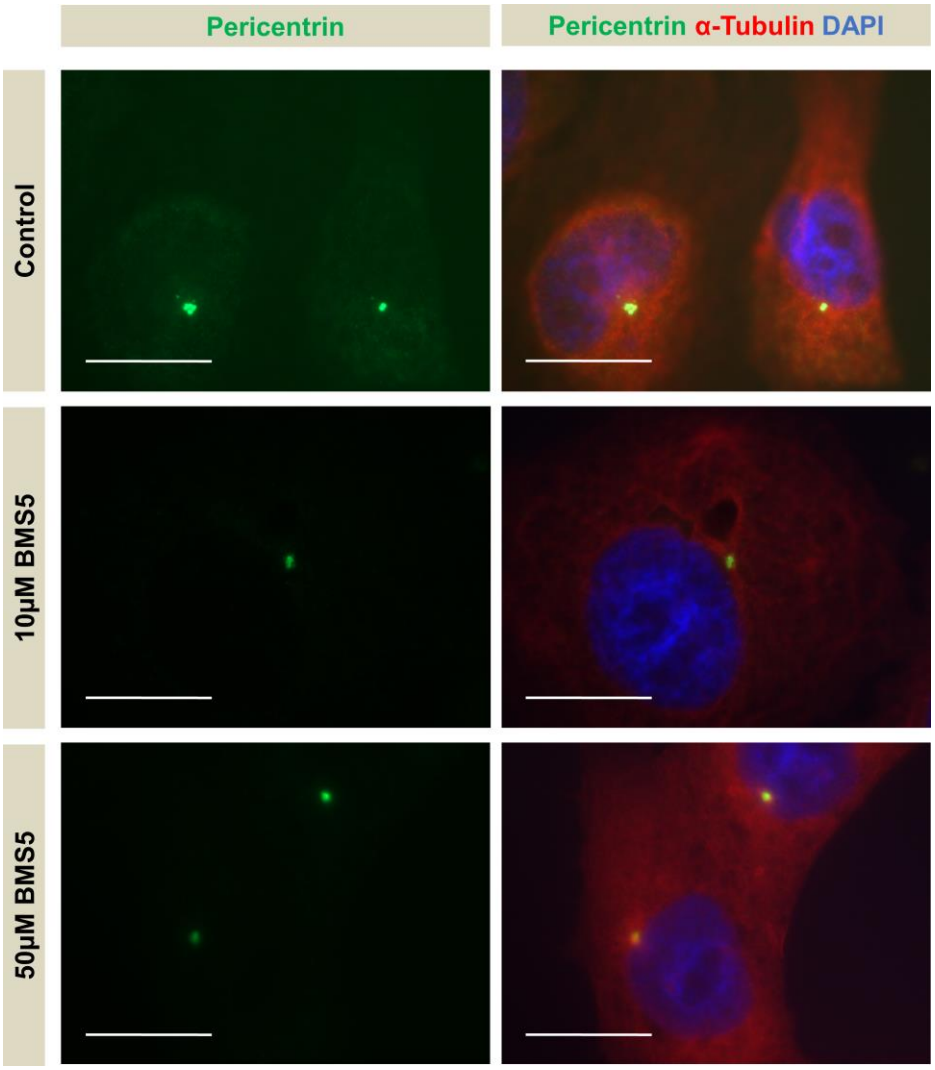



Figure 4.19 – Pericentrin and α-tubulin in HK2 cells cultured in 10μM and 50μM BMS5 (interphase).

HK2 cells in interphase cultured in BMS5 for 24 hours, fixed and immunofluorescently labelled with Pericentrin (green), α-tubulin (red), and DAPI (blue). There is no difference in Pericentrin (green) localisation in interphase cells cultured in 10μM or 50μM BMS5. Scale bars = 10μm. N=3.

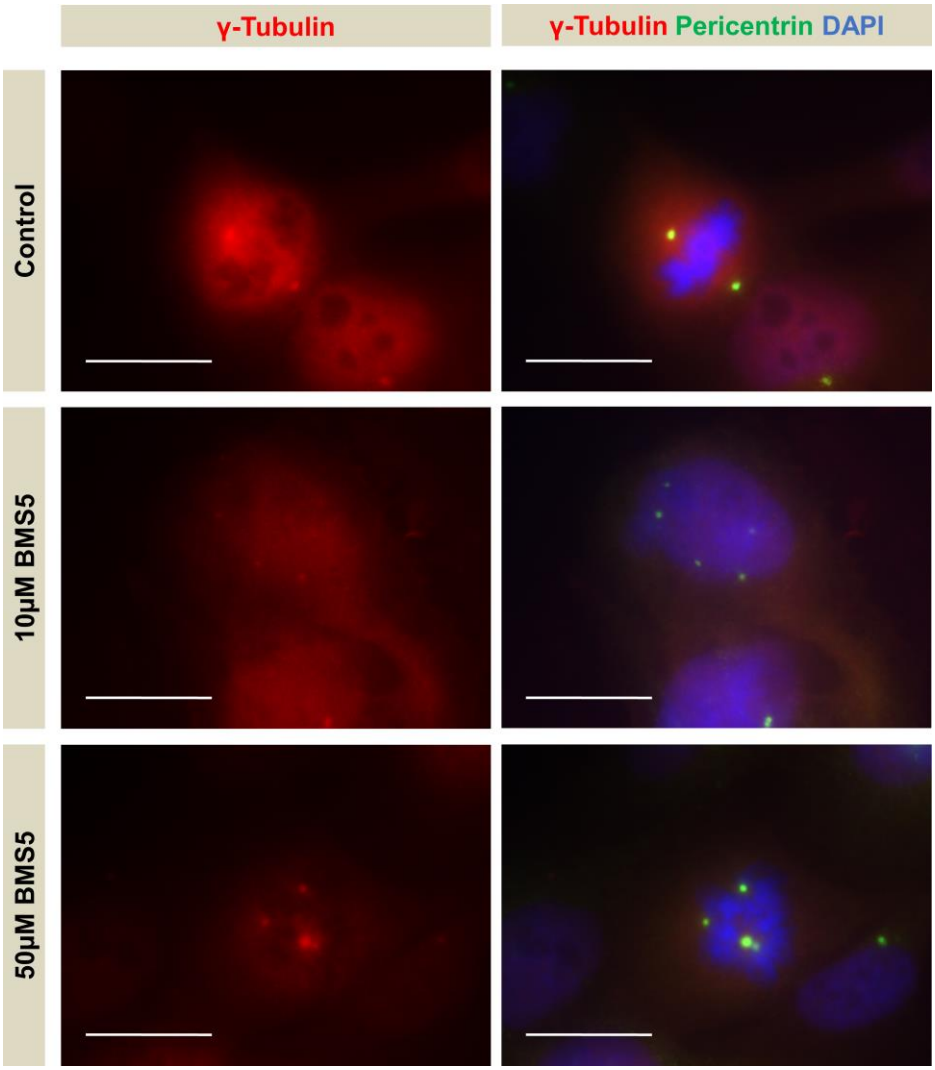



Figure 4.20 – γ-tubulin and Pericentrin in HK2 cells cultured in 10μM and 50μM BMS5.

HK2 cells in mitosis cultured in BMS5 for 24 hours, fixed and immunofluorescently labelled with gamma-tubulin (red), Pericentrin (green), and DAPI (blue). In cells cultured in 10μM or 50μM BMS5 gamma-tubulin (red) overlies with Pericentrin as in the controls. Scale bars = 10μm. N=3.

## 4.2.6 – BMS5 causes the inappropriate dispersal of SMC3

To look further at the mechanics of anaphase and why BMS5 treated cells cannot undergo this, the dispersal of SMC3 (structural maintenance protein 3), which holds the sister chromatids together as part of the cohesin complex until the spindle is formed and the cell is ready to undergo anaphase, was examined. When the cell is ready to undergo anaphase, the cohesin complex is cleaved and SMC3 is dispersed throughout the cell. Control cells in anaphase showed that SMC3 is dispersed throughout the cell whereas in interphase cells SMC3 was localised to the nucleus, SMC3 was also dispersed in cells cultures in BMS5 (Figure 4.21). This implies that SMC3 dispersal occurs in BMS5 treated cells even in the absence of a fully formed spindle.

From this it could be said that BMS5 and the inhibition of LIMK caused the inappropriate dispersal of SMC3, meaning that the chromatids were no longer held together. A possible reason for apoptosis is that aneuploidy might ensue if the cell cannot separate the chromosomes for 2 new daughter cells.

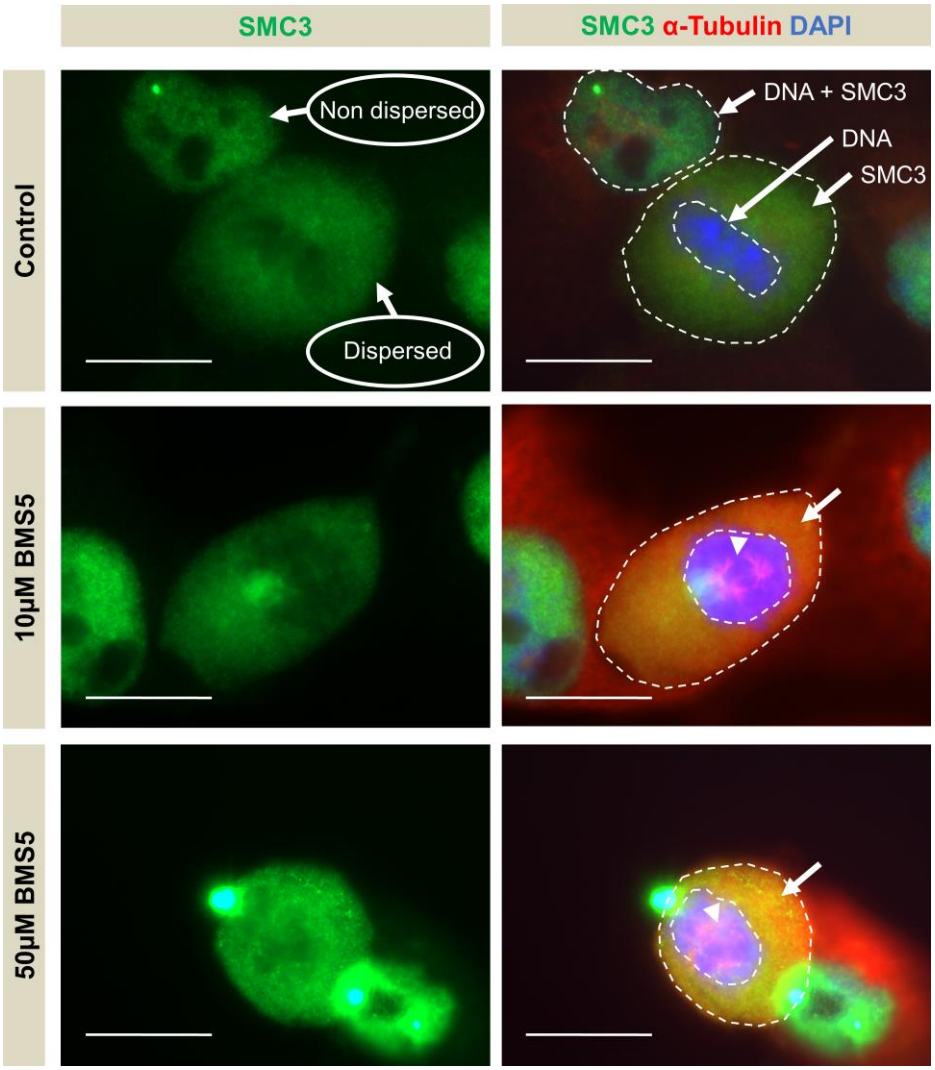



Figure 4.21 – SMC3 and α-tubulin in HK2 cells cultured in 10μM and 50μM BMS5.

HK2 cells in mitosis cultured in BMS5 for 24 hours, fixed and immunofluorescently labelled with SMC3 (green), α-tubulin (red), and DAPI (blue). 10μM and 50μM BMS5: Arrows = SMC3, arrow heads = DNA. In cells cultured in control media, 10μM BMS5, or 50μM BMS5 SMC3 (green) is dispersed in mitotic cells. Scale bars = 10μm. N=3.

### 4.2.7 – LIMK inhibition with BMS5 has no effect on Stathmin phosphorylation, or Vimentin

Stathmin has an important role in regulating microtubule dynamics by binding to and sequestering tubulin. It has been previously shown that when the phosphorylation sites on Stathmin were mutated very similar α-tubulin foci appear in cells (Marklund et al., 1996; Larsson et al., 1997). When Stathmin phosphorylation sites were mutated, localised α-tubulin foci appeared within the DNA compartment of cells in a manner similar to the α-tubulin foci observed with cells cultured in BMS5. It was therefore hypothesised that LIMK might phosphorylate Stathmin and if LIMK is inhibited by BMS5 then Stathmin would not become phosphorylated, providing a pathway to the generation of α-tubulin foci. When HK2 cells were cultured in BMS5, the phosphorylation state of Stathmin at residues 37 and 63 were unaffected by LIMK inhibition which excluded this as a mechanism for the formation of the α-tubulin foci (Figure 4.22, Figure 4.23).

Additionally Vimentin was examined as this is another cytoskeletal protein, which, among other tissues, is expressed in the developing kidney (Holthöfer et al., 1984) and therefore if BMS5 were to act on Vimentin then this could be a potential relevant pathway of action for BMS5 in both HK2 cells and embryonic kidneys. HK2 cells and embryonic kidneys shared a similar effect when treated with BMS5 of the inhibition of progression beyond metaphase. BMS5 also had effects on both α-tubulin and actin (albeit indirectly through Cofilin), we therefore looked to see if this additional filamentous protein would

be affected. HK2 cells grown in BMS5 showed no effects on Vimentin during mitosis (Figure 4.24).

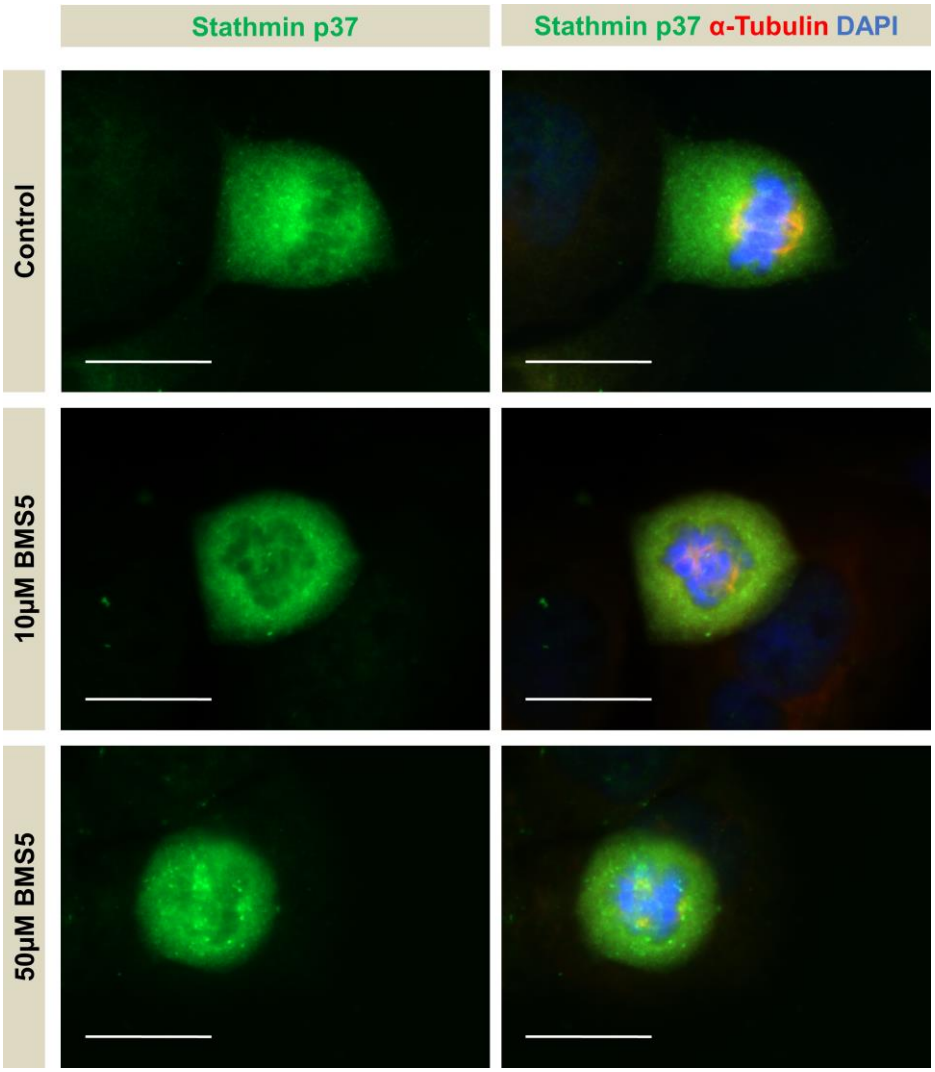



Figure 4.22 – Stathmin p37 and α-tubulin in HK2 cells cultured in 10μM and 50μM BMS5.

HK2 cells in mitosis cultured in BMS5 for 24 hours, fixed and immunofluorescently labelled with Stathmin p37 (green), α-tubulin (red), and DAPI (blue). Stathmin phosphorylation is unaffected by culturing HK2 cells in 10μM BMS5 or 50μM BMS5. Scale bars = 10μm. N=3.

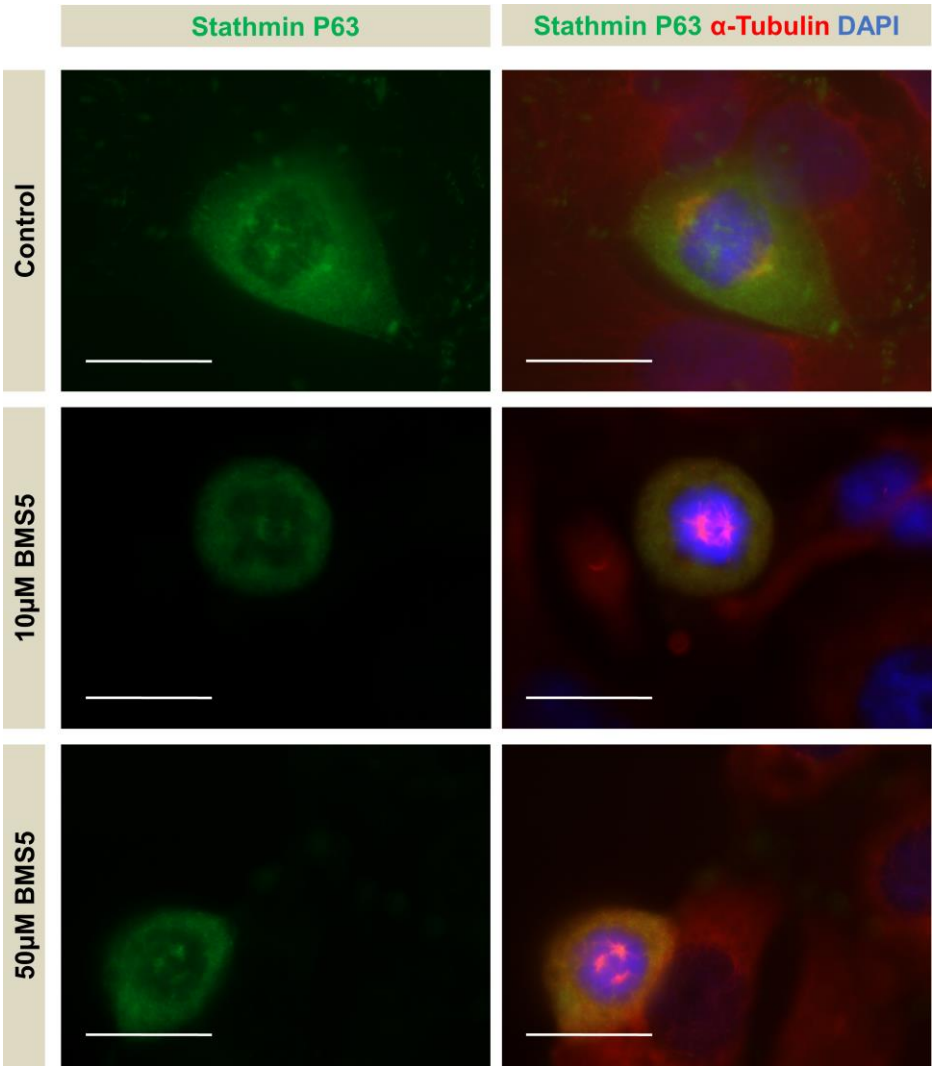



Figure 4.23 – Stathmin p63 and α-tubulin in HK2 cells cultured in 10μM and 50μM BMS5.

HK2 cells in mitosis cultured in BMS5 for 24 hours, fixed and immunofluorescently labelled with Stathmin p63 (green), α-tubulin (red), and DAPI (blue). Stathmin phosphorylation is unaffected by culturing HK2 cells in 10μM BMS5 or 50μM BMS5. Scale bars = 10μm. N=3.

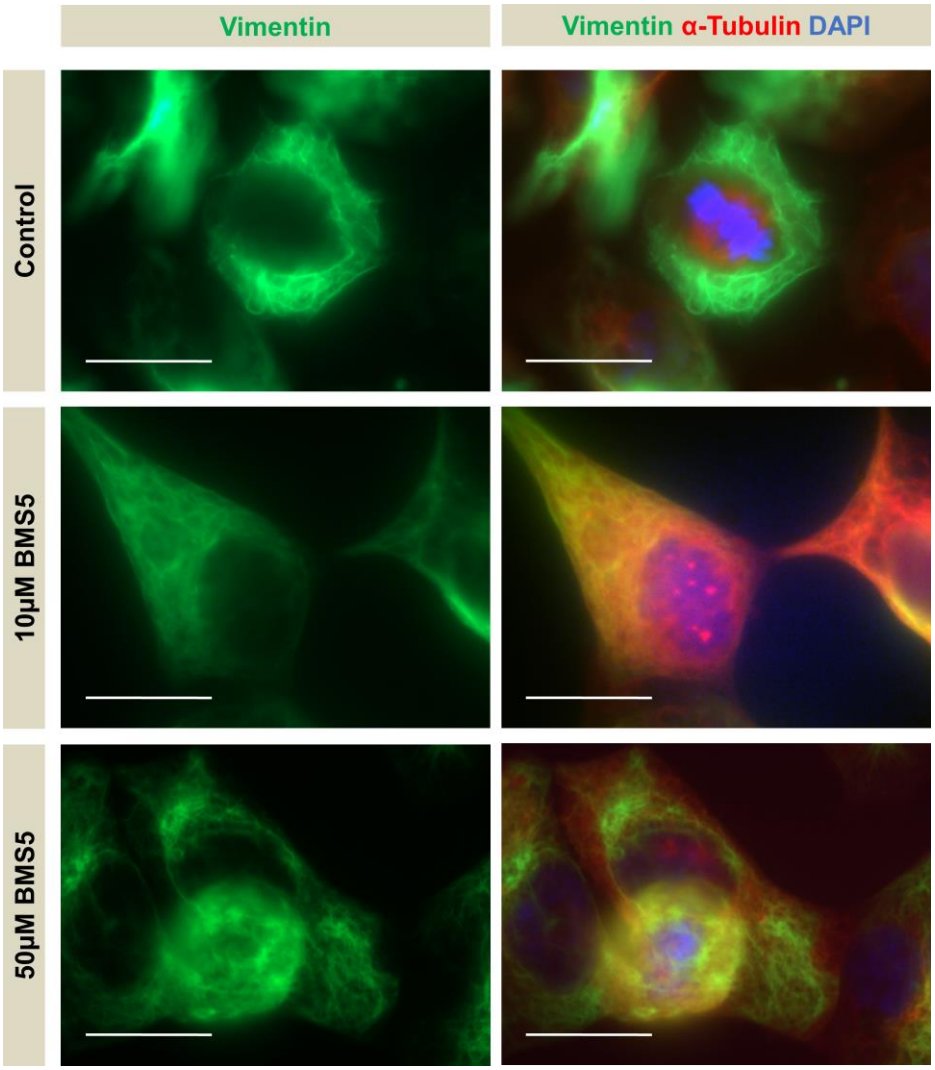



Figure 4.24 – Vimentin and α-tubulin in HK2 cells cultured in 10μM and 50μM BMS5.

HK2 cells in mitosis cultured in BMS5 for 24 hours, fixed and immunofluorescently labelled with Vimentin (green), α-tubulin (red), and DAPI (blue). Vimentin is unaffected by culturing HK2 cells in 10μM BMS5 or 50μM BMS5. Scale bars = 10μm. N=3.

### 4.2.8 – Mitotic inhibition by BMS5 is independent of cell type

In order to demonstrate that our observations were not cell type specific, 3T3 mouse embryonic fibroblast cells were cultured in the presence of BMS5. Similar to that seen in HK2 cells, α-tubulin foci were observed to form in cells undergoing mitosis at both 10μM and 50μM concentrations of BMS5 (Figure 4.25; arrows). In addition in 3T3 cells, BMS5 induced inhibition of mitosis was observed with a significant decrease in the percentage of mitotic cells in anaphase. Control cultures showed 12.42% ± 1.94 of mitotic cells in anaphase, whereas cells treated with 10μM or 50μM BMS5 both had 0% ± 0 in anaphase ($p=0.0006$, $n=3$). The total number of cells in mitosis in the field of view decreased from 52.33 ± 6.57 in controls to 26 ± 8.89 in cultures treated with 10μM BMS5 ($p=0.085$) and 21 ± 5.20 in cultures treated with 50μM BMS5 ($p=0.046$, $n=3$) (Figure 4.26). This shows that while BMS5 inhibited progression to anaphase in 3T3 cells the same as with HK2 cells, the total number of cells in mitosis decreased in 50μM BMS5 treated 3T3 cells compared to no difference in HK2 cells which suggests that BMS5 is having more of a cell death effect in mitosis in 3T3 cells compared to HK2 cells.

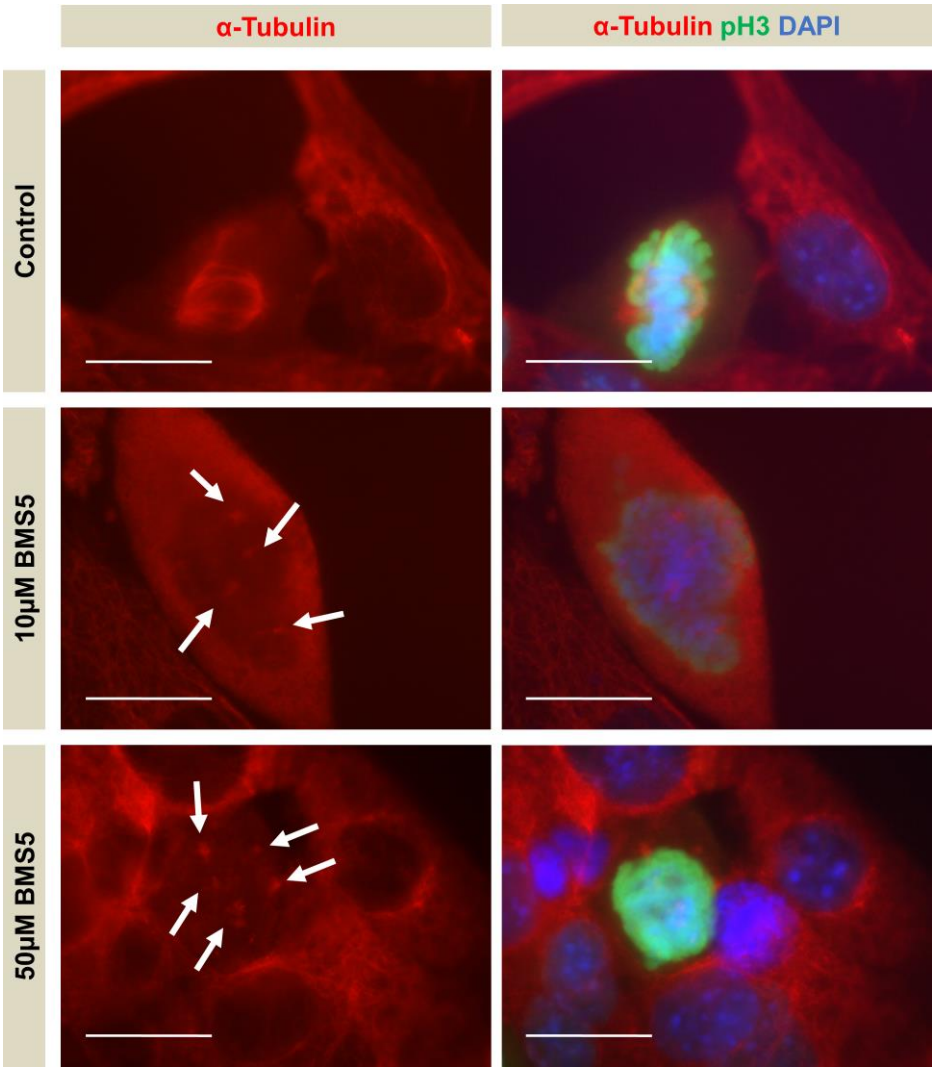



Figure 4.25 – α-tubulin and pH3 in 3T3 cells cultured in 10μM and 50μM BMS5.

3T3 cells in mitosis cultured in 10μM and 50μM BMS5 for 24 hours, fixed and immunofluorescently labelled with α-tubulin (red), pH3 (green), and DAPI (blue). α-tubulin foci (red, arrows) are present in 3T3 cells cultured in 10μM or 50μM BMS5. Scale bars = 10μm. N=3.

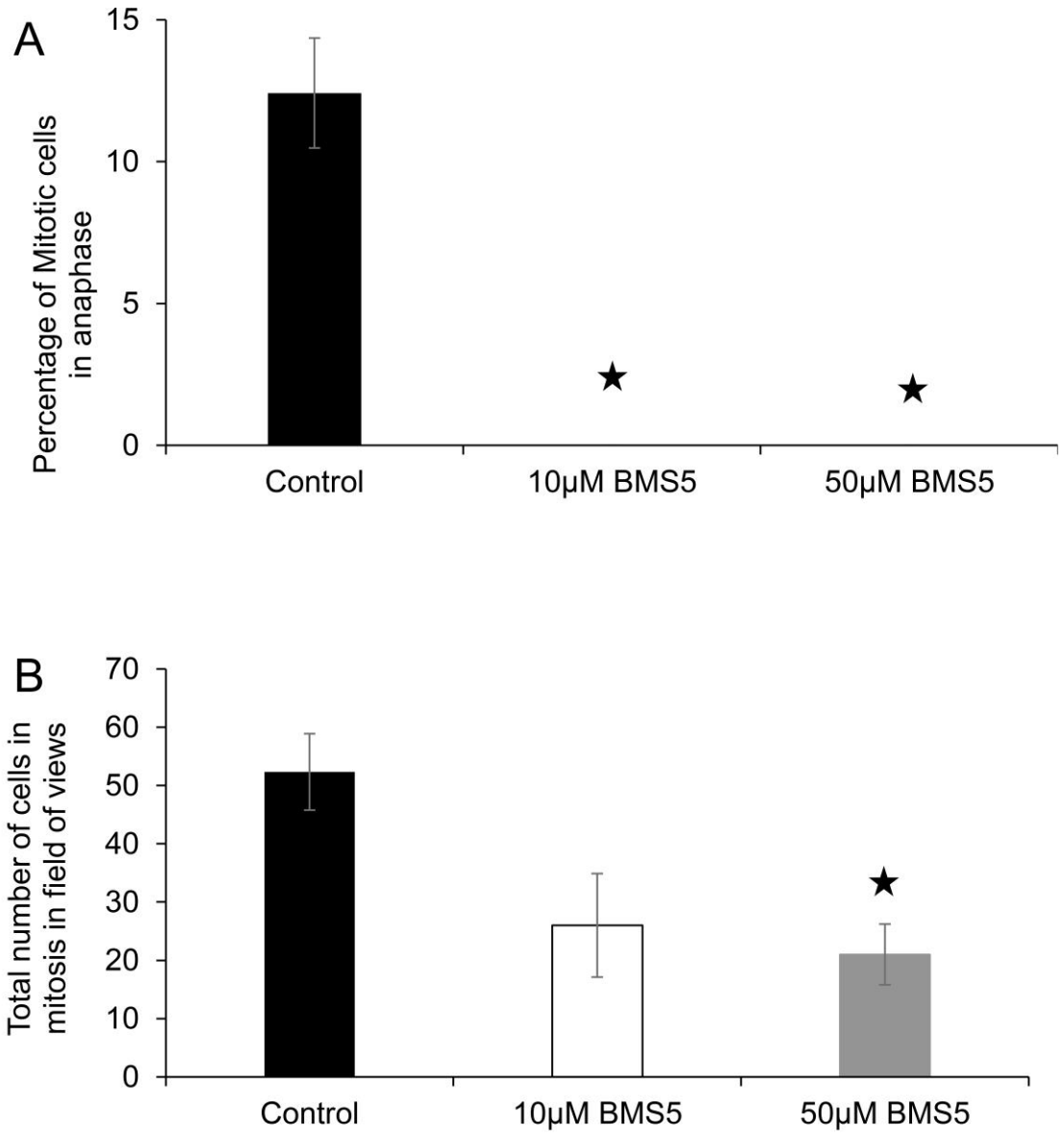



Figure 4.26 – Mitosis analysis on 3T3 cells cultured in 10μM and 50μM BMS5.

Graphs showing 3T3 cells cultured in 10μM and 50μM BMS5 for 24 hours, fixed and immunofluorescently labelled with pH3. (A) Percentage of mitotic cells in anaphase. Control cultures showed 12.42% ± 1.94 of mitotic cells in anaphase, whereas cells treated with 10μM or 50μM BMS5 both had 0% ± 0 in anaphase (p=0.0006, n=3). (B) Total number of cells in mitosis in field of views. The total number of cells in mitosis in the field of view decreased from 52.33 ± 6.57 in controls to 26 ± 8.89 in cultures treated with 10μM BMS5

(p=0.085) and 21 ± 5.20 in cultures treated with 50μM BMS5 (p=0.046, n=3). * p<0.05 compared to control.

## 4.2.9 – Is Cofilin phosphorylation responsible for the generation of α-tubulin foci?

This chapter also looked at whether the α-tubulin phenotype was due to LIMK's effects on Cofilin phosphorylation, therefore A23187 and histamine were used. Both the calcium ionophore, A23187 and the $Ca^{2+}$ mobilising agonist, Histamine, cause Cofilin dephosphorylation (Wang et al., 2005). This group showed both A23187 and histamine decreased the amount of Cofilin phosphorylation, but this loss was failed to have been observed both at the concentration they used (5μM A23187, 10mM Histamine) and at other concentrations (Figure 4.27, Figure 4.28).

The α-tubulin phenotype was not observed during mitosis in cells cultured in A23187 or Histamine (Figure 4.29, Figure 4.30). Wang et al., 2005 used shorter time points to analyse the reduction in Cofilin phosphorylation than we did. Therefore there might have been a reduction in Cofilin phosphorylation in our HK2 cells but we did not use the correct time points to see any effect. As such this work should be repeated using the same time points as Wang et al., 2005 in HK2 cells.

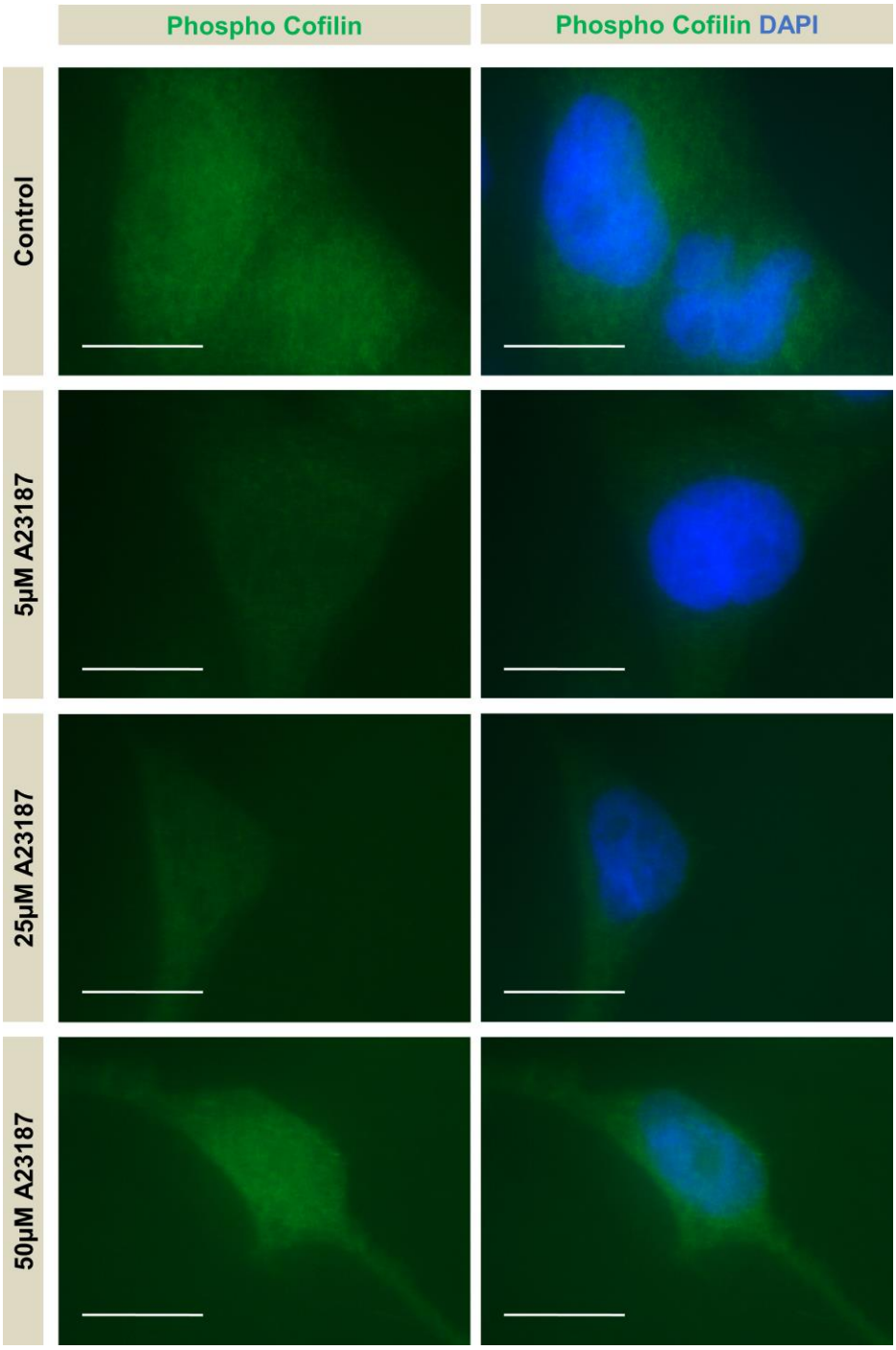



Figure 4.27 – Phosphorylated Cofilin in HK2 cells cultured in 5µM, 25µM and 50µM A23187.

HK2 cells cultured in A23187 for 24 hours, fixed and immunofluorescently labelled with phosphorylated Cofilin (green) and DAPI (blue). The amount of

phosphorylated Cofilin is unaffected in cells cultured in 50µM A23187 and only a slight decrease in 5µM and 25µM A23187. Scale bars = 10µm. N=3.

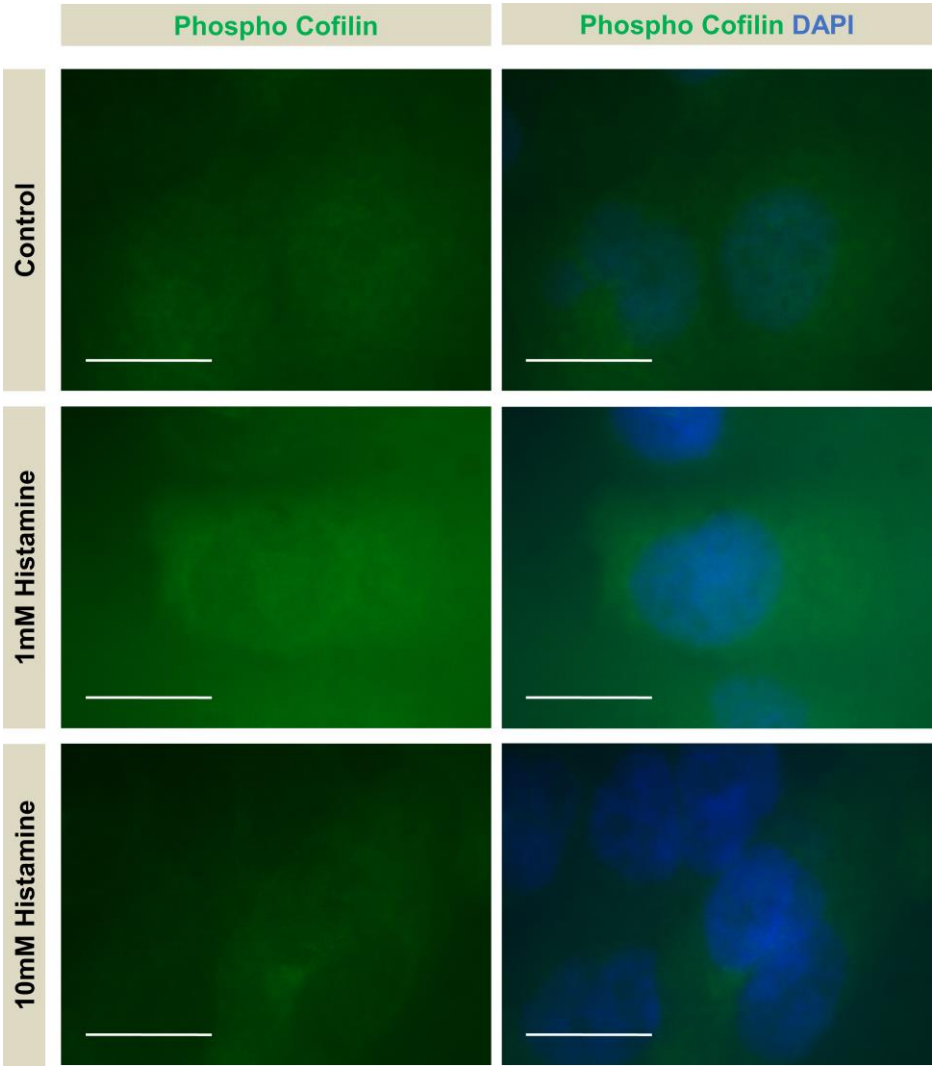



Figure 4.28 – Phosphorylated Cofilin in HK2 cells cultured in 1mM and 10mM Histamine.

HK2 cells cultured in Histamine for 24 hours, fixed and immunofluorescently labelled with phosphorylated Cofilin (green) and DAPI (blue). The amount of phosphorylated Cofilin is unaffected in cells cultured in 1mm or 10mM Histamine. Scale bars = 10µm. N=3.

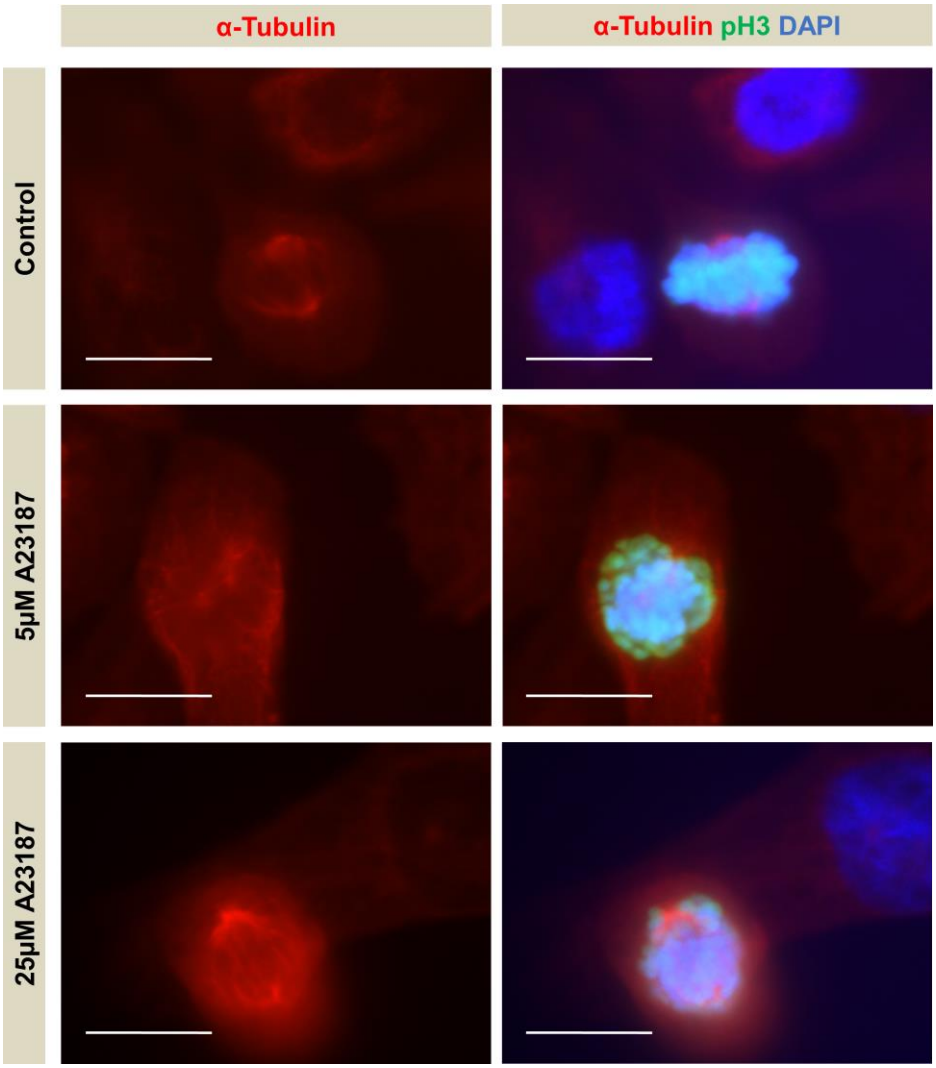



Figure 4.29 – α-tubulin and pH3 in HK2 cells cultured in 5μM and 50μM A23187.

HK2 cells cultured in A23187 for 24 hours, fixed and immunofluorescently labelled with α-tubulin (red), pH3 (green), and DAPI (blue). No α-tubulin (red) foci were observed in cells cultured in A23187 and α-tubulin localisation appeared normal compared to the control. Scale bars = 10μm. N=3.

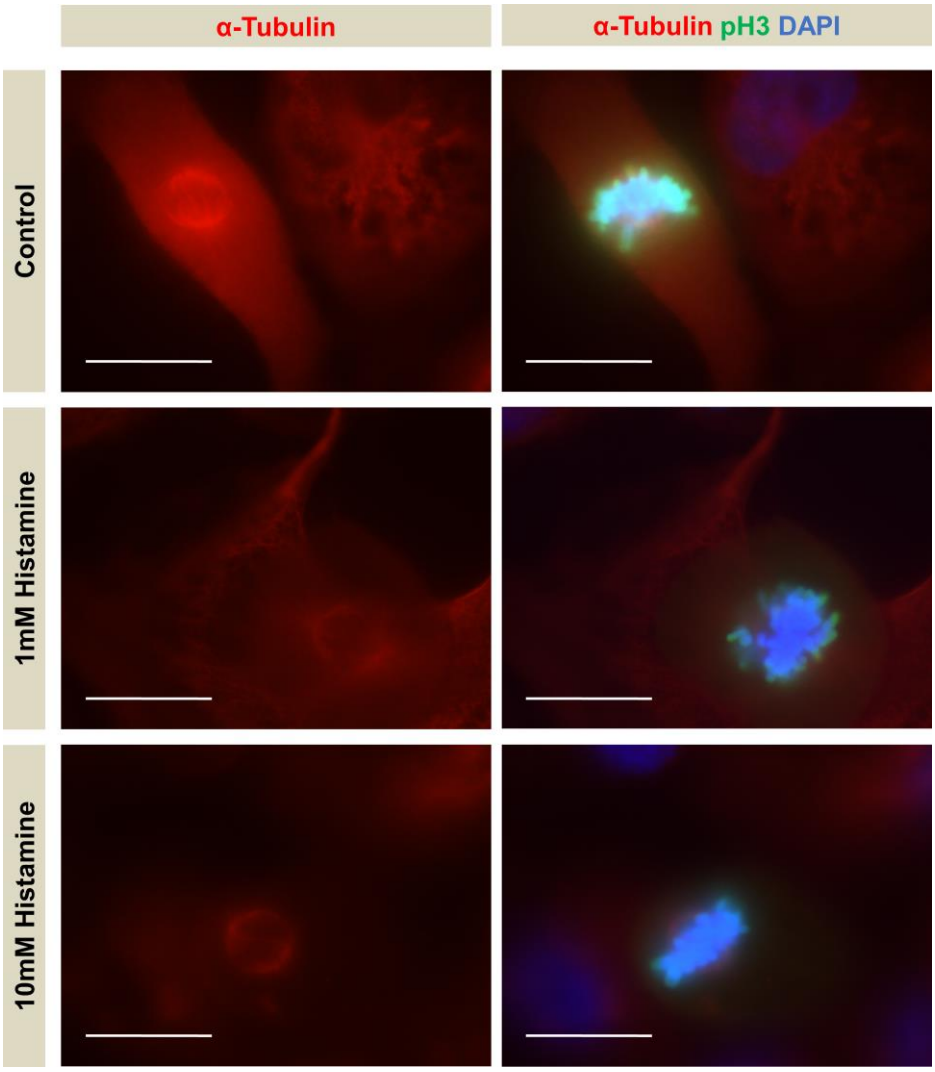



Figure 4.30 – α-tubulin and pH3 in HK2 cells cultured in 1mM and 10mM Histamine.

HK2 cells cultured in Histamine for 24 hours, fixed and immunofluorescently labelled with α-tubulin (red), pH3 (green), and DAPI (blue). No α-tubulin (red) foci were observed in cells cultured in Histamine and α-tubulin localisation appeared normal compared to the control. Scale bars = 10μm. N=3.

## 4.2.10 – Actin filament disruption is not the mechanism by which BMS5 generates α-tubulin foci

To see whether the effects seen with BMS5 can be explained by the downstream effect on actin, the loss of the ability to form actin filaments, an actin disrupter, Cytochalasin B, was used. Cytochalasin B is a cell permeable mycotoxin and acts by preventing new actin monomers being added at the growing end of actin filaments (Lin et al., 1980). To confirm that Cytochalasin B is disrupting the actin filaments HK2 cells were cultured in Cytochalasin B for 24 hours, fixed and labelled with Phalloidin. There was a complete loss of all actin filaments at 10μM and 30μM, and the actin network was severely damaged at 1μM Cytochalasin B (Figure 4.31).

When HK2 cells were cultured in the presence of Cytochalasin B the number of cells after 24 hours and 48 hours both were significantly lower than the controls for cells treated with both 1μM and 10μM Cytochalasin B ($p<0.0001$). After 48 hours, the number of cells in 1μM and 10μM Cytochalasin B were lower than the number cells before Cytochalasin B was added ($p<0.0001$, Figure 4.32). Cytochalasin B did not prevent cells reaching anaphase, control cells had 21.51% ± 2.68 of mitotic cells in anaphase, cells treated with 1μM Cytochalasin B had 15.14% ± 8.39 ($p=0.77$), cells treated with 10μM Cytochalasin B had 1.85% ± 1.85 ($p=0.068$), and cells treated with 30μM Cytochalasin B had 2.38% ± 2.38 ($p=0.076$, $n=3$). The control had 26.67 ± 8.37 cells in mitosis in the field of view, cells treated with 1μM Cytochalasin B had 24 ± 7.57 cells ($p=0.99$), cells treated with 10μM Cytochalasin B had 13 ± 2.89 cells (0.41), and cells treated with 30μM Cytochalasin B had 10.33 ± 2.03

cells (p=0.28, n=3) (Figure 4.33). While there was a numerical decrease in both the percentage of mitotic cells in anaphase and the number of cells in mitosis there was not a significant difference between the control and individual treatment groups. Due to the observation of a statistically significant decrease in the number of cells but no effect on mitosis an MTT assay was conducted on confluent HK2 cells to determine if Cytochalasin B would cause any inherent toxicity to the cells. There was only a significant decrease in mitochondrial activity when the concentration of Cytochalasin B was at 50µm or 100µM ($p=0.0044$ and $p<0.0001$ respectively), no significant decrease in mitochondrial activity was observed at 0.1µM ($p>0.99$), 1µM ($p=0.23$), 10µM ($p=0.38$), or 25µM ($p=0.086$) which would strongly imply that at the concentrations used in our HK2 cells (1µM, 10µM, and 30µM) Cytochalasin B was not toxic.

Cells cultured in Cytochalasin B were still able to form an α-tubulin spindle at all concentrations of Cytochalasin B, indicating that BMS5 effects on actin disruption was not responsible for the failure to form the spindle (Figure 4.34). Centrosome positioning and number was appeared to be unaffected by Cytochalasin B (Figure 4.35). In addition cells cultured in Cytochalasin B were able to disperse SMC3 correctly, as the mitotic spindle had already formed (Figure 4.36). These observations in Figure 4.34, Figure 4.35 and Figure 4.36, in addition to the failure to see anaphase stage nuclei, indicated that cells cultured in Cytochalasin B could reach metaphase but could not separate the chromosomes due to the lack of a normal actin filament network. This was dissimilar to BMS5, which forms no spindle.

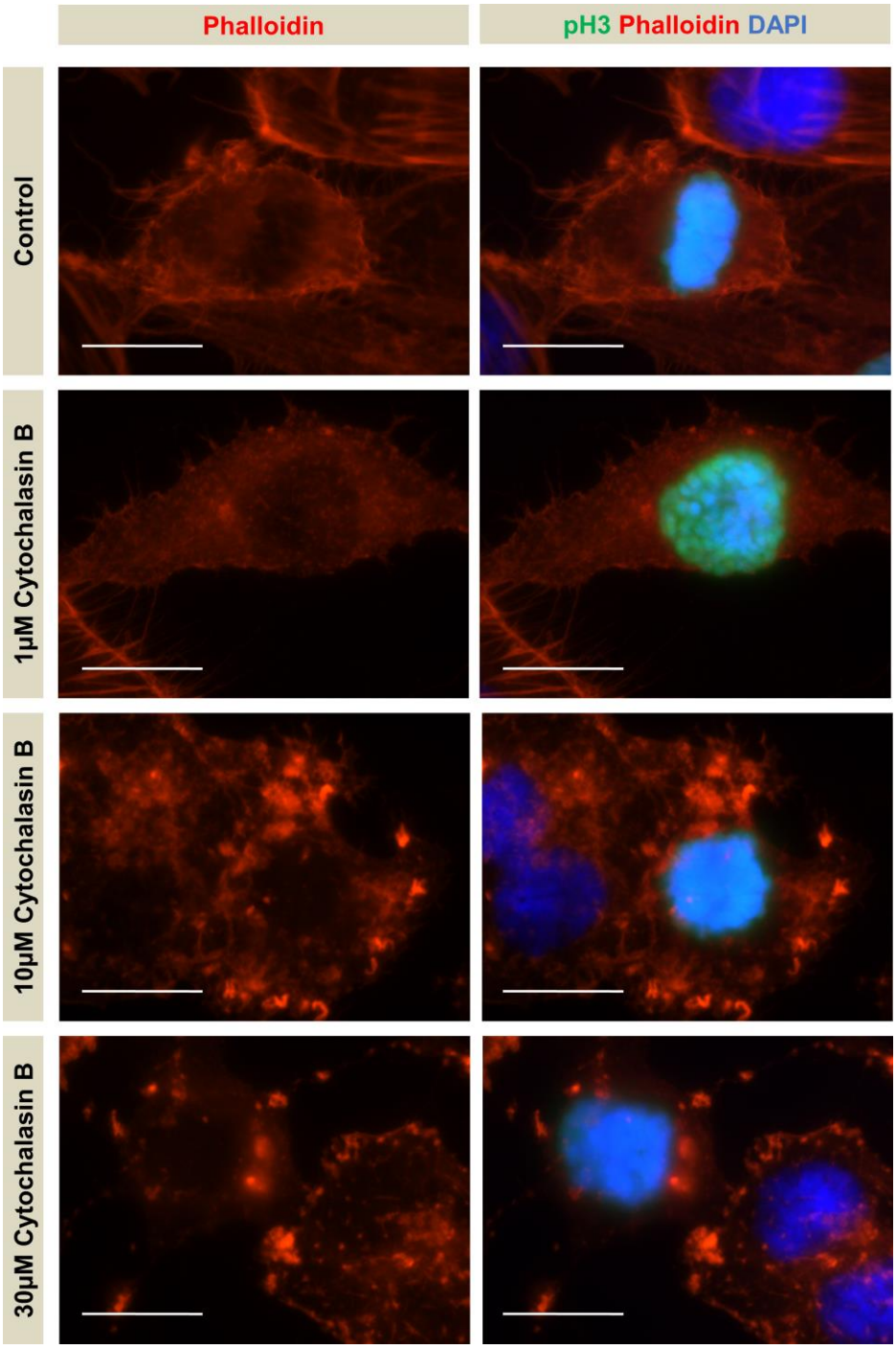



Figure 4.31 – Phalloidin and pH3 in HK2 cells cultured in 1µM, 10µM, and 30µM Cytochalasin B.

HK2 cells cultured in Cytochalasin B for 24 hours, fixed and labelled with Phalloidin (red), pH3 (green), and DAPI (blue). The actin (red) network is

severely disrupted at all concentrations of Cytochalasin B compared to the control. Scale bars = 10µm. N=3.

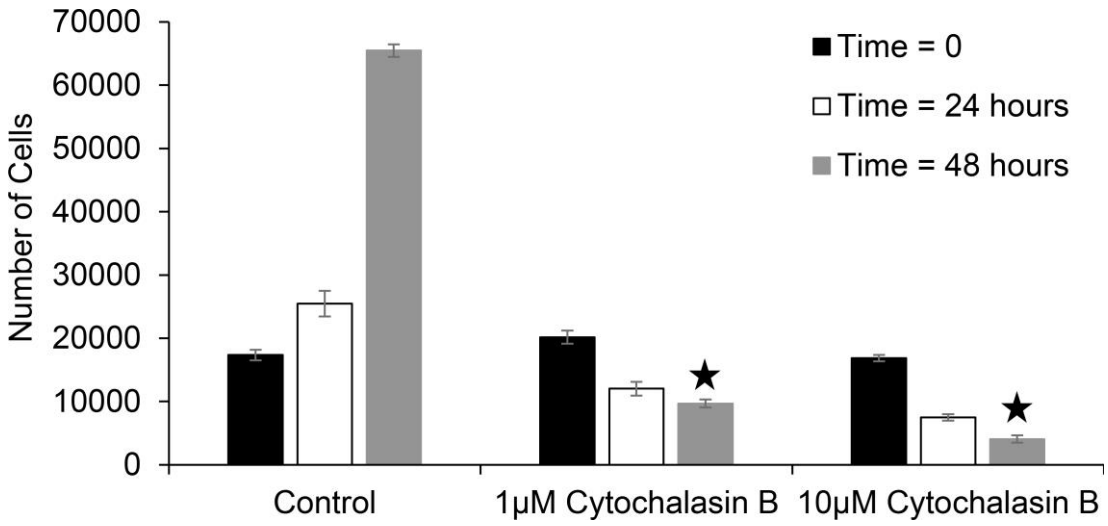



Figure 4.32 – Cell counts on HK2 cells cultured in 1µM, 10µM, and 30µM Cytochalasin B.

Graph showing cell counts from HK2 cells cultured in 1µm and 10µM Cytochalasin B for 0 hours, 24 hours and 48 hours. After 48 hours, the number of cells in 1µM and 10µM Cytochalasin B were lower than the number cells before Cytochalasin B was added (* $p<0.0001$, N=3).

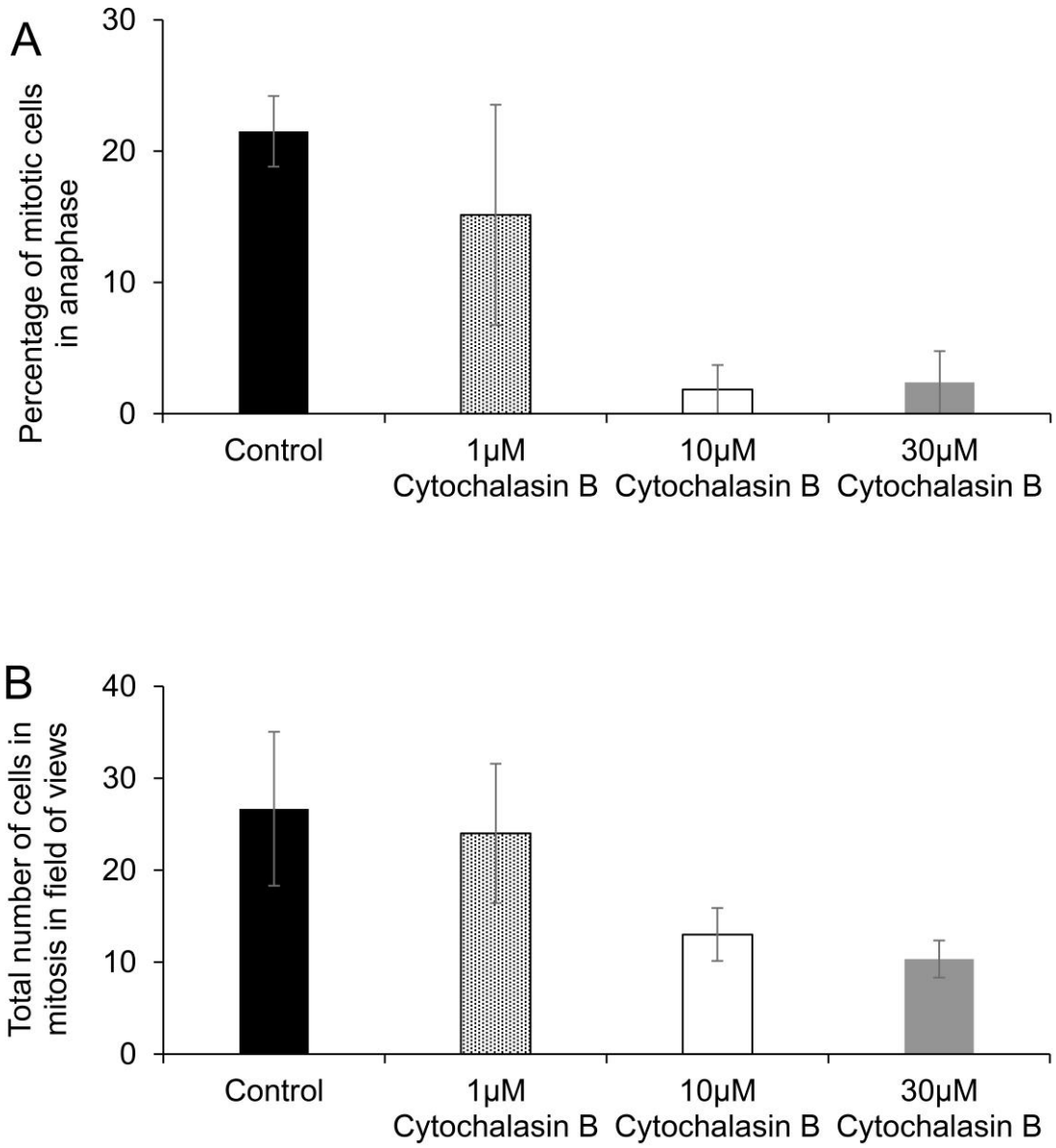



Figure 4.33 – Mitosis analysis on HK2 cells cultured in 1µM, 10µM, and 30µM Cytochalasin B.

Graphs showing HK2 cells cultured in 1µM, 10µM, and 30µM Cytochalasin B for 24 hours, fixed and immunofluorescently labelled with pH3. (A) Percentage of mitotic cells in anaphase. Cytochalasin B did not prevent cells reaching anaphase, control cells had 21.51% ± 2.68 of mitotic cells in anaphase, cells treated with 1µM Cytochalasin B had 15.14% ± 8.39 (p=0.77), cells treated with 10µM Cytochalasin B had 1.85% ± 1.85 (p=0.068), and cells treated with

30µM Cytochalasin B had 2.38% ± 2.38 (p=0.076, n=3). (B) Total number of cells in mitosis in field of views. The control had 26.67 ± 8.37 cells in mitosis in the field of view, cells treated with 1µM Cytochalasin B had 24 ± 7.57 cells (p=0.99), cells treated with 10µM Cytochalasin B had 13 ± 2.89 cells (0.41), and cells treated with 30µM Cytochalasin B had 10.33 ± 2.03 cells (p=0.28, n=3).

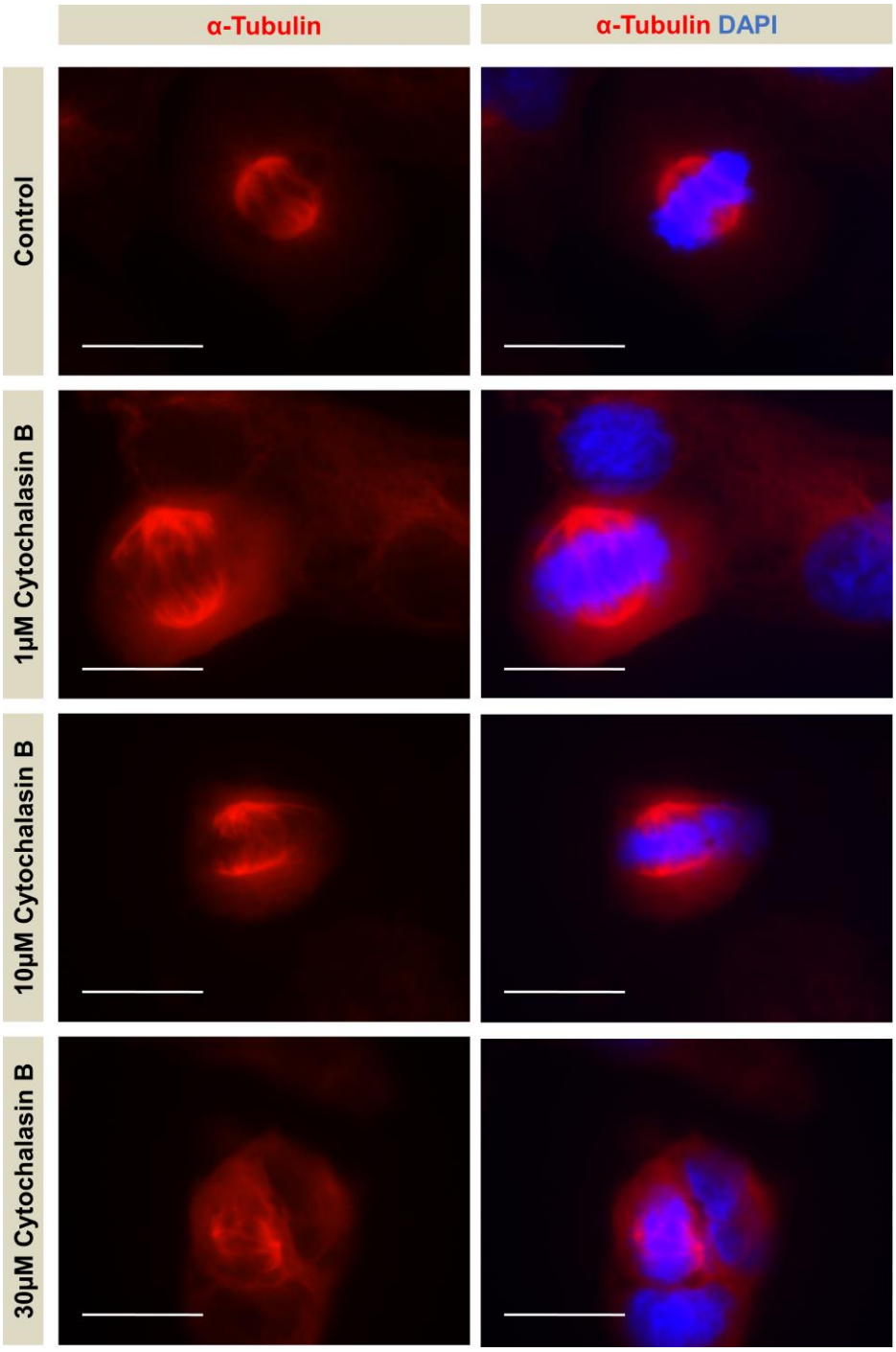



Figure 4.34 – α-tubulin in HK2 cells cultured in 1µM, 10µM, and 30µM Cytochalasin B.

HK2 cells cultured in Cytochalasin B for 24 hours, fixed and immunofluorescently labelled with α-tubulin (red) and DAPI (blue). The α-

tubulin (red) spindle appeared normal in cells cultured in 1µM, 10µM, and 30µM Cytochalasin B. Scale bars = 10µm. N=3.

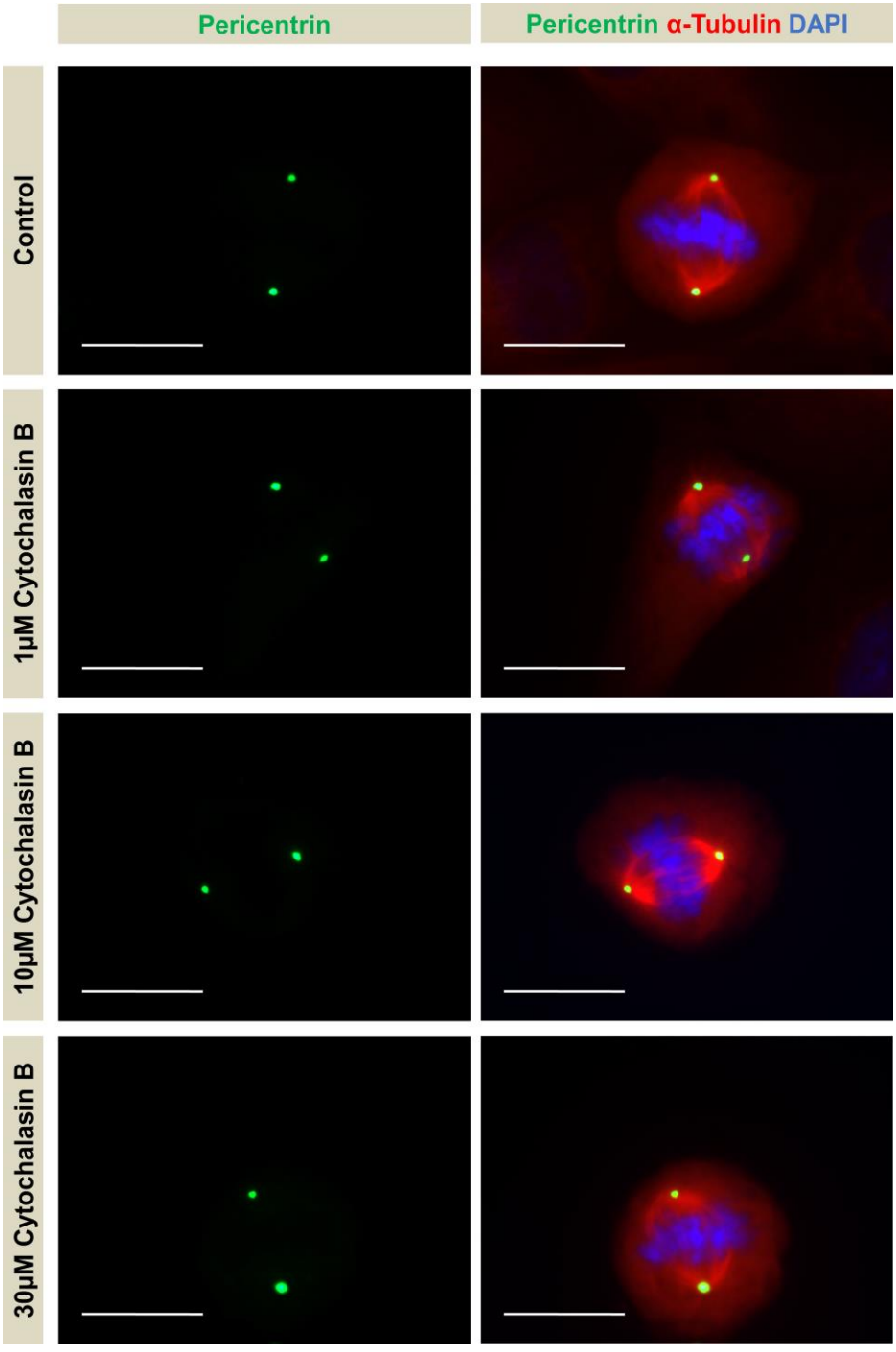



Figure 4.35 – Pericentrin and α-tubulin in HK2 cells cultured in 1µM, 10µM, and 30µM Cytochalasin B.

HK2 cells cultured in Cytochalasin B for 24 hours, fixed and immunofluorescently labelled with Pericentrin (green), α-tubulin (red), and DAPI (blue). Pericentrin appeared normal compared to the control in all concentrations of Cytochalasin B. Scale bars = 10μm. N=3.

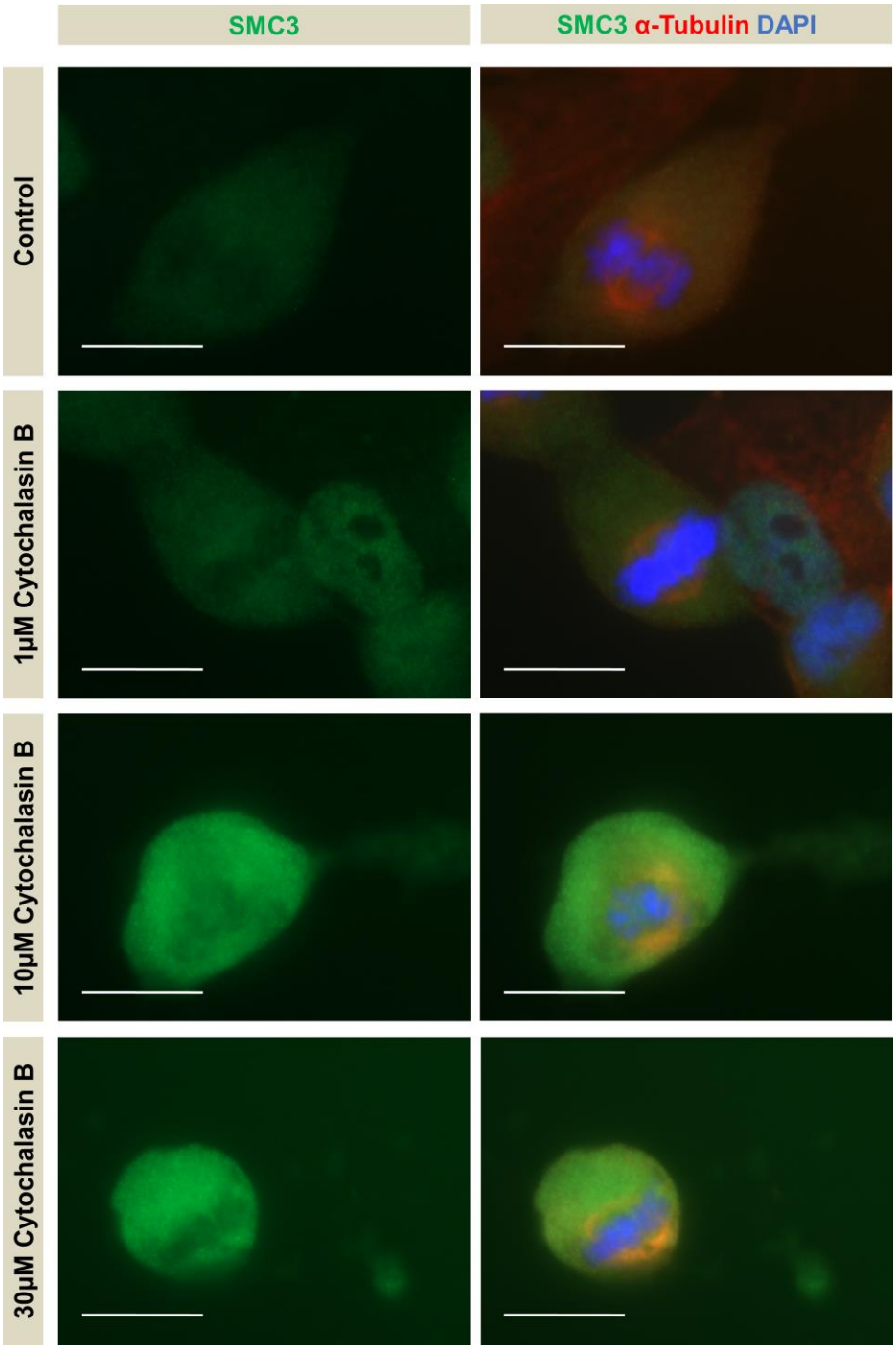



Figure 4.36 – SMC3 and α-tubulin in HK2 cells cultured in 1µM, 10µM, and 30µM Cytochalasin B.

HK2 cells cultured in Cytochalasin B for 24 hours, fixed and immunofluorescently labelled with SMC3 (green), α-tubulin (red), and DAPI

(blue). Cells cultured in Cytochalasin B can disperse SMC3 (green) in a similar manner to the control cells. Scale bars = 10µm. N=3.

### 4.2.11 – Mitosis inhibition cannot replicate the BMS5 phenotype in HK2 cells

Paclitaxel stabilises microtubules and prevents its disassembly, thereby inhibiting spindle assembly and mitosis (Schiff and Horwitz, 1980; Hornick et al., 2008). Therefore to see if the BMS5 effects were simply due to an inhibition of mitosis, Paclitaxel was used to see if this generated the same phenotype of α-tubulin foci in HK2 cells. First to confirm that paclitaxel inhibited mitosis in HK2 cells, it was looked to see if paclitaxel prevented cells from reaching anaphase. There was a decrease from 16.87% ± 1.86 of mitotic cells in anaphase in controls to 0% ± 0 in cells treated with 10µM paclitaxel ($p<0.0001$), and 0% ± 0 in cells treated with 50µM paclitaxel ($p<0.0001$, n=3, Figure 4.37). This is what would be expected with paclitaxel treatment, also as expected the number of cells in mitosis in the field of view increased significantly, controls cells had 46 ± 6.51 cells in mitosis, cells treated with 10µM paclitaxel had 147 ± 13.32 cells in mitosis ($p=0.12$), and cells treated with 50µM paclitaxel had 247.67 ± 49.52 cells in mitosis ($p=0.0073$, n=3, Figure 4.37). This indicated that the cells had become stalled in mitosis, due to the increase in the number of cells in mitosis, and were not dying in a comparable manner to cells cultured in BMS5.

To see whether simply stalling in mitosis would recreate the same α-tubulin phenotype and SMC3 dispersal, HK2 cells were cultured in paclitaxel for 24 hours, fixed and immunolabelled for α-tubulin and SMC3. There were multiple α-tubulin foci formed and there was dispersal of SMC3 in the control cultures and in 10μM paclitaxel and 50μM paclitaxel (Figure 4.38). Figure 4.37 and Figure 4.38 showed that inhibiting mitosis with paclitaxel caused multiple α-tubulin foci and the dispersal of SMC3, but crucially these cells did not die (increase in number of cells in mitosis) but instead were stalled in mitosis which indicated a different mechanism to how BMS5 caused a similar phenotype.

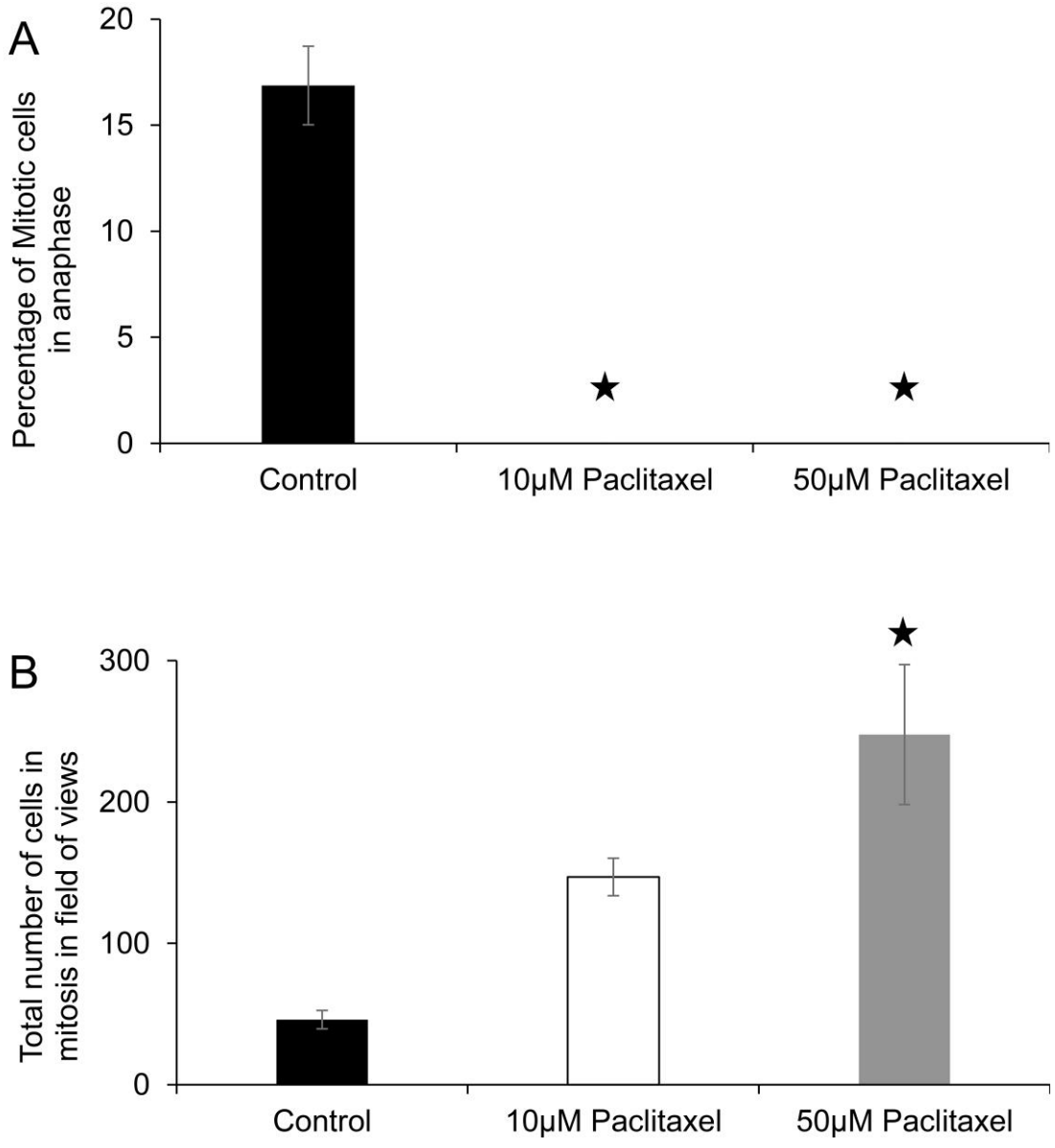



Figure 4.37 – Mitosis analysis on HK2 cells cultured in 10μM and 50μM Paclitaxel.

Graphs showing HK2 cells cultured in 10μM and 50μM Paclitaxel for 24 hours, fixed and immunofluorescently labelled with pH3. (A) Percentage of mitotic cells in anaphase. There is a decrease from 16.87% ± 1.86 of mitotic cells in anaphase in controls to 0% ± 0 in cells treated with 10μM paclitaxel ($p<0.0001$), and 0% ± 0 in cells treated with 50μM paclitaxel ($p<0.0001$, $n=3$). (B) Total number of cells in mitosis in field of views. The number of cells in

mitosis in the field of view increased significantly, controls cells had 46 ± 6.51 cells in mitosis, cells treated with 10µM paclitaxel had 147 ± 13.32 cells in mitosis ($p=0.12$), and cells treated with 50µM paclitaxel had 247.67 ± 49.52 cells in mitosis ($p=0.0073$, $n=3$). * $p<0.01$ compared to control.

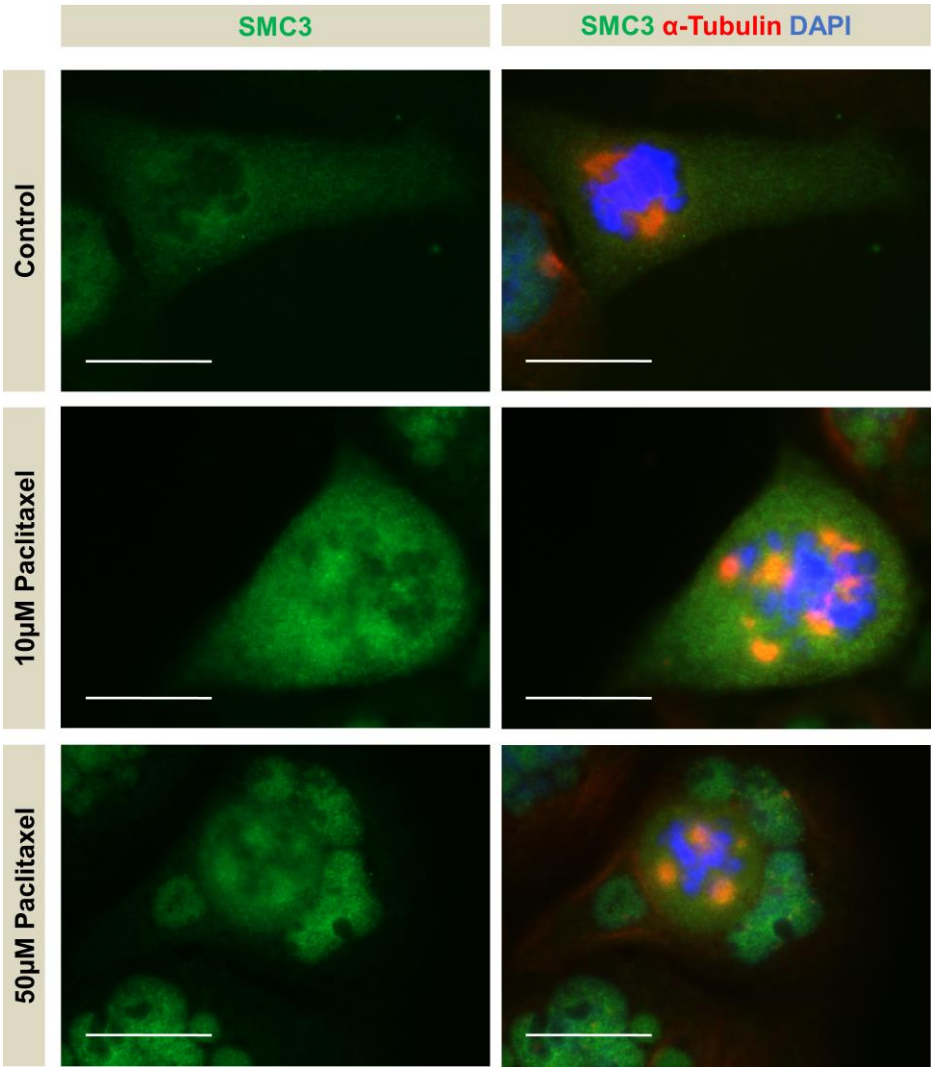



Figure 4.38 – SMC3 and α-tubulin in HK2 cells cultured in 10μM and 50μM Paclitaxel

HK2 cells cultured in Paclitaxel for 24 hours, fixed and immunofluorescently labelled with SMC3 (green), α-tubulin (red), and DAPI (blue). Multiple α-tubulin (red) foci are formed in cells cultured in 10μM and 50μM Paclitaxel and SMC3 (green) is dispersed in these cells. Scale bars = 10μm. N=3.

## 4.3 – Conclusions

This chapter showed that BMS5 induced LIMK inhibition prevented the completion of mitosis and caused a decrease in cell number but only in populations of cells undergoing mitosis, there was no observable effect on non-mitotic cells. BMS5 in mitotic cells caused the formation of the mitotic spindle, with multiple α-tubulin foci generated within the DNA area. Multiple centrosomes were also created in the absence of LIMK activity, however these did not overlie with the α-tubulin foci, but consisted of Pericentrin and γ-tubulin. BMS5 also causes the inappropriate dispersal of SMC3 from the cohesin complex in the absence of any spindle, which would be required to pull apart the chromosomes.

Slingshot activators (A23187 and Histamine) which decrease the amount of phosphorylated Cofilin in the cells, which LIMK inhibition also does, did not replicate the α-tubulin foci observation seen in cells cultured in BMS5. Though this was more a consequence of the slingshot activators, A23187 and Histamine, failing to cause a decrease in the amount of phosphorylated Cofilin present in HK2 cells. As mentioned in chapter 3 this is contrary to previously published work showing that A23187 and Histamine inducing a decrease in the amount of phosphorylated Cofilin.

In chapter 3 Paclitaxel could not replicate the inhibition of kidney growth or complete loss of Six2, and here it was shown that Paclitaxel did not produce the same α-tubulin foci observation. Paclitaxel produced α-tubulin foci but these were outside of the DNA compartment as opposed to within the DNA compartment as with BMS5. Paclitaxel stalled cells in mitosis and caused an

increase in the number of cells in mitosis compared to no difference in cells cultured in BMS5, this was the same observation as in embryonic kidneys. This shows again that Paclitaxel is not replicating the mechanism by which BMS5 stalls cells in mitosis implying that the observations seen with BMS5 is showing that LIMK is doing something other than simply stalling the cells in mitosis.

BMS5 successfully reduced Cofilin phosphorylation in HK2 cells which caused a reduction in the number of cells present after 24 and 48 hours. This cell number reduction was also true in HEPG2 and C2C12 cells, indicating that this is a universal effect regardless of cell type. To overcome the potential argument that this concentration (50μM) of BMS5 is too high and toxic to the cell, a number of experiments to determine BMS5's toxicity were performed. Using cell counts it was determined that BMS5 was only having this cell number decrease effect in cells undergoing mitosis and cells that were confluent and therefore not undergoing mitosis were unaffected. Thus showing that 50μM BMS5 is an appropriate concentration that reduces Cofilin phosphorylation and non-toxic to non-dividing cells. This also strongly argues that LIMK activity is crucial for the completion of mitosis. This chapter then looked further as to what effect LIMK inhibition has on mitosis and showed that LIMK inhibition prevented progressing beyond metaphase and prevented the formation of the mitotic spindle. The generation of α-tubulin foci within the DNA compartment of the cell during mitosis is different to the α-tubulin foci generated with Paclitaxel which are present outside of the DNA in the cytoplasm. The inappropriate dispersal of SMC3 in BMS5 cultured cells showed a mis-regulation of the spindle checkpoint mechanism in the absence

of active LIMK. SMC3 was also dispersed in cells cultured in Paclitaxel which is because the spindle checkpoint becomes activated (Sudo et al., 2004). This might suggest that the small microtubules emanating from the α-tubulin foci in BMS5 cultured cells have attached to the chromosomes and therefore have activated the spindle checkpoint.

# Chapter 5: Metanephric mesenchymal cell migration.

## 5.1 – Introduction

Chapter 4: showed that active LIMK was required for the completion of mitosis, but LIMK also has a well-documented role in cell migration (Nishita et al., 2005) via is phosphorylation of Cofilin which is crucial for actin turnover at cell lamellipodia. Thus a potential reason for the inhibition of kidney growth and loss of Six2 expression in the MM might be the inability for these cells to migrate in addition to them not being able to complete mitosis. LIMK might be involved in both of these, mitosis and cell migration, therefore this chapter investigated whether cell migration occurs during kidney development and examined the consequences of stopping cell migration.

The UB secretes Wnt9b to signal to the MM cells close to the UB tip to induce them to form nephrons, it was therefore hypothesised that at least some MM cells will need to migrate away from the UB tip towards the periphery of the organ. This is because even though the Six2 expressing MM cells expand via mitosis, some cells must migrate away from the UB tip to prevent becoming induced. If this cell migration was to not occur then all the Six2 MM cells would become induced and the Six2 pool of nephron progenitors (MM cells) would be used up quickly and only a few nephrons would be produced.

It has been shown that LIMK is required for path finding cells during breast cancer cell migration (Scott et al., 2010), and it is well known that LIMK and Cofilin are involved in cell migration (Zebda et al., 2000). Therefore if

metanephric mesenchymal cell migration occurred during kidney development then this would logically require regulation and consequently require LIMK to phosphorylate Cofilin and regulate the actin cytoskeleton.

Chapter 3 showed that LIMK acts to phosphorylate Cofilin in our embryonic kidneys because the LIMK inhibitor, BMS5, caused the loss of phosphorylated Cofilin (Figure 3.4). BMS5 also prevented cell division from completing so the cells won't migrate if they are undergoing mitosis and/or dying via apoptosis. Therefore to show what effects inhibition of migration alone it was necessary to employ alternative inhibitors of migration including the actin disrupter, Cytochalasin B, and the Arp2/3 inhibitor, CK666.

This chapter investigates whether MM cells migrate away from the UB towards the periphery of the kidney by injecting the MM with a fluorescent dye that labels the cell membranes enabling us to track where MM cells go. The effects of inhibiting cell migration in *ex-vivo* organ culture were also investigated.

## 5.2 – Results

### 5.2.1 – DiI labelled populations of cells in the metanephric mesenchyme separate

Kidneys were injected with the lipophilic fluorescent red dye, DiI which binds to the cell membrane and enabled us to track the movement of cells labelled with DiI. MM was injected approximately half way between the UB and the outside edge of the kidney then imaged immediately and after 24 hours in culture. There was clear separation of DiI labelled cells over 24 hours (Figure 5.1 and higher magnifications Figure 5.1). This indicated that these cells had migrated towards the periphery of the organ away from the UB. The original injection site still had cells labelled with DiI after 24 hours showing that some cells did not move, while there were multiple DiI labelled cells (or groups of cells) in the mesenchyme between the original injection site and the periphery of the kidney. Although not all injections were placed perfectly as there was a need to inject in the small region between the UB and the kidney periphery, 21 out of 30 kidneys were observed to have shown separation of DiI labelled cells over 24 hours. We believed that this was migration as opposed to proliferation due to the clear region of non DiI labelled area between the red spots after 24 hours, if it were proliferation or simply the act of kidney growing outwards causing this effect then we would expect to see a line of DiI labelled cells with no gaps as when cells divide the DiI in the membrane is shared between the daughter cells.

The kidneys were then whole mount immunofluorescently labelled with an antibody against the metanephric mesenchyme marker, Six2, to identify that it

was the Six2 cells that were injected. DiI labelled cells (indicated by the arrows) overlaid with Six2 labelled cells (Figure 5.2). Because it was shown that DiI labelled cells moved towards the periphery of the kidney it was therefore proposed that it was the Six2 expressing cells that were the ones moving.

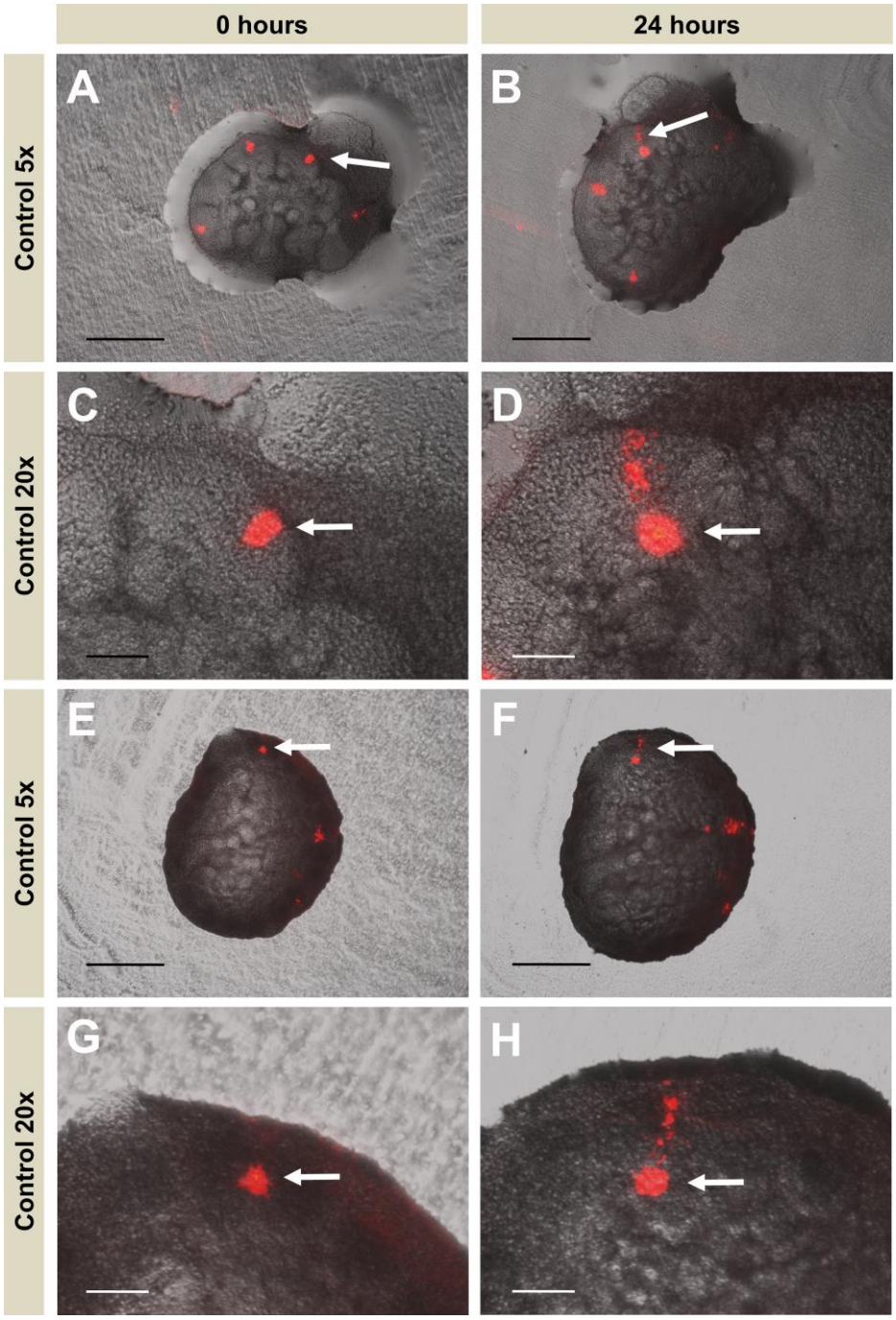



Figure 5.1 – DiI injected mesenchyme showing cells moving to the periphery of the kidney.

E12.5 kidneys DiI (red) microinjected into the mesenchyme (A, C, E, G) and cultured for 24 hours (B, D, F, H), with arrows showing indicating the original injection site and DiI labelled cells moving towards the periphery. Low 5x magnifications (A, B, E, F) showing the whole kidney, and high (20x)

magnifications (C, D, G, H) showing the selected DiI injection showing movement of DiI labelled cells towards the periphery of the kidney. Scale bars = 500µm (A, C, E, G), 100µm (B, D, F, H). 21 out of 30 kidneys were observed to have shown separation of DiI labelled cells over 24 hours.

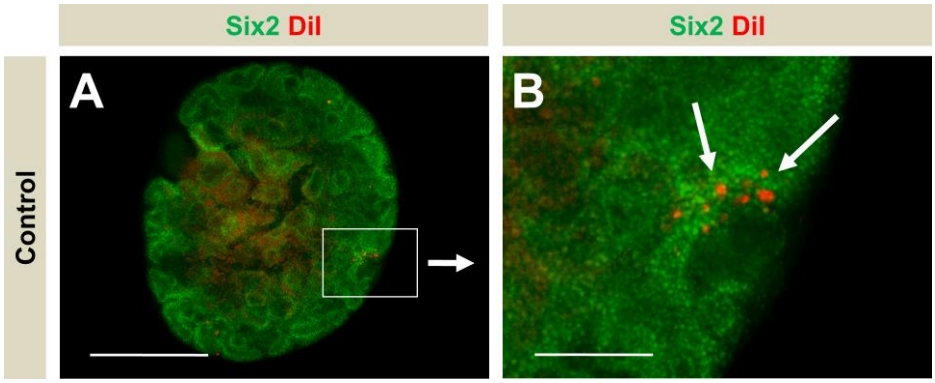



Figure 5.2 – DiI labelled cells overlay with Six2 in E12.5 kidneys.

E12.5 kidneys DiI (red) microinjected and cultured for 24 hours, fixed and whole mount immunofluorescently labelled with Six2 (green). (B) Is a higher magnification (20x) of the boxed region of (A, 5x), with arrows showing DiI (red) labelled cells overlaying with Six2 labelled cells. Scale bars = (A) 400µm and (B) 100µm.

## 5.2.2 – DiI labelled cells migrate towards the periphery of the kidney

To further support the evidence that this separation observed was due to migration, 1 embryonic kidney was injected with DiI and then a time lapse on a confocal laser scanning microscope was carried out over 16 hours (Figure 5.3), this showed one DiI labelled cell (arrow) moved around another stationary DiI labelled cell (arrow head). Images from a single Z stack (number 9) every 1 hour showed clear movement of a DiI labelled cell (approximately 10µm in diameter) migrating 78.9µm towards the periphery of the kidney (towards the bottom of the images), arrow indicating the stationary cell (arrow in the exact same position in every image), the stationary cell disappeared over the course of 16 hours, moving vertically within the kidney (Figure 5.4). Another region of the same kidney (Z stack number 10 from the top left corner of Figure 5.3) showed cells moving over the course of 16 hours, in particular the red cell (indicated by the arrow at 0 hours) moved towards the centre of the kidney (to the right of the images) at the end of the time points (16 hours; away from the arrow which is in the same position; Figure 5.5). The cell (part of the cell membrane labelled with DiI) indicated by the white arrow head in Figure 5.5 at 12 hours moved in the direction of the centre of the kidney (to the right of the images) then back out towards the periphery of the kidney (to the left and bottom left of the images) by 16 hours to the position indicated by the yellow arrow head (the white arrow head remained in the same position in every image). This showed that cells moved independently of each other in the same field of view (Figure 5.5).

In the same region as Figure 5.5 (top left corner of Figure 5.3) but on a higher Z-plane (Z stack number 13, 27.6µm vertical difference from Z stack number 10) there was a DiI labelled cell (indicated by the arrow at 0 hours) that migrated towards the periphery of the kidney (to the left and left bottom corner of the images) between 0 hours and 16 hours (Figure 5.6). Thus showing that cells migrated in opposite directions in the same region of the kidney, towards the centre in Figure 5.5 and towards the periphery in Figure 5.6.

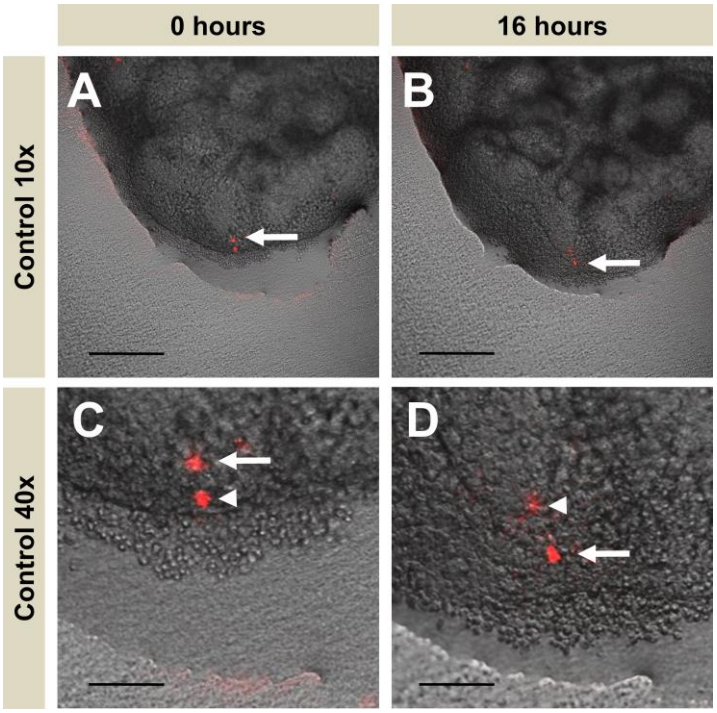



Figure 5.3 – Confocal images of DiI injected mesenchyme showing a cell moving towards the periphery of the kidney.

E12.5 kidney DiI (red) microinjected into the mesenchyme and cultured for 16 hours on a Zeiss LSM710 confocal microscope, with arrows showing a cell labelled with DiI migrating around a stationary cell (arrow head) over 16 hours. Scale bars = 200µm (A, B), 50µm (C, D).

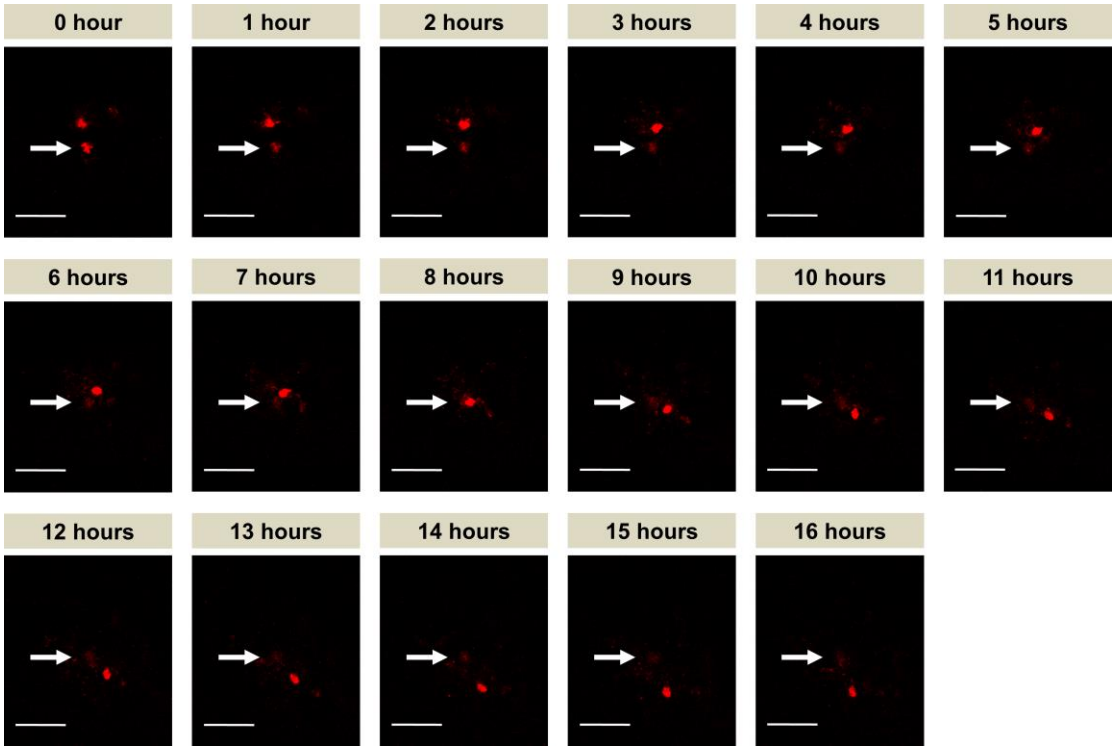



Figure 5.4 – Time lapse confocal images of a DiI labelled cell migrating in the kidney.

E12.5 kidney DiI (red) microinjected into the mesenchyme and cultured for 16 hours on a Zeiss LSM710 confocal microscope with images every 1 hour. Arrows indicating a stationary DiI labelled cell and another DiI labelled cell migrating around the stationary cell over 16 hours (arrow is in the same position in every image, bottom of the image is the edge of the kidney, top is the centre). Scale bars = 50µm.

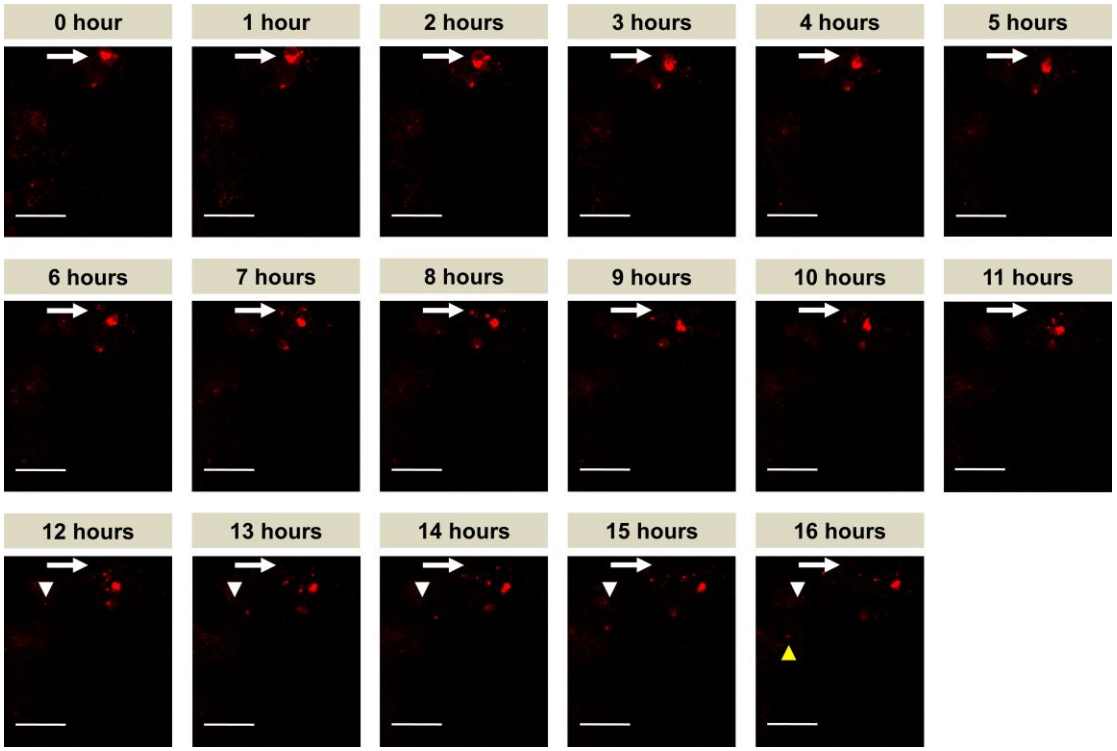



Figure 5.5 – Time lapse confocal images of DiI labelled cells migrating in the kidney.

E12.5 kidney DiI (red) microinjected into the mesenchyme and cultured for 16 hours on a Zeiss LSM710 confocal microscope with images every 1 hour. A DiI labelled cell (indicated by the arrow) is shown migrating towards the centre of the kidney (to the right of the images) over 16 hours (away from the stationary arrow). Another cell indicated by the white arrow head at 12 hours moved to the right (centre of the kidney) then back to the left and bottom of the images (periphery of the kidney) by 16 hours to the final position indicated by the yellow arrow head at 16 hours (the white arrowhead remains in the same position in each image). Scale bars = 50µm.

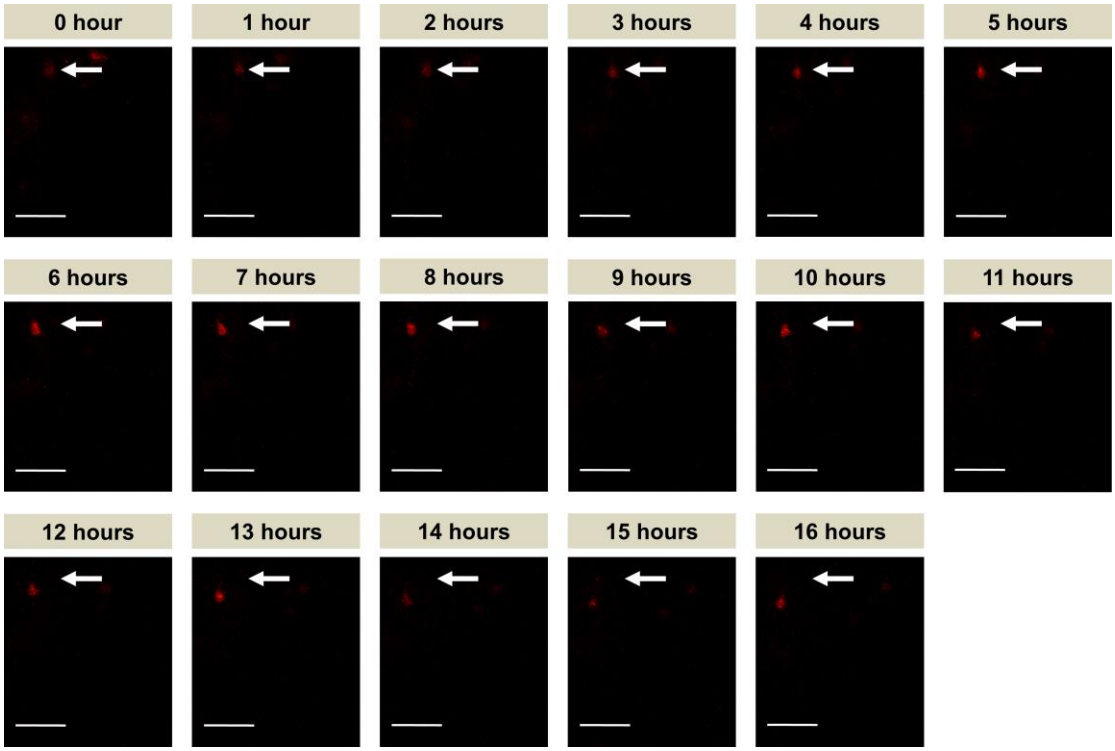



Figure 5.6 – Time lapse confocal images of a DiI labelled cell migrating towards the periphery of the kidney.

E12.5 kidney DiI (red) microinjected into the mesenchyme and cultured for 16 hours on a Zeiss LSM710 confocal microscope with images every 1 hour. A DiI labelled cell (indicated by the arrow) is shown migrating towards the periphery of the kidney (to the left and left bottom corner of the images) over 16 hours (away from the stationary arrow). Scale bars = 50µm.

### 5.2.3 – BMS5 stops cell movement in kidneys

BMS5 was used initially to look at LIMK mediated migration of metanephric mesenchyme cells. Culturing kidneys in BMS5 prevented DiI spot separation (Figure 5.7) as expected in 0 out of 7 kidneys but in addition this also had the effect of inhibiting mitosis (observed in 3.2.3), which meant the observation of DiI spot separation could not be concluded to be solely as a result of BMS5 inhibiting cell migration. Since BMS5 inhibited mitosis and causes apoptosis (Figure 3.10, Figure 3.11) then the lack of DiI separation could simply be because the cells were dying via apoptosis and therefore could not migrate if they were dying. This showed the need to find an inhibitor of cell migration that had no effect on mitosis.

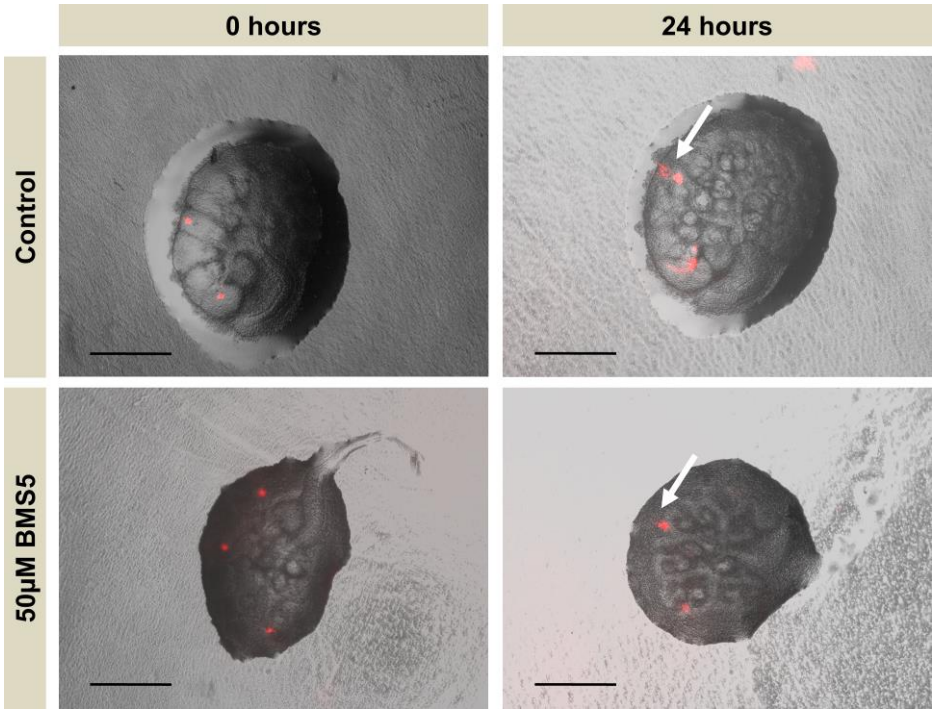



Figure 5.7 – Failure of DiI labelled cells to move in E12.5 kidneys cultured in 50µM BMS5.

E12.5 kidneys microinjected with DiI (red) and cultured in 50µM BMS5 for 24 hours. Arrows show movement of DiI labelled cells in the control kidney, and no movement in the kidney cultured in 50µM BMS5. Scale bars = 500µm. 0 out of 7 kidneys were observed to have shown separation of DiI labelled cells over 24 hours.

## 5.2.4 – Migration inhibitors in HK2 cells

To quantify BMS5s effect on cell migration a cell wounding assay was performed, which showed that control cells migrated 825.99µm ± 62.72, cells cultured in 10µM BMS5 migrated 667.00µm ± 62.49 (p=0.23), and cells cultured in 50µM BMS5 migrated 89.32µm ± 54.86 (p=0.0003, Figure 5.8). This showed that BMS5 affects migration in addition to mitosis.

Next this chapter looked to see if it was possible to inhibit cell migration without affecting mitosis. To this end we made use of two alternative migration inhibitors, CK666 and Cytochalasin B. CK666 inhibits actin polymerisation and thereby migration, by blocking Arp2/3 function and consequently preventing its ability to nucleate new actin filaments at branch points (1.3.2; Yang et al., 2012; Hetrick et al., 2013; Liu et al., 2013). Cytochalasin B is a cell permeable mycotoxin which prevents new actin monomers being added at the growing end of actin filaments and inhibits cell migration (Lin et al., 1980; Selden and Schwartz, 1979). To to verify and quantify these migration inhibitors, wound healing assays in HK2 cells were performed. HK2 cells were grown to confluence and ‘wounded’ with a tip of a 1ml pipette tip, the cell free gap was measure at the beginning and 24 hours later. Control cells migrated 736.3µm ± 41.2 whereas cells cultured in 100µM CK666 migrated only 374.3µm ± 24.6 ($p<0.0001$), 500µM CK666 migrated 67.6µm ± 12.3 ($p<0.0001$, n=4, Figure 5.9). For 1000µM CK666, control cells migrated 651.51µm ± 25.75 and 1000µM CK666 migrated only 96.04µm ± 36.26 ($p<0.0001$, n=4, Figure 5.9).

Cytochalasin B also inhibited cell migration; controls cells migrated 715.4µm ± 32.7 while cells cultured in 10µM Cytochalasin B migrated 148.1µm ± 26.8

($p<0.0001$), and 30µM Cytochalasin B migrated 48.9µm ± 22.7 ($p<0.0001$, Figure 5.10).

Blockade of phospholipase D with Butanol or FIPI has been demonstrated to inhibit cell migration (Nagasaki et al., 2008; Su et al., 2009). Butanol and FIPI was shown to stop migration in HK2 cells. With Butanol the control cells migrated 483.4µm ± 62.5, and cells cultured in 1.5% Butanol migrated 15.1µm ± 14.6 ($p=0.0019$, Figure 5.11). With FIPI, the control cells migrated 475.9µm ± 48.2, and cells cultured in 100µM FIPI migrated 303.4µm ± 16.8 ($p=0.028$, Figure 5.12).

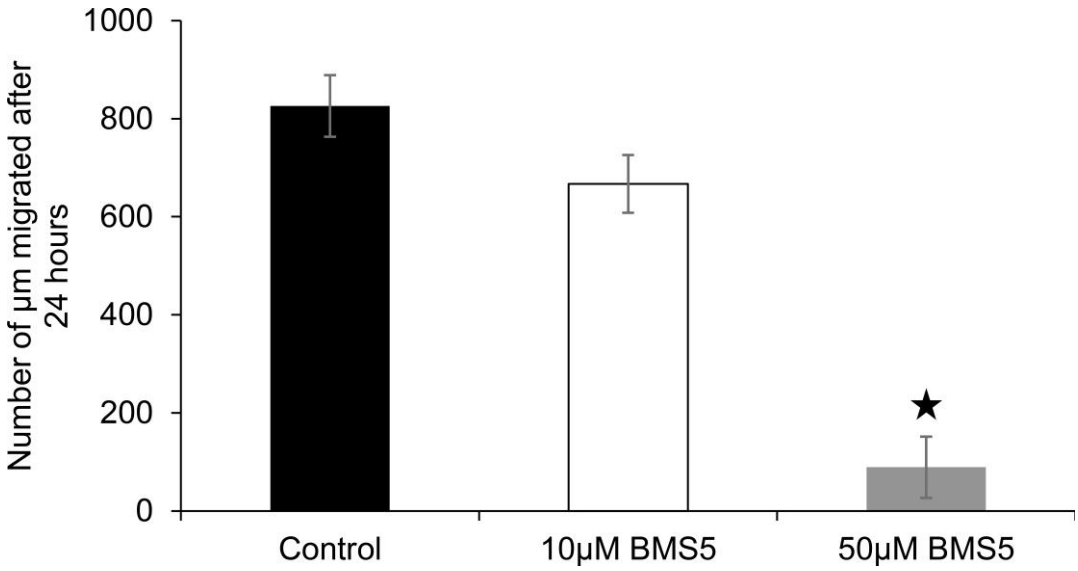



Figure 5.8 – Cell wound assay on HK2 cells cultured in 10µM and 50µM BMS5.

Graph showing a cell wound assay on HK2 cells cultured in 10µm and 50µM BMS5 for 24 hours, showing the number of µm cells migrated over 24 hours after creation of a cell free ‘wound’. Control cells migrated 825.99µm ± 62.72, cells cultured in 10µM BMS5 migrated 667.00µm ± 62.49 ($p=0.23$), and cells cultured in 50µM BMS5 migrated 89.32µm ± 54.86 ($p=0.0003$). * $p<0.001$ compared to control. N=3.

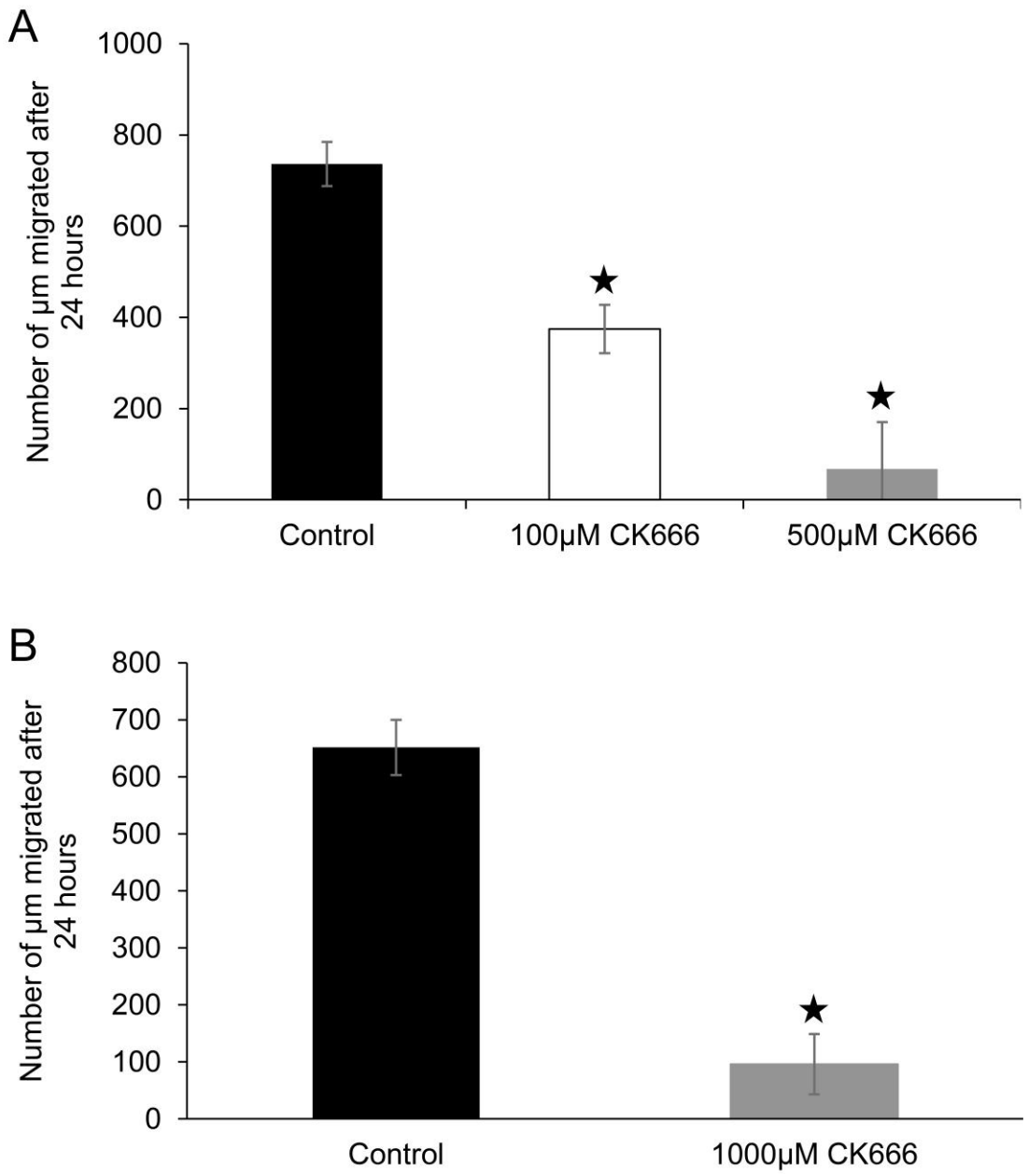



Figure 5.9 – Cell wound assays on HK2 cells cultured in 100µM, 500µM, and 1000µM CK666.

Graphs showing a cell wound assay on HK2 cells cultured in (A) 100µm and 500µM CK666, and (B) 1000µM CK666 for 24 hours, showing the number of µm cells migrated over 24 hours after creation of a cell free 'wound'. (A) Control cells migrated 736.3µm ± 41.2, cells cultured in 100µM CK666 migrated 374.3µm ± 24.6 ($p<0.0001$), and 500µM CK666 migrated 67.6µm ±

12.3 (p<0.0001, n=4). (B) Control cells migrated 651.51µm ± 25.75 and cells cultured in 1000µM CK666 migrated 96.04µm ± 36.26 (p<0.0001, n=4). * p<0.0001 compared to control.

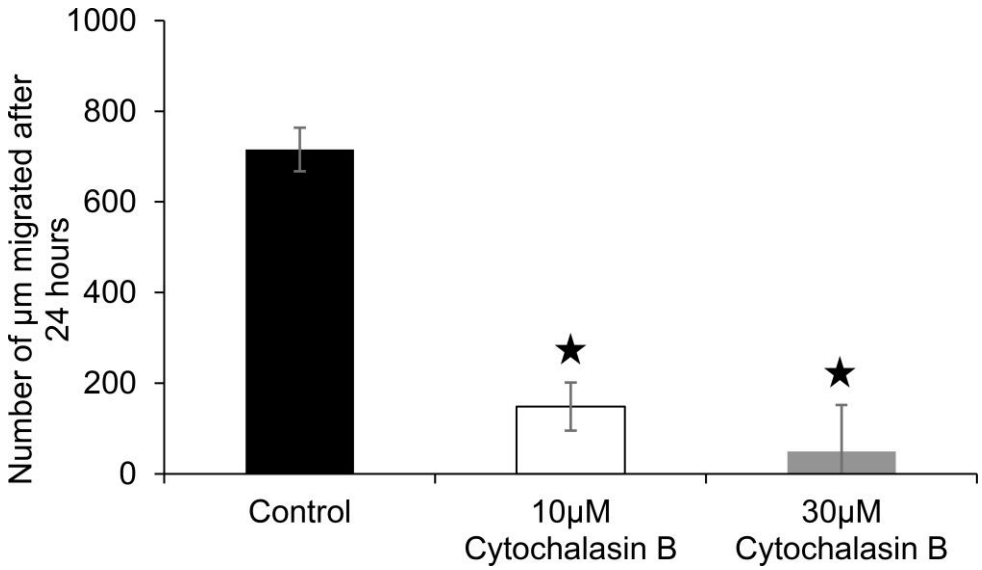



Figure 5.10 – Cell wound assay on HK2 cells cultured in 10µM and 30µM Cytochalasin B.

Graph showing a cell wound assay on HK2 cells cultured in 10µm and 30µM Cytochalasin B for 24 hours, showing the number of µm cells migrated over 24 hours after creation of a cell free 'wound'. Controls cells migrated 715.4µm ± 32.7, cells cultured in 10µM Cytochalasin B migrated 148.1µm ± 26.8 (p<0.0001), and cells cultured in 30µM Cytochalasin B migrated 48.9µm ± 22.7 (p<0.0001, N=3). * p<0.0001 compared to control.

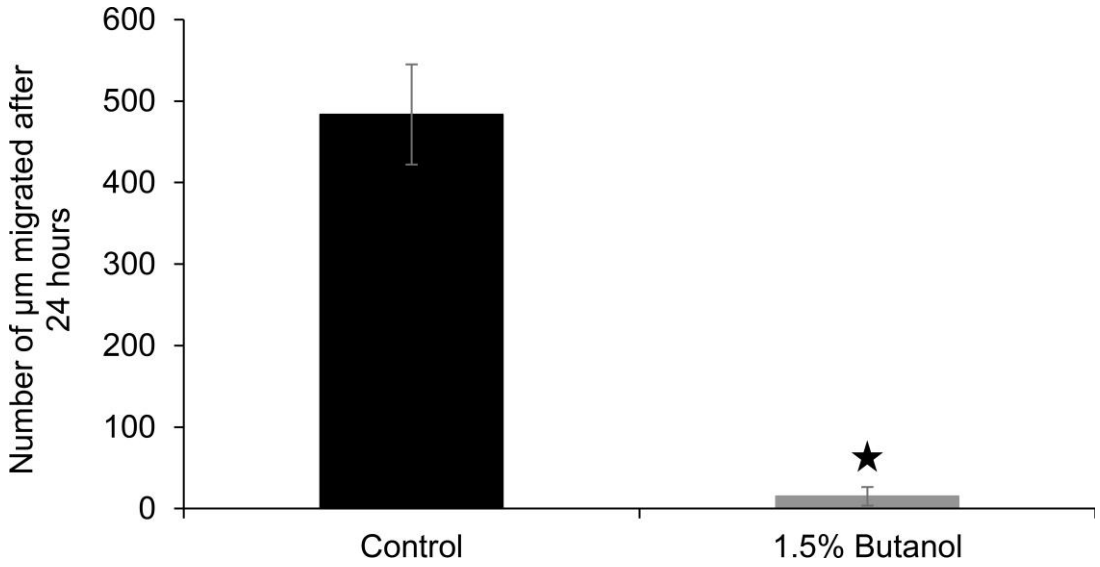



Figure 5.11 – Cell wound assay on HK2 cells cultured in 1.5% Butanol.

Graph showing a cell wound assay on HK2 cells cultured in 1.5% Butanol for 24 hours, showing the number of µm cells migrated over 24 hours after creation of a cell free 'wound'. Cells cultured in control media migrated 483.4µm ± 62.5, and cells cultured in 1.5% Butanol migrated 15.1µm ± 14.6 ($p=0.0019$). * $p<0.01$ compared to control. N=3.

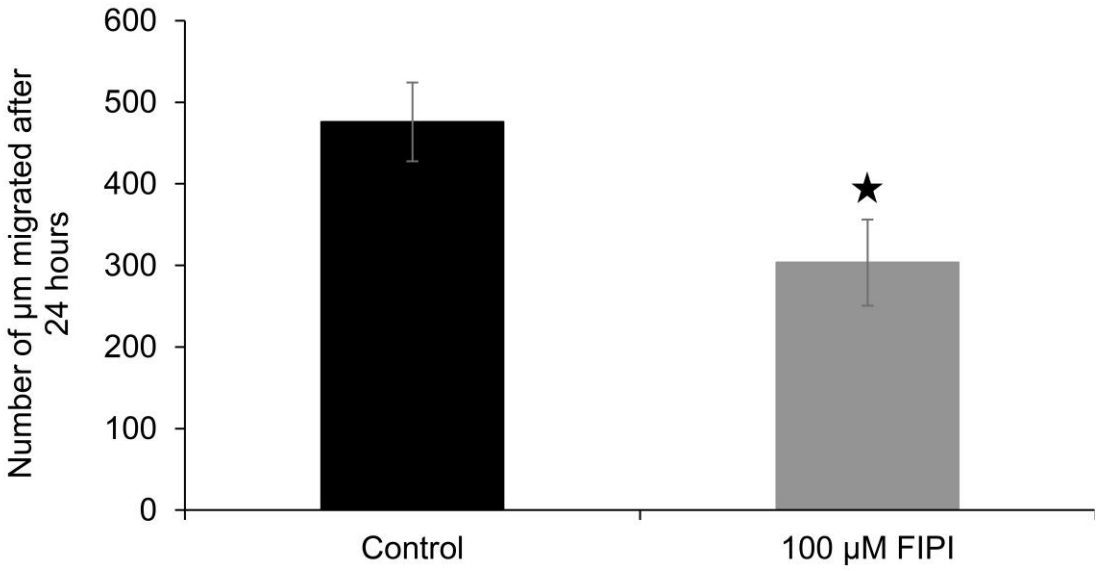



Figure 5.12 – Cell wound assay on HK2 cells cultured in 100µM FIPI.

Graph showing a cell wound assay on HK2 cells cultured in 100µm FIPI for 24 hours, showing the number of µm cells migrated over 24 hours after creation of a cell free ‘wound’. Cells cultured in control media migrated 475.9µm ± 48.2, and cells cultured in 100µM FIPI migrated 303.4µm ± 16.8 ($p=0.028$, $N=3$). * $p<0.05$ compared to control.

### 5.2.5 – Migration inhibitors stop mesenchyme cell migration

To see whether CK666 and Cytochalasin B inhibited cell migration in kidney development in addition to in a cell culture system embryonic kidneys were injected with DiI and then cultured in the presence or absence of 100µM, 500µM, 1000µM CK666, or 10µM, 30µM Cytochalasin B. CK666, an inhibitor of the Arp2/3 complex prevented the separation of the DiI cells indicating that this effectively inhibited migration at 500µM and at 1000µM (Figure 5.13). 29 out of 37 (78%) kidneys showed migration in controls whereas 3 out of 5 (60%) kidneys showed migration in 100µM CK666 cultured kidneys, 3 out of 6 (50%) kidneys showed migration at 500µM CK666, and only 1 out of 6 (20%) kidneys showed migration at 1000µM CK666. Cytochalasin B also showed no movement for DiI at 30µM (Figure 5.14); 3 out of 5 (60%) kidneys showed migration in 10µM Cytochalasin B cultured kidneys and only 1 out of 5 (20%) kidneys showed migration at 30µM CK666.

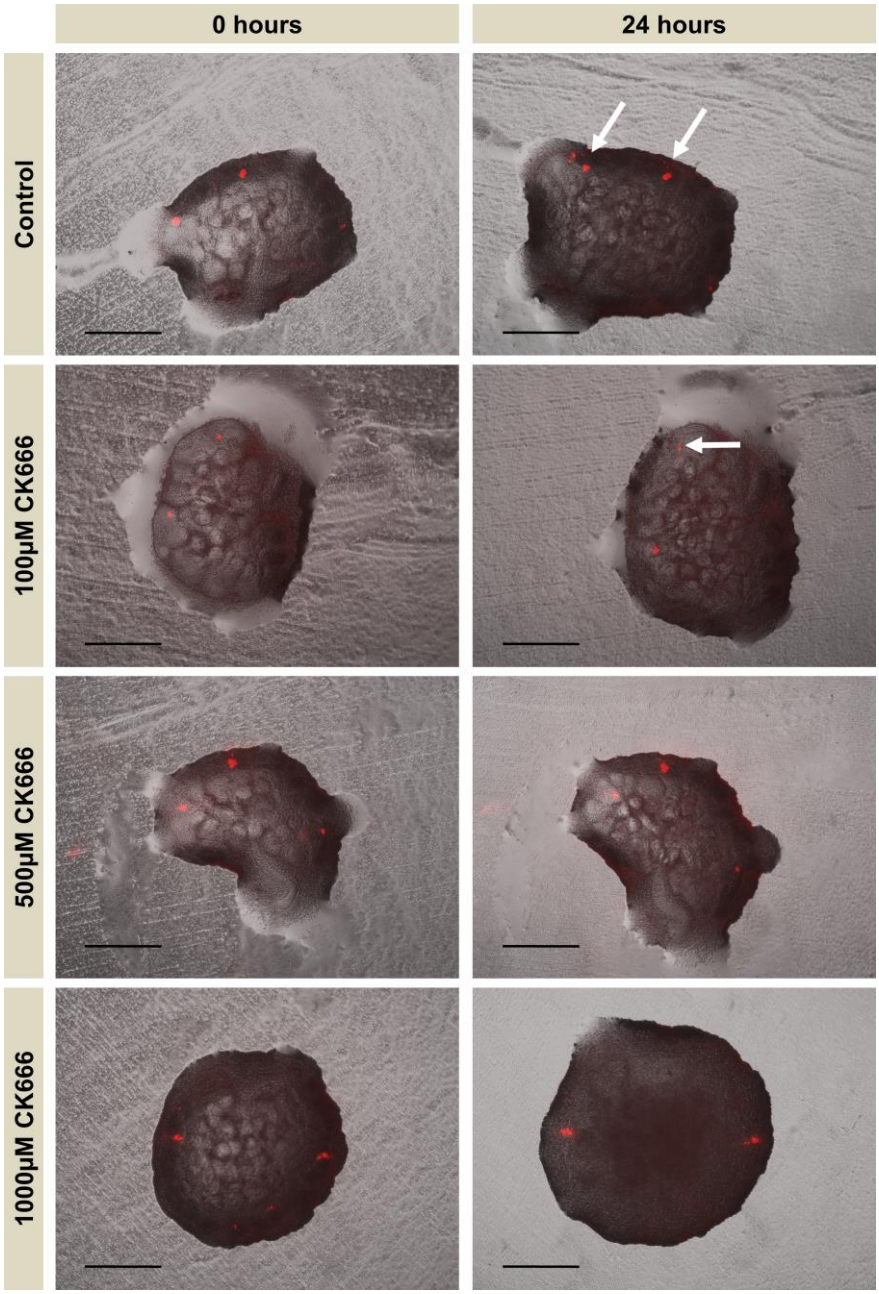



Figure 5.13 – DiI labelled cells not migrating in E12.5 kidneys cultured in CK666.

E12.5 kidneys microinjected with DiI (red) and cultured in 100µM, 500µM, and 1000µM CK666 for 24 hours. Arrows show movement of DiI labelled cells in the control kidney and the kidney cultured in 100µM CK666. No movement was observed in the kidneys cultured in 500µM and 1000µM CK666. Scale bars = 500µm. N>5.

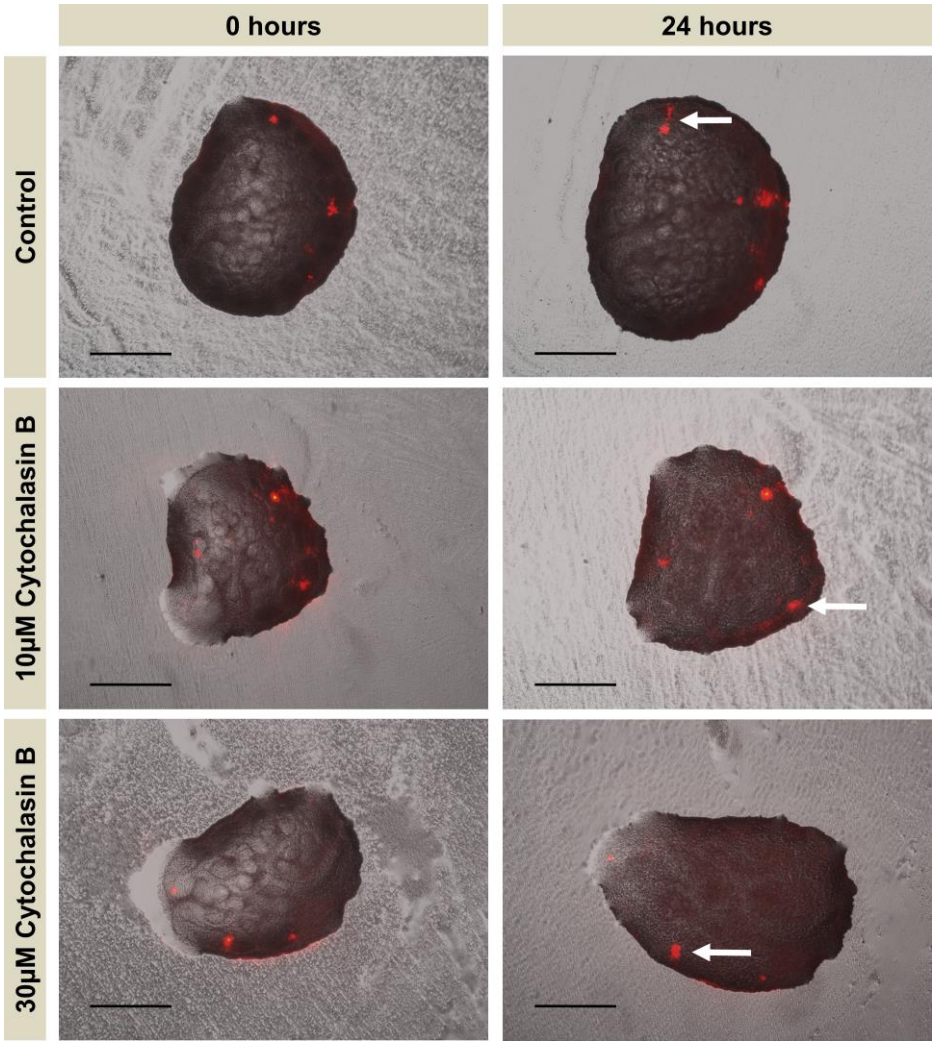



Figure 5.14 – DiI labelled cells not migrating in E12.5 kidneys cultured in Cytochalasin B.

E12.5 kidneys microinjected with DiI (red) and cultured in 10µM and 30µM Cytochalasin B for 24 hours. Arrows show movement of DiI labelled cells in the control kidney and no movement in the kidneys cultured in 10µM and 30µM Cytochalasin B. Scale bars = 500µm. N>5.

## 5.2.6 – Consequences of the inhibition of cell migration with Cytochalasin B

Due to the observation that Cytochalasin B inhibited migration (Figure 5.14) we looked to see what effect this had on the growth of the kidney. During 48 hours in culture control kidneys had grown 147.56% ± 4.60, and 10μM Cytochalasin B cultured kidneys had grown 131.19% ± 6.70 (p=0.079, n=5, Figure 5.15). When the concentration of Cytochalasin B was increased to 30μM control kidneys had grown 146.53% ± 3.86 over 48 hours, and kidneys cultured in 30μM Cytochalasin B had only grown to 132.24% ± 4.43 (p=0.041, n=5, Figure 5.15) of their original size.

This inhibition of growth was also apparent in light micrographs of kidneys cultured in Cytochalasin B. Kidneys cultured in both 10μM (Figure 5.16) and 30μM (Figure 5.17) Cytochalasin B appeared smaller with no further development of the UB and no generation of new renal vesicles apparent on the light micrographs. Kidneys were cultured in 10μM and 30μM Cytochalasin B and were whole mount immunofluorescently labelled for the detection of the metanephric mesenchyme marker, Six2, which showed that they had lost all Six2 expression at both 10μM (Figure 5.18) and 30μM (Figure 5.18) Cytochalasin B.

Kidneys were cultured in control or 10μM Cytochalasin B and immunofluorescently labelled for the detection of the mitotic marker pH3. Controls had 4.09% ± 1.53 of mitotic cells in anaphase and kidneys cultured in 10μM Cytochalasin B had 5.62% ± 1.07 of mitotic cells in anaphase (p=0.46, n=3). The total number of cells in mitosis in an average field of view

was 95.33 ± 6.80 in control kidneys, while kidneys cultured in 10μM Cytochalasin B had 27.11 ± 3.29 cells in mitosis (p=0.00083, n=3, Figure 5.19). When kidneys were cultured in 30μM Cytochalasin B, controls had 4.60% ± 0.15 of mitotic cells in anaphase and kidneys cultured in 30μM Cytochalasin B had 3.01% ± 0.89 of mitotic cells in anaphase (p=0.15, n=3). The total number of cells in mitosis in an average field of view was 95.00 ± 6.75 in control kidneys, and kidneys cultured in 30μM Cytochalasin B had 32.22 ± 6.06 cells in mitosis (p=0.0023, n=3, Figure 5.20). This showed that Cytochalasin B caused a significant reduction in the number of cells in mitosis at both 10μM and 30μM concentrations, thus Cytochalasin B did not exclusively affect migration in kidneys.

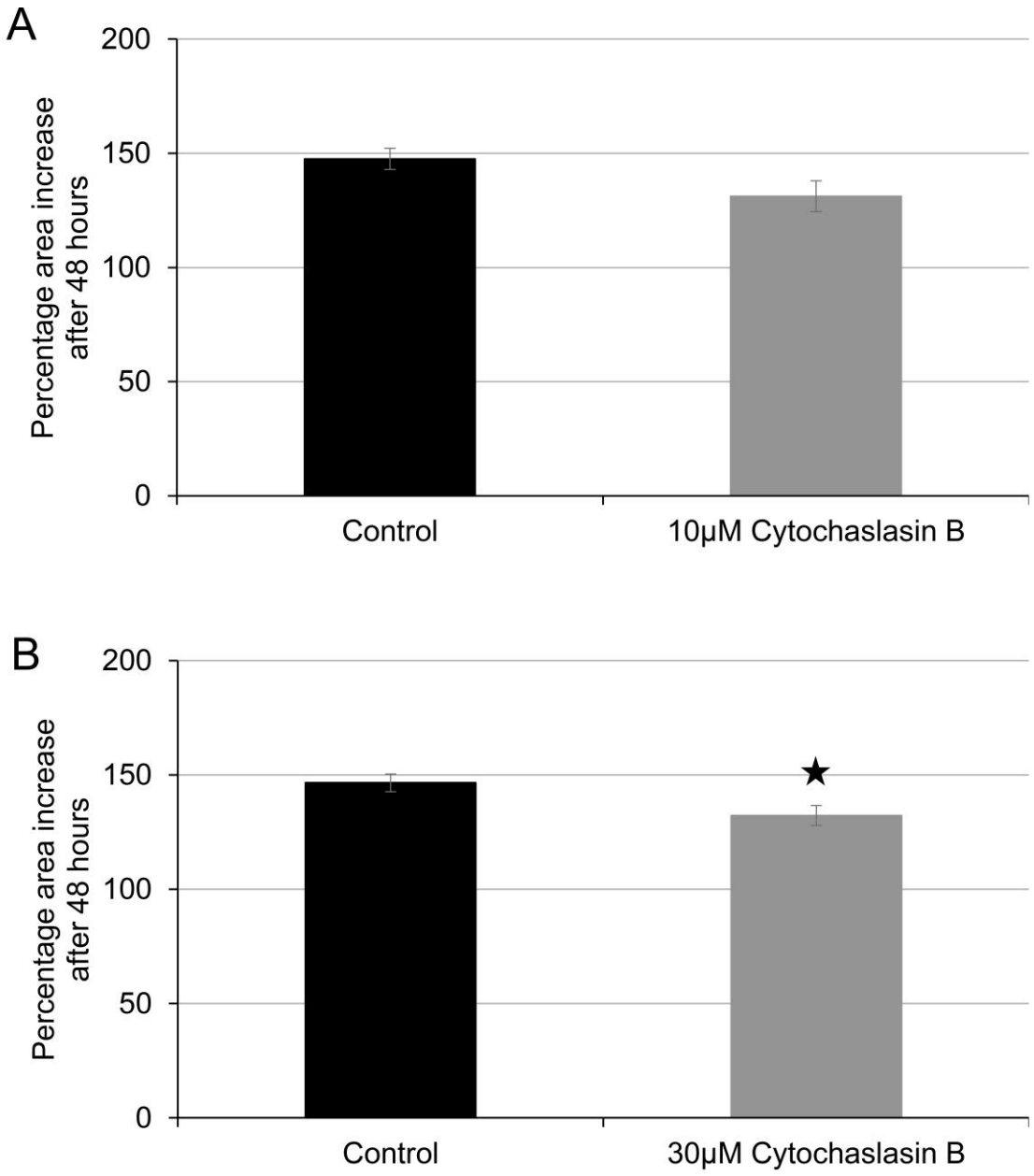



Figure 5.15 – Kidney size after 48 hours cultured in 10µM and 30µM Cytochalasin B.

Graph showing the percentage area increase over 48 hours in culture in (A) 10µM and (B) 30µM Cytochalasin B. (A) Control kidneys had grown 147.56% ± 4.60, and 10µM Cytochalasin B cultured kidneys had grown 131.19% ± 6.70 (p=0.079, n=5). (B) Control kidneys had grown 146.53% ± 3.86 over 48 hours,

and kidneys cultured in 30µM Cytochalasin B had only grown to 132.24% ± 4.43 (p=0.041, n=5). * p<0.05 compared to control.

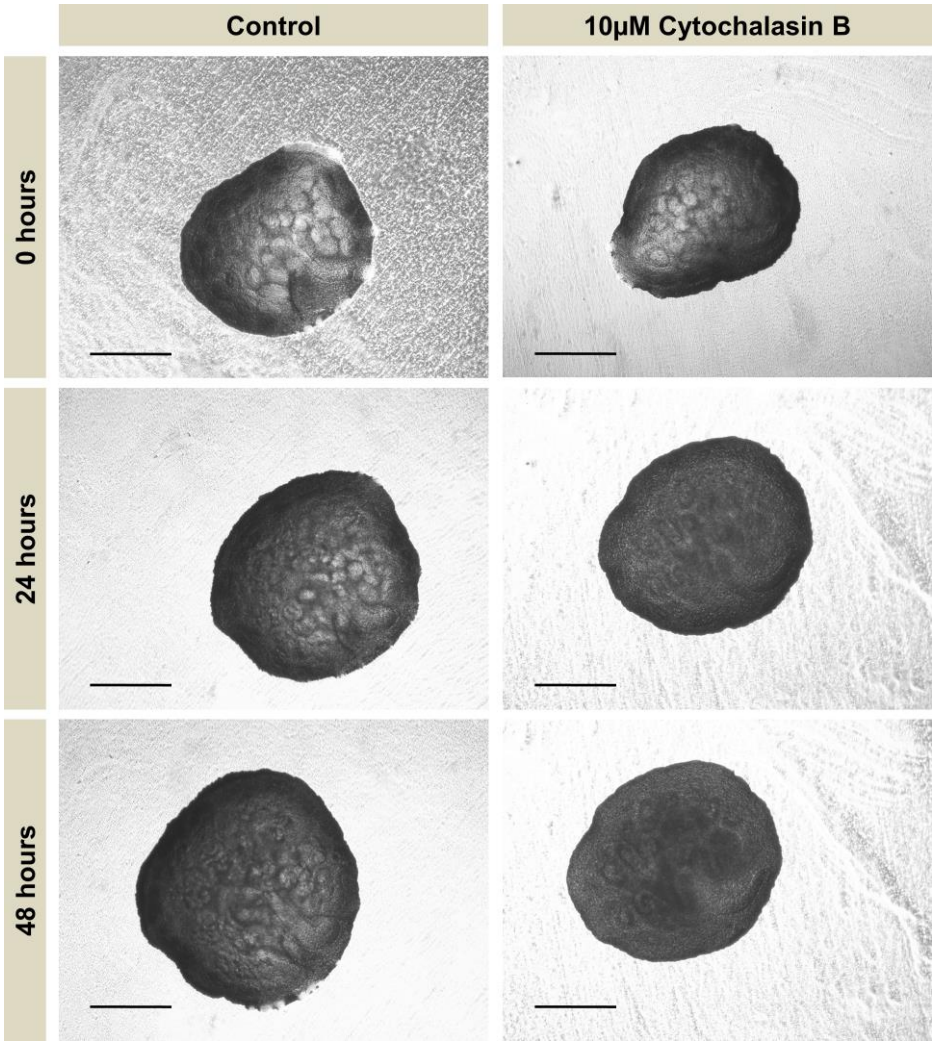



Figure 5.16 – Light micrographs of E12.5 kidneys cultured in 10µM Cytochalasin B.

E12.5 kidneys cultured in 10µM Cytochalasin B for 48 hours. Kidneys cultured in 10µM Cytochalasin B appeared smaller than controls after 48 hours. Scale bars = 500µm. N=3.

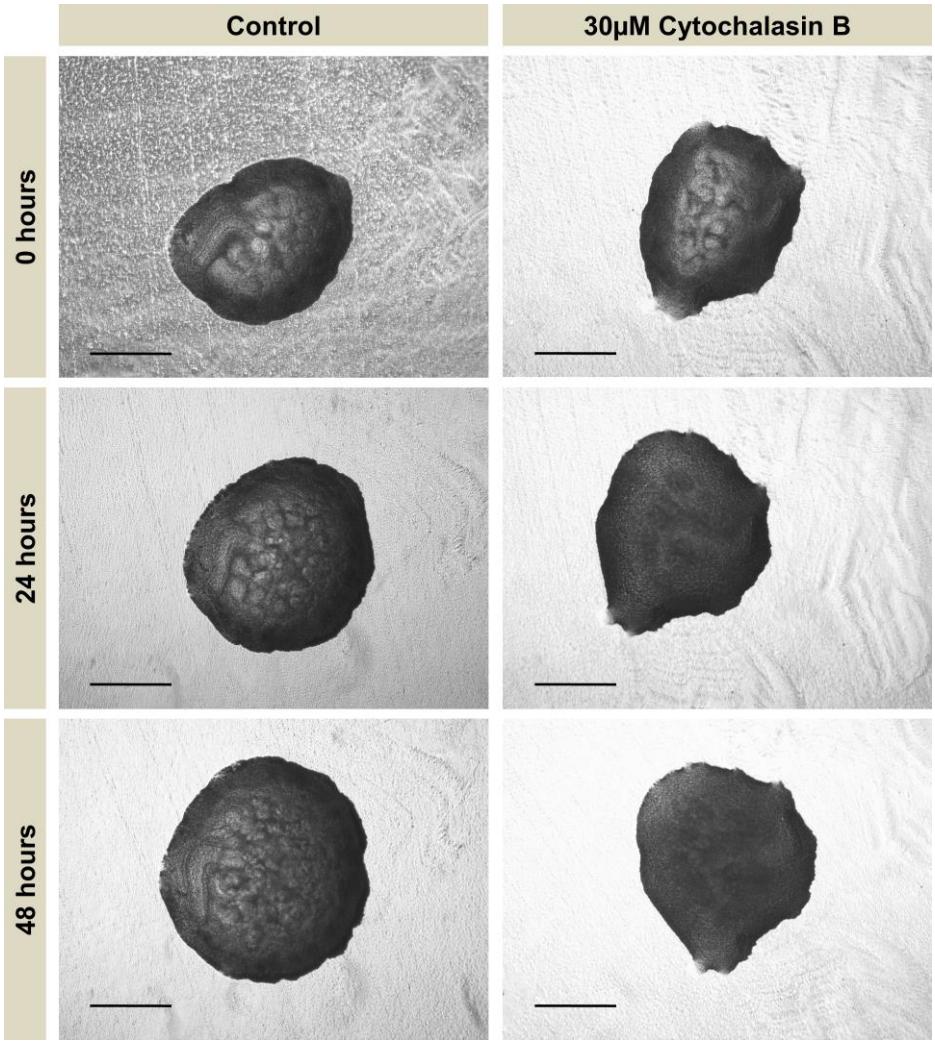



Figure 5.17– Light micrographs of E12.5 kidneys cultured in 30µM Cytochalasin B.

E12.5 kidneys cultured in 30µM Cytochalasin B for 48 hours. Kidneys cultured in 30µM Cytochalasin B appeared smaller than controls after 48 hours. Scale bars = 500µm. N=3.

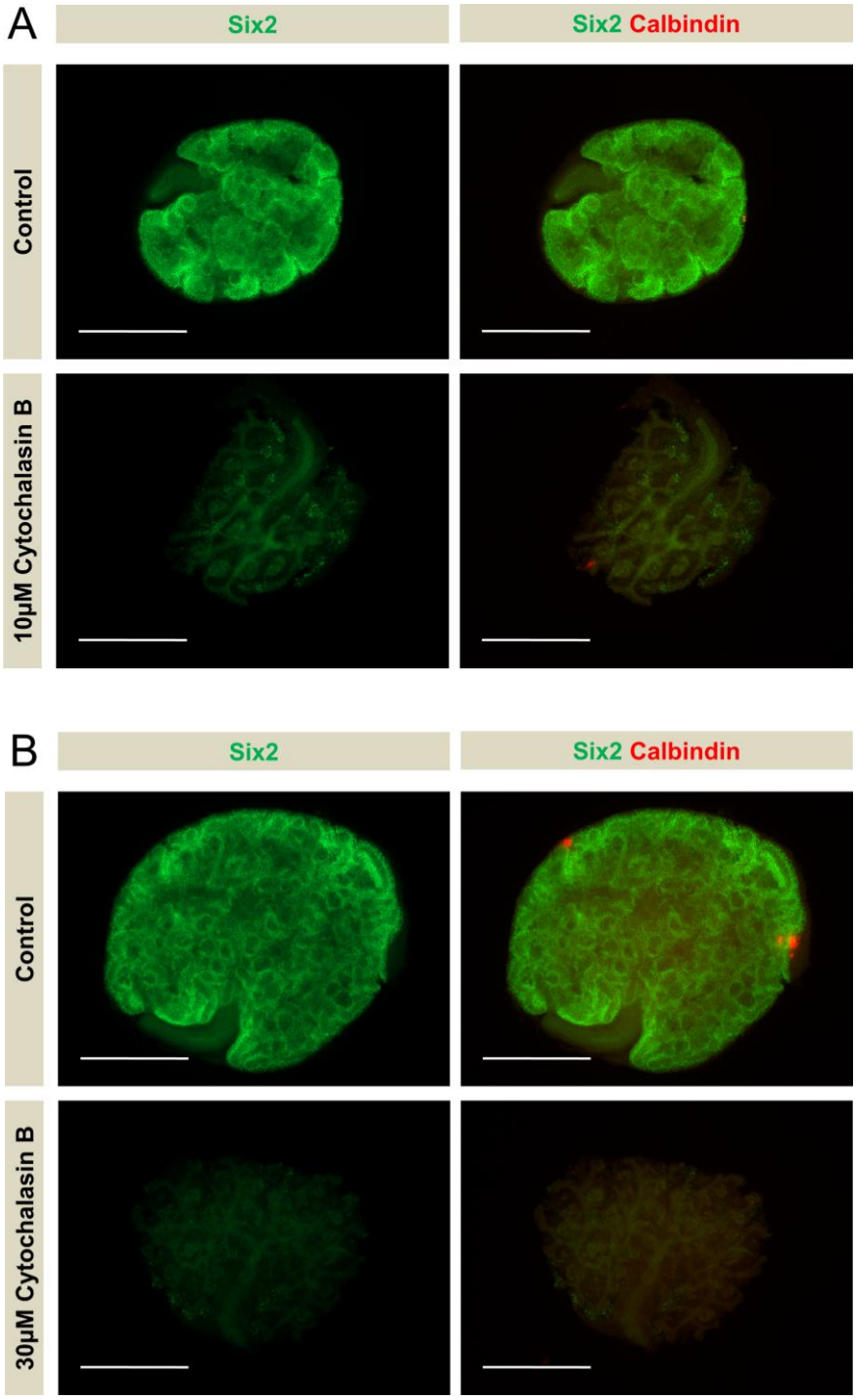



Figure 5.18 – Six2 in E12.5 kidneys cultured in 10μM and 30μM Cytochalasin B.

E12.5 kidneys cultured in (A) 10μM and (B) 30μM Cytochalasin B for 48 hours, fixed and whole mount immunofluorescently labelled with Six2 (green), and Calbindin (red). Kidneys cultured in both 10μM and 30μM Cytochalasin B

show no Six2 (green) expression compared to controls. Scale bars = 200µm. N=3.

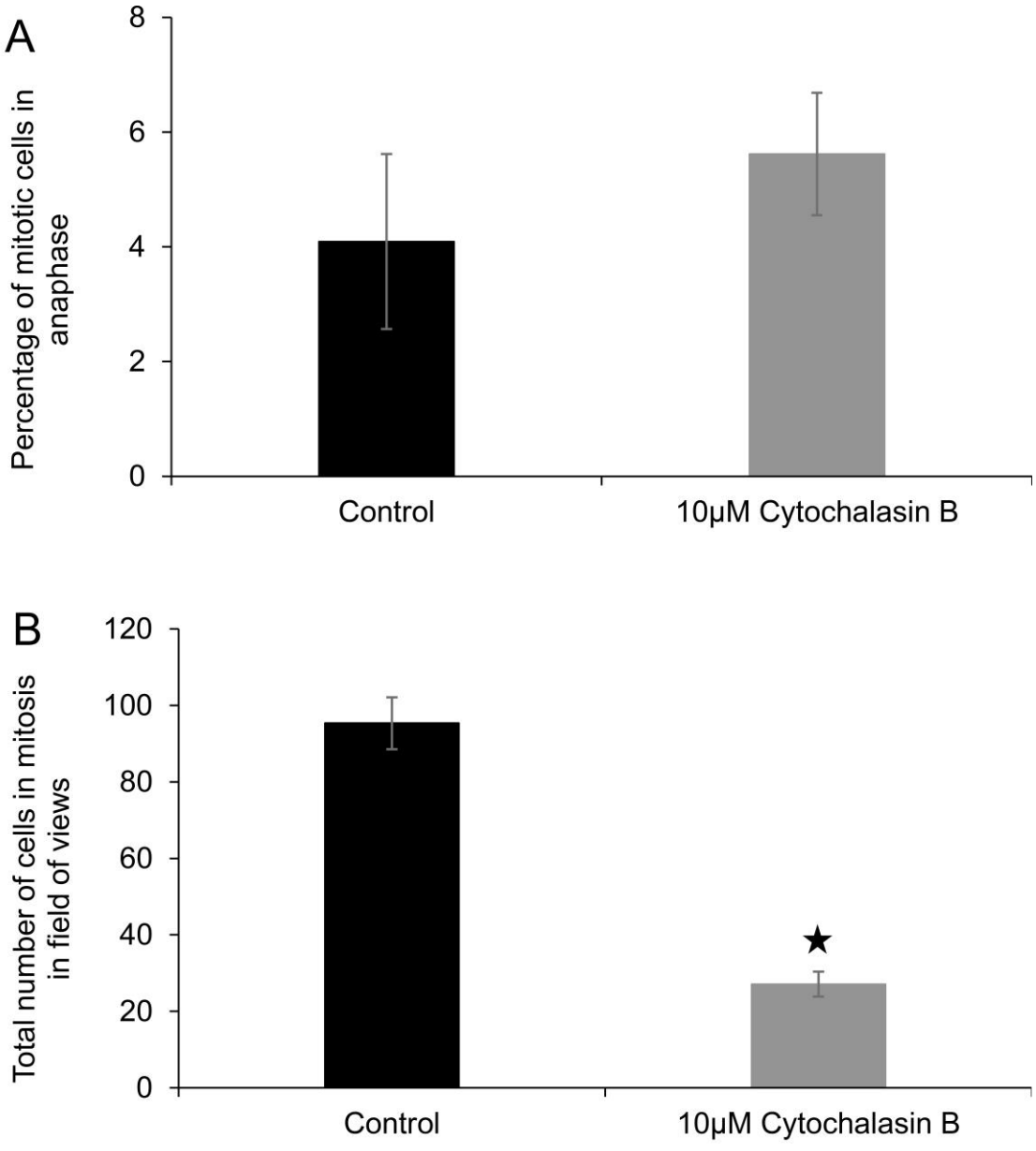



Figure 5.19 – Mitosis analysis of E12.5 kidneys cultured in 10µM Cytochalasin B.

Graphs showing kidneys cultured in 10µM Cytochalasin B for 48 hours, fixed and whole mount immunofluorescently labelled with pH3. (A) Percentage of mitotic cells in anaphase. Controls had 4.09% ± 1.53 of mitotic cells in

anaphase and kidneys cultured in 10μM Cytochalasin B had 5.62% ± 1.07 of mitotic cells in anaphase (p=0.46, n=3). (B) Total number of cells in mitosis in field of views. The total number of cells in mitosis in an average field of view was 95.33 ± 6.80 in control kidneys, while kidneys cultured in 10μM Cytochalasin B had 27.11 ± 3.29 cells in mitosis (p=0.00083, n=3). * p<0.001 compared to control.

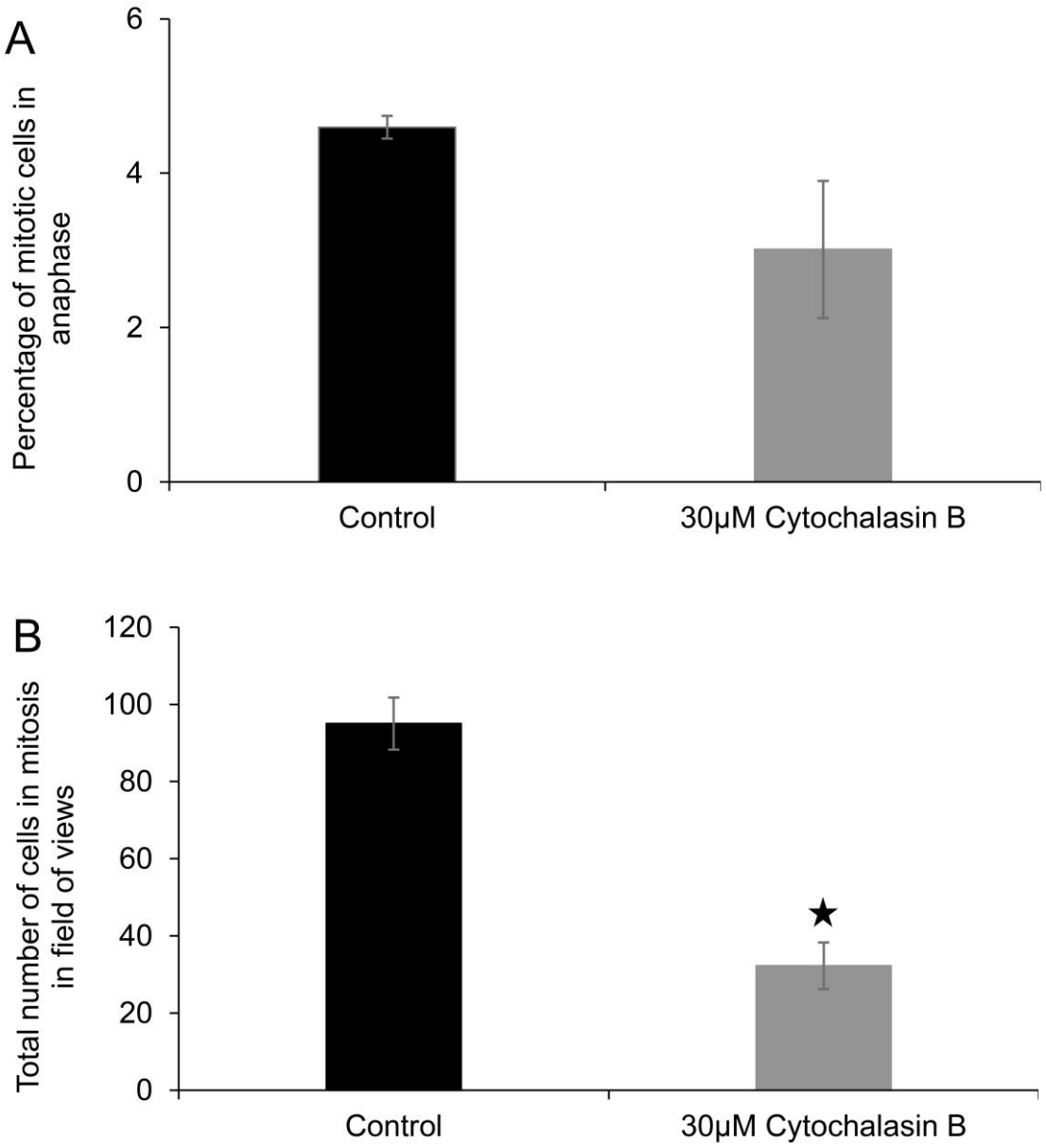



Figure 5.20 – Mitosis analysis of E12.5 kidneys cultured in 30μM Cytochalasin B.

Graphs showing kidneys cultured in 30μM Cytochalasin B for 48 hours, fixed and whole mount immunofluorescently labelled with pH3. (A) Percentage of mitotic cells in anaphase. Controls had 4.60% ± 0.15 of mitotic cells in anaphase and kidneys cultured in 30μM Cytochalasin B had 3.01% ± 0.89 of mitotic cells in anaphase ($p=0.15$, $n=3$). (B) Total number of cells in mitosis in field of views. The total number of cells in mitosis in an average field of view

was 95.00 ± 6.75 in control kidneys, and kidneys cultured in 30μM Cytochalasin B had 32.22 ± 6.06 cells in mitosis (p=0.0023, n=3). * p<0.01 compared to control.

## 5.2.7 – Does CK666 affect mitosis?

Cytochalasin caused the inhibition of mitosis (see 5.2.6) therefore another migration inhibitor, the Arp2/3 inhibitor CK666, was used to see if this only affected migration with no impact on mitosis in embryonic kidneys. Three concentrations (100μM, 500μM and 1000μM) were used because there was very little knowledge on the use of this inhibitor, and the papers that have used it used it at 100μM (Liu et al., 2013) or 200μM (Hetrick et al., 2013). A low concentration (100μM), five times this (500μM), and five times the higher concentration (1000μM) were used because with the BMS5 inhibitor we had to use five times the concentration in organ culture as opposed to previously published work due to the nature of culturing organs (see 3.2.1).

Kidneys cultured in CK666 for 48 hours were fixed and whole mount immunofluorescently labelled with pH3. The number of mitotic cells in anaphase and total number of mitotic cells in an average field of view were counted. When kidneys were cultured in 100μM CK666, controls had 2.39% ± 0.74 of mitotic cells in anaphase and kidneys cultured in 100μM CK666 had 2.16% ± 1.21 of mitotic cells in anaphase (p=0.88, n=3). The total number of cells in mitosis in an average field of view was 92.6 ± 7.11 in control kidneys, and kidneys cultured in 100μM CK666 had 94.2 ± 20.39 cells in mitosis (p=0.94, n=3, Figure 5.21). When kidneys were cultured in 500μM CK666,

controls had 3.40% ± 1.48 of mitotic cells in anaphase and kidneys cultured in 500µM CK666 had 2.55% ± 0.51 of mitotic cells in anaphase (p=0.64, n=2), while the total number of cell in mitosis in an average field of view was 101.00 ± 1.20 in control kidneys, while kidneys cultured in 500µM CK666 had 99.50 ± 2.10 cells in mitosis (p=0.60, n=2, Figure 5.22). And when kidneys were cultured in 1000µM CK666, controls had 3.76% ± 0.80 of mitotic cells in anaphase and kidneys cultured in 1000µM CK666 had 1.23% ± 0.50 of mitotic cells in anaphase (p=0.054, n=3), while the total number of cells in mitosis in an average field of view was 86.53 ± 13.69 in control kidneys, while kidneys cultured in 1000µM CK666 had 96.53 ± 4.33 cells in mitosis (p=0.52, n=3, Figure 5.23). Thus showing that neither 100µM, 500µM nor 1000µM CK666 had any significant effect on mitosis.

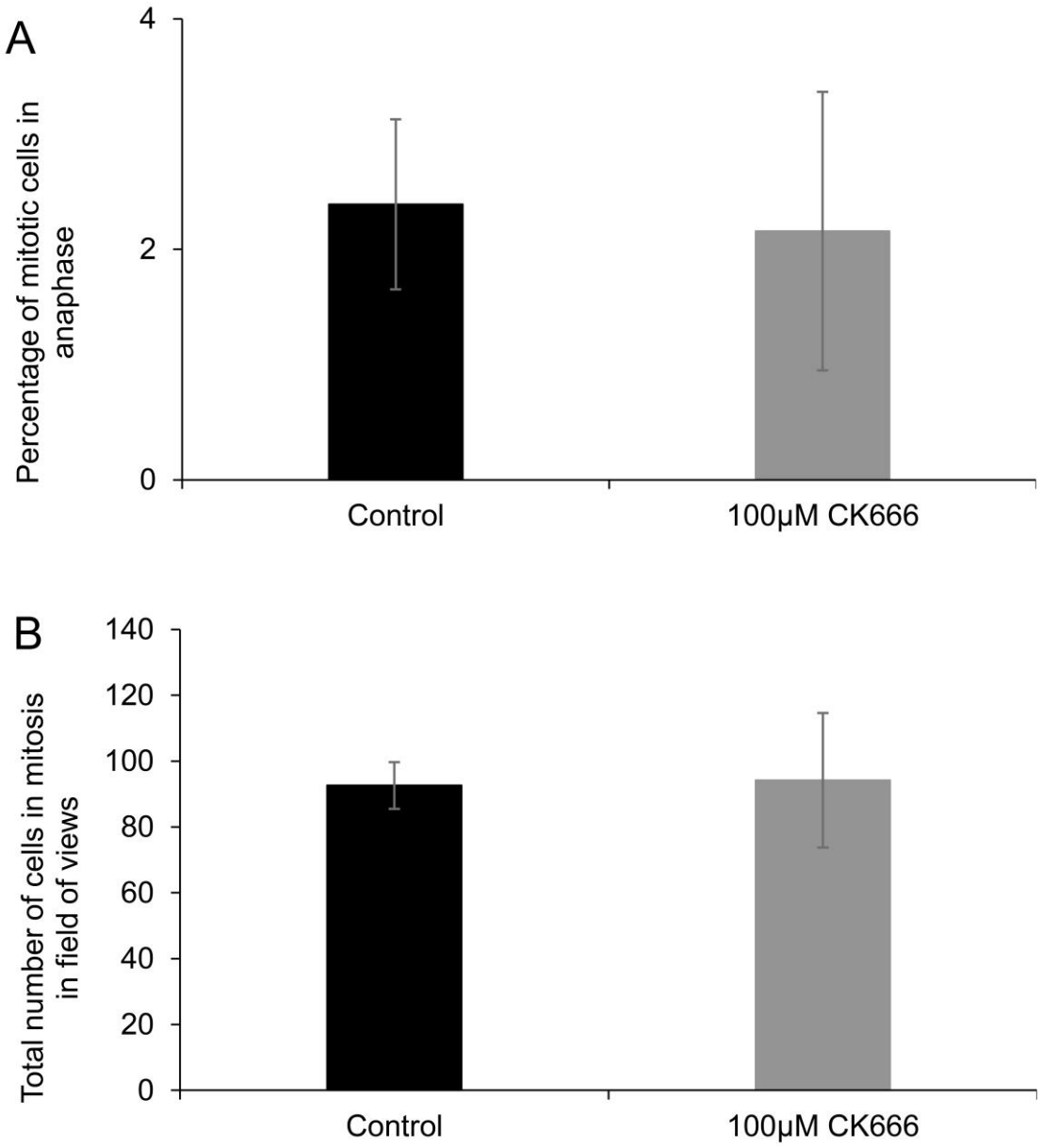



Figure 5.21 – Mitosis analysis of E12.5 kidneys cultured in 100µM CK666.

Graphs showing kidneys cultured in 100µM CK666 for 48 hours, fixed and whole mount immunofluorescently labelled with pH3. (A) Percentage of mitotic cells in anaphase. Controls had 2.39% ± 0.74 of mitotic cells in anaphase and kidneys cultured in 100µM CK666 had 2.16% ± 1.21 of mitotic cells in anaphase (p=0.88, n=3). (B) Total number of cells in mitosis in field of views. The total number of cells in mitosis in an average field of view was 92.6 ± 7.11

in control kidneys, and kidneys cultured in 100µM CK666 had 94.2 ± 20.39 cells in mitosis (p=0.94, n=3).

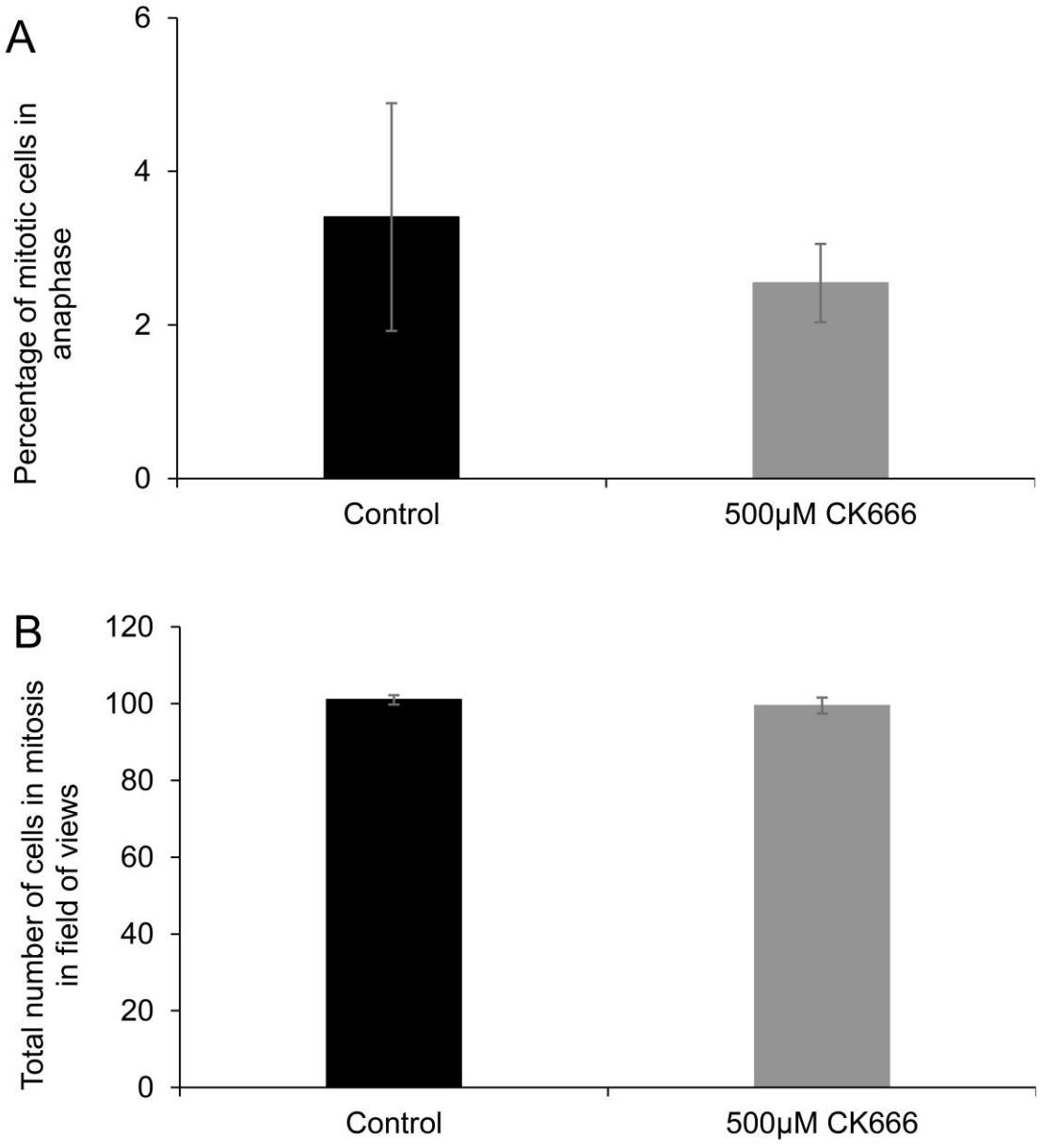



Figure 5.22 – Mitosis analysis of E12.5 kidneys cultured in 500µM CK666.

Graphs showing kidneys cultured in 500µM CK666 for 48 hours, fixed and whole mount immunofluorescently labelled with pH3. (A) Percentage of mitotic cells in anaphase. Controls had 3.40% ± 1.48 of mitotic cells in anaphase and kidneys cultured in 500µM CK666 had 2.55% ± 0.51 of mitotic cells in

anaphase (p=0.64, n=2). (B) Total number of cells in mitosis in field of views. The total number of cell in mitosis in an average field of view was 101.00 ± 1.20 in control kidneys, while kidneys cultured in 500μM CK666 had 99.50 ± 2.10 cells in mitosis (p=0.60, n=2).

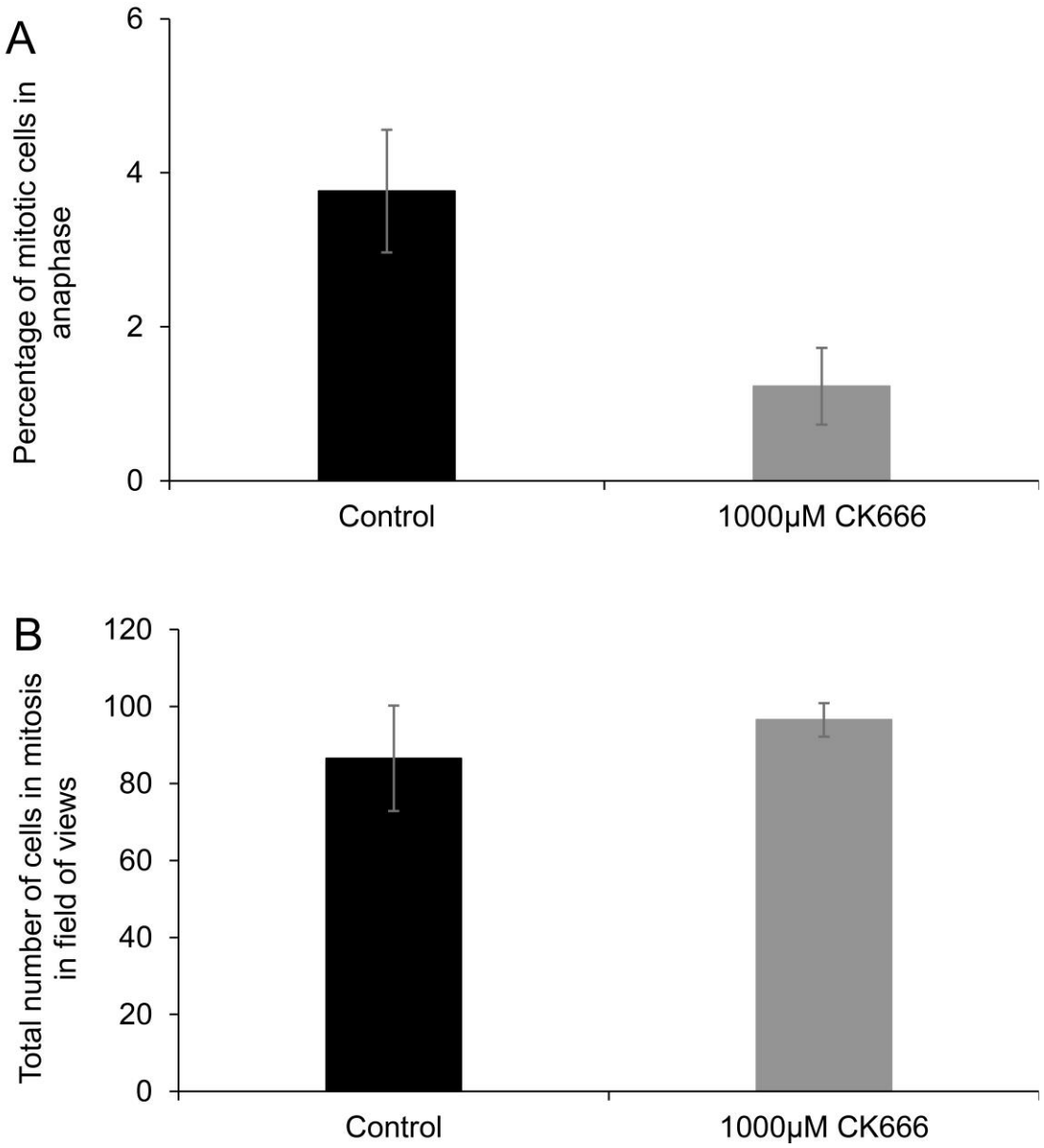



Figure 5.23 – Mitosis analysis of E12.5 kidneys cultured in 1000µM CK666.

Graphs showing kidneys cultured in 1000µM CK666 for 48 hours, fixed and whole mount immunofluorescently labelled with pH3. (A) Percentage of mitotic cells in anaphase. Controls had 3.76% ± 0.80 of mitotic cells in anaphase and kidneys cultured in 1000µM CK666 had 1.23% ± 0.50 of mitotic cells in anaphase (p=0.054, n=3). (B) Total number of cells in mitosis in field of views. The total number of cells in mitosis in an average field of view was 86.53 ±

13.69 in control kidneys, while kidneys cultured in 1000µM CK666 had 96.53 ± 4.33 cells in mitosis (p=0.52, n=3).

### 5.2.8 – Consequences of cell migration inhibition with CK666

CK666 had no significant effect on mitosis so we therefore looked at the effect CK666 had on the growth of the kidney. Kidneys were cultured in control media, 100µM CK666, or 500µM CK666 for 5 days and there was no significant impairment in growth compared to contralateral controls (Figure 5.24), however when kidneys were cultured in 1000µM CK666 over 5 days their growth was significantly impaired compared to contralateral controls at every time point after start of culture ($p<0.01$, Figure 5.24).

While this impairment of growth over 5 days compared to the effect seen with 50µM BMS5 was similar in that the end result of significantly smaller kidneys were seen after 5 days, their growth over 5 days was different. Kidneys cultured in 50µM BMS5 grew to about 150% in the first 2 days before shrinking to 122.97% ± 9.64 after 5 days cultured in 50µM BMS5 (Figure 5.25). When cultured in 1000µM CK666 kidney growth was limited to a maximum of 110.41% ± 2.41 after 72 hours, and stayed fairly constant over 5 days, which implied that CK666 prevented growth rather than the BMS5 effect of growing and dying off.

The appearance of kidneys cultured in CK666 was consistent with the growth measurements with kidneys that were cultured in 1000µM appeared

considerably smaller than their contralateral controls (Figure 5.28). This appearance suggests that they kidney cultured in 1000µM had simply halted growth and were not dying because the structure of the kidney appeared to be intact, this compared to kidneys treated in BMS5 in which the mesenchyme appeared to be disintegrating. Kidneys grown in 500µM CK666 appeared slightly smaller (Figure 5.27), and those cultured in 100µM CK666 appeared very similar to contralateral controls (Figure 5.26). The appearance of kidneys cultured in 1000µM CK666, while smaller, did not appear to be disintegrating as seen with kidneys cultured in 50µM BMS5 (Figure 5.29) which showed the mesenchyme to be disintegrating. This would suggest that the CK666 inhibitor was not causing cell death, which happened when kidneys were cultured in 50µM BMS5. Further to this when kidneys cultured in 1000µM CK666 for 48 hours were whole mount immunofluorescently labelled for the mesenchyme marker Six2, they appeared to have fewer Six2 expressing cells. However contrary to what was observed in kidneys cultured in 50µM BMS5, there were still some Six2 expressing cells present which would be appropriate because they were smaller kidneys. The amount of Six2 appeared to decrease as the concentration of CK666 increased, 100µM CK666 cultured kidneys appeared no different to the control, 500µM CK666 cultured kidneys appeared to have less Six2 expressing cells, and 1000µM CK666 cultured kidneys have much less Six2 expressing cells compared to the control (Figure 5.30) although this could not be quantified.

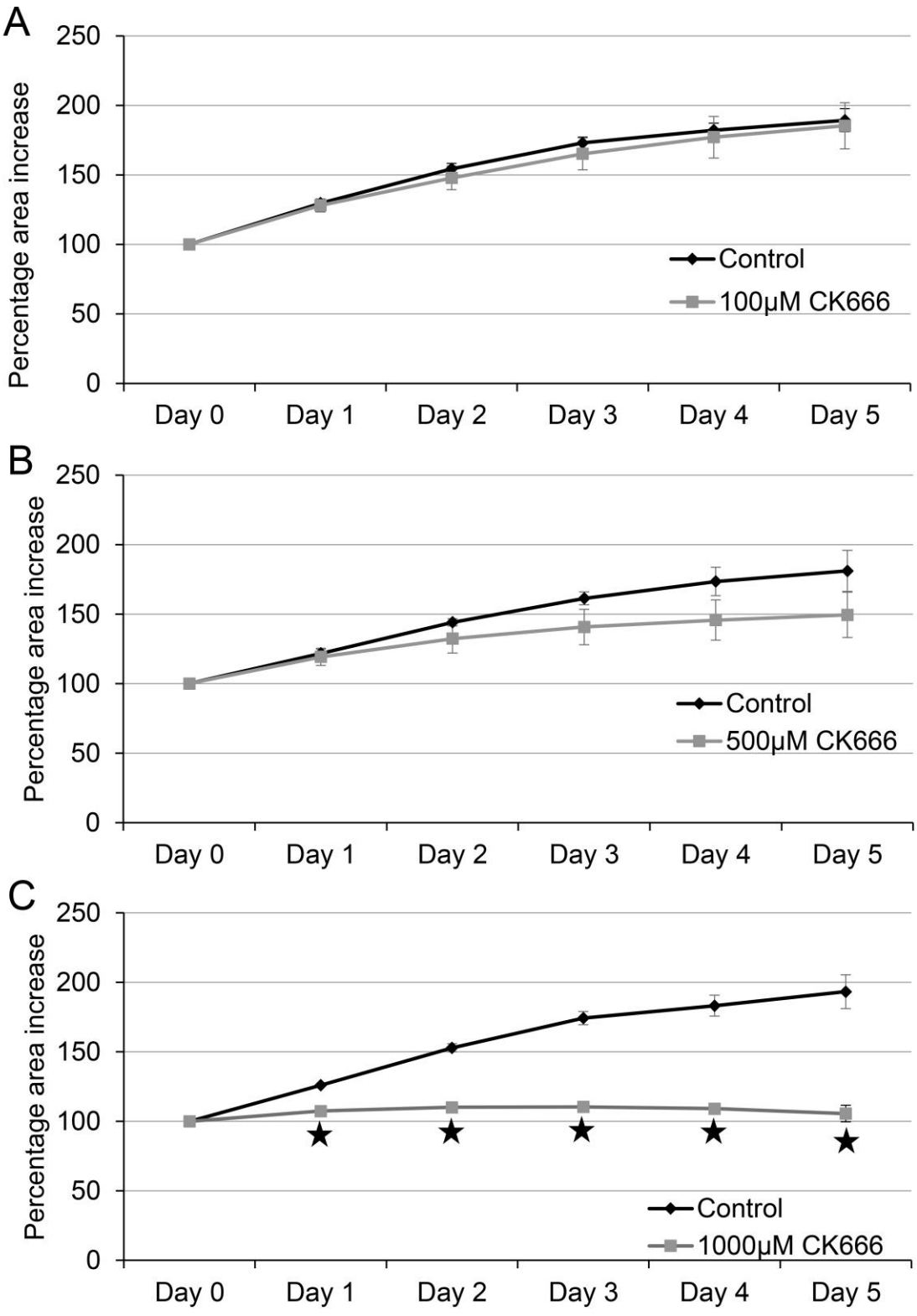



Figure 5.24 – Kidney size over 5 days cultured in 100µM, 500µM, and 1000µM CK666.

Graph showing the percentage area increase over 5 days in culture in (A) 100µM CK666, (B) 500µM CK666, and (C) 1000µM CK666. No significant difference was observed in kidneys cultured in 100µM CK666 or 500µM CK666 compared to controls. Kidneys cultured in 1000µM CK666 were significantly smaller over 5 days compared to contralateral controls at every time point after start of culture (* $p<0.01$). N=3.

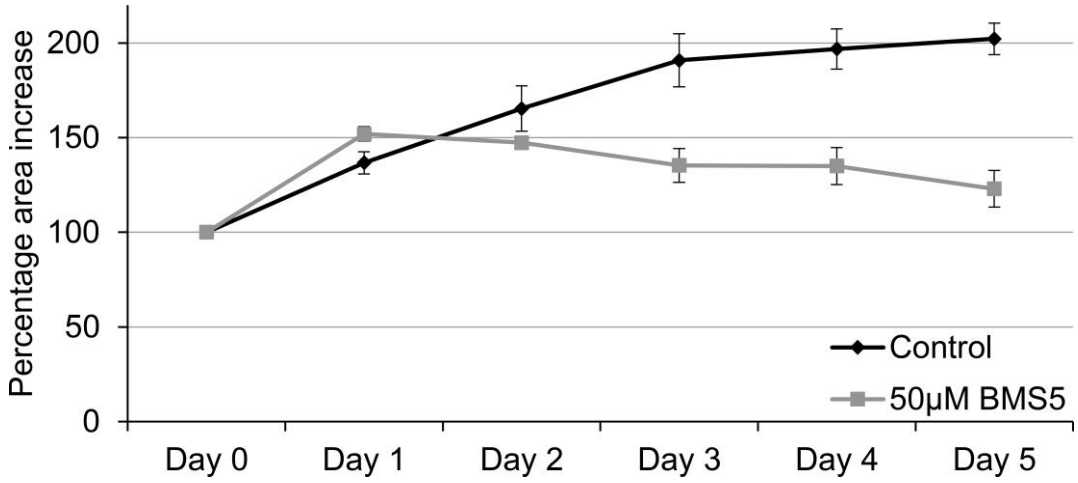



Figure 5.25 – Kidney size over 5days cultured in 50µM BMS5.

Graph showing the percentage area increase over 5 days cultured in 50µM BMS5. Kidneys cultured in 50µM BMS5 grew to about 150% in the first 2 days before shrinking to 122.97% ± 9.64 after 5 days cultured in 50µM BMS5. N=3.

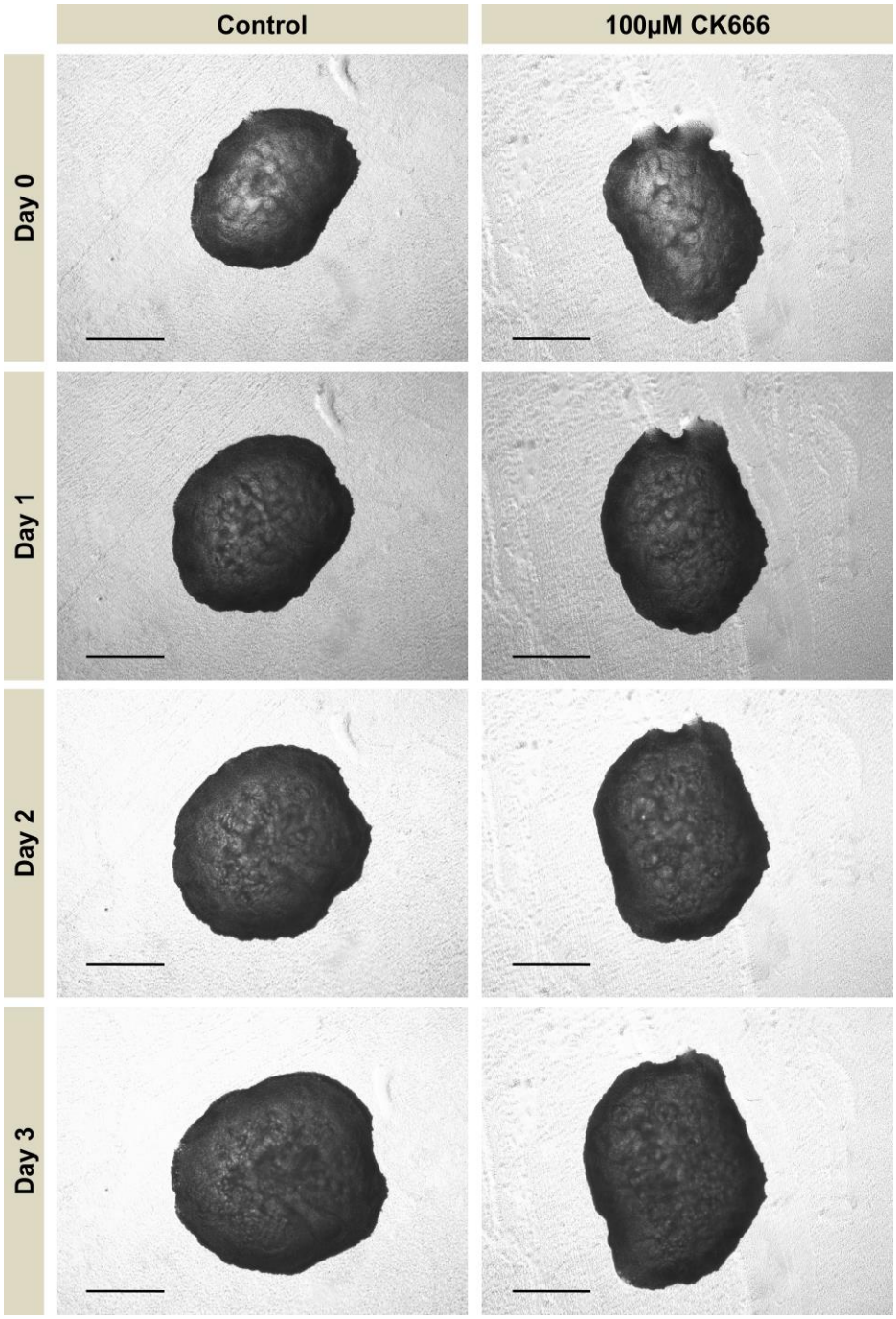



Figure 5.26 – Light micrographs of E12.5 kidneys cultured in 100µM CK666.

E12.5 kidneys cultured in 100µM CK666 for 3 days, images every 24 hours. Kidneys cultured in 100µM CK666 appeared similar to the kidneys cultured in control media. Scale bars = 500µm. N=3.

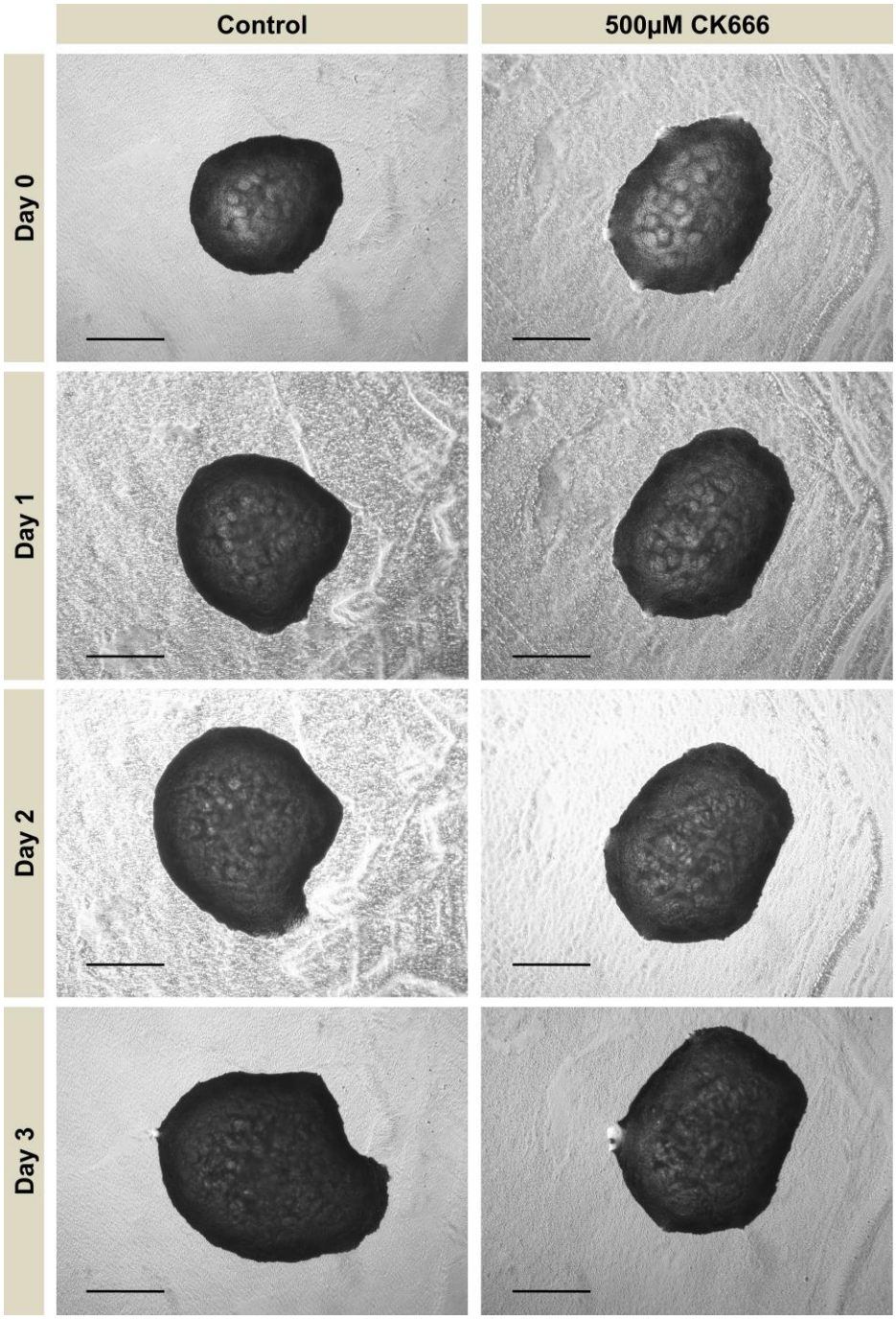



Figure 5.27 – Light micrographs of E12.5 kidneys cultured in 500µM CK666.

E12.5 kidneys cultured in 500µM CK666 for 3 days, images every 24 hours. Kidneys cultured in 500µM CK666 appeared slightly smaller compared to the kidneys cultured in control media. Scale bars = 500µm. N=3.

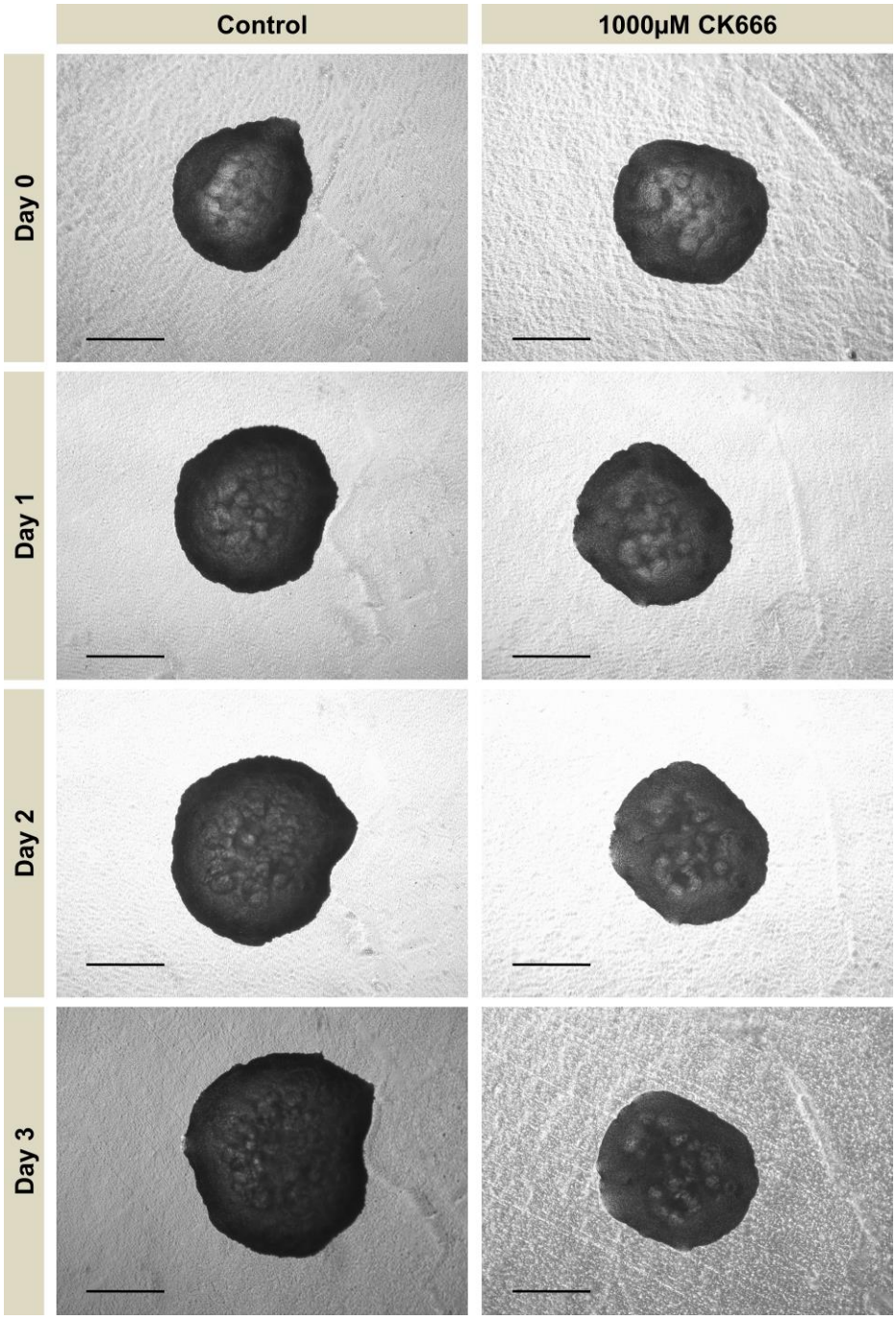



Figure 5.28 – Light micrographs of E12.5 kidneys cultured in 1000µM CK666.

E12.5 kidneys cultured in 1000µM CK666 for 3 days, images every 24 hours, showing kidneys cultured in 1000µM CK666 much smaller and no further growth compared to kidneys cultured in control media. Scale bars = 500µm. N=3.

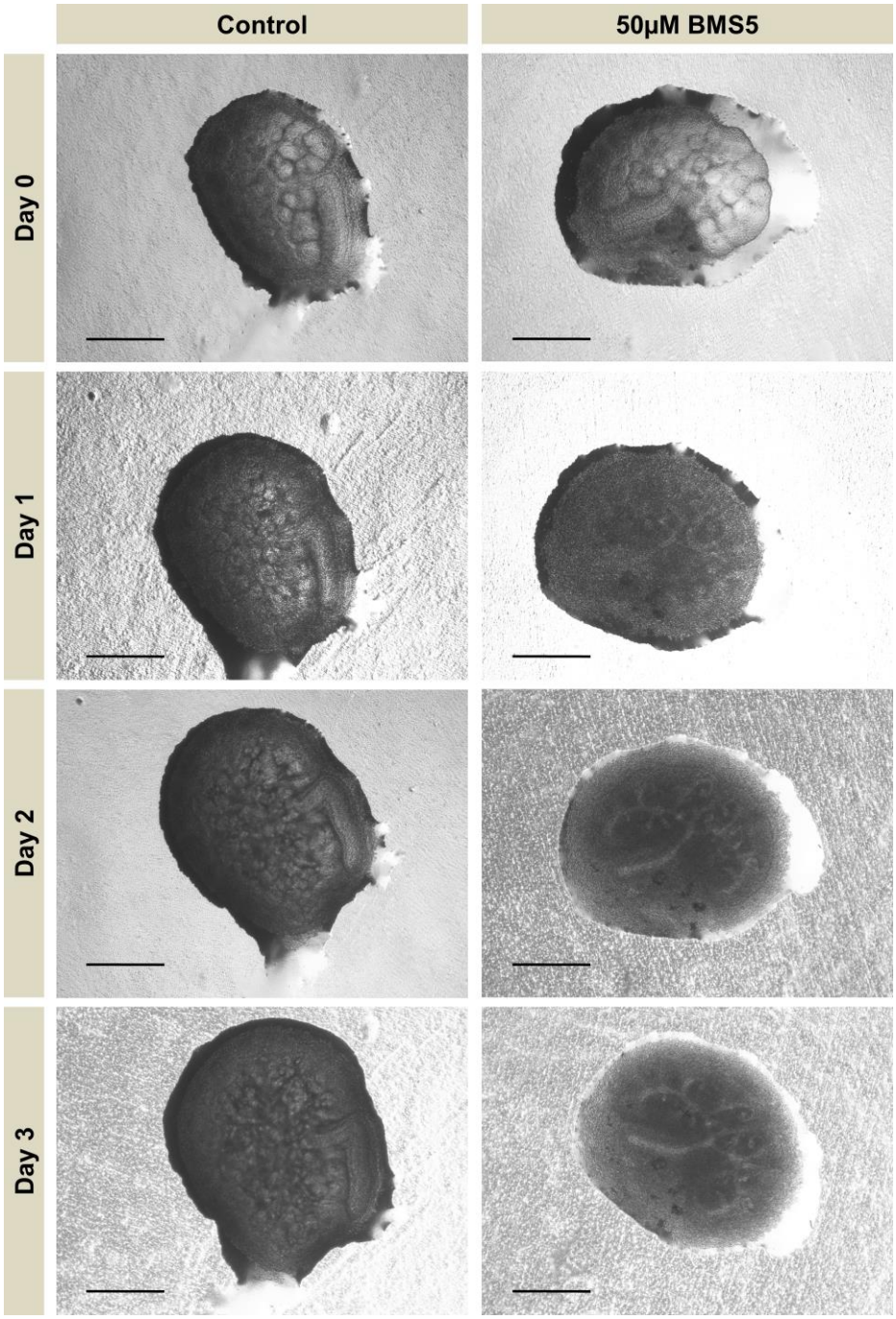



Figure 5.29 – Light micrographs of E12.5 kidneys cultured in 50µM BMS5.

E12.5 kidneys cultured in 50µM BMS5 for 3 days, images every 24 hours, showing kidneys cultured in 50µM BMS5 smaller and no further growth and the metanephric mesenchyme disintegrating. Scale bars = 500µm. N=3.

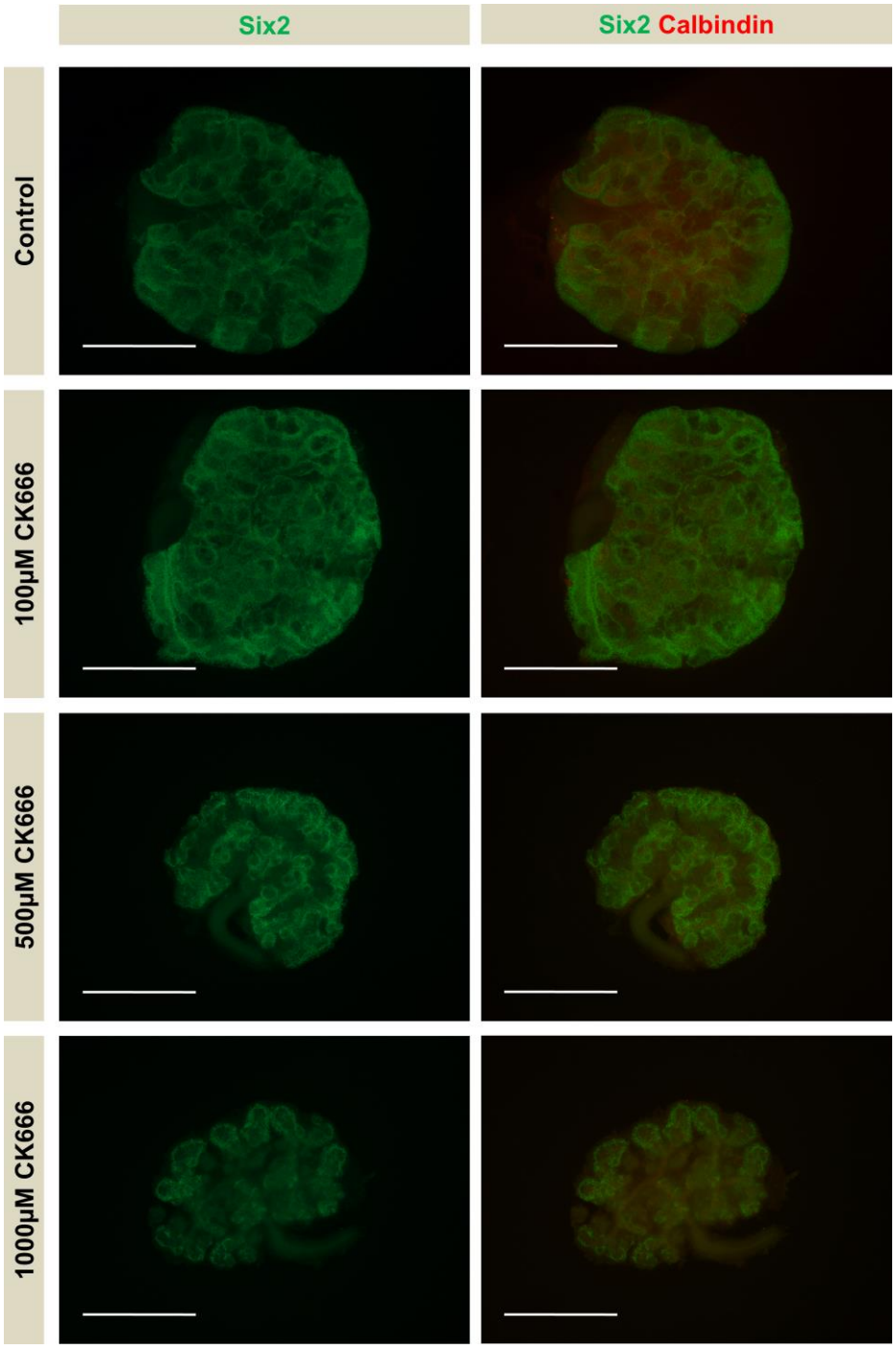



Figure 5.30 – Six2 in E12.5 kidneys cultured in 100µM, 500µM, and 1000µM CK666.

E12.5 kidneys cultured in 100µM, 500µM, and 1000µM CK666 for 48 hours, fixed and whole mount immunofluorescently labelled with Six2 (green), and Calbindin (red). The amount of Six2 (green) present in kidneys appeared to

decrease as the concentration of CK666 increased, kidneys cultured in 1000µM CK666 appear to have much less Six2 (green) than kidneys cultured in control media. Scale bars = 200µm. N=3.

## 5.2.9 – Can the effect of inhibiting migration with CK666 be reversed by transfer back to control media?

Next we looked to see if the impairment in growth with CK666 or BMS5 could be reversed by transfer back into control media after 24 hours and culturing in control media for a further 48 hours. This is to see if the effects seen with the treatments is temporary and can be reversed or if it is a permanent loss of Six2 that cannot be recovered from. Kidneys cultured in 100µm CK666 and 'rescued' had no significant difference in size (Figure 5.31), as would be expected since no significant difference was observed when cultured in 100µM CK666 for 5 days. The same was true for kidneys cultured in 500µM CK666 and 'rescued' (Figure 5.31) as there was no significant difference when cultured for 5 days either. This was again true when kidneys were cultured in 1000µM CK666 for 24 hours and 'rescued' as there was still a significant difference in the area of the kidney at all time points ($p<0.05$, Figure 5.31), showing that the significant impairment of growth observed over 5 days (Figure 5.24) could not be reversed by transferring the organs back into control media. The appearance of kidneys cultured in 100µM CK666 for 24 hours followed by 48 hours in control media were no different to controls (Figure 5.32), the same was true for those in 500µM CK666 (Figure 5.33).

When kidneys were cultured in 1000µM CK666 and transferred back into control media they appeared smaller as expected from the growth measurements (Figure 5.34) but the mesenchyme also looked to be disintegrating and appeared more comparable to kidneys cultured in 50µM BMS5 (Figure 5.29). Suggesting that instead of recovering after transfer back into control media, they become further damaged.

When kidneys were cultured in 50µM BMS5 for 24 hours followed by 48 hours in control media, the significant difference in percentage area increase between control and 50µM BMS5 was lost after 48 hours in control media ($p=0.064$, Figure 5.35) however the appearance of these ‘rescued’ kidneys would suggest that they were severely damaged (Figure 5.36) which implies that transferring back into control media did not result in recovery.

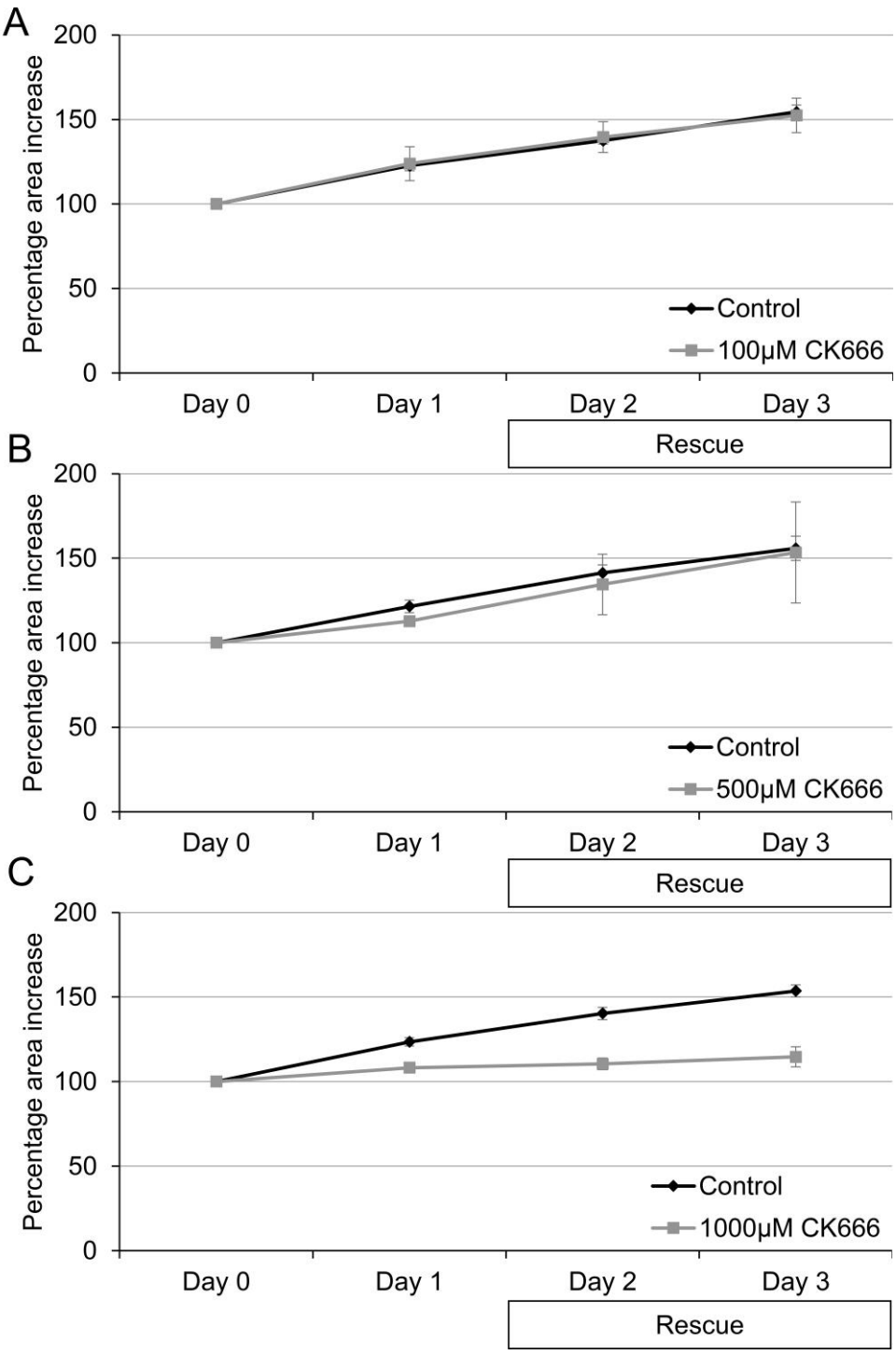



Figure 5.31 – Kidney size after 24 hours cultured in 100µM, 500µM, and 1000µM CK666, followed by 48 hour ‘rescue’.

Graph showing the percentage area increase over 24 hours in culture in (A) 100µM CK666, (B) 500µM CK666, and (C) 1000µM CK666, followed by 48 hours in control media. N=3.

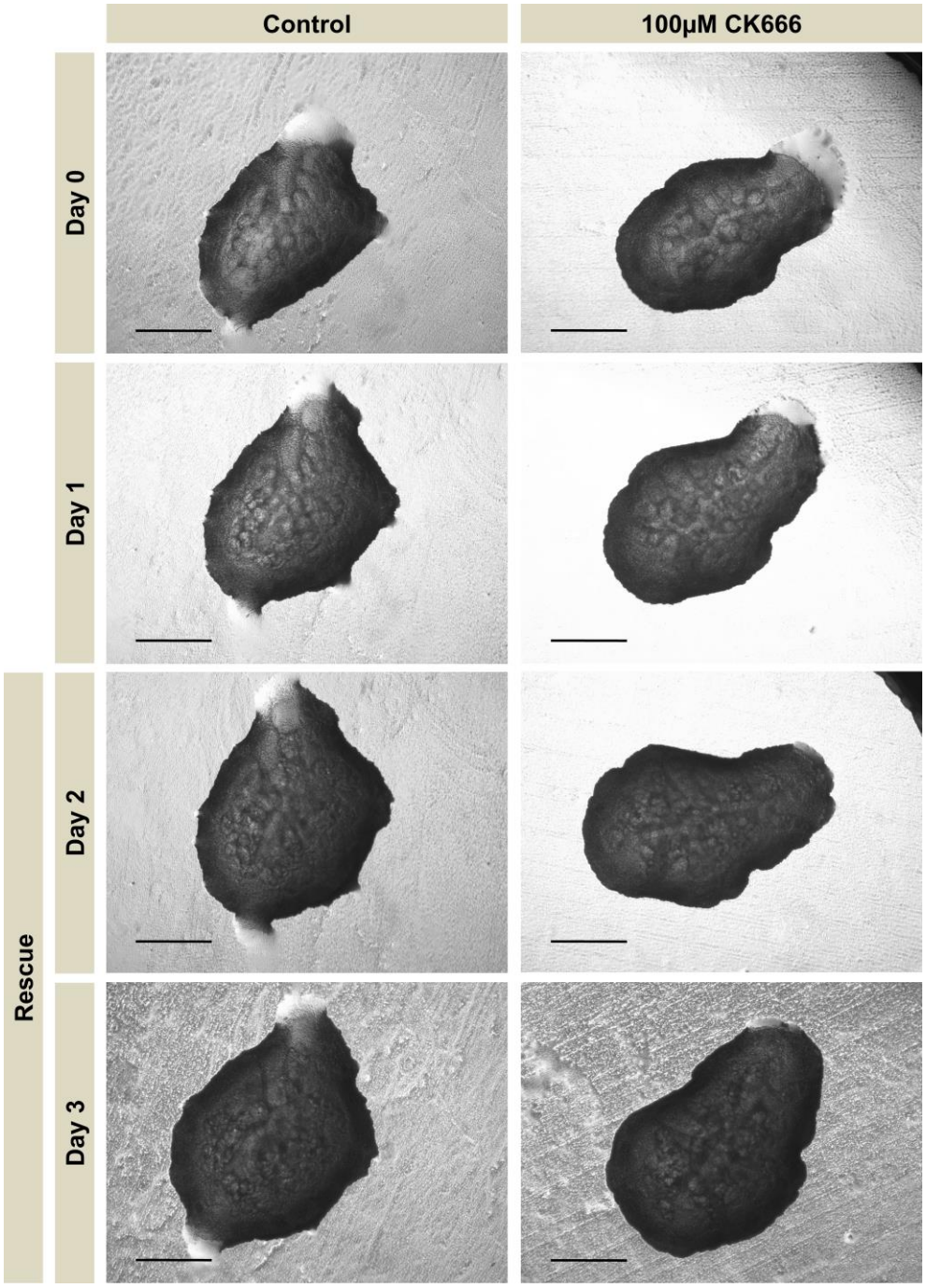



Figure 5.32 – Light micrographs of E12.5 kidneys cultured in 100µM CK666 for 24 hours followed by 48 hour ‘rescue’.

E12.5 kidneys cultured in 100µM CK666 for 24 hours then in control media for 48 hours, images every 24 hours. Kidneys cultured in 100µM CK666 for 24 hours followed by a 48 hour ‘rescue’ show no difference compared to kidneys cultured in control media. Scale bars = 500µm. N=3.

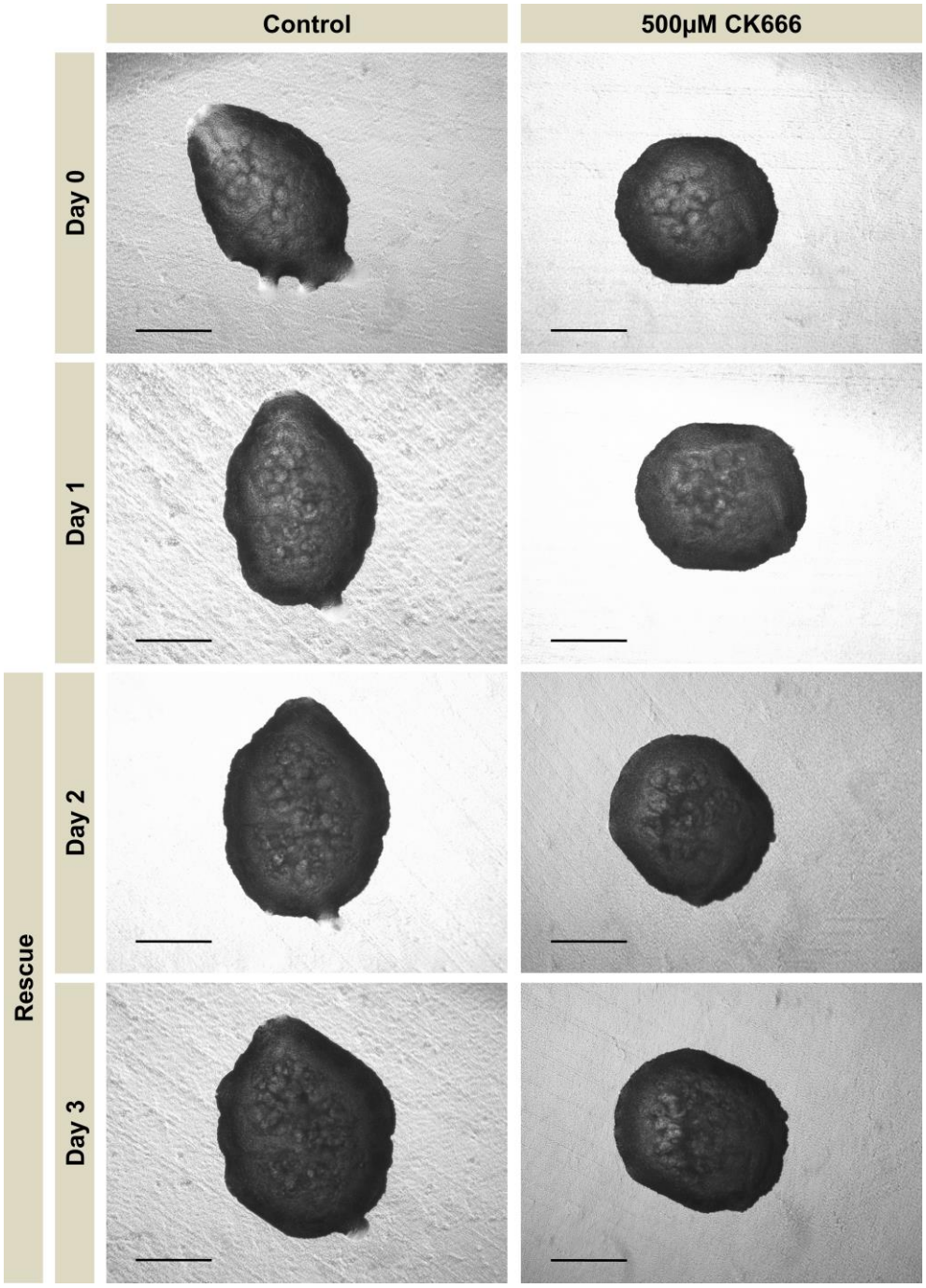



Figure 5.33 – Light micrographs of E12.5 kidneys cultured in 500µM CK666 for 24 hours followed by 48 hour ‘rescue’.

E12.5 kidneys cultured in 500µM CK666 for 24 hours then in control media for 48 hours, images every 24 hours. Kidneys cultured in 500µM CK666 for 24 hours followed by a 48 hour ‘rescue’ show no difference compared to kidneys cultured in control media. Scale bars = 500µm. N=3.

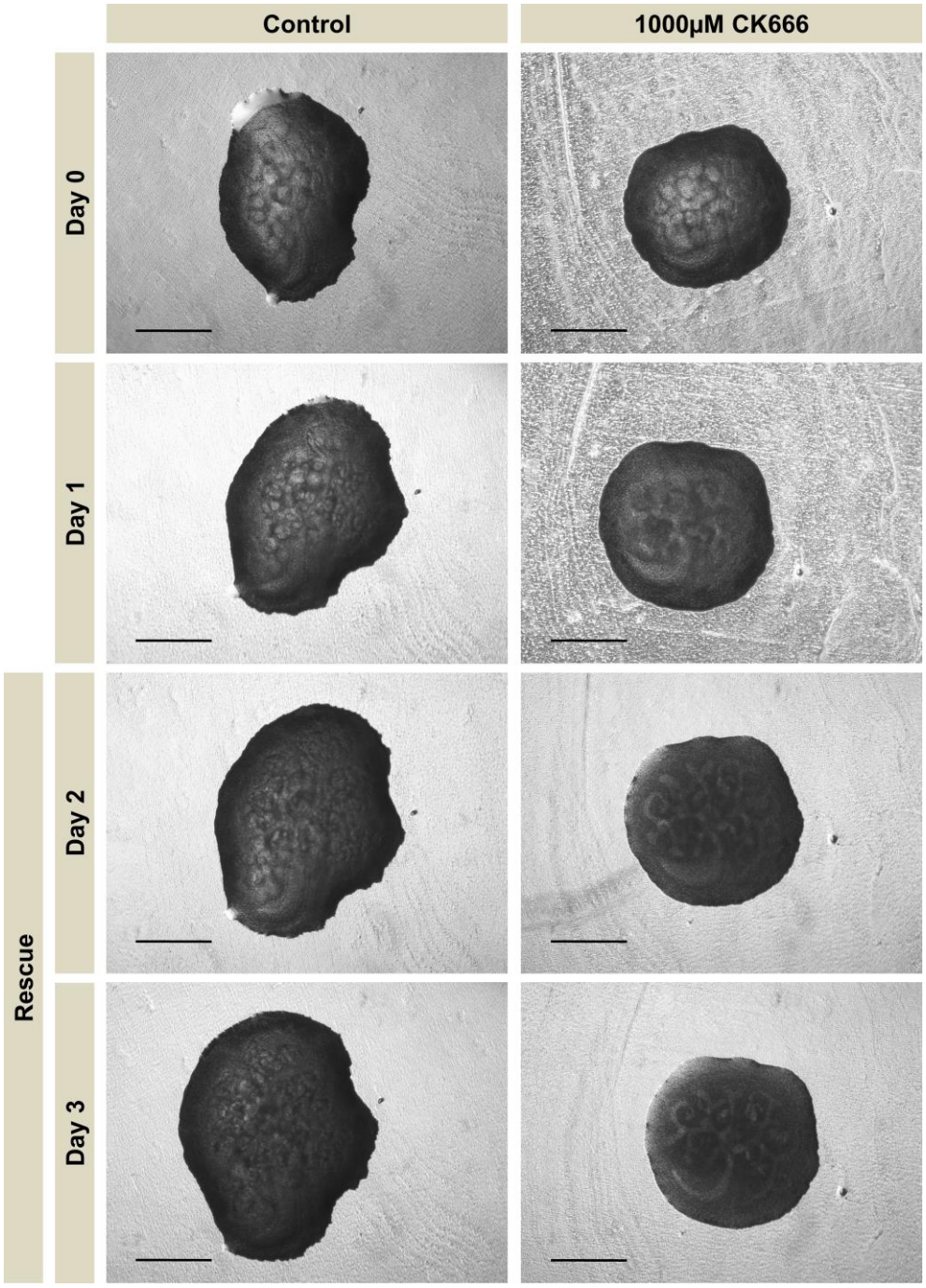



Figure 5.34 – Light micrographs of E12.5 kidneys cultured in 1000µM CK666 for 24 hours followed by 48 hour ‘rescue’.

E12.5 kidneys cultured in 1000µM CK666 for 24 hours then in control media for 48 hours, images every 24 hours. Kidneys cultured in 1000µM CK666 for 24 hours followed by a 48 hour ‘rescue’ show some impairment of growth compared to kidneys cultured in control media. Scale bars = 500µm. N=3.

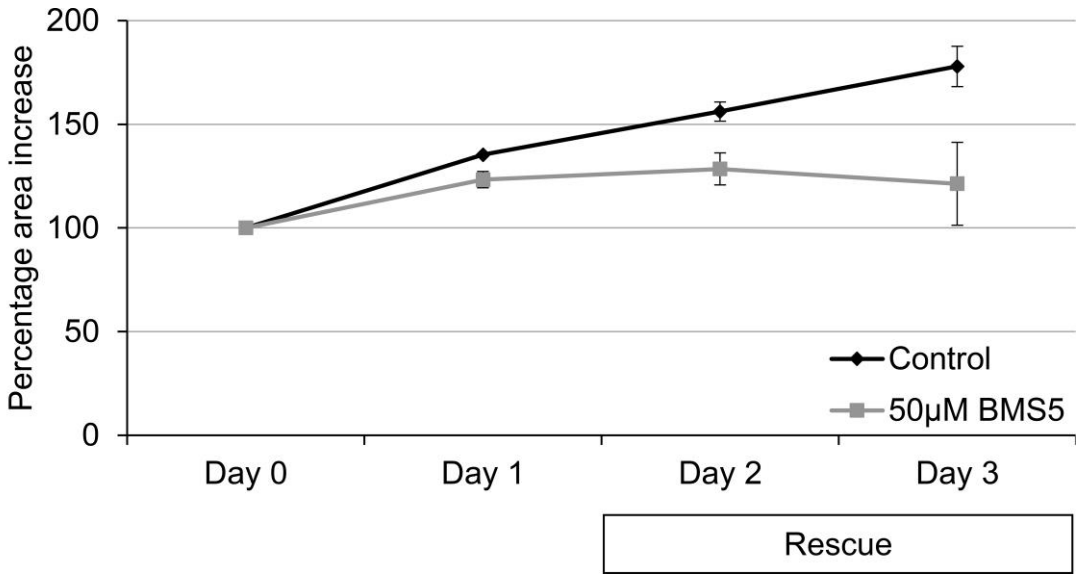



Figure 5.35 – Kidney size after 24 hours cultured in 50µM BMS5 followed by 48 hour ‘rescue’.

Graph showing the percentage area increase over 24 hours in culture in 50µM BMS5, followed by 48 hours in control media. There is no significant difference at any time point between kidneys cultured in control media and those in 50µM BMS5. N=3.

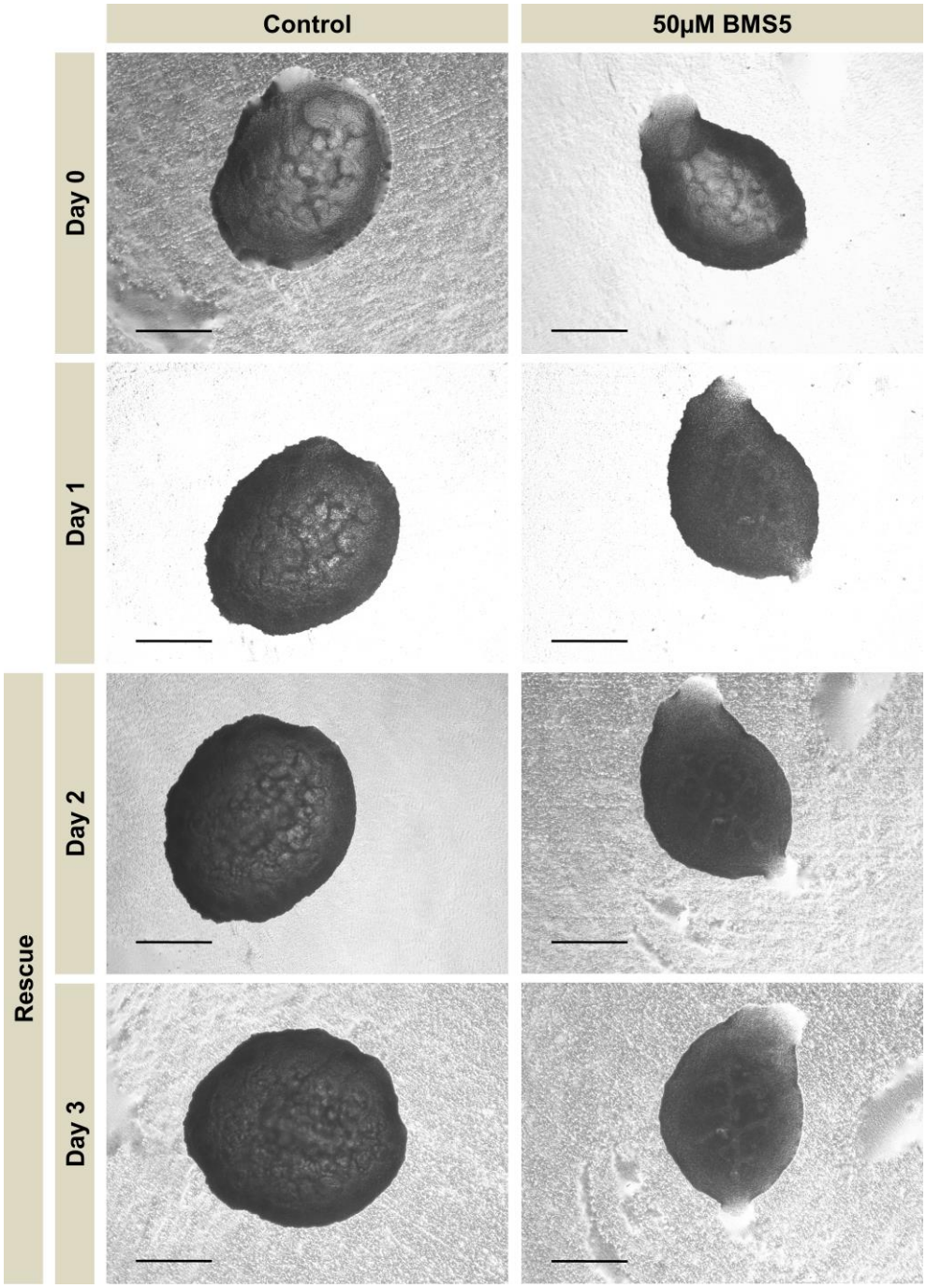



Figure 5.36 – Light micrographs of E12.5 kidneys cultured in 50µM BMS5 for 24 hours followed by 48 hour ‘rescue’.

E12.5 kidneys cultured in 50µM BMS5 for 24 hours then in control media for 48 hours, images every 24 hours. Kidneys cultured in 50µM BMS5 for 24 hours followed by a 48 hour ‘rescue’ are smaller than those in control media. Scale bars = 500µm. N=3.

## 5.2.10 – Can the inhibition of growth with migration inhibitors be replicated with an anti-MMP9 antibody?

MMP9 is required for normal kidney development (Arnould et al., 2009) and the addition of MMP9 antibodies in kidney culture has been shown to prevent further growth and development (Lelongt et al., 1997). The addition of 2 different MMP9 antibodies in kidney culture at varying concentrations in an attempt to prevent cell migration, by preventing the breakdown of the extracellular matrix by MMP9, did not yield any observable phenotype. There was no observable difference between control and 1µg/ml (Figure 5.37) or 5µg/ml (Figure 5.38) MMP9 antibody cultured organs (n=4), while there was no significant difference in the percentage area grown over 48 hours. During 48 hours in culture control kidneys had grown 144.45% ± 0.98 while 1µg/ml MMP9 cultured kidneys had grown 154.68% ± 4.83 (p=0.084, n=4)). When the concentration of MMP9 antibody was increased to 5µg/ml control kidneys had grown 144.86% ± 6.13 over 48 hours while 5µg/ml MMP9 cultured kidneys had grown 148.00% ± 9.45 (p=0.79, n=4, Figure 5.39).

This would imply that the MMP9 antibody might not have worked as expected so an alternative MMP9 antibody from a different manufacturer was used, yet this did not have any different observable effect at either 1µg/ml (Figure 5.40) or 5µg/ml (Figure 5.41) concentrations (n=1). At 1µg/ml MMP9 (Novus) the control kidney had grown 156.43% over 48 hours while the MMP9 cultured kidney grew 135.15%, while at 5µg/ml MMP9 (Novus) the control kidney grew 144.50% while the 5µg/ml MMP9 cultured kidney grew 135.44%. The MMP9 cultured kidneys did not grow as much as the controls, although this was a

small difference. Since a 10% difference was not significant in the 1µg/ml MMP9 (Millipore) cultured kidneys this suggested that even at the highest concentration of the Novus MMP9 antibody there would be unlikely to be a significant effect (though this was not repeated). It was noteworthy that the manufacturer did not provide information whether it would work against mouse MMP9.

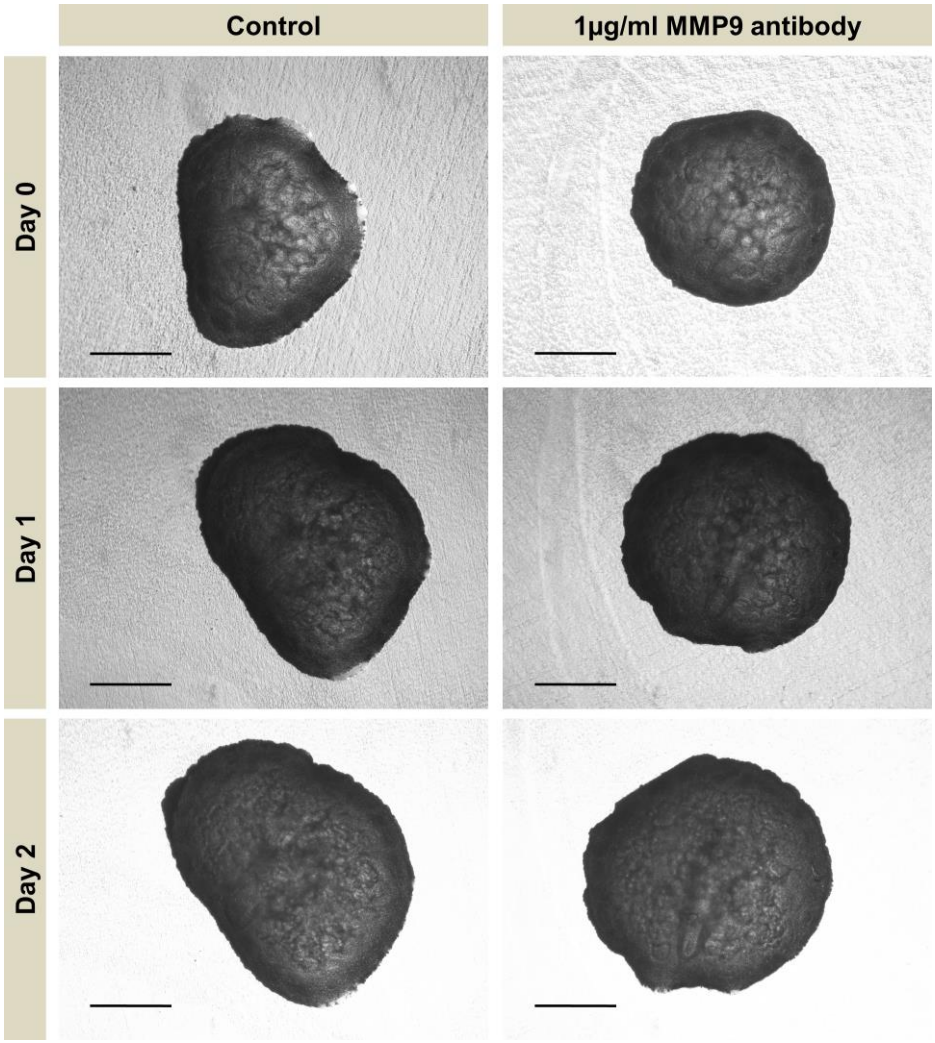



Figure 5.37 – Light micrographs of E12.5 kidneys cultured in 1µg/ml MMP9 antibody.

E12.5 kidneys cultured in 1µg/ml MMP9 antibody for 48 hours, images every 24 hours. There is no observable difference in kidneys cultured in 1µg/ml MMP9 antibody compared to kidneys cultured in control media. Scale bars = 500µm. N=4.

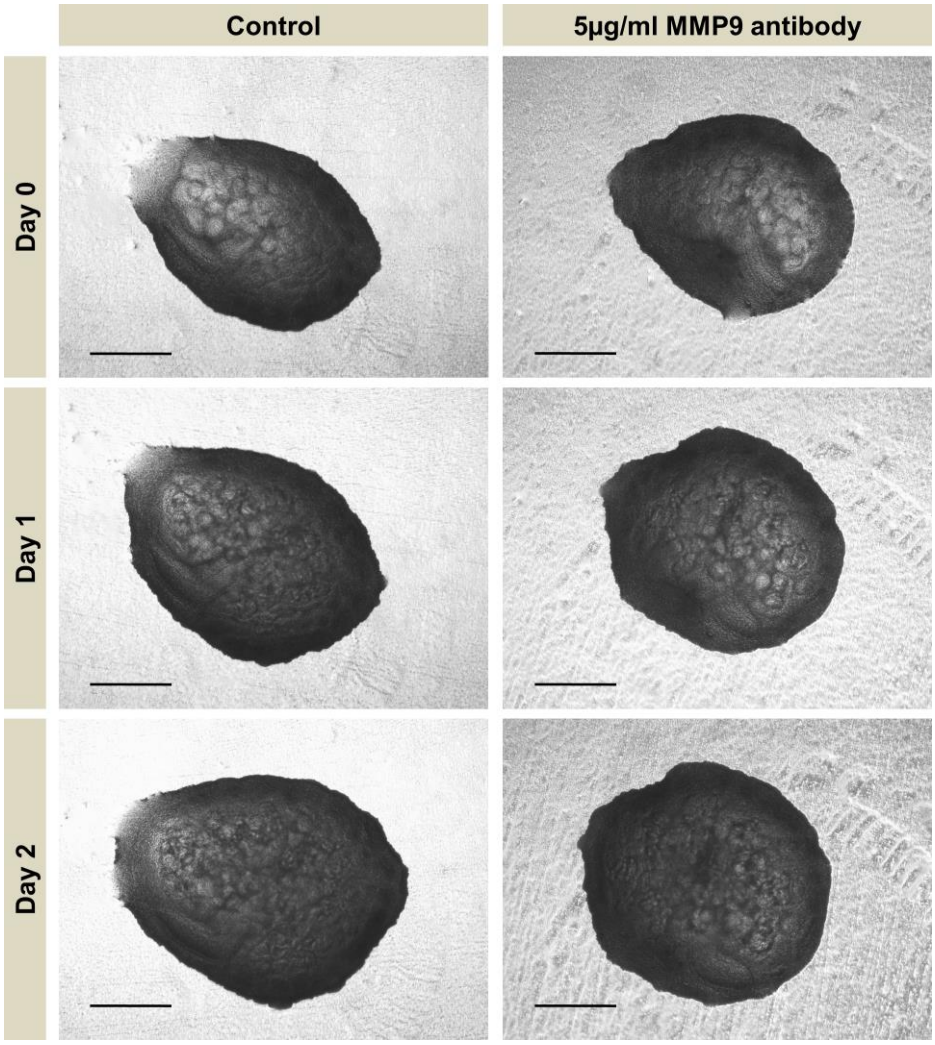



Figure 5.38 – Light micrographs of E12.5 kidneys cultured in 5µg/ml MMP9 antibody.

E12.5 kidneys cultured in 5µg/ml MMP9 antibody for 48 hours, images every 24 hours. There is no observable difference in kidneys cultured in 5µg/ml MMP9 antibody compared to kidneys cultured in control media. Scale bars = 500µm. N=4.

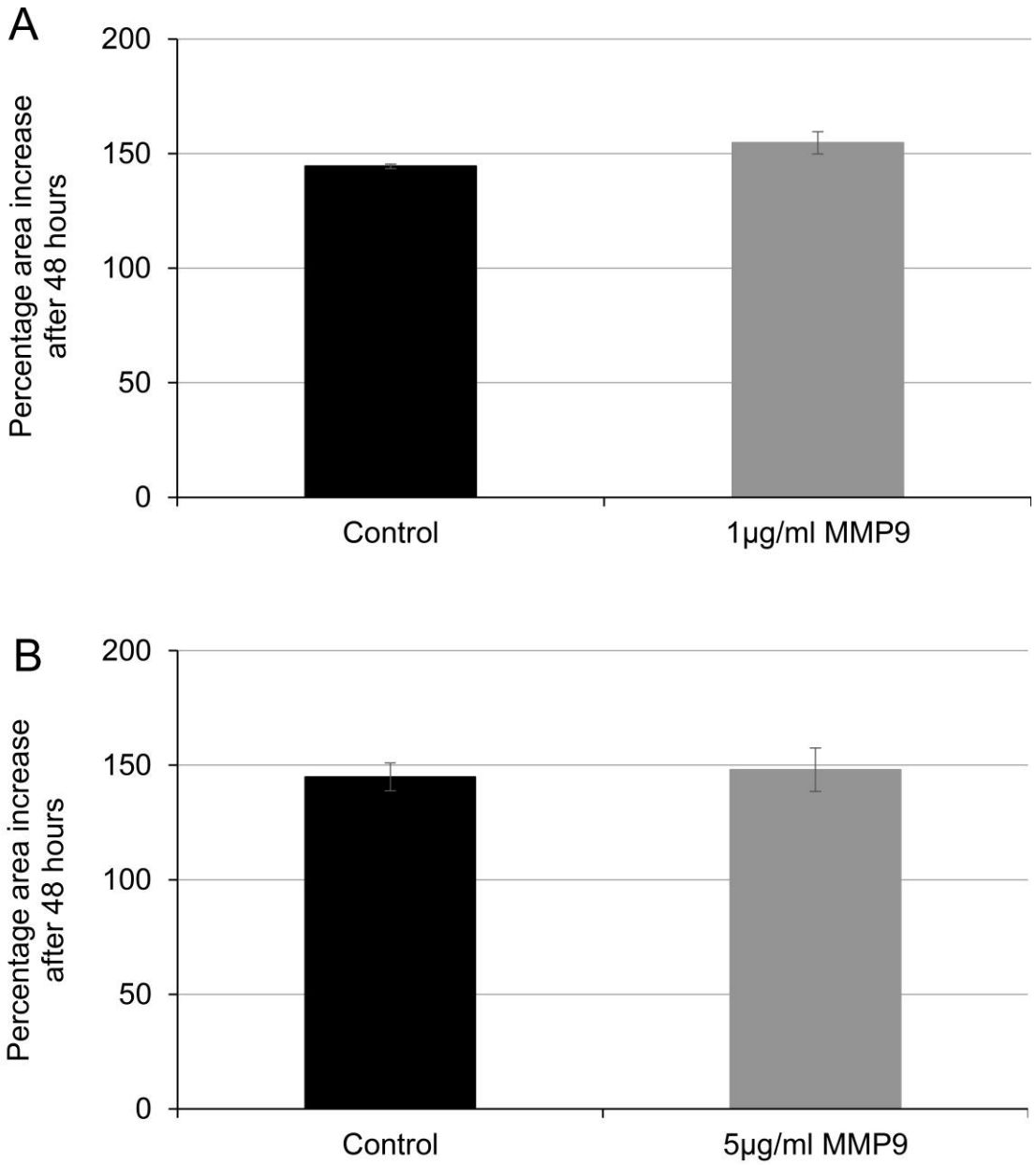



Figure 5.39 – Kidney size after 48 hours cultured in 1µg/ml and 5µg/ml MMP9 antibody.

Graph showing the percentage area increase over 48 hours in culture in (A) 1µg/ml and (B) 5µg/ml MMP9 antibody. (A) Control kidneys had grown 144.45% ± 0.98 while 1µg/ml MMP9 cultured kidneys had grown 154.68% ± 4.83 ($p=0.084$, $n=4$). (B) Control kidneys had grown 144.86% ± 6.13 over 48

hours while 5µg/ml MMP9 cultured kidneys had grown 148.00% ± 9.45 (p=0.79, n=4).

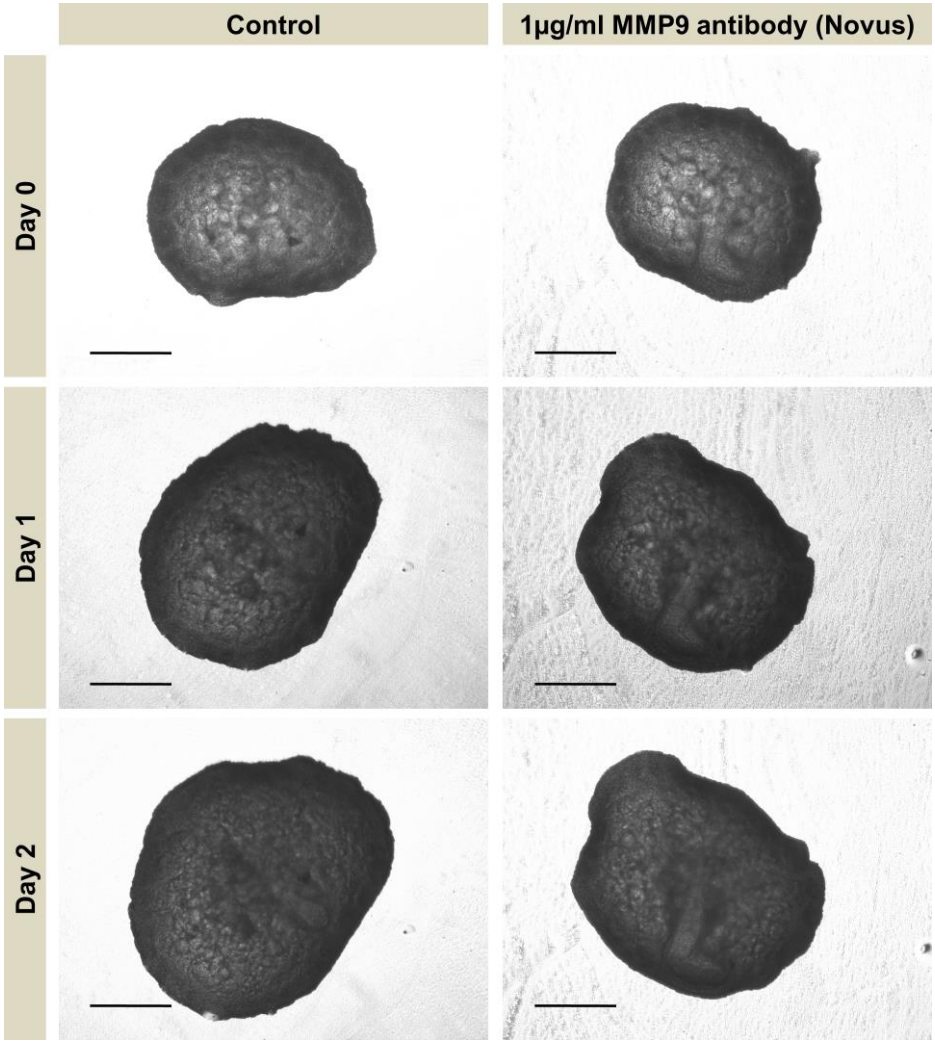



Figure 5.40 – Light micrographs of E12.5 kidneys cultured in 1µg/ml MMP9 (Novus) antibody.

E12.5 kidneys cultured in 1µg/ml MMP9 antibody (Novus) for 48 hours, images every 24 hours (n=1). There is no observable difference in a kidney cultured in 1µg/ml MMP9 antibody (Novus) compared to a kidney cultured in control media. Scale bars = 500µm.

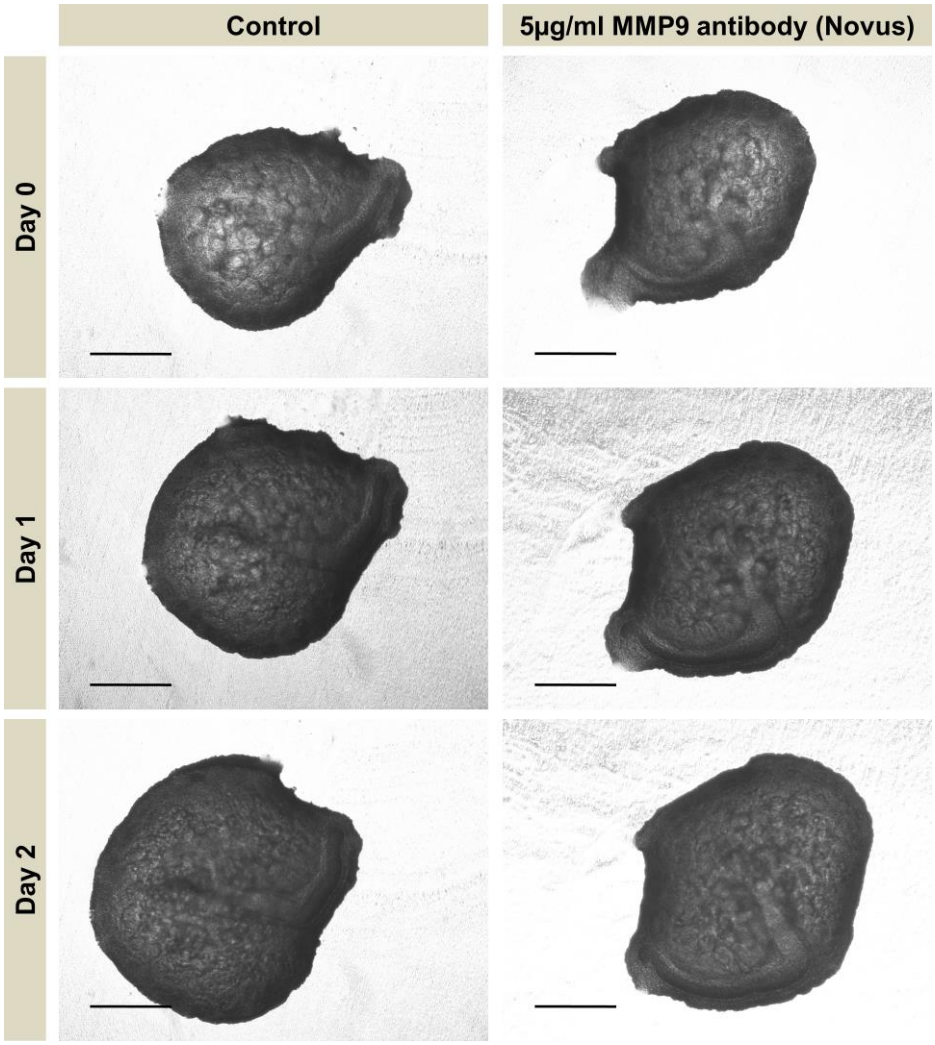



Figure 5.41 – Light micrographs of E12.5 kidneys cultured in 5µg/ml MMP9 (Novus) antibody.

E12.5 kidneys cultured in 5µg/ml MMP9 antibody (Novus) for 48 hours, images every 24 hours (n=1). There is no observable difference in a kidney cultured in 5µg/ml MMP9 antibody (Novus) compared to a kidney cultured in control media. Scale bars = 500µm.

## 5.3 – Conclusions

This chapter investigated whether MM cells migrate away from the UB to the periphery of the kidney during development. The hypothesis for this was that these cells would need to move away from the inductive stimulus (WNT9b), being released for the UB tips that induce MM cells to form nephrons, to have enabled some of the cells to have continued to proliferate and expand the population of nephron progenitors. Using a technique of micro-injecting DiI into the mesenchyme, which binds to cell membranes, to track the cells it was shown that some of the MM cells moved away from the UB over the course of 24 hours. Time lapse confocal microscopy also demonstrated that these cells migrated away from the UB, and in one case a cell appeared to have migrated around a stationary cell. The limitation of this was only using one kidney for the time lapse confocal microscopy work, this was due to time and cost restraints. Further work repeating this to gain statistically valid results would be necessary to show that these cells do indeed migrate. Although the work with DiI injecting and imaging over 24 hours showed that 21 out of 30 kidneys had some DiI separation indicated that this was repeatable.

This metanephric mesenchymal migration was stopped by a number of migration inhibitors, including an actin disrupter, Cytochalasin B, and an Arp2/3 inhibitor, CK666. Cytochalasin B stopped metanephric mesenchymal cell migration (lack of movement of DiI labelled cells) and slowed the growth of the kidney over 48 hours at the highest (30μM) concentration. Kidneys cultured in Cytochalasin B had no Six2 present, but to be able to say that it was the inhibition of metanephric mesenchymal cell migration that caused this

loss of Six2 it was necessary to look at how Cytochalasin B affected mitosis in embryonic kidneys. Cytochalasin B did not affect the percentage of mitotic cells in anaphase suggesting that cells in kidneys cultured in Cytochalasin B could still progress through mitosis to divide, however there was a decrease in the number of cells in mitosis. As such Cytochalasin B did have a detrimental effect on mitosis in embryonic kidneys, therefore the loss of Six2 could not be attributed to the inhibition of metanephric mesenchymal cell migration.

Therefore another inhibitor of cell migration was used, CK666, which inhibited the Arp2/3 complex. Initially it was checked to see if CK666 had any effect on mitosis, kidneys cultured in 100µM, 500µM or 1000µM CK666 had no effect on neither the number of mitotic cells in anaphase nor the number of cells in mitosis. 1000µM CK666 effectively stopped migration while having no significant effect on mitosis, compared to the other migration inhibitors which did have an impact on mitosis (BMS5 and Cytochalasin B). The act of inhibiting this metanephric mesenchymal cell migration resulted in the inhibition of further growth with organs cultured in CK666 being significantly smaller than their contralateral controls, although the mesenchyme appeared fairly normal unlike the mesenchyme disintegration seen with 50µM BMS5. This suggested that the metanephric mesenchyme needed to be able to migrate away from the UB (inductive source) in order to facilitate development. The observation of fewer Six2 expressing cells present in kidneys cultured in 1000µM CK666 would imply that these cells needed to migrate away from an inductive stimulus to self-renew and proliferate, if these cells could not migrate then it would be plausible that these cells became induced to form nephrons and hence lost Six2 expression.

Normal kidney development requires MMP9 which is involved in breaking down the extracellular matrix to enable cells to migrate through. Therefore a technique of adding anti-MMP9 antibodies into the media of kidney culture was used, which prevented further growth and development (Lelongt et al., 1997), to see if this metanephric mesenchymal cell migration required active MMP9. Two different MMP9 antibodies were used but neither produced any effects on kidney growth as seen with other migration inhibitors such as CK666. This showed that either the MMP9 antibodies did not work in our mouse embryonic kidneys (the Millipore antibody specifically says it works on mouse MMP9) or the method of culturing kidneys in media containing MMP9 did not allow the desired effect of preventing MMP9 from degrading the extracellular matrix. Or if the MMP9 antibodies did stop MMP9 mediated extracellular matrix degradation then the inhibition of migration by this method (MMP9 inactivation) did not have an effect during kidney development and as such metanephric mesenchymal cell migration did not require MMP9. A future experiment to clarify whether the anti-MMP9 antibodies are working in our embryonic kidneys would be to use gelatin Zymography to see if the activity of MMP9 is stopped or decreased by the addition of anti-MMP9 antibodies (Toth and Fridman, 2001; Toth et al., 2012).

This chapter has shown that metanephric mesenchyme cells migrated towards the periphery of the kidney and that this migration was necessary for the continued growth of the kidney and expansion of the Six2 expressing nephron progenitor population.

# Chapter 6: Discussion

## 6.1 – LIM kinase role in mitosis

This thesis showed that active LIMK was crucial for the completion of mitosis during kidney development and in HK2 cells. Active LIMK was required for the formation of normal α-tubulin spindles, the correct number and positioning of centrosomes and the appropriate dispersal of SMC3. Using a specific inhibitor of LIMK chapter 3 showed that kidneys cultured in BMS5 showed reduced growth, loss of mesenchyme definition, and loss of Six2 expression in the metanephric mesenchyme cells. In addition kidneys cultured in BMS5 showed an increase in apoptosis after 18 hours, suggesting that BMS5 caused cells to undergo cell death. The cells were being induced to undergo apoptosis because BMS5 prevented the completion of mitosis, with kidney cells being stopped at metaphase. There was a significant reduction in the number of mitotic cells in anaphase after culture in BMS5, this also occurred in HK2 cells which were used to look at the mitotic machinery further using immunofluorescence techniques. In HK2 cells the inhibition of LIMK by BMS5 resulted in the formation of multiple (frequently more than two) α-tubulin foci, and multiple centrosomes which did not always overly with the α-tubulin foci. This suggested that LIMK was required for the formation of the α-tubulin spindle beyond the stage of individual foci. The mitotic spindle forms from the pericentriolar matrix around a centrosome and therefore it can be concluded that active LIMK was required for the α-tubulin spindle to form at the centrosome. Not only did BMS5 prevented the mitotic spindle from forming, it also caused the inappropriate dispersal of SMC3. SMC3 is normally only

dispersed once the spindle checkpoint has been activated after the kinetochores on the centromere of the chromatid have attached to the microtubules ready for the sister chromatids to be pulled apart. Inhibition of LIMK caused SMC3 to be dispersed throughout the cytoplasm of mitotic cells, thus implying that the spindle checkpoint had been activated. Since the α-tubulin foci observed in cells cultured in the LIMK inhibitor were within the DNA compartment of mitotic cells it was entirely plausible that the kinetochores had attached to the very short microtubules present in the α-tubulin foci and this triggered the spindle checkpoint. If this were to be the case then the role of active LIMK would be to cause the formation of the α-tubulin spindle at the centrosomes and for active LIMK to prevent the over-duplication of the centrosomes.

Using siRNA to knockdown both LIMK1 and LIMK2 resulted in multiple Pericentrin dots, but with relatively normal α-tubulin spindles arising from these (Heng et al., 2012). siRNA mediated knockdown of LIMK1 and LIMK2 was attempted but failed to achieve knockdown using 2 different transfection reagents (DharmaFECT 1 and FuGENE HD) at a variety of different siRNA concentrations recommended by the siRNA manufacturer and the transfection reagent manufacturer and using immunofluorescent labelling of LIMK1 and LIMK2 as the end point. This suggested that HK2 cells were not easily transfectable with siRNAs and while this would have been a useful addition to this thesis, Heng et al., 2012 showed a different effect with using LIMK1 and LIMK2 siRNAs compared to the LIMK inhibitor BMS5. The difference between using siRNA and an inhibitor could be due to the different cell types or because with using siRNAs no protein is present, while with an inhibitor the

protein is present but not active which could have a different effect if the cell compensates for having no LIMK protein present. Another possibility would have been that the BMS5 inhibitor was having an off target effect. This thesis ruled out BMS5 being toxic to the cells by showing no effect on HK2 or C2C12 cells grown to confluence and therefore it can be said that BMS5 only caused a cell death effect in cells undergoing mitosis.

Other groups had shown that Cofilin dephosphorylation can be achieved by increasing calcium levels using A23187 or Histamine (Wang et al., 2005). They stated that A23187 and Histamine decreased the amount of phosphorylated Cofilin in 293T and Hela cells, and other groups had shown that A23187 has decreased the amount of phosphorylated Cofilin in other cell types including HT4 cells (neural cell line; Meberg et al., 1998) and neutrophils (Zhan et al., 2003). However this loss of phosphorylated Cofilin was not observed using both HK2 cells and embryonic kidneys at several concentrations, therefore despite other groups using this method in a variety of cell types this could not be replicated. Although we used a different time point to look for the loss of Cofilin phosphorylation, this work in kidneys and HK2 cells should be repeated using the same time points as used in previous studies. The lack of phosphorylated Cofilin in LIMK inhibited cells and kidneys could not be said to be responsible for the effects observed.

During the course of this PhD Petrilli et al. (2014) showed that BMS5 caused the same α-tubulin foci that we observed in mitotic cells, although contrary to our findings they suggested that the cells only become stalled in mitosis. Chapter 4 showed that the cell number decreased in a number of different cell types in different species, indicating that not only did BMS5 stalled cells in

mitosis but also caused their death. In addition beyond the fact that BMS5 prevented spindle assembly, generated α-tubulin foci and prevented the completion of mitosis, it was shown that BMS5 prematurely caused the release of SMC3, normally released only just prior to chromosome separation. The dispersal of SMC3 meant that the chromosomes could be separated and if there is no spindle assembly to pull them apart and cause cell separation then the cell would logically have a diploid number of chromosomes and it is possible that because of this then the cell would want to prevent aneuploidy and undergo apoptosis or mitotic catastrophe (Castedo et al., 2004).

LIM kinases had been recently shown during the course of this work to interact with Aurora A (Ritchey et al., 2012; Johnson et al., 2012), which is located at the centrosomes and mitotic spindle microtubules (Hannak et al., 2001; Toya et al., 2011). Inhibition of LIMK with BMS5 caused mitotic arrest by “decreasing Aurora A activation”, although they did not show the same cell death observation shown in this thesis (Petrilli et al., 2014).

BMS5 was used by Petrilli et al. (2014) at a concentration of 4μM rather than our 10μM or 50μM for their observation of α-tubulin foci and stalling of mitosis. Their reasoning was that 4μM was close to the $IC_{50}$ value (3.9μM) for mouse Schwann cell viability (the cell they used) and when they increased BMS5 to 10μM they got a reduction in cell viability. This thesis showed that our concentrations of BMS5 was not toxic and the observation of cell death was due to a LIMK mediated mechanism and therefore using a lower concentration of BMS5 (such as 4μM) would not allow investigation of all of the mechanisms of LIMK or downstream effects of LIMK.

Inhibition of Aurora A with the pharmacological inhibitor MLN8054 causes cells to arrest in mitosis but only temporarily, and crucially these cells with no active Aurora A can still divide, albeit with aneuploidy and subsequent cell death (Hoar K et al., 2007). This thesis did not show any cell division in embryonic kidneys or HK2 cells after culturing in BMS5, thus implying that while LIMK inhibition with BMS5 may impact upon Aurora A activation (Petrilli et al., 2014) this did not explain why embryonic kidney cells or HK2 cells failed to divide, although it might partly explain the cell death effect shown with LIMK inhibition.

This thesis shows a role for LIMK during kidney development. LIMK is required for the continued proliferation and expansion of the Six2 metanephric mesenchyme cells. This is most likely due to LIMK's role allowing the cell cycle to progress unhindered rather than a specific kidney development mechanism within the Six2 cells. When LIMK is inhibited with BMS5 the cell cannot complete mitosis and undergoes cell death, this happens in a variety of cell types including HK2, C2C12 and HEPG2 cells. This thesis does not show any direct specific effect of LIMK during kidney development, the effects seen when culturing embryonic kidneys in BMS5 are due to BMS5 preventing the highly proliferative metanephric mesenchyme cell population from undergoing cell mitosis.

## 6.2 – Metanephric mesenchymal cell migration

Chapter 5 showed that DiI labelled metanephric mesenchyme cells migrated away from the UB tip towards the periphery of the kidney (Chapter 5). Initially

it was shown that groups of DiI labelled cells that appeared to be in the metanephric mesenchyme separated and some DiI labelled cells moved towards the periphery of the kidney. This was further confirmed by using live time lapse confocal microscopy, over 16 hours a DiI labelled cell moved away from the UB towards the periphery of the kidney.

We believed this to be cell migration but this movement could be due to the UB pushing the mesenchyme cells away though the observation of a separation of DiI labelled cells rather than all of them moving away would argue against the UB pushing idea. In addition the observation that one DiI labelled cell remained stationary while the other moved around it in Figure 5.4 would again argue that this was actual cell migration rather than cell being pushed. In the same kidney there was one DiI labelled cell moving towards the centre of the kidney and another cell in the same region (albeit 27.6µm vertical difference) moving in the opposite direction towards the periphery of the kidney (Figure 5.5; Figure 5.6), thus showing cells moving in opposing directions further implying that this was migration rather than pushing. Another way to ascertain whether this cell movement was migration was to use an inhibitor of cell migration, cell wounding assays were used on HK2 cells to test a number of cell migration inhibitors, both Cytochalasin B and CK666 showed inhibition of cell migration.

By culturing kidneys that had been injected with DiI in CK666 or Cytochalasin B it was shown that this movement of DiI labelled cells ceases. Only 20% of kidneys injected with DiI showed cell movement in both 1000µM CK666 and 30µM Cytochalasin B compared to 78% in control kidneys, while Cytochalasin

B had a significant impact on mitosis, CK666 did not and thus implied that the movement of DiI labelled cells was cell migration.

If metanephric mesenchymal cell migration occurred during kidney development then there must be a reason for it. The hypothesis for this migration was that these cells needed to migrate away from the inductive signalling from the UB tip to prevent all the metanephric mesenchyme cells being induced to form nephrons. If this migration did not occur then all the metanephric mesenchyme cells would be induced to form nephrons as they would be too close to the UB tip. To look at this, kidneys were cultured in the cell migration inhibitor CK666 and chapter 5 (5.2.8) looked at whether the kidney continued to grow and what happened to the Six2 expressing metanephric mesenchyme cells. Kidneys cultured in CK666 showed no further growth and there was a loss of Six2 expression, this showed that inhibiting cell migration prevented further growth of the kidney and either caused the Six2 expressing cells to become used up and induced to form renal vesicles or they died off. By comparing the loss of Six2 to that seen with BMS5 (Figure 3.8) it was shown that while BMS5 caused total loss of Six2 and it was shown that this was due to apoptosis (Figure 3.11), CK666 did not show total loss of Six2 and some Six2 expressing cells remained around the tips of the UB. A further experiment would be to use a renal vesicle marker such as WT1 and see if there were more renal vesicles forming in kidney cultured in CK666, though there might be an issue in that if cell migration is required to form a renal vesicle after they have become induced then this end point might not answer this question. This experiment of immunostaining for WT1 was not performed in this project due to time constraints. In addition

migration was inhibited globally, not only in the metanephric mesenchyme, so cell migration would also be inhibited in the UB. If cell migration is required for growth of the UB then it cannot be said for certain that the observation of no further kidney growth and loss of Six2 expression is solely due to the inhibition of metanephric mesenchymal cell migration as the UB might impact upon this. A possible way to separate this would be to specifically inhibit cell migration only in the metanephric mesenchyme by using Cre-Lox recombination to specifically delete ArpC3 (a component of the Arp2/3 complex) in Cited1 expressing cells. Cited1 is another marker of the metanephric mesenchyme and unlike Six2 it is switched off earlier before the renal vesicles have formed and therefore would be more likely to catch only the non-induced metanephric mesenchyme cells. This could be carried out by crossing a Cited1-cre mouse (Boyle et al., 2008) with an ArpC3 floxed mouse (Kim et al., 2013) thereby generating mice which have ArpC3 deleted only in the Cited1 expressing metanephric mesenchyme cells thus migration can still occur in the UB but not the metanephric mesenchyme.

It is possible that whatever determines metanephric mesenchymal cell migration away from the UB is what determines the end of nephrogenesis. If the signal to stop producing more nephron progenitors is via stopping the cells from migrating away from their inductive source and thus can no longer continue to proliferate then metanephric mesenchymal cell migration is involved in regulating the end of nephrogenesis and by default the number of nephrons in the kidney. The results in this thesis would support this idea, because when cell migration was stopped with CK666 then the Six2 expressing metanephric mesenchyme stopped expanding, and it was

therefore hypothesised that these cells would now become induced to form nephrons. Further studies will be required to specifically stop only this radially cell migration away from the UB, to see if these cells would indeed form nephrons.

## 6.3 – Limitations and future directions

This thesis showed the stalling of mitosis after culturing HK2 cells in BMS5, which inhibits LIMK. Synchronisation of HK2 cells was attempted after the work shown although this was not achieved, using a different cell type would be appropriate as the stalling in mitosis by BMS5 appears to be non-cell type specific. Synchronisation of cells in mitosis would allow better quantification of how many cells cultured in BMS5 are stalled in mitosis and at precisely what stage they are stalled. The work utilising A23187 and Histamine in an attempt to replicate the effect observed with BMS5 by increasing Cofilin dephosphorylation used time points that in hindsight were too long to see the effect of Cofilin dephosphorylation and as such this needs to be repeated using shorter time points to observe the Cofilin dephosphorylation and to observe any effects arising from this.

A limitation of this study was that we used the pharmacological inhibitor BMS5 which will be toxic at high doses, it would therefore be useful to compliment this approach with using siRNA to knockdown LIMK thus bypassing the toxicity issues associated with addition of BMS5.

Increasing the number of replicates would allow for more certainty in the results and also allow quantification of the number of branches within the kidney. Kidneys cultured in BMS5 showed a reduced number of branches compared to their contralateral control, and quantification of this would be necessary to confirm this observation.

While this thesis hypothesises that cells migrate within the metanephric mesenchyme, we only show that cells move within this compartment. This could be a result of ‘pushing’ by the ureteric bud tip, and the identity of the cells that move has not been confirmed. This thesis showed the Di I labelled cells to overlie that which are labelled with the Six2 antibody, further confocal images would be required to confirm this observation. In addition other markers of the metanephric mesenchyme should be used to analyse which cells are moving, such as using Cited1, Pax2, or FoxD1 for labelling the stroma. In addition labelling with the renal vesicle marker, WT1, would allow the number of renal vesicles to be quantified in kidneys cultured in BMS5 and CK666, this was not performed in this thesis due to time limitations.

## 6.4 – Significance and conclusions

The mechanism by which the kidney forms nephrons, and how many are produced is important to adult health because a number of studies have shown that a lower nephron number results in hypertension and renal disease later in life (Hoy et al., 2008). The exact mechanism by which an organism determines the number of nephrons in the kidney is unknown, though it has been shown to be linked with birth weight (Mañalich et al., 2000; Hughson et al., 2003). A maternal diet of low protein results in a lower nephron number (Langley-Evans et al., 1999), and intrauterine growth retardation measured by birth weight also results in a lower nephron number (Hinchliffe et al., 1992). Kidney development determines nephron number in most cases which, if impaired, can result in hypertension later in life which has been recently reported to cost the NHS £2 billion a year although this includes all causes of hypertension which can be lifestyle related or genetic (Public Health England, 2014). This shows an importance of studying how the kidney develops in particular how nephron progenitors survive and ultimately switch off nephrogenesis during adult health.

Williams-Beuron syndrome is a genetic disorder in which LIMK1 is one of the genes deleted (Tassabehji et al., 1996). And while 18% of patients have renal abnormalities (Pober et al., 1993; Pankau et al., 1996), it cannot be said that the deletion of LIMK1 is the cause of these renal abnormalities. Though due to my observation that LIMK is required for the continued proliferation of mesenchyme cells during kidney development it is possible that the deletion

of LIMK in Williams-Beuron syndrome contributes to the renal abnormalities seen in patients.

In the Williams-Beuron syndrome phenotype only the LIMK1 gene is deleted and there is no evidence of the deletion of LIMK2, therefore because my work focuses on the inhibition of both LIMK1 and LIMK2 with BMS5 then some of the effects seen could be due to loss of LIMK2 activity. There also could be a compensatory effect if the cells only lose LIMK1, as seen in the phenotype in Williams-Beuron syndrome, where LIMK2 might compensate to some effect for the loss of LIMK1. This taken together with the fact that the LIMK1/2 double knockout mouse is viable and clearly the cells can divide would suggest that while inhibiting LIMK when the protein is present results is cell death, removing the LIMK protein does not have the same effect. Thus having no protein present has a different effect compared to the protein being present but having no activity.

This thesis investigated the role of LIMK and metanephric mesenchymal cell migration during mouse kidney development, showing that LIMK is required for the continued proliferation and expansion of the Six2 metanephric mesenchyme cells. Active LIMK is required for cells to correctly assemble the mitotic spindle and for normal activation of the spindle checkpoint, without active LIMK the cells cannot progress beyond metaphase and die via apoptosis. Metanephric mesenchyme cells migrate radially away from the UB towards the periphery of the kidney and without this migration, the kidney begins to lose its pool of Six2 metanephric mesenchyme cells and the kidney no longer develops.

This thesis has provided novel insight into the role of LIMK in the progression of mitosis and showed that a subset of metanephric mesenchyme cells migrate towards the periphery of the kidney during development. Further work will aim to understand how LIMK is involved in the activation of the spindle checkpoint leading to the dispersal of SMC3 and why metanephric mesenchymal cells need to migrate.

# Chapter 7: References

Acquaviva C., and Pines J. (2006). The anaphase-promoting complex/cyclosome: APC/C. J Cell Sci. 119(Pt 12), 2401-4.

Agnew B.J., Minamide L.S., and Bamburg J.R. (1995). Reactivation of phosphorylated actin depolymerizing factor and identification of the regulatory site. J Biol Chem. 270(29), 17582-7.

Al-Awqati Q., and Oliver J.A. (2002). Stem cells in the kidney. Kidney Int. 61(2), 387-95.

Alberts B., Johnson A., Lewis J., Raff M., Roberts K., and Walter P. (2008). Molecular biology of the cell, panel 17-1, pp. 1072-1073x. Garland Science, New York.

Amano M., Ito M., Kimura K., Fukata Y., Chihara K., Nakano T., Matsuura Y., and Kaibuchi K. (1996). Phosphorylation and activation of myosin by Rho-associated kinase (Rho-kinase). J Biol Chem. 271(34), 20246-9.

Amano T., Kaji N., Ohashi K., and Mizuno K. (2002). Mitosis-specific activation of LIM motif-containing protein kinase and roles of cofilin phosphorylation and dephosphorylation in mitosis. J Biol Chem. 277(24), 22093-102.

Arber S., Barbayannis F.A., Hanser H., Schneider C., Stanyon C.A., Bernard O., and Caroni P. (1998). Regulation of actin dynamics through phosphorylation of cofilin by LIM-kinase. Nature. 393(6687), 805-9.

Arnould C., Lelièvre-Pégorier M., Ronco P., and Lelongt B. (2009). MMP9 limits apoptosis and stimulates branching morphogenesis during kidney development. J Am Soc Nephrol. 20(10), 2171-80.

Barak H., and Boyle S.C. (2011). Organ culture and immunostaining of mouse embryonic kidneys. Cold Spring Harb Protoc. 2011(1), pdb.prot5558.

Basson M.A., Akbulut S., Watson-Johnson J., Simon R., Carroll T.J., Shakya R., Gross I., Martin G.R., Lufkin T., McMahon A.P., Wilson P.D., Costantini F.D., Mason I.J., and Licht J.D. (2005). Sprouty1 is a critical regulator of GDNF/RET-mediated kidney induction. Dev Cell. 8(2), 229-39.

Basson M.A., Watson-Johnson J., Shakya R., Akbulut S., Hyink D., Costantini F.D., Wilson P.D., Mason I.J., and Licht J.D. (2006). Branching morphogenesis of the ureteric epithelium during kidney development is coordinated by the opposing functions of GDNF and Sprouty1. Dev Biol. 299(2), 466-77.

Bayés M., Magano L.F., Rivera N., Flores R., and Pérez Jurado L.A. (2003). Mutational mechanisms of Williams-Beuren syndrome deletions. Am J Hum Genet. 73(1), 131-51.

Beaudouin J., Gerlich D., Daigle N., Eils R., and Ellenberg J. (2002). Nuclear envelope breakdown proceeds by microtubule-induced tearing of the lamina. Cell. 108(1), 83-96.

Bernard O. (2007). Lim kinases, regulators of actin dynamics. Int J Biochem Cell Biol. 39(6), 1071-6.

Bompard G., and Caron E. (2004). Regulation of WASP/WAVE proteins: making a long story short. J Cell Biol. 166(7), 957-62.

Boyle S., Misfeldt A., Chandler K.J., Deal K.K., Southard-Smith E.M., Mortlock D.P., Baldwin H.S., and de Caestecker M. (2008). Fate mapping using Cited1-CreERT2 mice demonstrates that the cap mesenchyme contains self-renewing progenitor cells and gives rise exclusively to nephronic epithelia. Dev Biol. 313(1), 234-45.

Boyle S.C., Kim M., Valerius M.T., McMahon A.P., and Kopan R. (2011). Notch pathway activation can replace the requirement for Wnt4 and Wnt9b in mesenchymal-to-epithelial transition of nephron stem cells. Development. 138(19), 4245-54.

Bravo-Cordero J.J., Magalhaes M.A., Eddy R.J., Hodgson L., and Condeelis J. (2013). Functions of cofilin in cell locomotion and invasion. Nat Rev Mol Cell Biol. 14(7), 405-15.

Brodbeck S., Besenbeck B., and Englert C. (2004). The transcription factor Six2 activates expression of the Gdnf gene as well as its own promoter. Mech Dev. 121(10), 1211-22.

Brophy P.D., Ostrom L., Lang K.M., and Dressler G.R. (2001). Regulation of ureteric bud outgrowth by Pax2-dependent activation of the glial derived neurotrophic factor gene. Development. 128(23), 4747-56.

Campbell A.K., and Siddle K. (1976). The effect of intracellular calcium ions on adrenaline-stimulated adenosine 3':5'-cyclic monophosphate concentrations in pigeon erythrocytes, studied by using the ionophore A23187. Biochem J. 158(2), 211-21.

Carroll T.J., Park J.S., Hayashi S., Majumdar A., and McMahon A.P. (2005). Wnt9b plays a central role in the regulation of mesenchymal to epithelial transitions underlying organogenesis of the mammalian urogenital system. Dev Cell. 9(2), 283-92.

Castedo M., Perfettini J.L., Roumier T., Andreau K., Medema R., and Kroemer G. (2004). Cell death by mitotic catastrophe: a molecular definition. Oncogene. 23(16), 2825-37.

Cha J.H., Kim Y.H., Jung J.Y., Han K.H., Madsen K.M., and Kim J. (2001). Cell proliferation in the loop of henle in the developing rat kidney. J Am Soc Nephrol. 12(7), 1410-21.

Chan S.K., Riley P.R., Price K.L., McElduff F., Winyard P.J., Welham S.J., Woolf A.S., and Long D.A. (2010). Corticosteroid-induced kidney dysmorphogenesis is associated with deregulated expression of known

cystogenic molecules, as well as Indian hedgehog. Am J Physiol Renal Physiol. 298(2), F346-56.

Cheng H.T., Kim M., Valerius M.T., Surendran K., Schuster-Gossler K., Gossler A., McMahon A.P., and Kopan R. (2007). Notch2, but not Notch1, is required for proximal fate acquisition in the mammalian nephron. Development. 134(4), 801-11.

Chi X., Michos O., Shakya R., Riccio P., Enomoto H., Licht J.D., Asai N., Takahashi M., Ohgami N., Kato M., Mendelsohn C., and Costantini F. (2009). Ret-dependent cell rearrangements in the Wolffian duct epithelium initiate ureteric bud morphogenesis. Dev. Cell. 17, 199-209.

Christiansen J.J., and Rajasekaran A.K. (2006). Reassessing epithelial to mesenchymal transition as a prerequisite for carcinoma invasion and metastasis. Cancer Res. 66(17), 8319-26.

Coleman M.L., Sahai E.A., Yeo M., Bosch M., Dewar A., and Olson M.F. (2001). Membrane blebbing during apoptosis results from caspase-mediated activation of ROCK I. Nat Cell Biol. 3(4), 339-45.

Coles H.S., Burne J.F., and Raff M.C. (1993). Large-scale normal cell death in the developing rat kidney and its reduction by epidermal growth factor. Development. 118(3), 777-84.

Cuddihy A.R., and O'Connell M.J. (2003). Cell-cycle responses to DNA damage in G2. Int Rev Cytol. 222, 99-140.

Dan C., Kelly A., Bernard O., and Minden A. (2001). Cytoskeletal changes regulated by the PAK4 serine/threonine kinase are mediated by LIM kinase 1 and cofilin. J Biol Chem. 276(34), 32115-21.

Davidson, A.J. (2009). Mouse kidney development (January 15, 2009), StemBook, ed. The Stem Cell Research Community, StemBook, doi/10.3824/stembook.1.34.1, http://www.stembook.org/node/532

DesMarais V., Ghosh M., Eddy R., and Condeelis J. (2005). Cofilin takes the lead. J Cell Sci. 118(Pt 1), 19-26.

Ding Y., Milosavljevic T., and Alahari S.K. (2008). Nischarin inhibits LIM kinase to regulate cofilin phosphorylation and cell invasion. Mol Cell Biol. 28(11), 3742-56.

dos Remedios C.G., Chhabra D., Kekic M., Dedova I.V., Tsubakihara M., Berry D.A., and Nosworthy N.J. (2003). Actin binding proteins: regulation of cytoskeletal microfilaments. Physiol Rev. 83(2), 433-73.

Dressler G. (2002). Tubulogenesis in the developing mammalian kidney. Trends Cell Biol. 12(8), 390-5.

Dressler G.R. (2009). Advances in early kidney specification, development and patterning. Development. 136(23), 3863-74.

Edwards D.C., Sanders L.C., Bokoch G.M., and Gill G.N. (1999). Activation of LIM-kinase by Pak1 couples Rac/Cdc42 GTPase signalling to actin cytoskeletal dynamics. Nat Cell Biol. 1(5), 253-9.

Edwards M., Zwolak A., Schafer D.A., Sept D., Dominguez R., and Cooper J.A. (2014). Capping protein regulators fine-tune actin assembly dynamics. Nat Rev Mol Cell Biol. 15(10), 677-89.

Forer A., and Wilson P.J. (2000). Evidence that kinetochore fibre microtubules shorten predominantly at the pole in anaphase flea-beetle spermatocytes. Chromosome Res. 8(2), 151-63.

Fackler O.T, and Grosse R. (2008). Cell motility through plasma membrane blebbing. J Cell Biol. 181(6), 879-84.

Fang Y., Vilella-Bach M., Bachmann R., Flanigan A., and Chen J. (2001). Phosphatidic acid-mediated mitogenic activation of mTOR signaling. Science. 294(5548), 1942-5.

Francke U. (1999). Williams-Beuren syndrome: genes and mechanisms. Hum Mol Genet. 8(10), 1947-54.

Friedl P., Noble P.B., Walton P.A., Laird D.W., Chauvin P.J., Tabah R.J., Black M., and Zänker K.S. (1995). Migration of coordinated cell clusters in mesenchymal and epithelial cancer explants in vitro. Cancer Res. 55(20), 4557-60.

Gerace L., and Blobel G. (1980). The nuclear envelope lamina is reversibly depolymerized during mitosis. Cell. 19(1), 277-87.

Giuliani S., Perin L., Sedrakyan S., Kokorowski P., Jin D., and De Filippo R. (2008). Ex vivo whole embryonic kidney culture: a novel method for research in development, regeneration and transplantation. J Urol. 179(1), 365-70.

Glotzer M. (2005). The molecular requirements for cytokinesis. Science. 307(5716), 1735-9.

Gohla A., Birkenfeld J., and Bokoch G.M. (2005). Chronophin, a novel HAD-type serine protein phosphatase, regulates cofilin-dependent actin dynamics. Nat Cell Biol. 7(1), 21-9.

Goldschmidt-Clermont P.J., Furman M.I., Wachsstock D., Safer D., Nachmias V.T., and Pollard T.D. (1992). The control of actin nucleotide exchange by thymosin beta 4 and profilin. A potential regulatory mechanism for actin polymerization in cells. Mol Biol Cell. 3(9), 1015-24.

Grieshammer U., Le Ma, Plump A.S., Wang F., Tessier-Lavigne M., and Martin G.R. (2004). SLIT2-mediated ROBO2 signaling restricts kidney induction to a single site. Dev Cell. 6(5), 709-17.

Grieshammer U., Cebrián C., Ilagan R., Meyers E., Herzlinger D., and Martin G.R. (2005). FGF8 is required for cell survival at distinct stages of nephrogenesis and for regulation of gene expression in nascent nephrons. Development. 132(17), 3847-57.

Grobstein C. (1953). Inductive epitheliomesenchymal interaction in cultured organ rudiments of the mouse. Science. 118(3054), 52-5.

Gruber S., Haering C.H., and Nasmyth K. (2003). Chromosomal cohesin forms a ring. Cell. 112(6), 765-77.

Gupta I.R., Lapointe M., and Yu O.H. (2003). Morphogenesis during mouse embryonic kidney explant culture. Kidney Int. 63(1), 365-76.

Han L., Stope M.B., de Jesús M.L., Oude Weernink P.A., Urban M., Wieland T., Rosskopf D., Mizuno K., Jakobs K.H., and Schmidt M. (2007). Direct stimulation of receptor-controlled phospholipase D1 by phospho-cofilin. EMBO J. 26(19), 4189-202.

Hannak E., Kirkham M., Hyman A.A., and Oegema K. (2001). Aurora-A kinase is required for centrosome maturation in Caenorhabditis elegans. J Cell Biol. 155(7), 1109-16.

Hartman H.A., Lai H.L., and Patterson L.T. (2007). Cessation of renal morphogenesis in mice. Dev Biol. 310(2), 379-87.

Heng Y.W., Lim H.H., Mina T., Utomo P., Zhong S., Lim C.T., and Koh C.G. (2012). TPPP acts downstream of RhoA-ROCK-LIMK2 to regulate astral microtubule organization and spindle orientation. J Cell Sci. 125(Pt 6), 1579-90.

Hetrick B., Han M.S., Helgeson L.A., and Nolen B.J. (2013). Small molecules CK-666 and CK-869 inhibit actin-related protein 2/3 complex by blocking an activating conformational change. Chem Biol. 20(5), 701-12.

Hinchliffe S.A., Lynch M.R., Sargent P.H., Howard C.V., and Van Velzen D. (1992). The effect of intrauterine growth retardation on the development of renal nephrons. Br J Obstet Gynaecol. 99(4), 296-301.

Hoar K., Chakravarty A., Rabino C., Wysong D., Bowman D., Roy N., and Ecsedy J.A. (2007). MLN8054, a small-molecule inhibitor of Aurora A, causes spindle pole and chromosome congression defects leading to aneuploidy. Mol Cell Biol. 27(12), 4513-25.

Holthöfer H., Miettinen A., Lehto V.P., Lehtonen E., and Virtanen I. (1984). Expression of vimentin and cytokeratin types of intermediate filament proteins in developing and adult human kidneys. Lab Invest. 50(5), 552-9.

Hornick J.E., Bader J.R., Tribble E.K., Trimble K., Breunig J.S., Halpin E.S., Vaughan K.T., and Hinchcliffe E.H. (2008). Live-cell analysis of mitotic spindle formation in taxol-treated cells. Cell Motil Cytoskeleton. 65(8), 595-613.

Hoy W.E., Bertram J.F., Denton R.D., Zimanyi M., Samuel T., and Hughson M.D. (2008). Nephron number, glomerular volume, renal disease and hypertension. Curr Opin Nephrol Hypertens. 17(3), 258-265.

Hughson M., Farris A.B. 3rd., Douglas-Denton R., Hoy W.E., and Bertram J.F. (2003). Glomerular number and size in autopsy kidneys: the relationship to birth weight. Kidney Int. 63(6), 2113-22.

Hum S., Rymer C., Schaefer C., Bushnell D., and Sims-Lucas S. (2014). Ablation of the renal stroma defines its critical role in nephron progenitor and vasculature patterning. PLoS One. 9(2), e88400.

Humphreys B.D., Lin S.L., Kobayashi A., Hudson T.E., Nowlin B.T., Bonventre J.V., Valerius M.T., McMahon A.P., and Duffield J.S. (2010). Fate tracing reveals the pericyte and not epithelial origin of myofibroblasts in kidney fibrosis. Am J Pathol. 176(1), 85-97.

Johnson E.O., Chang K.H., Ghosh S., Venkatesh C., Giger K., Low P.S., and Shah K. (2012). LIMK2 is a crucial regulator and effector of Aurora-A-kinase-mediated malignancy. J Cell Sci. 125(Pt 5), 1204-16.

Karner C.M., Das A., Ma Z., Self M., Chen C., Lum L., Oliver G., and Carroll T.J. (2011). Canonical Wnt9b signaling balances progenitor cell expansion and differentiation during kidney development. Development. 138(7), 1247-57.

Kawano Y., Fukata Y., Oshiro N., Amano M., Nakamura T., Ito M., Matsumura F., Inagaki M., and Kaibuchi K. (1999). Phosphorylation of myosin-binding subunit (MBS) of myosin phosphatase by Rho-kinase in vivo. J Cell Biol. 147(5), 1023-38.

Kelly T., Mueller S.C., Yeh Y., and Chen W.T. (1994). Invadopodia promote proteolysis of a wide variety of extracellular matrix proteins. J Cell Physiol. 158(2), 299-308.

Kim I.H., Racz B., Wang H., Burianek L., Weinberg R., Yasuda R., Wetsel W.C., and Soderling S.H. (2013). Disruption of Arp2/3 results in asymmetric structural plasticity of dendritic spines and progressive synaptic and behavioral abnormalities. J Neurosci. 33(14), 6081-92.

Kim J., Lee G.S., Tisher C.C., and Madsen K.M. (1996). Role of apoptosis in development of the ascending thin limb of the loop of Henle in rat kidney. Am J Physiol. 271(4 Pt 2), F831-45.

Kobayashi A., Kwan K.M., Carroll T.J., McMahon A.P., Mendelsohn C.L., and Behringer R.R. (2005). Distinct and sequential tissue-specific activities of the LIM-class homeobox gene Lim1 for tubular morphogenesis during kidney development. Development. 132(12), 2809-23.

Kobayashi A., Valerius M.T., Mugford J.W., Carroll T.J., Self M., Oliver G., and McMahon A.P. (2008). Six2 defines and regulates a multipotent self-

renewing nephron progenitor population throughout mammalian kidney development. Cell Stem Cell. 3(2), 169-81.

Krawczyk W.S. (1971). A pattern of epidermal cell migration during wound healing. J Cell Biol. 49(2), 247-63.

Kume T., Deng K., and Hogan B.L. (2000). Murine forkhead/winged helix genes Foxc1 (Mf1) and Foxc2 (Mfh1) are required for the early organogenesis of the kidney and urinary tract. Development. 127(7), 1387-95.

Kuure S., Vuolteenaho R., and Vainio S. (2000). Kidney morphogenesis: cellular and molecular regulation. Mech Dev. 92(1), 31-45.

Kwiatkowski D.J. (1999). Functions of gelsolin: motility, signaling, apoptosis, cancer. Curr Opin Cell Biol. 11(1), 103-8.

Langley-Evans S.C., Welham S.J., and Jackson A.A. (1999). Fetal exposure to a maternal low protein diet impairs nephrogenesis and promotes hypertension in the rat. Life Sci. 64(11), 965-74.

Larsson N., Marklund U., Gradin H.M., Brattsand G., and Gullberg M. (1997). Control of microtubule dynamics by oncoprotein 18: dissection of the regulatory role of multisite phosphorylation during mitosis. Mol Cell Biol. 17(9), 5530-9.

Lee W.C., Berry R., Hohenstein P., and Davies J. (2008). siRNA as a tool for investigating organogenesis: The pitfalls and the promises. Organogenesis. 4(3), 176-81.

Lelongt B., Trugnan G., Murphy G., and Ronco P.M. (1997). Matrix metalloproteinases MMP2 and MMP9 are produced in early stages of kidney

morphogenesis but only MMP9 is required for renal organogenesis in vitro. J Cell Biol. 136(6), 1363-73.

Levinson R.S., Batourina E., Choi C., Vorontchikhina M., Kitajewski J., and Mendelsohn C.L. (2005). Foxd1-dependent signals control cellularity in the renal capsule, a structure required for normal renal development. Development. 132(3), 529-39.

Li R., Doherty J., Antonipillai J., Chen S., Devlin M., Visser K., Baell J., Street I., Anderson R.L., and Bernard O. (2013). LIM kinase inhibition reduces breast cancer growth and invasiveness but systemic inhibition does not reduce metastasis in mice. Clin Exp Metastasis. 30(4), 483-95.

Lin D.C., Tobin K.D., Grumet M., and Lin S. (1980). Cytochalasins inhibit nuclei-induced actin polymerization by blocking filament elongation. J Cell Biol. 84(2), 455-60.

Lindström N.O., Neves C., McIntosh R., Miedzybrodzka Z., Vargesson N., and Collinson J.M. (2011). Tissue specific characterisation of Lim-kinase 1 expression during mouse embryogenesis. Gene Expr Patterns. 11(3-4), 221-32.

Lindström N.O., Lawrence M.L., Burn S.F., Johansson J.A., Bakker E.R., Ridgway R.A., Chang C.H., Karolak M.J., Oxburgh L., Headon D.J., Sansom O.J., Smits R., Davies J.A., and Hohenstein P. (2015). Integrated β-catenin, BMP, PTEN, and Notch signalling patterns the nephron. Elife. 4, e04000.

Liu Z., Yang X., Chen C., Liu B., Ren B., Wang L., Zhao K., Yu S., and Ming H. (2013). Expression of the Arp2/3 complex in human gliomas and its role in the migration and invasion of glioma cells. Oncol Rep. 30(5), 2127-36.

Low S.H., Li X., Miura M., Kudo N., Quiñones B., and Weimbs T. (2003). Syntaxin 2 and endobrevin are required for the terminal step of cytokinesis in mammalian cells. Dev Cell. 4(5), 753-9.

Luster A.D., Alon R., and von Andrian U.H. (2005). Immune cell migration in inflammation: present and future therapeutic targets. Nat Immunol. 6(12), 1182-90.

Machesky L.M., and Insall R.H. (1998). Scar1 and the related Wiskott-Aldrich syndrome protein, WASP, regulate the actin cytoskeleton through the Arp2/3 complex. Curr Biol. 8(25), 1347-56.

Mañalich R., Reyes L., Herrera M., Melendi C., and Fundora I. (2000). Relationship between weight at birth and the number and size of renal glomeruli in humans: a histomorphometric study. Kidney Int. 58(2), 770-3.

Marklund U., Larsson N., Gradin H.M., Brattsand G., and Gullberg M. (1996). Oncoprotein 18 is a phosphorylation-responsive regulator of microtubule dynamics. EMBO J. 15(19), 5290-8.

Mashiach-Farkash E., Rak R., Elad-Sfadia G., Haklai R., Carmeli S., Kloog Y., and Wolfson H.J. (2012). Computer-based identification of a novel LIMK1/2 inhibitor that synergizes with salirasib to destabilize the actin cytoskeleton. Oncotarget. 3(6), 629-39.

Meberg P.J., Ono S., Minamide L.S., Takahashi M., and Bamburg J.R. (1998). Actin depolymerizing factor and cofilin phosphorylation dynamics: response to signals that regulate neurite extension. Cell Motil Cytoskeleton. 39(2), 172-90.

Meng Y., Takahashi H., Meng J., Zhang Y., Lu G., Asrar S., Nakamura T., and Jia Z. (2004). Regulation of ADF/cofilin phosphorylation and synaptic function by LIM-kinase. Neuropharmacology. 47(5), 746-54.

Meng Y., Zhang Y., Tregoubov V., Janus C., Cruz L., Jackson M., Lu W.Y., MacDonald J.F., Wang J.Y., Falls D.L., and Jia Z. (2002). Abnormal spine morphology and enhanced LTP in LIMK-1 knockout mice. Neuron. 35(1), 121-33.

Meraldi P., and Nigg E.A. (2002). The centrosome cycle. FEBS Lett. 521(1-3), 9-13.

Meyer T.N., Schwesinger C., Sampogna R.V., Vaughn D.A., Stuart R.O., Steer D.L., Bush K.T., and Nigam S.K. (2006). Rho kinase acts at separate steps in ureteric bud and metanephric mesenchyme morphogenesis during kidney development. Differentiation. 74(9-10), 638-47.

Michos O., Panman L., Vintersten K., Beier K., Zeller R., and Zuniga A. (2004). Gremlin-mediated BMP antagonism induces the epithelial-mesenchymal feedback signaling controlling metanephric kidney and limb organogenesis. Development. 131(14), 3401-10.

Miki H., Suetsugu S., and Takenawa T. (1998). WAVE, a novel WASP-family protein involved in actin reorganization induced by Rac. EMBO J. 17(23), 6932-41.

Minshull J., Sun H., Tonks N.K., and Murray A.W. (1994). A MAP kinase-dependent spindle assembly checkpoint in Xenopus egg extracts. Cell. 79(3), 475-86.

Moritz M., and Agard D.A. (2001). Gamma-tubulin complexes and microtubule nucleation. Curr Opin Struct Biol. 11(2), 174-81.

Moriyama K., Iida K., and Yahara I. (1996). Phosphorylation of Ser-3 of cofilin regulates its essential function on actin. Genes Cells. 1(1), 73-86.

Morris A.R., Drawbridge J., and Steinberg M.S. (2003). Axolotl pronephric duct migration requires an epidermally derived, laminin 1-containing extracellular matrix and the integrin receptor alpha6beta1. Development 130, 5601–5608.

Mouneimne G., DesMarais V., Sidani M., Scemes E., Wang W., Song X., Eddy R., and Condeelis J. (2006). Spatial and temporal control of cofilin activity is required for directional sensing during chemotaxis. Curr Biol. 16(22), 2193-205.

Mugford J.W., Yu J., Kobayashi A., and McMahon A.P. (2009). High-resolution gene expression analysis of the developing mouse kidney defines novel cellular compartments within the nephron progenitor population. Dev Biol. 333(2), 312-23.

Mullins R.D., Heuser J.A., and Pollard T.D. (1998). The interaction of Arp2/3 complex with actin: nucleation, high affinity pointed end capping, and formation of branching networks of filaments. Proc Natl Acad Sci U S A. 95(11), 6181-6.

Musacchio A., and Salmon E.D. (2007). The spindle-assembly checkpoint in space and time. Nat Rev Mol Cell Biol. 8(5), 379-93.

Nagasaki A., Inotsume K., Kanada M., and Uyeda T.Q. (2008). Phospholipase D is essential for keratocyte-like migration of NBT-II cells. Cell Struct Funct. 33(1), 27-33.

Nakai S., Sugitani Y., Sato H., Ito S., Miura Y., Ogawa M., Nishi M., Jishage K., Minowa O., and Noda T. (2003). Crucial roles of Brn1 in distal tubule formation and function in mouse kidney. Development. 130(19), 4751-9.

Nasmyth K. (2001). Disseminating the genome: joining, resolving, and separating sister chromatids during mitosis and meiosis. Annu Rev Genet. 35, 673-745.

Nishita M., Tomizawa C., Yamamoto M., Horita Y., Ohashi K., and Mizuno K. (2005). Spatial and temporal regulation of cofilin activity by LIM kinase and Slingshot is critical for directional cell migration. J Cell Biol. 171(2), 349-59.

Niwa R., Nagata-Ohashi K., Takeichi M., Mizuno K., and Uemura T. (2002). Control of actin reorganization by Slingshot, a family of phosphatases that dephosphorylate ADF/cofilin. Cell. 108(2), 233-46.

Ohashi K., Nagata K., Maekawa M., Ishizaki T., Narumiya S., and Mizuno K. (2000). Rho-associated kinase ROCK activates LIM-kinase 1 by phosphorylation at threonine 508 within the activation loop. J Biol Chem. 275(5), 3577-82.

Ohashi K., Sampei K., Nakagawa M., Uchiumi N., Amanuma T., Aiba S., Oikawa M., and Mizuno K. (2014). Damnacanthal, an effective inhibitor of LIM-kinase, inhibits cell migration and invasion. Mol Biol Cell. 25(6), 828-40.

Packard A., Georgas K., Michos O., Riccio P., Cebrian C., Combes A.N., Ju A., Ferrer-Vaquer A., Hadjantonakis A.K., Zong H., Little M.H., and Costantini F. (2013). Luminal mitosis drives epithelial cell dispersal within the branching ureteric bud. Dev Cell. 27(3), 319-30.

Pankau R., Partsch C.J., Winter M., Gosch A., and Wessel A. (1996). Incidence and spectrum of renal abnormalities in Williams-Beuren syndrome. Am J Med Genet. 63(1), 301-4.

Pardee A.B. (1989). G1 events and regulation of cell proliferation. Science. 246(4930), 603-8.

Park J.S., Valerius M.T., and McMahon A.P. (2007). Wnt/beta-catenin signaling regulates nephron induction during mouse kidney development. Development. 134(13), 2533-9.

Park J.S., Ma W., O'Brien L.L., Chung E., Guo J.J., Cheng J.G., Valerius M.T., McMahon J.A., Wong W.H., and McMahon A.P. (2012). Six2 and Wnt regulate self-renewal and commitment of nephron progenitors through shared gene regulatory networks. Dev Cell. 23(3), 637-51.

Pepicelli C.V., Kispert A., Rowitch D.H., and McMahon A.P. (1997). GDNF induces branching and increased cell proliferation in the ureter of the mouse. Dev Biol. 192(1), 193-8.

Pober B.R., Lacro R.V., Rice C., Mandell V., and Teele R.L. (1993). Renal findings in 40 individuals with Williams syndrome. Am J Med Genet. 46(3), 271-4.

Poladia D.P., Kish K., Kutay B., Hains D., Kegg H., Zhao H., and Bates C.M. (2006). Role of fibroblast growth factor receptors 1 and 2 in the metanephric mesenchyme. Dev Biol. 291(2), 325-39.

Pole R.J., Qi B.Q., and Beasley S.W. (2002). Patterns of apoptosis during degeneration of the pronephros and mesonephros. J Urol. 167(1), 269-71.

Pollard T.D., and Borisy G.G. (2003). Cellular motility driven by assembly and disassembly of actin filaments. Cell. 112(4), 453-65.

Prudent R., Vassal-Stermann E., Nguyen C.H., Pillet C., Martinez A., Prunier C., Barette C., Soleilhac E., Filhol O., Beghin A., Valdameri G., Honoré S., Aci-Sèche S., Grierson D., Antonipillai J., Li R., Di Pietro A., Dumontet C., Braguer D., Florent J.C., Knapp S., Bernard O., and Lafanechère L. (2012). Pharmacological inhibition of LIM kinase stabilizes microtubules and inhibits neoplastic growth. Cancer Res. 72(17), 4429-39.

Public Health England. (2014). New figures show high blood pressure costs NHS billions each year. Public Health England press release. First published: 18 November 2014, https://www.gov.uk/government/news/new-figures-show-high-blood-pressure-costs-nhs-billions-each-year .

Qiao J., Uzzo R., Obara-Ishihara T., Degenstein L., Fuchs E., and Herzlinger D. (1999). FGF-7 modulates ureteric bud growth and nephron number in the developing kidney. Development. 126(3), 547-54.

Rak R., Haklai R., Elad-Tzfadia G., Wolfson H.J., Carmeli S., and Kloog Y. (2014). Novel LIMK2 Inhibitor Blocks Panc-1 Tumor Growth in a mouse xenograft model. Oncoscience. 1(1), 39-48.

Range R.C., Venuti J.M., and McClay D.R. (2005). LvGroucho and nuclear beta-catenin functionally compete for Tcf binding to influence activation of the endomesoderm gene regulatory network in the sea urchin embryo. Dev Biol. 279(1), 252-67.

Ridley A.J., Schwartz M.A., Burridge K., Firtel R.A., Ginsberg M.H., Borisy G., Parsons J.T., and Horwitz A.R. (2003). Cell migration: integrating signals from front to back. Science. 302(5651), 1704-9.

Ritchey L., Ottman R., Roumanos M., and Chakrabarti R. (2012). A functional cooperativity between Aurora A kinase and LIM kinase1: implication in the mitotic process. Cell Cycle. 11(2), 296-309.

Roose J., Molenaar M., Peterson J., Hurenkamp J., Brantjes H., Moerer P., van de Wetering M., Destrée O., and Clevers H. (1998). The Xenopus Wnt effector XTcf-3 interacts with Groucho-related transcriptional repressors. Nature. 395(6702), 608-12.

Ross-Macdonald P., de Silva H., Guo Q., Xiao H., Hung C.Y., Penhallow B., Markwalder J., He L., Attar R.M., Lin T.A., Seitz S., Tilford C., Wardwell-Swanson J., and Jackson D. (2008). Identification of a nonkinase target mediating cytotoxicity of novel kinase inhibitors. Mol Cancer Ther. 7(11), 3490-8.

Sainio K., Suvanto P., Davies J., Wartiovaara J., Wartiovaara K., Saarma M., Arumäe U., Meng X., Lindahl M., Pachnis V., and Sariola H. (1997). Glial-cell-line-derived neurotrophic factor is required for bud initiation from ureteric epithelium. Development. 124, 4077–4087.

Salina D., Enarson P., Rattner J.B., and Burke B. (2003). Nup358 integrates nuclear envelope breakdown with kinetochore assembly. J Cell Biol. 162(6), 991-1001.

Schiff P.B., and Horwitz S.B. (1980). Taxol stabilizes microtubules in mouse fibroblast cells. Proc Natl Acad Sci U S A. 77(3), 1561-5.

Schooley A., Vollmer B., and Antonin W. (2012). Building a nuclear envelope at the end of mitosis: coordinating membrane reorganization, nuclear pore complex assembly, and chromatin de-condensation. Chromosoma. 121(6), 539-54.

Scott R.W., Hooper S., Crighton D., Li A., König I., Munro J., Trivier E., Wickman G., Morin P., Croft D.R., Dawson J., Machesky L., Anderson K.I., Sahai E.A., and Olson M.F. (2010). LIM kinases are required for invasive path generation by tumor and tumor-associated stromal cells. J Cell Biol. 191(1), 169-85.

Selden S.C. 3rd., and Schwartz S.M. (1979). Cytochalasin B inhibition of endothelial proliferation at wound edges in vitro. J Cell Biol. 81(2), 348-54.

Self M., Lagutin O.V., Bowling B., Hendrix J., Cai Y., Dressler G.R., and Oliver G. (2006). Six2 is required for suppression of nephrogenesis and progenitor renewal in the developing kidney. EMBO J. 25(21), 5214-28.

Sequeira Lopez M.L., and Gomez R.A. (2011). Development of the renal arterioles. J Am Soc Nephrol. 22(12), 2156-65.

Shakya R., Jho E.H., Kotka P., Wu Z., Kholodilov N., Burke R., D'Agati V., and Costantini F. (2005). The role of GDNF in patterning the excretory system. Dev Biol 283, 70–84.

Shawlot W., and Behringer R.R. (1995). Requirement for Lim1 in head-organizer function. Nature. 374(6521), 425-30.

Short K.M., Combes A.N., Lefevre J., Ju A.L., Georgas K.M., Lamberton T., Cairncross O., Rumballe B.A., McMahon A.P., Hamilton N.A., Smyth I.M., and Little M.H. (2014). Global quantification of tissue dynamics in the developing mouse kidney. Dev Cell. 29(2), 188-202.

Skippen A., Jones D.H., Morgan C.P., Li M., and Cockcroft S. (2002). Mechanism of ADP ribosylation factor-stimulated phosphatidylinositol 4,5-bisphosphate synthesis in HL60 cells. J Biol Chem. 277(8), 5823-31.

Song X., Chen X., Yamaguchi H., Mouneimne G., Condeelis J.S., and Eddy R.J. (2006). Initiation of cofilin activity in response to EGF is uncoupled from cofilin phosphorylation and dephosphorylation in carcinoma cells. J Cell Sci. 119(Pt 14), 2871-81.

Srinivas S., Goldberg M.R., Watanabe T., D'Agati V., al-Awqati Q., and Costantini F. (1999). Expression of green fluorescent protein in the ureteric bud of transgenic mice: a new tool for the analysis of ureteric bud morphogenesis. Dev Genet. 24(3-4), 241-51.

Stark K., Vainio S., Vassileva G., and McMahon A.P. (1994). Epithelial transformation of metanephric mesenchyme in the developing kidney regulated by Wnt-4. Nature. 372(6507), 679-83.

Su W., Yeku O., Olepu S., Genna A., Park J.S., Ren H., Du G., Gelb M.H., Morris A.J., and Frohman M.A. (2009). 5-Fluoro-2-indolyl des-chlorohalopemide (FIPI), a phospholipase D pharmacological inhibitor that alters cell spreading and inhibits chemotaxis. Mol Pharmacol. 75(3), 437-46.

Sudo T., Nitta M., Saya H., and Ueno N.T. (2004). Dependence of paclitaxel sensitivity on a functional spindle assembly checkpoint. Cancer Res. 64(7), 2502-8.

Sumi T., Matsumoto K., Takai Y., and Nakamura T. (1999). Cofilin phosphorylation and actin cytoskeletal dynamics regulated by rho- and Cdc42-activated LIM-kinase 2. J Cell Biol. 147(7), 1519-32.

Sumi T., Matsumoto K., and Nakamura T. (2002). Mitosis-dependent phosphorylation and activation of LIM-kinase 1. Biochem Biophys Res Commun. 290(4), 1315-20.

Svitkina T.M., Bulanova E.A., Chaga O.Y., Vignjevic D.M., Kojima S., Vasiliev J.M., and Borisy G.G. (2003). Mechanism of filopodia initiation by reorganization of a dendritic network. J Cell Biol. 160(3), 409-21.

Takahashi H., Koshimizu U., Miyazaki J., and Nakamura T. (2002). Impaired spermatogenic ability of testicular germ cells in mice deficient in the LIM-kinase 2 gene. Dev Biol. 241(2), 259-72.

Tassabehji M., Metcalfe K., Fergusson W.D., Carette M.J., Dore J.K., Donnai D., Read A.P., Pröschel C., Gutowski N.J., Mao X., and Sheer D. (1996). LIM-kinase deleted in Williams syndrome. Nat Genet. 13(3), 272-3.

Taylor E.W. (1965). The mechanism of colchicine inhibition of mitosis. i. kinetics of inhibition and the binding of h3-colchicine. J Cell Biol. 25, SUPPL, 145-60.

Toshima J., Toshima J.Y., Amano T., Yang N., Narumiya S., and Mizuno K. (2001a). Cofilin phosphorylation by protein kinase testicular protein kinase 1 and its role in integrin-mediated actin reorganization and focal adhesion formation. Mol Biol Cell. 12(4), 1131-45.

Toshima J., Toshima J.Y., Takeuchi K., Mori R., and Mizuno K. (2001b). Cofilin phosphorylation and actin reorganization activities of testicular protein kinase 2 and its predominant expression in testicular Sertoli cells. J Biol Chem. 276(33), 31449-58.

Toth M., and Fridman R. (2001). Assessment of Gelatinases (MMP-2 and MMP-9 by Gelatin Zymography. Methods Mol Med. 57, 163-74.

Toth M., Sohail A., and Fridman R. (2012). Assessment of gelatinases (MMP-2 and MMP-9) by gelatin zymography. Methods Mol Biol. 878, 121-35.

Toya M., Terasawa M., Nagata K., Iida Y., and Sugimoto A. (2011). A kinase-independent role for Aurora A in the assembly of mitotic spindle microtubules in Caenorhabditis elegans embryos. Nat Cell Biol. 13(6), 708-14.

van Rheenen J., Song X., van Roosmalen W., Cammer M., Chen X., Desmarais V., Yip S.C., Backer J.M., Eddy R.J., and Condeelis J.S. (2007). EGF-induced PIP2 hydrolysis releases and activates cofilin locally in carcinoma cells. J Cell Biol. 179(6), 1247-59.

Vega Q.C., Worby C.A., Lechner M.S., Dixon J.E., and Dressler G.R. (1996). Glial cell line-derived neurotrophic factor activates the receptor tyrosine kinase RET and promotes kidney morphogenesis. Proc Natl Acad Sci USA. 93, 10657–10661.

Wang Y., Shibasaki F., and Mizuno K. (2005). Calcium signal-induced cofilin dephosphorylation is mediated by Slingshot via calcineurin. J Biol Chem. 280(13), 12683-9.

Watanabe K., Ueno M., Kamiya D., Nishiyama A., Matsumura M., Wataya T., Takahashi J.B., Nishikawa S., Nishikawa S., Muguruma K., and Sasai Y. (2007). A ROCK inhibitor permits survival of dissociated human embryonic stem cells. Nat Biotechnol. 25(6), 681-6.

Weijer C.J. (2009). Collective cell migration in development. J Cell Sci. 122(Pt 18), 3215-23.

Welham S.J., Riley P.R., Wade A., Hubank M., and Woolf A.S. (2005). Maternal diet programs embryonic kidney gene expression. Physiol Genomics. 22(1), 48-56.

Wu B., Sahoo D., and Brooks J.D. (2013). Comprehensive gene expression changes associated with mouse postnatal kidney development. J Urol. 189(6), 2385-90.

Xu J., Liu H., Park J.S., Lan Y., and Jiang R. (2014). Osr1 acts downstream of and interacts synergistically with Six2 to maintain nephron progenitor cells during kidney organogenesis. Development. 141(7), 1442-52.

Yang N., Higuchi O., Ohashi K., Nagata K., Wada A., Kangawa K., Nishida E., and Mizuno K. (1998). Cofilin phosphorylation by LIM-kinase 1 and its role in Rac-mediated actin reorganization. Nature. 393(6687), 809-12.

Yang Q., Zhang X.F., Pollard T.D., and Forscher P. (2012). Arp2/3 complex-dependent actin networks constrain myosin II function in driving retrograde actin flow. J Cell Biol. 197(7), 939-56.

Yao H., Wang G., Guo L., and Wang X. (2013). Phosphatidic acid interacts with a MYB transcription factor and regulates its nuclear localization and function in Arabidopsis. Plant Cell. 25(12), 5030-42.

Yin H.L., and Janmey P.A. (2003). Phosphoinositide regulation of the actin cytoskeleton. Annu Rev Physiol. 65, 761-89.

Yonezawa N., Nishida E., Iida K., Yahara I., and Sakai H. (1990). Inhibition of the interactions of cofilin, destrin, and deoxyribonuclease I with actin by phosphoinositides. J Biol Chem. 265(15), 8382-6.

Yoo Y., Ho H.J., Wang C., and Guan J.L. (2010). Tyrosine phosphorylation of cofilin at Y68 by v-Src leads to its degradation through ubiquitin-proteasome pathway. Oncogene. 29(2), 263-72.

Zebda N., Bernard O., Bailly M., Welti S., Lawrence D.S., and Condeelis J.S. (2000). Phosphorylation of ADF/cofilin abolishes EGF-induced actin nucleation at the leading edge and subsequent lamellipod extension. J Cell Biol. 151(5), 1119-28.

Zhan Q., Bamburg J.R., and Badwey J.A. (2003). Products of phosphoinositide specific phospholipase C can trigger dephosphorylation of

cofilin in chemoattractant stimulated neutrophils. Cell Motil Cytoskeleton. 54(1), 1-15.

Zhang L., Valdez J.M., Zhang B., Wei L., Chang J., and Xin L. (2011). ROCK inhibitor Y-27632 suppresses dissociation-induced apoptosis of murine prostate stem/progenitor cells and increases their cloning efficiency. PLoS One. 6(3), e18271.

Zhao H., Kegg H., Grady S., Truong H.T., Robinson M.L., Baum M., and Bates C.M. (2004). Role of fibroblast growth factor receptors 1 and 2 in the ureteric bud. Dev Biol. 276(2), 403-15.